

STUDIES OF VOLTAGE-ACTIVATED POTASSIUM CHANNELS IN A
MAMMALIAN CELL LINE

Thesis submitted for the degree of

Doctor of Philosophy

at the University of Leicester

by

Iftikhar Ahmad Khan BSc (Bradford)

Department of Cell Physiology and Pharmacology

University of Leicester

October 1998

UMI Number: U536424

All rights reserved

INFORMATION TO ALL USERS

The quality of this reproduction is dependent upon the quality of the copy submitted.

In the unlikely event that the author did not send a complete manuscript and there are missing pages, these will be noted. Also, if material had to be removed, a note will indicate the deletion.



UMI U536424

Published by ProQuest LLC 2013. Copyright in the Dissertation held by the Author.
Microform Edition © ProQuest LLC.

All rights reserved. This work is protected against
unauthorized copying under Title 17, United States Code.



ProQuest LLC
789 East Eisenhower Parkway
P.O. Box 1346
Ann Arbor, MI 48106-1346

ABSTRACT

The biophysical properties of a delayed rectifier (Kv1.5) and an A-type (Kv4.2) K⁺-channel were investigated using a Murine Erythroleukemia (MEL) cell line. Genomic DNA clones of full length human Kv1.5 gene (isolated and sequenced from an adult heart cDNA library) and a cDNA sequence encoding Kv4.2 (isolated from rat hippocampus) were stably transfected into MEL cells by electroporation. Gene expression was regulated by the locus control region of the human β -globin gene; channels were expressed after induction of cells to undergo erythroid differentiation by addition of dimethyl sulphoxide.

The whole cell configuration of the patch clamp technique was used to characterise the biophysical properties of the two channels, which are distinguishable by rates of current inactivation. The voltage-dependence of current activation was used to construct current-voltage relationships. Selectivity of Kv1.5 for K⁺ ions was assessed, and reversal potentials measured with different external K⁺ concentrations. The voltage-dependence of steady state activation, (a measure of the channel open probability) and steady state inactivation were examined, and the time course of activation and inactivation calculated in terms of classical Hodgkin-Huxley equations.

Synthetic 'ball' peptides based upon the sequence of the amino-terminal structural motif that causes fast inactivation (analogous to a 'ball and chain' occluding the pore internally) in *Shaker* K⁺ channels were included in pipette solutions during recordings. Blocking/unblocking rates, and association/dissociation rate constants were calculated to characterise the effect on Kv1.5 and Kv4.2 currents. Kv1.5 does not undergo fast inactivation unlike Kv4.2, but these peptides caused Kv1.5 inactivation to speed up to resemble an A-type current. The mutation L7E caused peptides to become inactive; the double mutation E12K,D13K made the peptide more potent. Even Kv4.2 currents inactivated significantly more quickly. These results imply that there is a high degree of conservation of the ball receptor from *Shaker* to Kv4.2 and Kv1.5.

Table of contents

TITLE	i
ABSTRACT	ii
TABLE OF CONTENTS	iii
LIST OF FIGURES	ix
LIST OF TABLES	xiii
ACKNOWLEDGEMENTS	xiv
CHAPTER ONE: General Introduction	1
1.1 Ionic channels	5
1.2 The patch clamp technique	6
1.2.1 Patch clamp configurations	8
1.3 Voltage-activated potassium channels	11
1.3.1 The action potential	12
1.3.1.1 The Hodgkin-Huxley Model	14
1.3.1.2 The cardiac action potential	18
1.4 Potassium channel gene cloning	23
1.4.1 The role of <i>Drosophila melanogaster</i>	26
1.4.2 Molecular structure and function of voltage-activated potassium channels	28
1.4.2.1 Transmembrane domains and the voltage sensor	30
1.4.2.2 The pore region	32

1.4.2.3	N-type inactivation	34
1.4.2.4	C-type inactivation	36
1.4.3	Alternative splicing, genomic complexity and the generation of diversity	37
1.4.3.1	Alternative splicing	37
1.4.3.2	Multiple gene families	38
1.4.3.3	Heteromultimeric channels	41
1.4.4	Nomenclature for vertebrate voltage-activated potassium channels	43
1.5	Introduction to work carried out	49
CHAPTER TWO: METHODS AND MATERIALS		50
2.1	Molecular Biology Methods	51
2.1.1	Expression of cloned potassium channel genes in Murine erythroleukemia (MEL) cells by locus activation	51
2.1.1.1	Murine erythroleukemia cells	51
2.1.1.2	The locus control region	54
2.1.1.3	Kv1.5	56
2.1.1.4	Kv4.2	58
2.2	Cell Culture Methods	59
2.2.1	Maintenance, storage and induction of Murine erythroleukemia cells	60
2.2.1.1	Incubation media	60
2.2.1.2	Subculture of cells	61

2.2.1.3	Storage of cell stocks in liquid nitrogen	61
2.2.1.4	Induction of transfected cells	62
2.3	Electrophysiological Methods and Equipment	64
2.3.1	Micropipette fabrication	64
2.3.2	Solutions	66
2.3.2.1	External bath solutions	67
2.3.2.2	Internal bath solutions	68
2.3.3	The patch clamp set-up	70
2.3.3.1	Microscope	70
2.3.3.2	Micromanipulator	71
2.3.3.3	Air Table and Faraday cage	71
2.3.3.4	Headstage and Amplifier	73
2.3.3.5	Computer and interface	76
2.3.3.6	Oscilloscope	76
2.3.3.7	Filters	77
2.3.4	Recording using the Axopatch 200A amplifier	77
2.3.5	Data Analysis	82
2.3.5.1	Data Storage and Software	82
2.3.5.2	Leak subtraction	82
2.3.5.3	Curve fitting	83

**CHAPTER THREE: WHOLE CELL RECORDING OF VOLTAGE-ACTIVATED
DELAYED RECTIFIER POTASSIUM CURRENTS FROM Kv1.5 CHANNELS**

	85
3.1 Introduction	86
3.2 Results	88
3.2.1 The voltage dependence of Kv1.5	89
3.2.2 The reversal potential and selectivity of Kv1.5	90
3.2.3 Voltage dependence of steady-state activation for Kv1.5	97
3.2.4 Hodgkin-Huxley activation kinetics	100
3.2.5 Steady state inactivation in Kv1.5	101
3.2.6 The recovery from inactivation of Kv1.5	103
3.3 Discussion	104

**CHAPTER FOUR: WHOLE CELL RECORDING OF VOLTAGE-ACTIVATED
TRANSIENT POTASSIUM CURRENTS FROM Kv4.2 CHANNELS**

	128
4.1 Introduction	129
4.2 Results	131
4.2.1 The voltage dependence of Kv4.2	132
4.2.2 Hodgkin-Huxley parameters	133
4.2.3 Voltage-dependence of activation	135
4.2.4 Voltage-dependence of steady-state inactivation	141
4.3 Discussion	142

CHAPTER FIVE: THE EFFECT OF ShB INACTIVATING BALL PEPTIDES ON Kv1.5 AND Kv4.2 WHOLE CELL CURRENTS	161
5.1 Introduction	162
5.2 Results	165
5.2.1 The effects of ShB inactivating ball peptide on Kv1.5 currents	170
5.2.2 Voltage dependence of steady state activation of Kv1.5	171
5.2.3 Voltage dependence of steady state inactivation of Kv1.5	172
5.2.4 Recovery from inactivation	173
5.2.5 Inactive mutant variant of the ShB inactivating ball peptide	175
5.2.6 The kinetics of the block of Kv1.5 by ShB inactivating ball peptide	176
5.2.7 A mutant of the ShB inactivating ball peptide with increased positive charge	180
5.2.8 The effects of the ShB:E12K,D13K inactivating ball peptide on Kv4.2 currents	185
5.2.9 The effect of peptide on the voltage dependence of steady state activation and inactivation in Kv4.2	187
5.2.10 Hodgkin-Huxley parameters	189
5.2.11 The kinetics of the block of Kv4.2 by 200 μ M ShB:E12K,D13K inactivating ball peptide	190
5.3 Discussion	193

CHAPTER SIX: GENERAL DISCUSSION	237
REFERENCES	245

List of Figures

CHAPTER ONE

1.1	Patch Clamp configurations	9
1.2	Changes in membrane potential and ionic conductances during an action potential	13
1.3	The cardiac action potential	19
1.4	Membrane topology of voltage-activated channels	29
1.5	High conservation of potassium channel sequence identity between the same subfamily in different species compared to that between subfamilies in the same species	40

CHAPTER TWO

2.1	The patch clamp set-up	72
2.2A	The patch clamp headstage is a resistive feedback current to voltage converter	75
2.2B	Command potentials are applied to the pipette and removed from subsequent headstage recorded operational amplifier voltage output via a differential operational amplifier	75

CHAPTER THREE

3.1	Voltage dependence of Kv1.5	109
-----	-----------------------------	-----

3.2	Reversal potential and selectivity of Kv1.5	111
3.3	Selectivity of Kv1.5	113
3.4	Time constants of deactivation	115
3.5	Voltage dependence of activation for Kv1.5	117
3.6	Activation curves with increased external potassium	119
3.7	Hodgkin-Huxley activation kinetics	121
3.8	Kv1.5 Steady state inactivation	123
3.9	Steady state inactivation with increased external potassium	125
3.10	Kv1.5 Recovery from inactivation	127

CHAPTER FOUR

4.1	Current-voltage relationship for Kv4.2	148
4.2	Hodgkin-Huxley activation parameters	150
4.3	Voltage dependence of activation of Kv4.2	152
4.4	Correction of reduction in peak current due to inactivation	154
4.5	Activation curve with 70 mM K ⁺ external bath solution	156
4.6	Plots of τ_{decay} against membrane potential	158
4.7	Voltage dependence of steady state inactivation of Kv4.2	160

CHAPTER FIVE

5.1	The effect of ShakerB inactivating ball peptide on Kv1.5	202
5.2	The effect of ShakerB inactivating ball peptide illustrated using scaled current traces	204

5.3	The effect of ShakerB inactivating ball peptide on the voltage dependence of activation and inactivation of Kv1.5	206
5.4	The effect of ShakerB inactivating ball peptide on the recovery from inactivation of Kv1.5	208
5.5	The effect of the inactive ShB:L7E ball peptide illustrated using scaled currents	210
5.6	An explanation of the parameters used in the equations used to determine blocking rates etc.	212
5.7	The variation of 200 μ M ShakerB inactivating ball peptide blocking/unblocking rates, association/dissociation rate constants and equilibrium dissociation rate constants of Kv1.5 with membrane potential	214
5.8	The variation of 100 μ M ShakerB inactivating ball peptide blocking/unblocking rates, association/dissociation rate constants and equilibrium dissociation rate constants of Kv1.5 with membrane potential	216
5.9	The effect of ShB:E12K,D13K inactivating ball peptide on Kv1.5 illustrated using scaled currents	218
5.10	The variation of 100 μ M ShB:E12K,D13K inactivating ball peptide blocking/unblocking rates, association/dissociation rate constants and equilibrium dissociation rate constants of Kv1.5 with membrane potential	220
5.11	Comparison of blocking and unblocking rates, association rate constants and equilibrium dissociation rate constants for different peptides with Kv1.5 at a +60 mV pulse	222
5.12	Comparison of τ_{fast} values at +60 mV	224

5.13	The effect of 200 μ M ShB:E12K,D13K inactivating ball peptide on Kv4.2	226
5.14	The effect of ShB:E12K,D13K inactivating ball peptide on Kv4.2 illustrated using scaled currents	228
5.15	The effect of 200 μ M ShB:E12K,D13K inactivating ball peptide on the voltage dependence of activation and inactivation of Kv4.2	230
5.16	Hodgkin-Huxley activation parameters	232
5.17	The variation of 200 μ M ShB:E12K,D13K inactivating ball peptide blocking and unblocking rates of Kv4.2 with membrane potential	234
5.18	The variation of 200 μ M ShB:E12K,D13K inactivating ball peptide association/dissociation rate constants and equilibrium dissociation rate constants of Kv4.2 with membrane potential	236

List of tables

1.1a	Classification of cloned voltage-gated (Kv) members of S4 superfamily	45
1.1b	Classification of cloned S4 superfamily K ⁺ channels (non-Kv)	46
1.2	Classification of cloned Kir channels of the inward rectifier superfamily	48
2.1	Ionic composition of external bath solutions	67
2.2	Ionic composition of internal pipette solutions	68
3.1	Comparison of activation parameters of Kv1.5 with previous studies	105
4.1	Comparison of activation parameters of Kv4.2 with previous studies	143
4.2	Comparison of inactivation parameters of Kv4.2 with previous studies	144
5.1	Amino acid sequence and net charges of the <i>Shaker</i> B derived synthetic ball peptides	166

Acknowledgements

ALHUMDU LILLAHI RABILAL AMEEN

I would like to give my eternal thanks to my family for their love, support and encouragement throughout my studies. I extend this to all my relatives and friends.

I am extremely grateful to my supervisors, Professor Nick Standen and Dr. Noel Davies for their invaluable guidance, support, kindness and above all, patience. Thank you for dragging this thesis out of me. I thank Hafeez Mohammed, Dr. Amar Hanif and Dr. Aziz Asghar for assistance with proof-reading and Haji Fiaz Ali Raja for his tremendous help in the lapidation of the Jamra-i-Aqaba.

I am very lucky to have worked with some extremely friendly, supportive, fun people. Thank you to all my colleagues (past) in the Ion Channel Group in the Department of Cell Physiology and Pharmacology, University of Leicester, and to my colleagues (present) in the Department of Physiology at the University of Leeds.

Finally, I would like to thank anyone that is not mentioned by name that assisted me in my research and in my daily life.

بِسْمِ اللَّهِ الرَّحْمَنِ الرَّحِيمِ

CHAPTER ONE

General Introduction

Ion channels represent a diverse group of selective pore-forming proteins found in, and functioning as the elementary excitable elements of the plasma membranes of most eukaryotic cells. The remarkable ubiquity of potassium channels is matched to their diversity of function.

Cell membranes consist of phospholipids, cholesterol and other lipids arranged in a double layer, with the hydrophobic portions facing one another in the interior of the membrane, and the hydrophilic portions on the external and internal surfaces of the membrane. Proteins are incorporated into the membrane. Some proteins are attached to the inner or outer surface of the cell membrane and others penetrate all the way through the membrane so that they form a bridge from one side to the other. The membrane is selectively permeable to solutes, thus the watery interior of the cell is protected from its extracellular surroundings, and the transport of specific substances can be controlled. Essential molecules such as carbohydrates, amino acids and lipids can enter and stay in the cell, and waste products are transported out of the cell. Chemical communication with the cell occurs through the transduction of the message of signalling molecules through the membrane. Hormones for example are recognised by specific sites on receptor proteins in the membrane that recognise and selectively bind the hormone at high affinity, and pass on the message of the hormone into the cell.

Uncharged molecules pass through the cell membrane quite easily, because they can pass through the hydrophobic phase; charged ions require transport proteins in order to pass through. There are two sorts of transport proteins, channels and carriers.

Some of the transmembrane proteins form the aqueous pores, or channels, that allow ions and other small hydrophilic molecules to cross the membrane. The regulated passage through the membrane of electrically charged ions such as sodium, calcium, potassium and chloride occurs through protein channels specific for the ion. In addition to ionic channels, mechanisms exist for active ion transport by membrane-bound carriers utilising energy in the form of the hydrolysis of adenosine triphosphate (ATP), either directly or indirectly. These include the Na^+ / K^+ -ATPase pump transporting sodium out, and potassium into the cell, as mentioned above (three sodium ions leave the cell and two potassium ions enter for every ATP molecule that is broken down); the Ca^{2+} -ATPase pump transporting calcium ions out of the cell, or from the cytoplasm to the sarcoplasmic reticulum; and the proton pump for H^+ ions. The rates of transport of these ions by these mechanisms are much lower than that for passage through ion channels since the carrier must change conformation for each ion transported. There are also secondary active co-transporters that use the Na^+ gradient, which in turn is maintained by the primary active Na^+ / K^+ -ATPase pump.

In this way, the cell maintains concentration gradients for ions across the membrane. The passive transport of ions through ion channels occurs down an electrochemical gradient. The electrochemical gradient for each ion is a combination of the electrical potential difference between the cytoplasm and the extracellular tissue fluid and the concentration gradient for the ion. The conductance of the membrane for these ions can be varied via the opening or closing of the channels by a gating mechanism which allows ions to enter or exit from the cell, and the gate can only be open or closed. Each individual channel gate is independent of the others, responding to regulation by either electrochemical

gradient or chemical (for example hormonal) messenger in a statistical manner.

Channel gating is of a random, chance nature, and the mean number of open gates and thus open channels can be predicted, but one cannot say which individual channels will be open. Channel selectivity ensures permeability to certain particular ions or ion types. Some channels are highly selective for potassium, sodium, calcium or chloride ions for example, with measurements of selectivity showing that in the order of less than one in a thousand 'undesired' ion gets through. Other channels are less selective, allowing through all cations for example.

At rest, the inside of the cell is always negative with respect to the outside. There is a much higher relative permeability to potassium ions compared to sodium ions, and there are energy-expending metabolic processes actively pumping sodium ions out of the cell, and potassium ions in, thereby causing the concentration of sodium ions outside the cell to exceed that inside the cell. There is a lower concentration of potassium ions outside the cell compared to the inside; the concentration gradient, which would tend to drive the potassium ions out of the cell is matched by the potential gradient attempting to drive them in. Because of the selective permeability to potassium, this sets up a resting membrane potential.

1.1 Ionic channels

Each ionic channel can be regarded as a macromolecule that responds, individually and specifically to a certain stimulus, for example, membrane potential changes in the case of voltage-activated channels.

As mentioned above, gating, the response of an ion channel to a stimulus, appears to be a simple opening or closing of the pore, regulating the flux of up to 10^7 ions per second, flowing through the open pore typically for milliseconds. Selective permeability restricts the passage of ions through the open pore with remarkable discrimination, allowing the chosen ions to flow passively down their electrochemical gradients.

The functions of ionic channels include setting the resting membrane potentials (and therefore regulating the electrical excitability of the cell), producing action potentials and modulating action potential frequencies. Signals or electrical information are transduced by, for example, the gating of the flow of Ca^{2+} ions, initiating calcium regulated cellular responses. This can cause, for instance neurotransmitter release and hormonal secretion. Ion channels can control the volume of the cell, regulating the net flow of ions across epithelial cells of secretory and resorptive tissues. They are also known to function in cellular mechanisms of learning and memory (Rudy, 1988; Hille, 1992; Salkoff, Baker, Butler, Covarrubias, Pak, and Wei, 1992; Stühmer, Ruppersberg, Schröter, Sakmann, Stocker, Giese, Perschke, Baumann and Pongs, 1989).

1.2 The patch clamp technique

The study of ion channels was greatly enhanced by the development of the patch clamp technique by Erwin Neher and Bert Sakmann (1976), with refinements of the technique detailed in a further paper in 1981 (Hamill, Marty, Neher, Sakmann and Sigworth) which has proved to be seminal. This technique enabled the currents passing through individual ion channels to be resolved and measured for the first time, overcoming previously unfavourable levels of background noise. Dynamic molecular mechanisms were revealed, whereas previously the classic work on the membrane ionic theory of excitation carried out by workers such as Hodgkin and Huxley from the 1950s onwards was at a macroscopic level. Thus, the activity of single macromolecules could be observed. A tremendous explosion of work has resulted from these advancements in electrophysiological methods.

The patch clamp technique allows the current through individual channels to be measured directly from a small patch of voltage clamped membrane. This portion of membrane, typically 5 - 20 μm^2 in area, is electrically isolated by a mechanically stable, high resistance seal, typically in the order of tens of gigaohms ($10^9 \Omega$), formed between the small diameter tip (in the order of 1 micron) of a heat polished glass pipette and the cell membrane. The glass pipette is connected to an amplifier, which allows the voltage of the patch of membrane to be controlled, and the tiny membrane currents flowing through the patch to be measured. Sakmann, Neher and colleagues found that the application of slight suction through the pipette, and optimising the shape and size of the pipette, as well as cleaning the cell surface (for example, using collagenase to remove connective tissue and extracellular

matrix) all helped in the formation of high quality seals. The glass pipette is itself non-conductive. It is important to ensure that there is no leak of current between the interior of the pipette and the extracellular fluid. Due to the high resistance of the seal, currents flowing through the patch of membrane inside the seal flow into the pipette and then into the current measurement circuitry of the amplifier.

Unitary membrane currents can be typically in the order of picoamps, (10^{-12} A), so the great problem was of resolving these currents from the background noise associated with the membrane, pipette and recording electronics. Some of this noise is the result of random (Brownian) thermal movements of electrons and causes spontaneous fluctuations in baseline current in the absence of any detectable signal - these could be 100 times greater than the size of the signal, thus drowning it out. The seal formed between the glass pipette and the membrane needs to be in the order of gigaohms because a high resistance seal minimises the noise. The variance of the current noise, σ^2 (units in A^2) through a resistor is related to the Johnson voltage noise (or thermal noise) due to the resistance R (Ω), by:

$$\sigma^2 = \frac{4kTB}{R}$$

(Equation 1.1)

where k is Boltzmann's constant ($1.381 \times 10^{-23} \text{ J K}^{-1}$), T is the absolute temperature in Kelvins ($K = ^\circ\text{C} + 273$) and B is the bandwidth of the current recording (also equal to the low pass filter frequency) in Hz. A higher seal resistance decreases the value of σ^2 , with a resistance of $10 \text{ G}\Omega$ at $20 \text{ }^\circ\text{C}$ at a bandwidth of 1 kHz giving a value of 0.04 pA for σ (standard deviation of current noise) compared to a value of

0.4 pA for a resistance of 100 M Ω . A higher seal resistance also means that less of the current flowing through the membrane patch will be lost through the seal to the extracellular fluid. Thus electrical isolation of the membrane patch is improved.

1.2.1 Patch clamp configurations

Once the gigaohm seal (or ‘gigaseal’) has formed, it is mechanically stable as well as electrically. From this ‘*cell-attached*’ configuration, with which Neher and Sakmann first made recordings from the nicotinic acetylcholine receptor activated channel in frog skeletal muscle, various other patch clamp configurations can be set up. These are shown in Figure 1.1 below.

The clamped membrane patch can be ruptured, giving direct low resistance access to the cytoplasm of the cell without breaking the seal between the pipette and cell membrane. This allows the exchange of materials between the interior of the cell and the contents of the pipette, for example. This is known as the ‘*whole-cell*’ configuration of recording. The patch pipette is thus able to record voltage or current changes from the whole of the cell membrane since it is in contact with the interior of the cell, but the noise level of this recording set-up does not allow single channel currents to be resolvable.

Alternatively, cell-free membrane patches (either ‘*inside-out*’ or ‘*outside-out*’) can be formed, retaining the high resistance seal between the pipette and membrane. From the cell-attached configuration, the pipette is withdrawn from the cell surface after a seal has formed, causing a membrane vesicle to occlude the tip.

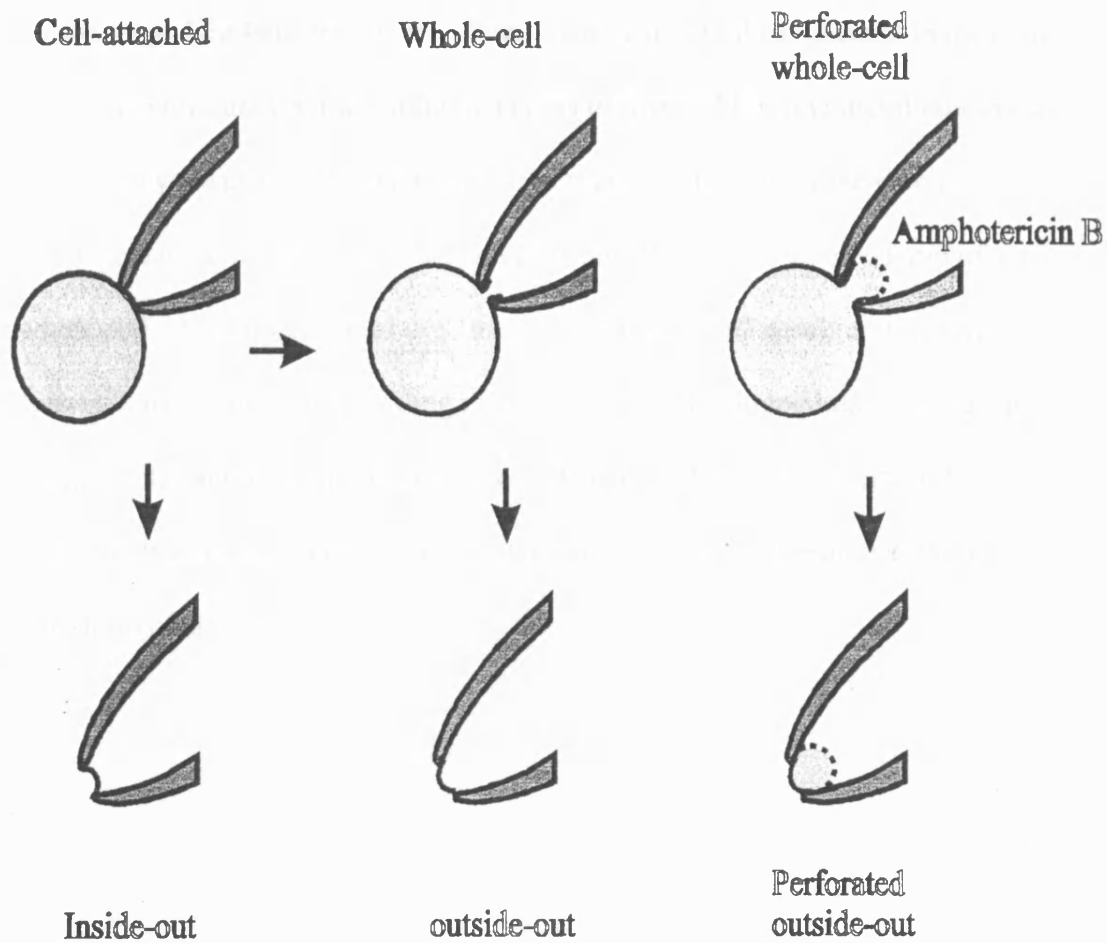


FIGURE 1.1: Patch Clamp configurations.

This vesicle disrupts on exposure to air to give an inside-out patch. An outside-out patch can be formed by withdrawing the pipette during the whole-cell configuration. Cell-free membrane patch configurations allow single-channel recordings, control of the potential across the membrane and exposure of either face of the membrane to solution changes during the course of electrophysiological measurements.

An alternative configuration for making whole cell recordings involves the use of a pore-forming polyene antibiotic such as Amphotericin B in the patch electrode solution. Amphotericin B makes pores in the membrane of diameter 0.8

nm (Holz and Finkelstein, 1970). After the gigaohm seal has formed in the cell-attached configuration, the antibiotic begins to permeabilise the membrane patch enclosed by the electrode. After about ten minutes, the membrane patch is permeable to monovalent ions, allowing current flow, and voltage clamp of the whole cell. The advantage of this '*perforated whole cell*' configuration over conventional whole cell recording is that most soluble intracellular cytoplasmic components cannot escape from the cell. This is particularly important, for example, where second messenger systems are involved in the activation or inhibition of currents.

1.3 Voltage-activated potassium channels

Potassium channels form the most extensive and diverse group of voltage-gated ion channels. The negative equilibrium potential for potassium ions under physiological conditions leads to potassium channels tending to dampen excitation. The equilibrium potential is that membrane potential at which there is no net flow of ions through the channel, that is, the electrochemical forces are in balance. For potassium ions, the equilibrium potential, E_K , is given by the Nernst equation, where:

$$E_K = \frac{RT}{zF} \ln \frac{[K^+]_o}{[K^+]_i}$$

(Equation 1.2)

where E_K is expressed in mV; R is the gas constant ($8.315 \text{ J K}^{-1} \text{ mol}^{-1}$); T is the absolute temperature in Kelvins ($K = ^\circ\text{C} + 273$); F is Faraday's constant, the quantity of charge carried by one mole of single charged ions ($9.648 \times 10^4 \text{ C mol}^{-1}$); z is the valency of potassium ions (+1); and $[K^+]_o$ and $[K^+]_i$ represent the concentrations of potassium ions outside and inside the cell respectively.

A simple generalisation is that potassium channels provide the outward current that sodium and calcium currents must overcome to depolarise the membrane. Because the potassium equilibrium potential is normally negative to the resting membrane potential, an increase in potassium conductance leads to hyperpolarisation of the membrane, moving the potential of the membrane away from the threshold level which needs to be reached in order to generate an action

potential (see below). However, this simplification does not allude to the 'anomalous' inward rectification role of an important family of potassium channels.

The variety of potassium channel types display a diversity of biophysical properties, with each cell type genetically programmed to suit its special purpose by selecting required channels. This is customisation to fill a specialised role. The very large number of different potassium channels compared to for example, calcium channels, indicates that different tissues or organs achieve their diverse and characteristic electrical activity using different complements of these potassium channels. This can be seen in cardiac muscle, skeletal muscle, smooth muscle, neurones, pancreatic cells and so on.

1.3.1 The action potential

Action potentials occur in response to sufficiently strong stimuli in nerve and muscle cells, which are said to be excitable. Sodium channels are activated when a stimulus depolarises the resting membrane potential beyond a critical threshold potential, and the membrane transiently becomes more permeable to sodium ions. This increase in sodium conductance causes a large influx of positively charged sodium ions into the cell, and as the cell membrane depolarises further, even more sodium channels open. However, inactivation of the sodium channels also begins very quickly, and sodium conductance decreases, along with a slow and sustained rise in potassium conductance, as potassium channels open. This has the effect of re-establishing the negative resting potential of the cell, as positively charged potassium ions leave the cell.

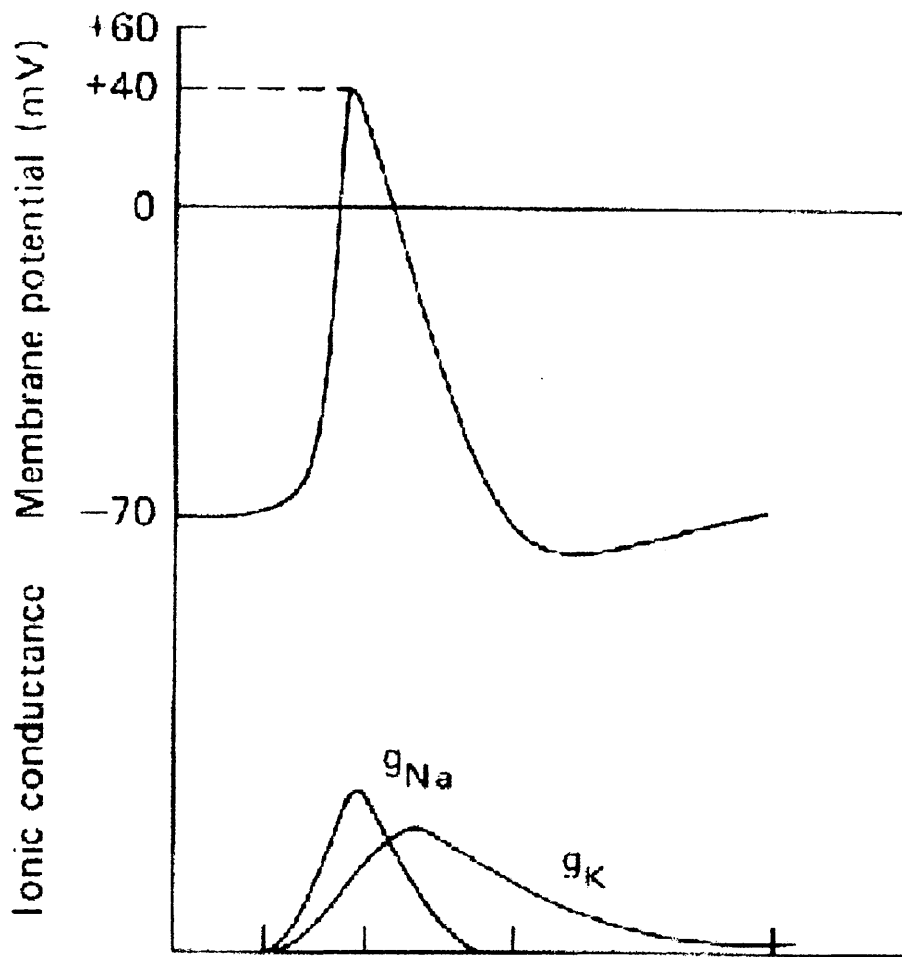


FIGURE 1.2 Changes in membrane potential and ionic conductances during an action potential (in a squid giant axon). g_{Na} and g_K represent sodium and potassium conductances. From Keynes and Aidley (1991).

1.3.1.1 The Hodgkin-Huxley Model

Hodgkin and Huxley described the action potential in squid axon in these terms using the voltage clamp technique to measure ionic currents flowing across the membrane in response to changes in membrane potential. The giant squid axon is up to 1mm in diameter, allowing the potential inside to be measured and controlled with wire electrodes placed inside the axon. Analysis of these currents allowed Hodgkin and Huxley to derive equations to describe the voltage dependence of the potassium and sodium conductances, and the time course of the changes of these in response to controlled changes in the membrane potential. As a kinetic description, this model still stands up today in the face of ever more sophisticated techniques used to evaluate how the kinetics of measured behaviour agree with the putative structure of these channels.

The Hodgkin and Huxley model provided a description for nerve impulses in terms of the movements of potassium and sodium ions through the membranes of nerve axons. Channel gating was described in terms of electrically charged gating particles which are free to move within the plasma membrane in response to step changes in the membrane potential; when particular binding sites associated with the opening of the channel are occupied by the gating charges, the channel opens, and allows ions to pass through. Some part of the channel structure detects the change in the electric field. The opening and closing of these channels is voltage and time dependent.

Using the voltage clamp technique, Hodgkin and Huxley (1952) were able to clamp the membrane potential of squid axons, and determined that upon depolarisation there was a fast inward sodium current passing through voltage-gated sodium channels, followed by a longer lasting potassium current passing through voltage-gated potassium channels. The sodium and potassium currents were separated by manipulating the sodium content of the recording solutions to allow recording at a potential when no sodium current flowed, leaving just potassium current. Subtracting the potassium current trace from that representing sodium and potassium gave the isolated sodium current. The relationship between the conductances of these ions and the membrane potential was determined by altering the clamped potentials, and this led to deduction of the nature and time course of the conductances of the action potential. The sodium conductance forms the upstroke of the action potential as many sodium channels open, and then they begin to close or become inactivated. The potassium channels open after a delay compared to sodium channels, and the potassium conductance rises; there is now significant current flow out of the axon, in a direction opposite to that of the earlier sodium current. This potassium channel displays no voltage sensitive inactivation over the time scale of the action potential, and the channel continues to conduct potassium ions out of the cell, until the membrane potential is brought back towards its resting level.

The activation of this potassium channel in response to depolarisation sets up a self-shutting negative feedback loop. The depolarisation, which activates the channel causing positively charged potassium ions to flow out of the cell, is thus opposed. In the absence of inactivation of the sodium channel and activation of the

potassium channel, a positive feedback loop that causes in rushing sodium ions would cause the depolarisation to persist.

There are various characteristics of the triggering of action potentials that are concerned with changes in the permeability of membranes to ions. The resting potential is not a sharp cut-off point for activation of channel activity; a threshold level of depolarisation has to be reached for the action potential to be triggered. If the threshold level is not reached, there is no action potential. Once triggered, the action potential is 'all-or-none', the amplitude of the action potential is fixed, and is independent of the strength of the stimulus setting it off so long as it has reached the threshold level. After an excitable cell has generated an action potential, there is an absolute refractory period during which another action potential cannot be triggered. This absolute refractory period therefore sets the rate at which the excitable cell can generate action potentials. Following this absolute refractory period, there is a period during which it is possible to elicit a second action potential, but the threshold stimulus intensity is higher than usual. This period, the relative refractory period, corresponds to a period when the sodium channels have recovered from inactivation, but the potassium current is still high.

From these characteristics, it can be seen that in, for example, the nervous system, it is the control of the frequency of the action potential discharges that is important, since other factors such as amplitude of the action potential are fixed.

The potassium channel described in the squid giant axon by Hodgkin and Huxley, as mentioned above, contributed to the repolarising phase of the neuronal action potential. This channel persisted in the open state without inactivating while depolarisation lasted, and because of the delayed nature of its activation compared to the activation and initiation of inactivation of the sodium channel, it became known

as a delayed rectifier (the current-voltage relationship shows rectification, see Chapter 3). The action of tetraethylammonium (TEA) ions reduces this current and causes the action potential to be prolonged (Hille, 1967).

A second type of potassium channel, first described in molluscan neurones by Connor and Stevens (1971) was the transient outward (or A-current). This channel actually underwent inactivation as opposed to the delayed rectifier, which did not to any great degree. At membrane potentials more positive to -50 mV, the transient outward potassium channel exhibited almost complete steady state inactivation. This meant that it could not be activated by depolarising stimuli unless from more hyperpolarised potentials. This characteristic allows the channel to be involved in regulating the interspike interval and thus action potential firing frequency, since the inactivated state would need to be reversed before activation due to a depolarising stimuli could occur. This current is blocked by 4-aminopyridine, leading to uncontrolled repetitive firing.

Other types of neuronal potassium channels include the calcium-dependent channels, with either high conductance, (BK_{Ca}) or small conductance. BK_{Ca} seems to contribute to the repolarisation of the action potential (Adams, Constanti, Brown and Clark, 1982). Receptor-coupled potassium channels can be opened by the action of specific neurotransmitters activating several different receptor types (for example 5-HT, γ -aminobutyric acid (GABA) or adenosine receptors). Alternatively, calcium-activated potassium channels may be closed by the activation of a separate set of receptors. The M current, a slowly inactivating non-inactivating voltage-dependent potassium current first discovered in frog sympathetic neurons (Brown and Adams, 1980) is turned off by muscarinic receptor agonists in these cells. In hippocampal neurons, the M-current is inhibited by muscarinic agonists (Halliwell

and Adams, 1982) and serotonin (Colino and Halliwell, 1987) and is activated by somatostatin (Moore, Madamba, Joels and Siggins, 1988).

1.3.1.2 The cardiac action potential

In nerves and skeletal muscle, action potentials are of short duration, with cells depolarising and repolarising typically in the order of milliseconds. However the cardiac action potential lasts for hundred of milliseconds. It is this regenerative cardiac action potential that propagates through the heart and initiates cardiac contraction.

In heart cells, potassium channel currents are important in maintaining the normal cell resting potential, and controlling the duration of the action potential. The physiological function of the heart by the propagation of the action potential through the body of the heart requires a complex pattern of electrical activity in the different types of cardiac cells, for example, there are differing resting potentials. These differences in resting potentials can affect the number of available channels and thus conduction velocity through the heart. These variations in electrical activity are due to the variation in ion channel distribution, a reflection of the biophysical characteristics of the cells in each region.

Cardiac potassium channels are a very diverse group. They include voltage-activated delayed rectifiers, inward rectifiers and transient-outward (or A-type) potassium channels (all discussed in greater detail below). Both Kv1.5 (delayed rectifier) and Kv4.2 (transient-outward), the potassium channels studied in this project are found in the heart. There are ligand-gated potassium channels such as

the acetylcholine activated muscarinic potassium channel, the adenosine-triphosphate (ATP) sensitive potassium channel, the intracellular sodium activated potassium channel, and the calcium activated potassium channel. Amongst others, there are stretch-activated potassium channels in the heart. A list of all presently known vertebrate cardiac ionic currents has been compiled by Boyett, Harrison, Janvier, McMorn, Owen and Shui (1996).

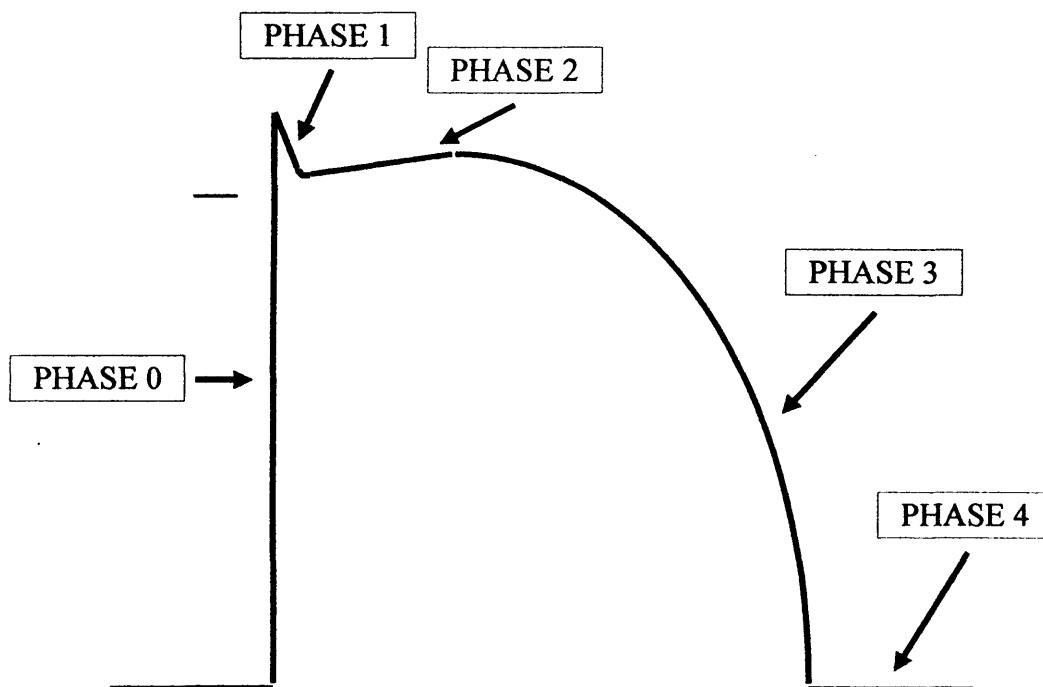


FIGURE 1.3 The cardiac action potential

The cardiac action potential varies in characteristics such as duration and shape between the different regions of the heart, and can include at least five distinct phases, termed phase 0 through to phase 4 as shown in Figure 1.3 above, which is a composite schematic picture, not necessarily representing the activity in each part of the heart (Deal, England, and Tamkun, 1996).

Phase 0 is the equivalent of the upstroke in the action potential found in most excitable cells, caused by the rapid influx of sodium ions through voltage-activated sodium channels; this influx of sodium ions lasts for 1 - 2 ms, because as the membrane depolarises, the channel inactivates. Once these channels are inactivated, they cannot open again until the inactivation is reversed by the membrane repolarising to the resting membrane potential. Thus, the cell is unable to respond to a further stimulus that would again normally trigger an action potential.

During Phase 1, there is an incomplete, rapid repolarisation phase achieved by the activation of a transient outward potassium current. This current is important in setting the initial plateau level, hence the membrane potential of this plateau influences the behaviour of subsequently activated channels, and the duration of the action potential. It can be seen that, although the activation of the transient outward potassium current is rapid in response to the depolarisation, from its slope it is not as rapid as the sodium current. This channel inactivates quite rapidly, thus setting the level of the plateau.

Phase 2 is the plateau of the cardiac action potential, which is responsible for the length of the action potential. There is minimal net flow of current due to a balance of an inactivating inward calcium current, and a slowly activating outward voltage-activated potassium current. This potassium current is a delayed rectifier, with a slower time course of activation in response to the depolarisation, and does not undergo inactivation over this period of time, as seen in the transient outward potassium current. The membrane potential can remain at this relatively depolarised plateau level for several hundred milliseconds, and it is the delayed rectifier which is responsible for ending the plateau phase, and repolarising the cell back towards the resting membrane potential.

In phase 3, the permeability of the membrane to K^+ ions increases rapidly with time, and the sodium and calcium channels are all inactivated. The resulting repolarisation activates inwardly rectifying potassium channels that open at relatively negative potentials. Inward rectification means that the channel passes inward current more easily than outward current, and conductance increases with increasing hyperpolarisation. The low conductance at potentials positive to E_K appears to be due to a voltage dependent block by intracellular polyamines and Mg^{2+} ions (Matsuda, Saigusa and Irisawa, 1987; Fakler, Brandle, Bond, Glowatzki, Konig, Adelman, Zenner and Ruppertsberg, 1994; Ficker, Tagliatela, Wible, Henley and Brown, 1994; Stanfield, Davies, Shelton, Khan, Brammar, Standen and Conley, 1994). The gating of inward rectifiers depends upon the external potassium concentration. Changes of external potassium alters both the reversal potential and the voltage dependence of channel gating.

The inward rectifiers regulate the resting membrane potential, maintaining it at quite a negative level close to the potassium equilibrium potential, whereas the voltage-activated outward potassium channels control the action potential duration. The long depolarisation during the plateau phase is possible because the large resting currents through inwardly rectifying channels are shut off at depolarised membrane potentials during the action potential. If the current through the inward rectifiers still flowed at depolarised potentials, then it would be antagonistic to the balance between the delayed rectifier potassium channel and the inward voltage-activated calcium channel, altering the overall minimal net flow of current during the plateau phase. A type of 'metabolic economy' is thus achieved by the inward rectifiers being closed at these membrane potentials.

Phase 4 represents the resting state, the time period between action potentials. The inward rectifier potassium channels help to stabilise the resting membrane potential of the cell by opposing depolarisation. Here, small amounts of outward current is passed in the voltage range a few millivolts positive to the potassium equilibrium potential, maintaining the resting membrane potential close to it.

There are also other currents involved in the cardiac action potential, mentioned briefly above. These include the current through the inwardly rectifying muscarinic potassium channel, which is responsible for the negative inotropic and chronotropic effects seen with vagal stimulation and the ATP-sensitive potassium channel. However, since these are not strictly voltage-activated potassium channels, they are not mentioned here in any depth.

It must also be remembered that the above is a composite picture of the cardiac action potential, all phases not necessarily occurring in all parts of the heart, and in all species.

To conclude, the roles of all types of voltage-activated potassium channels are related to stabilisation of the membrane potential, bringing it closer to the potassium equilibrium potential and away from the firing threshold. They set the resting potential, keeping fast action potentials short, and modulate the frequency during bursts of action potentials.

The different voltage-activated potassium channel types are distinguished and defined by their characteristic activation in response to changes to the membrane potential, and the time courses of these responses with regard to gating, inactivation etc. The currents passing through these channels can be categorised as

delayed rectifiers, fast transient (or A-type) and inward rectifiers. However, within the categories for delayed rectifier and fast transient potassium channel currents, there exist wide ranges of these biophysical properties (that is to say, ranges of potential for channel conduction, activation / inactivation time constants etc.) such that overlap may occur. It can be argued that there is a spectrum of voltage-activated potassium channels, ranging from delayed rectifier like to fast transient like, belonging to the same superfamily of ion channels (Hille, 1992; Jan and Jan, 1992).

1.4 Potassium channel gene cloning

Genetic information is stored in the form of double-stranded deoxyribonucleic acid (DNA) in the nucleus of every cell, specifying the construction of every protein in the organism. The sequence of nucleotides of DNA contains the information determining the sequence of amino acids in the resultant polypeptide chain. A gene is a portion of DNA that codes for a single polypeptide sequence enabling an appropriate number of amino acids in the production of a particular protein. These coding sequences, called exons, are interrupted at various positions by non-coding intervening sequences, or introns.

Genetic information stored in the nucleus in the form of DNA is transcribed in the cytoplasm to synthesise proteins using messenger ribonucleic acid (mRNA) as a template. Initially, each strand of DNA, containing introns and exons is transcribed, the formation of mRNA being controlled by a polymerase, which is normally prevented from acting by a repressor protein on the DNA and is activated when the repressor is removed (derepression). Selected introns can be excised out,

the exons spliced together and some processes of modification of termini occur before leaving the nucleus. This is known as post-transcriptional modification. When mRNA migrates into the cytoplasm, ribosomes, which will carry and facilitate the growing peptide, become attached to the mRNA. In the process called translation, amino acids carried to the ribosomes by transfer RNA (tRNA) are assembled into a polypeptide chain as the ribosomes move along the length of the mRNA. The mRNA contains initiation and termination signals, and the exact coding sequence for the order of the amino acids to be assembled in the polypeptide chain to form the protein. Post-translational modification, the last step, involves the cleavage of bonds within the new protein, modification of certain amino acids in the chain (for example by glycosylation or phosphorylation) and the folding of the protein into its characteristic configuration or tertiary structure. The completed protein is then delivered to its site of action, for example, ion channel proteins are inserted into the membrane of the cell, with their appropriate subunit configurations and receptor linkages etc.

The analysis of the detailed structure and function of genes has been made possible by the great advances in recombinant DNA technology. The study of ion channels has particularly benefited from this. The understanding of the effects of the alteration or mutation of a single gene could be seen clearly in the phenotype of the *Shaker* mutants of the *Drosophila* fruit fly, that is to say that using a combination of molecular biology and electrophysiology, this alteration could be traced in the changes to the resulting ionic currents. This principle led to extensive further research, especially with the advances in molecular biology approaches such as expression cloning and genome sequencing.

Recombinant DNA technology and gene mapping have made it possible to analyse genes and their mRNA and to define defects at a molecular level. The gene can be isolated and incorporated into a suitable vector allowing the introduction of the gene into other organisms, such as bacteria or eukaryotic cells. Cloning produces multiple copies of the gene, and various strategies exist for subsequent selection and harvesting. The primary or amino acid sequence can be determined for positive identification of the gene.

Gene probes can be used to identify the presence of a particular gene due to the simple result of the property of hybridisation whereby strands of DNA will associate and stick together (hydrogen bonds) if their base sequences are complementary. Gene probes therefore utilise DNA with a base sequence that is complementary to that of the gene. This cDNA can be synthesised by the enzyme reverse transcriptase when mixed with any purified mRNA isolated from cells or tissues, and cloned or inserted into vectors such as bacterial plasmids for the purpose of purification and amplification. Plasmids consist of a circular ring of DNA into which a foreign DNA can be inserted after cleaving to a linear structure using specific bacterial enzymes called restriction endonucleases, which act, at specific sites. The foreign DNA is broken up using these restriction enzymes and mixed with the plasmids together with ligase enzymes to seal the gaps. As a result, a proportion of the plasmids now contain the foreign DNA and reform back into their initial circular shape. These plasmids can be introduced into a suitable host bacterium (for example *Escherichia coli*), and through the use of selection techniques such as the conferment of antibiotic resistance, large quantities can be grown to produce the required DNA. Hybridisation is used again to screen for particular clones containing the inserted DNA.

Many gene libraries have been constructed, consisting of cloned DNA fragments of known sequence growing in suitable hosts such as *Escherichia coli*. Gene libraries allow the production of gene probes, and the easier identification of genes by comparison with already known amino acid sequences.

1.4.1 The role of *Drosophila melanogaster*

Shaker mutants of the *Drosophila* fruit fly were found to shake their legs under ether anaesthesia, and other abnormalities of behaviour were found, for example, wing scissoring even during consciousness. The larvae of the *Shaker* mutant showed an abnormally prolonged release of neurotransmitter at the neuromuscular junction, leading Jan, Jan and Dennis (1977) to propose that the pathology of this mutant might involve defective potassium channels in the nerve terminal membrane. Alterations in the duration of action potentials can cause large variations in the amount of neurotransmitter released at the neuromuscular junction.

It was subsequently shown that abnormal potassium conductances caused the *Shaker* mutant to show abnormally long delays in repolarisation of nerve terminals. The potassium channel blocker 4-aminopyridine (4-AP) was able to mimic the *Shaker* phenotype in normal fruit flies (Tanouye, Ferrus and Fujita, 1981). In addition, the fast transient potassium channel, I_A , was found, by voltage-clamp analysis, to be selectively affected by all the *Shaker* mutations which did not affect any other ionic currents (Salkoff, 1983). The resulting phenotypes from these mutations vary from those completely lacking I_A to those with reduced levels. One mutant, designated *Sh*⁵, showed alterations in kinetic and voltage sensitivity properties suggesting a subtle change in the structure of the channel.

All this evidence, arising from the specific linkage of various phenotypic defects due to mutations of the *Shaker* locus to a single class of ion channel, offered the idea that the *Shaker* gene encodes a structural component of the fast transient potassium channel, I_A . However, the characterisation of the potassium channel was difficult to prove because there were at the time no antibodies or high affinity ligands for biochemical purification. The strategies employed by Noda and associates (1982; 1984; 1986) to sequence the sodium channel and the nicotinic acetylcholine receptor (AChR) were not then applicable to genes encoding potassium channels, since channel proteins needed to be purified and characterised before the genes could be isolated. Partial amino acid sequences of the sodium channel and the subunits of the acetylcholine receptor were used to design oligonucleotide probes in order to find the corresponding cDNA clones.

The technique of chromosomal walking (Papazian, Schwarz, Tempel, Jan and Jan, 1987; Kamb, Iverson and Tanouye, 1987) allowed the *Shaker* gene to be precisely located by mapping with cloned genomic DNA (containing introns) isolated from regions containing physical markers, for example point mutations, deletions (bases lost from the DNA) or translocations (where there is rearrangement within a chromosome, or transfer between non-homologous chromosomes). In this way, genomic DNA was used to identify transcripts on RNA blots, or as a probe to isolate or 'fish out' cDNA clones from a mRNA library to identify coding regions. Repeated cloning of overlapping genomic DNA fragments in a library is equivalent to 'walking' along the chromosome. Thus, genomic DNA was isolated from the *Shaker* locus, alterations in the DNA of mutants were mapped and cDNA clones from the region characterised.

The discovery of the nucleotide sequences of two cDNA clones from the *Shaker* locus, ShA1 and ShA2 (Tempel, Papazian, Schwarz, Jan and Jan, 1987) provided more evidence to support the hypothesis that DNA from the *Shaker* locus did actually encode for a potassium channel. The *Shaker* protein product predicted from conceptual translation of the cDNA sequences contained a region homologous to vertebrate voltage-dependent sodium channels, in particular, the presumed voltage-sensing S4 region (see below). Hydropathy analysis implied that the protein had a hydrophobic core and six membrane spanning domains flanked at amino (N) and carboxyl (C) terminal ends by hydrophilic ends, presumed to be cytoplasmic. These results, allied to the precise isolation, localisation and characterisation of the cDNA to the *Shaker* locus by the same group, supported the hypothesis that *Shaker* encodes for a structural component of the fast transient potassium channel.

This was confirmed when *Xenopus oocytes* injected with the mRNA *in vitro* transcribed from ShA1 and another clone, ShB1, passed transient outward potassium currents under voltage clamp. These currents had similar ion selectivities, kinetic properties and pharmacological sensitivities to the A-current in *Drosophila* muscle (Timpe, Schwarz, Tempel, Papazian, Jan and Jan, 1988).

1.4.2 Molecular structure and function of voltage-activated potassium channels

Studies of voltage-activated potassium channels using various cloned cDNAs and genomic DNAs in expression systems have made it possible to relate certain structures within the polypeptide sequence to certain functions. Channel protein sequencing, plus other studies such as hydropathy plots (where the

distribution of amino acids between the membrane and aqueous phases on the basis of chemical nature is studied) have shown that voltage-gated potassium, calcium and sodium channels have structural similarities. The *Shaker* channel peptide is highly homologous to a single domain that is repeated four times in the formation of both the α -subunit of the sodium channel (Noda, Shimizu, Tanabe, Takai, Kayano, Ikeda, Takahashi, Nakayama, Kanaoka, Minamino, Kanagawa, Matsuo, Raftery, Hirose, Inayama, Hayashida, Miyata and Numa, 1984) and the α_1 -subunit of calcium channels (Tanabe, Takashima, Mikami, Flockerzi, Takahashi, Kangawa, Kojima, Matsuo, Hirose and Numa, 1987). This is shown in Figure 1.4 below.

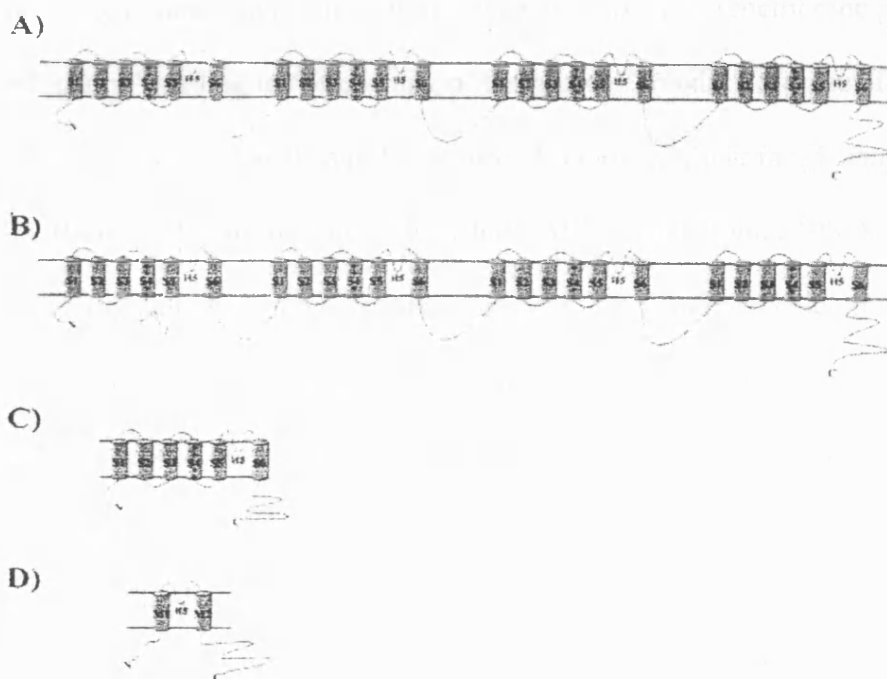


FIGURE 1.4 Membrane topology of voltage-activated channels: A) Na^+ channel, B) Ca^{2+} channel, C) K^+ channel and D) inward rectifier K^+ channel.

1.4.2.1 Transmembrane domains and voltage sensor

Each domain of the sodium and calcium channels, and the cDNA product from *Shaker*, consists of six hydrophobic segments each about 20 amino acids long, termed S1 to S6. These are bordered by hydrophilic (and therefore likely to be non-membrane) amino and carboxyl terminal sequences facing the cytoplasmic side, and varying greatly in length. The S1-S6 segments are capable of forming α -helices which could span the membrane. In each case, a pattern of five positively charged amino acids, either arginine or lysine, spaced three residues (i.e. every third residue is positive) apart in a S4 segment is consistent with a voltage sensor that could move within the membrane electric field in response to a change in membrane potential, a form of 'gating' leading to the opening of the channel (Noda, Shimizu, Tanabe, Takai, Kayano, Ikeda, Takahashi, Nakayama, Kanaoka, Minamino, Kanagawa, Matsuo, Raftery, Hirose, Inayama, Hayashida, Miyata and Numa, 1984). This net positive charge in this region is highly conserved, even amongst calcium and sodium channels, implying a common gating mechanism amongst the channels. The S4 segment is proposed to span the membrane, within the channel protein, and its involvement in the mechanism of voltage sensing was first shown in the sodium channel (Stühmer, Conti, Suzuki, Wang, Noda, Yahagi, Kubo, and Numa, 1989). Activation of voltage-activated channels involves conformational changes as regularly spaced positive charges are moved leading to detectable gating currents as the channel moves from a closed to an open state. However, amongst others, there are some cyclic-nucleotide gated cation channels that contain S4 sequences; these do not open in response to membrane depolarisations, therefore this phenomenon is not as straightforward as it first appears.

Site-directed mutagenesis and expression experiments of the S4 segment have explored the consequences of substitution of some of the positively charged residues. By injecting mRNAs made from the mutated cDNA into *Xenopus* oocytes and performing voltage-clamp experiments, Stühmer and colleagues found that substituting basic residues of the S4 region with neutral or acidic residues, thus decreasing the net positive charge, affected the voltage sensitivity of activation for sodium channels in almost a linear fashion (Stühmer, Conti, Suzuki, Wang, Noda, Yahagi, Kubo, and Numa, 1989). Papazian, Timpe, Jan and Jan (1991) found that neutralisation or reversal of the positive charges changed voltage sensitivity of *Shaker* potassium channels indicating that the S4 region contains a major part of the voltage sensing machinery, and is indeed involved in voltage-dependent activation, but not just in a simple electrostatic manner; it was found that interchanging arginine and lysine residues (therefore conserving charge) still caused changes in voltage sensitivity. It is thought that the chemical interactions of side chains are also significant. It can not be assumed either that it is solely the S4 region, which is responsible for sensing voltage. Indeed, the inward rectifier class of voltage-activated potassium channels does not possess an S4 region. Also, the voltage sensitivity of glutamate receptors sensitive to NMDA is due to voltage-dependent block by external magnesium ions.

1.4.2.2 The pore region

H5, a 21 amino acid portion of the extracellular loop between S5 and S6 containing hydrophilic residues, could form part of the pore, or ion conduction pathway. This stretch is sometimes called the P region or the SS1-SS2 link, and is thought to dip into the membrane from the outside, but not actually traverse it. The H5 segment is highly conserved among voltage-dependent potassium channels, and this pattern is also seen with voltage-activated sodium and calcium channels, with their four times repeated set of similar six transmembrane domains. Thus, it can be assumed that the four potassium channel subunits assemble in a symmetrical manner around a central axis along which the P region is aligned. The inner part of the pore lining is thought to be comprised of the intracellular S4-S5 loop and the intracellular end of the S6 segment (Isacoff, Jan and Jan, 1991). Each of the four domains thus contributes to forming a quarter of an aqueous conduction pathway for potassium ions to pass through when the channel is open.

It is thought that the P region confers some aspect of selectivity on the channel. Heginbotham, Abramson and MacKinnon (1992) formed a chimera, swapping the H5 region of a cyclic-nucleotide-gated channel which is a non-specific cation channel, for that from a *Shaker* potassium channel. The chimera channel had the selectivity and conductance of the cyclic nucleotide-gated channel. Similarly, Hartmann, Kirsch, Drewe, Tagliatela, Joho and Brown (1991) made a chimera using sections of two voltage-activated potassium channels, Kv3.1 and Kv2.1, from different gene sub-families (see 'Multiple gene families' below), swapping the section containing the H5 region of one with the corresponding section from the

other. The first channel had a single channel conductance three times that of the second, and the chimera, containing the H5 region from the first channel had the conductance of that channel.

From a similar analysis of chimeric potassium channels, it seems that the S6 region of the *Shaker* potassium channel also forms part of the pore. Lopez, Jan and Jan (1994) formed a chimera, using the S6 region from Kv3.1 and transplanting it into the *Shaker* channel, causing it to exhibit the single-channel conductance (a fourfold increase) as well as sensitivities to tetraethylammonium ions and barium ions of Kv 3.1. Three non-conserved residues in the S6 segment were said to affect the single channel conductance. The transplantation of the S6 segment into the chimera did not affect the voltage-dependence or kinetic properties of channel gating, thus the overall structure of the channel was not affected. Lopez, Jan and Jan concluded that the pore of voltage-activated potassium channels is likely to be formed by the S6 segment in addition to the H5 region and the S4-S5 intracellular loop.

Voltage-activated potassium channels are closed in hyperpolarised membranes and are converted to the open state when activated upon depolarisation (Hille, 1984). Open channels can either relax back into the closed state or else inactivation occurs causing the conduction of ions to stop despite a maintained depolarising stimulus (the term *deactivation* is used when conduction of ions stops due to the end of stimulus). Many voltage-activated channels inactivate with time even when the membrane potential is maintained at a depolarised level that would have initially opened the channel. Inactivated channels will not open in response to depolarisation, unless the inactivation is reversed by repolarisation, but the channel

must first enter the closed state. Inactivation can be fast (on a scale of milliseconds) or slow (on a scale of seconds), this difference in time course is due to these being distinct processes with distinct molecular mechanisms.

1.4.2.3 N-type inactivation

A 'ball and chain' model for fast inactivation has been suggested, in which an inactivation particle, the ball, tethered on the intracellular surface of the channel by a chain at the amino-terminus of the polypeptide, is able to move to a receptor site on the intracellular mouth of the pore to bind and block the pore, causing inactivation (Armstrong and Bezanilla, 1977). This fast inactivation process can be specifically prevented by treatment of the intracellular surface of the sodium channel with proteolytic enzymes (Armstrong, Bezanilla and Rojas, 1973). This model was first proposed with sodium channels, but was extended to include potassium channels also (Hoshi, Zagotta and Aldrich, 1990). The inactivation ball in potassium channels has been proposed to consist of a hydrophobic core, next to a region of positive charge.

A systematic study of deletion mutants showed that those with the first 19 amino acid residues of the amino-terminus of *ShakerB* removed did not undergo fast inactivation, and the next 60 amino acids are also crucial in determining the rate of inactivation. Point mutations of positively charged amino acids in the amino-terminus polypeptide chain slow down inactivation, implying that these positive charges correspond to possible negative charges at a potential binding site at the pore.

Synthetic peptides corresponding to the first 20 amino acid portion, or the ball of the *ShakerB* amino-terminus were found to restore fast inactivation to deletion mutants of *ShakerB* with the amino-terminus removed (Zagotta, Hoshi and Aldrich, 1990). Synthetic ball peptides were added to the intracellular side of the cell membrane in the inside-out configuration of the patch clamp technique. These synthetic ball peptides were found to even cause inactivation of calcium-activated potassium channels in coronary smooth muscle (Toro, Stefani and Latorre, 1992), rat brain (Foster, Chung, Zagotta, Aldrich and Levitan, 1992) and rat skeletal muscle (Beirão, Davies and Stanfield, 1994), but ATP-dependent potassium channels in rat skeletal muscle were found not to be blocked (Beirão, Davies and Stanfield, 1994).

The positively charged and hydrophobic amino acid residues of the ball region are thought to interact with a receptor at the intracellular mouth of the pore, thus the ball can occlude the pore. This receptor may include amino acid residues in the short intracellular loop between the S4 and S5 transmembrane segments (Isacoff, Jan and Jan, 1991). This short intracellular loop may contribute along with the H5 region between S5 and S6, to the formation of the lower part of the pore as mentioned above. Point mutations of charged hydrophilic amino acid residues within this loop to neutral hydrophilic ones and mutations of hydrophobic residues to (hydrophobic but lacking side chains) alanine reduce fast inactivation, but also channel conductance.

1.4.2.4 C-type inactivation

In contrast to this ball and chain model which depends upon the composition of the amino terminus, slow inactivation appears to be linked to the carboxyl terminus in the S6 segment; *ShakerA* and *ShakerB* alternative splice variants have differing time courses of C-type inactivation due to their differing carboxyl termini; *ShakerB* has slower slow inactivation. The characteristics of C-type inactivation were studied in the absence of N-type inactivation (portions of the N-terminus, amino acid residues 6 to 46 were deleted) by the use of point mutants. A hydrophobic alanine at position 463 in the S6 region of *ShakerB* changed to valine, as in *ShakerA*, speeded up the inactivation by nearly 100 times, to a value similar to that of *ShakerA* (Hoshi, Zagotta and Aldrich, 1991). C-type inactivation may be due to a conformational change at the extracellular mouth of the pore. Choi, Aldrich and Yellen (1991) found that tetraethylammonium (TEA) ions applied intracellularly blocked N-type inactivation; the intracellular site for TEA blockade of open channels is thought to be located in the middle portion of the H5 which doubles back as a hair pin to form the pore region; a point mutation in the middle of H5, from threonine to serine, removing a side-chain substantially reduces TEA block, placing this residue at the tip of the hairpin (Yellen, Jurman, Abramson and MacKinnon, 1991). Thus, simple competition between TEA ions and the inactivating ball at adjoining binding sites could explain the block of N-type inactivation. When TEA ions were applied extracellularly, C-type inactivation was blocked. External TEA block is known to be affected by mutations to the extracellular mouth of the pore, and a 'foot in the door' model has been proposed

whereby the channel cannot close when occupied by a blocker (Choi, Aldrich and Yellen, 1991), an effect confirmed with other permeant ions.

1.4.3 Alternative splicing, genomic complexity and the generation of diversity

1.4.3.1 Alternative splicing

The gene encoding the *Shaker* locus in *Drosophila* was found to be large and complex, with cDNA clones hybridising to different patterns of genomic sites. The implication of this was that the *Shaker* locus is a complex transcriptional unit, subject to alternative exon splicing (Papazian, Schwarz, Tempel, Jan and Jan, 1987; Schwarz, Tempel, Papazian, Jan and Jan, 1988). As mentioned above, post-transcriptional modifications to the mRNA involve the excision of selected intervening non-coding sequences, or introns, to generate multiple different secondary transcripts. Potentially, exons in between introns are also removed. Therefore, this differential mRNA splicing involves the selection of different combinations of exons from the same primary transcript, leading to a whole family of proteins. There are more than 23 different exons coded for by the *Shaker* gene in *Drosophila*, and alternative splicing of 10 different variants of *Shaker* protein product. Therefore, several related channel products, passing kinetically distinguishable currents are derived from the same gene by alternative splicing. The relative abundance of these different alternative splices may be developmentally regulated and tissue specific.

1.4.3.2 Multiple gene families

There are different genetic mechanisms for generating diversity of *Shaker*-like potassium channel genes between *Drosophila* and mammals. In contrast, the mammalian K⁺ channel genes have no introns in the coding region, rather the sub-families consist of a large number of distinct homologous genes, and the diversity of these channels seems to derive from gene duplication and divergence, that is to say, the existence of separate distinct genes coding for different types of channel. However, in the *Shaw*-like sub-family (see below) encoding mammalian channels, cDNAs encoding alternative splices of a member of this family were cloned and expressed in oocytes (Luneau, Williams, Marshall, Levitan, Oliva, Smith, Antanavage, Folander, Stein, Swanson, Kaczmarek and Buhrow, 1991).

From the sequencing of *Shaker*-related clones (Kamb, Iverson and Tanouye, 1987; Iverson, Tanouye, Lester, Davidson and Rudy, 1988; Schwarz, Tempel, Papazian, Jan and Jan, 1988; Jan and Jan, 1990) it was likely that the predicted protein products had identical core regions, and differing amino and carboxyl terminal ends. The central core region is encoded by relatively few exons within a shorter stretch of the genomic DNA compared to the distribution of the exons encoding for the variable terminal ends over a comparatively broader region of the gene. The *Shaker* locus seems to code for at least four different protein products, based upon the uniqueness of their amino and carboxyl termini. Within this scheme, there is further variation due to alternative splicing.

Multiple genes encoding different potassium channel polypeptides were found after it was seen that when most of the *Shaker* locus was deleted from the genome, a number of other potassium channels were still present (Solc, Zagotta and

Aldrich, 1987; Solc and Aldrich, 1988). Butler, Wei, Baker and Salkoff (1989) isolated several *Shaker*-like cDNAs residing at different chromosomal loci to *Shaker*, by screening a *Drosophila* cDNA library at low stringency using a cDNA probe derived from the *Shaker* S1-S6 presumed membrane spanning domains. Three 'sister' genes to *Shaker* were found, *Shab*, *Shaw* and *Shal*. They shared structural similarity with *Shaker*, with similar hydrophobicity plots over the presumed membrane spanning regions S1 to S6 reflecting a highly conserved core region. It was also found that there was variation in the patterns of expression of these *Shaker*-like genes during the different developmental stages of *Drosophila*, with the *Shab* gene not expressed in adult flies.

Like *Shaker*, the *Shab*, *Shaw* and *Shal* expression cloning in *Xenopus* oocytes gave potassium currents (Wei, Covarrubias, Butler, Baker, Pak and Salkoff, 1990) sharing general features such as selectivity and voltage-gating, but differing in other some more detailed biophysical properties such as inactivation, kinetics etc. Also, a comparison of *Drosophila* channel proteins with homologues from mouse brain showed that each of the *Shaker*-like gene subfamilies has homologous mammalian sub-family homologues. The mammalian homologues of the *Shaker* protein were found to be significantly more closely related to the *Drosophila Shaker* protein in the S1-S6 region than to the other mammalian sub-family members within a species (Salkoff, Baker, Butler, Covarrubias, Pak and Wei, 1992) - the mouse versions of the *Shaker* gene was found to have more than 70 % identity with that of the *Drosophila*, compared to only about 40 % identity with the mouse versions of the other subfamily genes. This is shown in Figure 1.5 below.

Shaker, Shab, Shaw and *Shal* therefore represent separate conserved gene sub-families. Shared identity between *Drosophila* and mammalian protein homologues implies a high level of conservation and common ancestry.

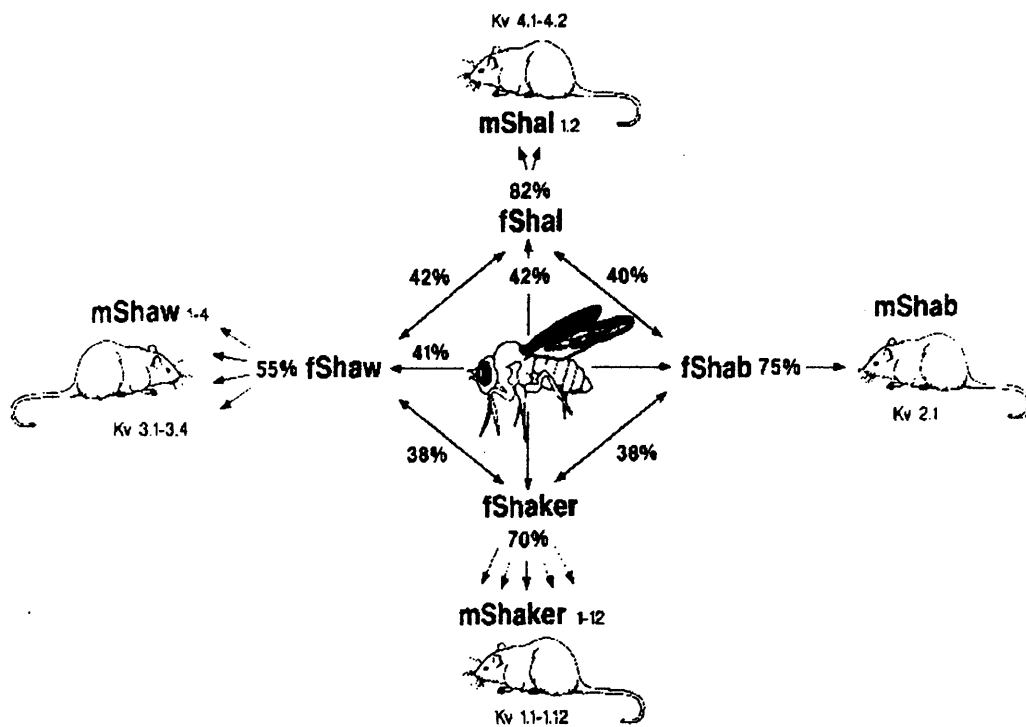


Figure 1.5 High conservation of potassium channel sequence identity between the same subfamily in different species compared to that between subfamilies in the same species. (from Salkoff, Baker, Butler, Covarrubias, Pak and Wei, 1992)

1.4.3.3 Heteromultimeric channels

Another mechanism for the generation of diversity is the formation of heteromultimeric channels comprised of different subunits from within the same subfamily, as opposed to homomultimeric channels, which are assembled, from four identical subunits. Heteromultimers have been demonstrated *in vitro* for Kv1.1 and Kv1.4 channels from rat brain (Ruppersberg, Schröter, Sakmann, Stocker, Sewing and Pongs, 1990) and for *ShakerA* and a non-inactivating deletion mutant of *ShakerB* (MacKinnon, 1991) mRNAs co-injected into *Xenopus* oocytes. *In vivo*, the subunits of both Kv1.1 and Kv1.2 were co-localised by antibody immunoprecipitation, when antibodies were raised against only one of the channels in mouse brain (Wang, Kunkel, Martin, Schwartzkroin and Tempel, 1993). This supported the finding that mRNAs for these channels injected into *Xenopus* oocytes produced a functional channel with hybrid properties.

These heteromultimeric channels have not been demonstrated for subunits from different subfamilies. Covarrubias, Wei and Salkoff (1991) showed that *Shaker*, *Shab*, *Shal*, and *Shaw* form potassium channels that act independently of one another; within a subfamily, hybrid heteromultimers can be formed. There appears to be some constraint on non-similar subfamily heteromultimer assembly controlled by a particular region of the polypeptide sequence called the T1 domain. This domain comprises 104 residues in the cytoplasmic region between the N-terminus and S1 in the *ShakerB* variant, and substitution of this region into chimeras allows members of other subfamilies not normally forming heteromultimers with *ShakerB* to do so (Shen, Chen, Boyer and Pfaffinger, 1993). Deletion of this T1

region through removal of the N-terminus will not allow *Shaker*B subunits to bind to each other at all (Li, Jan and Jan, 1992).

From these various mechanisms, great diversity is generated. It is difficult to calculate the number of different functional proteins that may be generated from each gene, or indeed the total number of similar genes within the genome for a species. Heteromultimer assembly of different members of a subfamily makes the number of potential potassium channels even greater. This provides a great deal of adaptability and customisation, which is tissue/species specific, in order to fulfil specialised roles. A large number of mammalian potassium channels grouped into these sub-families have since been cloned. All have slightly different biophysical properties, for example, activation and inactivation. Thus, there appears to be a spectrum of characteristics in *Drosophila* and mammalian voltage-activated potassium channel genes, an overlap of biophysical properties. Within the *Shaker* channel gene subfamily, the characteristics change from A-type to delayed rectifier, that is to say, inactivation rates vary from very rapid to extremely slow. The mechanisms of adding further diversity discussed above serve to provide cells with potassium channels with precise properties suited for fulfilling their precise roles.

It was assumed by analogy with the voltage-dependent sodium and calcium channels, that the complete functional potassium channel is formed from four channel peptide subunits assembling together. This implies a tetramer of four homologous domains, therefore showing similarities to calcium and sodium channels which consist of a four times repeated domain forming a single large subunit (Agnew, 1988; Tempel, Papazian, Schwarz, Jan and Jan, 1987; MacKinnon, 1991).

This is supported by evidence from experiments involving the expression of different types of subunits in a functional channel, and the use of specific potassium channel ligands such as tetraethylammonium ions (TEA) and charybdotoxin (CTX) to elucidate this stoichiometry. Two different cDNA transcripts (differing greatly in biophysical properties such as activation or pharmacological blocking) expressed simultaneously in the same oocyte, expressed channels with properties intermediate (rather than simply a mixture) to those of the individual channels encoded by the cDNAs of heteromultimeric *Shaker* (Isacoff, Jan and Jan, 1990) and mammalian potassium channels (Christie, North, Osborne, Douglass and Adelman, 1990; MacKinnon, 1991; Ruppersburg, Schröter, Sakmann, Stocker, Sewing and Pongs, 1990).

Point mutations at the charybdotoxin binding site (causing insensitivity to this toxin) in one of the cDNA transcripts forming such heteromultimeric channels were used to compare binding kinetics with the 'normal' subunits, yielding conclusive evidence of four subunits in *Shaker*-like channels (MacKinnon, 1991). This ability to form heteromultimers greatly increases the potential number of different possible potassium channels *in vivo*.

1.4.5 Nomenclature for vertebrate voltage-activated potassium channel genes

In response to the differing name schemes assigned by different laboratories to the emerging families of voltage-gated potassium channels Chandy, Douglass, Gutman, Jan, Joho, Kaczmarek, McKinnon, North, Numa, Philipson, Ribera, Rudy, Salkoff, Swanson, Steiner, Tanouye and Tempel (1991) adopted a unified and

simplified nomenclature scheme for the *Shaker*-like subfamilies representing mammalian homologues of the four *Drosophila* potassium channel genes.

Each gene is prefixed 'Kv' (i.e. K^+ channel gene, voltage-activated), and following this, the subfamily assigned number (1,2,3 and 4 respectively for *Shaker*, *Shab*, *Shaw* and *Shal*) and the order in which the gene was identified. For example, the first discovered gene in the *Shaker*-related subfamily, previously designated MBK1, RCK1 and HK1 in the mouse, rat and human respectively, is now known as Kv1.1. This nomenclature is based on the principle of sequence-relatedness of homologues between species, and the name applies to a cloned gene rather than to a channel. The name does not include the tissue or species of origin, though this can be included.

Gutman and Chandy (1993) updated this nomenclature list to include the rat IK8 and K13 genes, which were assigned to subfamilies 5 and 6 respectively. These genes also comprise a family of K^+ channels with six putative membrane-spanning domains. The Human Gene Mapping Workshop human locus names applied to the human homologues of all the genes are included, as are the accession numbers for K^+ channel gene sequences in the GenBank/EMBL cDNA databases.

Also included in the Gutman and Chandy nomenclature are other mammalian potassium-selective channels such as the calcium-activated potassium channel designated the K_{Ca} family; the mammalian homologues of the *Drosophila eag* (*ether-a-gogo*) gene which are members of a family of voltage-activated cyclic nucleotide-binding K^+ channels.

TABLE 1.1a: Classification of cloned voltage-gated (Kv) members of S4

superfamily

<u>NOMENCLATURE</u> (family/subfamily)	<u>HUMAN</u>	<u>RAT</u>	<u>MOUSE</u>	<u>CURRENT</u>	<u>TISSUE</u>
Kv/Shaker (Kv1 subfamily)					
Kv1.1	HuK(I)	RCK1	MBK2	delayed rectifier	CNS
		RBK1	MK1		
		RK1			
Kv1.2	HuK(IV)	BK2	MK2	delayed rectifier	Heart/CNS
		RCK5	MK5		
		NGK1			
		RK2			
		RAK			
Kv1.3	HuK(III)	RCK3	MK3	delayed rectifier	T cells/CNS
	hPCN3	RGK5			
	HLK3	KV3			
	HGK3				
Kv1.4	HuK(II)	RCK4	MK4	A-type	Heart/CNS
	hPCN2	RK8			
	HK1	RHK1			
		RK4			
Kv1.5	HuK(VI)	KV1		delayed rectifier	Heart/CNS
	hPCN1	RK3			
	HK2	RMK2			
	HCK2				
Kv1.6	HBK2	RCK2	MK2	delayed rectifier	CNS
	HuK(v)	KV2	MK6		
Kv1.7		RK6		delayed rectifier	
Kv/Shab (Kv2 subfamily)					
Kv2.1		DRK1	mShab	delayed rectifier	Heart/CNS
Kv2.2		cDRK			CNS
Kv/Shaw (Kv3 subfamily)					
Kv3.1	NGK2	Raw2	NGK2	delayed rectifier	T cells
	hKv3.1	KV4	mShaw22		
Kv3.2	HKShIIIA	RShaw12	mShaw12	delayed rectifier	CNS
		RKShIIIA			
		Raw1			
Kv3.3	hKv3.3	RKShIIID	mShaw19	A-type	CNS
	HKShIIID				
Kv3.4	HKShIIIC	Raw3	mKv3.4	A-type	SKM/CNS
Kv/Shal (Kv4 subfamily)					
Kv4.1			mShal	A-type	CNS
Kv4.2		RShal1		A-type	Heart/CNS
		RK5			
Kv4.3		RKShIVB		A-type	
Kv/Kv5.1 (Kv5 subfamily)		Ik8			
Kv/Kv6.1 (Kv6 subfamily)		K13			

TABLE 1.1b: Classification of cloned S4 superfamily K⁺ channels (non-Kv)

NOMENCLATURE (family/subfamily)	HUMAN	RAT	MOUSE	CURRENT	TISSUE
Ca²⁺-activated/maxi-K(BK)	hslo		mslo		
KvLQT	KvLQT1				Heart
EAG		r-eag	m-eag		
	HERG				Heart

(Notes:SkM = skeletal muscle

SmM = smooth muscle)

Inward rectifiers were included with the prefix Kir in subfamilies again on the basis of sequence relatedness, there being higher amino acid sequence similarity within subfamilies, compared to that between subfamilies. Gutman and Chandy arranged the (at the time) three known inward rectifier genes, ROMK1, IRK1 and GIRK1 to three subfamilies. ROMK1 or Kir1.1 was the first discovered (Ho, Nichols, Lederer, Lyton, Vassilev, Kanazirska and Hebert, 1993), isolated by expression cloning in *Xenopus* oocytes from a rat kidney cDNA library. ROMK1 has weak inward rectification properties, weak voltage-dependence and no time-dependent gating. IRK1, or Kir2.1 as mentioned above, is a classic strong inward rectifier passing little outward current on depolarisation, resembling inward rectifiers described in native tissues of many different types. The gene was first cloned from by Kubo, Baldwin, Jan and Jan (1993) from a mouse macrophage cell line. GIRK1 or Kir3.1 is a G-protein-coupled agonist activated strong inward rectifier, first cloned by Kubo, Reuveny, Slesinger, Jan and Jan (1993) from rat heart by homology screening using Kir2.1 and Kir1.1 clones.

Douppnik, Davidson and Lester (1995) adopted the nomenclature of Gutman and Chandy to assign the inward rectifiers to five different subfamilies. As well as newly discovered species homologues and new members within the three subfamilies of Gutman and Chandy, two new subfamilies with low sequence identity with other inward rectifier channels were added.

TABLE 1.2: Classification of cloned Kir channels of the inward rectifier superfamily.

<u>NOMENCLATURE</u>	<u>HUMAN</u>	<u>RAT</u>	<u>MOUSE</u>	<u>TISSUE</u>
Kir 1.0 subfamily				
Kir1.1a	ROMK1	ROMK1		Kidney/CNS
Kir1.1b	ROMK2	ROMK2		Kidney
	ROMK1B			
Kir1.1c	ROMK3			Heart/CNS/SkM
	ROMK1A			
Kir1.1d	ROMK4			Heart/Kidney/CNS/SkM
Kir1.1e	ROMK5			Heart/CNS
	ROMK1C			
Kir 2.0 subfamily				
Kir2.1	HH-IRK1	rb-IRK1	IRK1	Heart/Brain
	Hirk1		mb-IRK1	
			IRK1	
Kir2.2		rb-IRK-2	mb-IRK2	Brain
Kir2.3	HIR	BIR11	mb-IRK3	Brain
	Hirk2			
	hrk1			
Kir3.0 subfamily				
Kir3.1	GIRK1	GIRK1	GIRK1	Heart/CNS
		KGA		
		KGB		
Kir3.2a,b	GIRK2		GIRK2	CNS
			GIRK2B	
Kir3.3			GIRK3	CNS
Kir3.4	hcKATP	rcKATP		Heart
	GIRK4	CIR		
Kir4.0 subfamily				
Kir4.1		BIR10		Brain
Kir5.0 subfamily				
Kir5.1		BIR9		Brain
Kir6.0 subfamily				
Kir6.1	KCNJ8	uKATP-1		
Kir6.2		BIR		Heart/pancreatic b-cells

1.5 Introduction to work carried out

The aims of the project described were concerned with the analysis and characterisation of the properties of two different types of voltage gated potassium channel, A-type and delayed rectifier. To enable the study of such a phenomenon in isolation, when the normal physiological cellular environment has many other electrical signals and complicated interactions, a heterologous expression system was used. Molecular biology techniques were used to clone or produce identical message molecules coding for the channel protein under study. By a process known as transfection, these were introduced into a cell line, which was found to be electrically silent in the absence of the channel protein. Expression of the functional channel protein from the coding message was triggered by chemically induced cellular events. The patch clamp technique was used to study the membrane currents passing through these ion channels when a change in the membrane potential was imposed upon the cell. Synthetic peptides, corresponding to an integral structural component thought to be involved in inactivation of the A-type potassium channel were used in experiments with the delayed rectifier, which lacks these structures and has different inactivation characteristics. These peptides were also used in experiments with the A-type channel, to augment the inactivation inherent in these channels.

CHAPTER TWO

Methods and Materials

2.1 Molecular Biology Methods

2.1.1 Expression of cloned potassium channel genes in Murine erythroleukemia (MEL) cells by locus activation

2.1.1.1 Murine erythroleukemia cells

This project utilised the most commonly used erythroid tissue culture system, murine erythroleukemia (MEL) cells. MEL cells are Friend virus complex transformed erythroid progenitor cells, a process which arrests them at the pro-erythroid stage of development, and makes them oncogenic.

MEL cells can be cultured indefinitely at this stage, and these cells do not produce haemoglobin. However, several chemical agents, for example dimethyl sulphoxide (DMSO), can cause induction of terminal erythroid differentiation analogous to normal *in vivo* erythrocyte maturation. It is thought that treatment with DMSO causes a depolarising effect on the membrane potential of the cells, which in turn triggers intracellular events. The differentiation process involves specific alterations in ion transport associated with a reduction in cell volume and overall loss of cellular material (Delpire and Gullans, 1994). One characteristic change during this process is the high level synthesis of adult globin proteins. This fact allows the use of MEL cells as an erythroid expression system.

Previous methods used to express cloned ion channel genes have included several systems using transient expression in non-mammalian cells. These include the injection of in vitro transcribed RNA into *Xenopus* oocytes; cloning of the sequence into plasmid vectors inserted into a baculovirus-infected insect cell line and expression of ion channel genes using *Vaccinia* virus vectors, for both *Xenopus* oocytes and mammalian cells.

The fact that most of these systems employed non-mammalian cells meant that an exogenous, mammalian channel protein product has possibly been subjected to different post-translational modifications than would occur in mammalian cells. Also, the environment of the cell may lack other endogenous protein products normally found in mammalian cells, for example, second messenger systems, or these might differ. In contrast to this, MEL cells produce the full complement of products on induction and differentiation, as seen in normal erythrocytes in development. These include, for example, the outer membrane ion transporting proteins e.g. the $\text{Na}^+ / \text{Cl}^-$ symport, Ca^{2+} and Na^+ / K^+ ATPases, and exchangers for $\text{Cl}^- / \text{HCO}_3^-$ and Na^+ / H^+ , all these being active ion transporters (Shelton, Davies, Antoniou, Grosveld, Needham, Hollis, Brammar and Conley, 1992).

The stable transfection of the independent transcription unit into MEL cells is described below. Stable transfection is obviously preferable for detailed studies of the properties of expressed channels, compared to transient expression systems which can be time-consuming, requiring preparation manipulation, cloning and injection of sequences for each 'single shot'. In comparison, after simple electrophysiological screening, a stable, long term tissue culture system such as MEL is easy to maintain or store.

The MEL C-88 cell line used (Deisseroth and Hendrick, 1978) did not produce any detectable voltage-dependent currents in native untransfected, or uninduced transfected cells. Therefore, only cloned heterologous (that is, *external*) voltage-dependent channels expressed in this system could be studied in isolation with no endogenous currents to interfere with electrophysiological recordings.

While being free from endogenous voltage-dependent currents, Arcangeli, Wanke, Olivotto, Camagni and Ferroni (1987) have reported a calcium-activated potassium channel (K_{Ca}), a chloride channel, and a stretch-activated channel in MEL cells, the latter two being labile. Under conventional whole-cell recording conditions, K_{Ca} channel activity can be minimised by the attempt to minimise the free concentration of Ca^{2+} in pipette solutions, particularly by the use of EGTA buffering.

MEL cells have many advantageous characteristics as an expression system. They are semi-adherent floaters, very easy to culture (see Cell Culture Methods, below). They are resilient, being able to survive cryogenic storage in liquid nitrogen, and induction with DMSO. No enzymatic treatment is necessary before patch clamping, and high-resistance seals are relatively easy to achieve.

2.1.1.2 The locus control region

Two methods, employing β -globin gene-activation elements were used to regulate the expression of the potassium channel genes hPCN1 (Kv1.5) and RShall (Kv4.2), both employing the globin protein-producing properties of the MEL cell to give stable expression by locus activation. These methods were developed by the ICI Joint Laboratory Ion Channel Group at the University of Leicester.

The locus control region (LCR) is a DNA sequence which in addition to the full coding sequence and an activatable promoter, gives an independent transcription unit which can be stably introduced into MEL cells by electroporation.

Electroporation is a method for introducing foreign DNA or chromosomes into a cell by brief exposure to a high voltage which results in the temporary formation of small pores in the cell membrane, increasing permeability and allowing the uptake of DNA or chromosomes from the surrounding buffer.

MEL cells need to be actively growing in logarithmic log phase and healthy before electroporation. Linear expression construct DNA is introduced into a Bio-Rad Gene Pulsar™ electroporation cuvette (Bio-Rad, UK) together with sterile electroshock buffer (140 mM NaCl, 25 mM HEPES pH7.5, and 0.75 mM Na₂HPO₄) washed cells, and placed into the electroporation machine set at 960 μ F and 250 V.

DMSO induction causes cell differentiation, expressing the transgene, and synthesising the protein product, which is then assembled into homo-tetrameric potassium channels post-translation, and inserted into the cell plasma membrane.

In erythroid cells, the LCR is found upstream from, and directly influences the specific activation of β -globin genes. A gene (such as a potassium channel gene)

covalently linked to the LCR and stably expressed in erythroid tissue culture cells such as MEL cells will undergo expression linked to the erythroid specific expression of β -globin. The promoter is a region of DNA involved in the binding of RNA polymerase to initiate transcription. The LCR has a preference for acting on the nearest promoter, so a natural gene and its own native β -globin promoter, placed downstream from the LCR gives an expression system for heterologous potassium channel genes in MEL cells.

In the case of hPCN1/Kv1.5, the natural human gene was directly activated from chromosomal sequences from a genomic library, with chromosomal sequences flanking the protein coding sequence forming the native promoter.

Human β -globin sequences have been found to be fully functional in MEL cells, with the endogenous mouse globin gene switching on the human β -globin gene through the LCR. This leads to the production of equal amounts of endogenous mouse β -globin mRNA and human β -globin message.

This provided a route for the expression of single-stranded cDNA from a cDNA library, as used for RShal1/Kv4.2. The cDNA was inserted within a human β -globin 'backbone' prior to joining downstream to the LCR. Inserting the cDNA immediately after the β -globin promoter provides a functional promoter for it, activating vital transcriptional start and stop signals, as well as mRNA processing and maturation signals.

Below is an account in more detail of how the ICI Joint lab Ion Channel Group at the University of Leicester produced the channels used in this project.

2.1.1.3 hPCN1/Kv1.5

An adult male heart cDNA library was screened. A polymerase chain reaction (PCR) probe corresponding to the S4 segment of the MBK1 (Kv1.1) channel used the principle of simple hybridisation to look for, purify and multiply suitable cDNA clones derived from mRNA.

The mRNA content of a tissue represents the fraction of the coding sequence that is being actively expressed, whereas the DNA is representative of all molecular subtypes of the genotype. Total RNA is isolated from cells by mechanical and chemical means and then mRNA separated from other non-messenger RNAs.

The chances of finding a correct sequence is proportional to the relative abundance of a message in the mRNA population from the tissue. This is because the cDNA clones are formed from the mRNA by the use of the enzyme reverse transcriptase which utilises the mRNA as a template to synthesise a single-stranded cDNA copy.

A cDNA sequence which was thus purified and sequenced was found to correspond to most of the sequence of hPCN1 found by Philipson, Hice, Schaefer, LaMendola, Bell, Nelson and Steiner (1991) in human insulinoma, though it lacked the N-terminal region up to the S2 segment. A full-length cDNA needs to be recovered in order for a coupling to a promoter, therefore this cDNA could not be used for expression.

However, it was used as a probe in a human genomic library contained in a cosmid vector. The vector allows the continued replication and maintenance of the

human genome placed therein. Genomic DNA clones corresponding to the cDNA probe were isolated and sequenced. These were found to be full-length coding sequences for hPCN1, that is, the actual human gene.

Further manipulations yielded an additional region contiguous upstream to the protein-coding region, that included a promoter which could be activated by the locus control region of the β -globin gene in MEL cells.

Cell lines that expressed the transfected gene were isolated by introduction of a second gene that encoded a selectable marker, in this case resistance to the antibiotic geneticin G418 sulphate (Sambrook, Fritsch and Maniatis, 1989). Geneticin is an aminoglycoside, toxic to both eukaryotic and prokaryotic cells. The dominant resistance genes are bacterial in derivation, but can be expressed in eukaryotic cells when the Neo DNA sequence is linked to endogenous DNA sequences. Introduction of these genes confers resistance, and cells are selected by their ability to grow in medium containing geneticin. Following electroporation (as described above), cells were diluted at very low density in fresh culture medium (see Cell Culture Methods, below), and G418 sulphate was added at a concentration of 1 mg / ml after 24 hours to select for successful transfectants. Clonal colonies became visible after about two weeks, and these were separated and grown as independent multiple cell lines, which then required electrophysiological screening analysis after DMSO induction to confirm successful stable transfection.

2.1.1.4 RShall/Kv4.2

The cDNA sequence encoding RShall (Baldwin, Tsaur, Lopez, Jan and Jan, 1991) was supplied to the ICI Joint Laboratory Ion Channel Group by Dr. Timothy Baldwin, University of California at San Francisco. This cDNA sequence was stably expressed in MEL cells by the following route.

The full length cDNA sequence for RShall was linked to the β -globin locus control region via direct insertion into the MEL cell expression cassette pEC3 (Needham, Gooding, Hudson, Antoniou, Grosveld and Hollis, 1992), which contains a multiple cloning segment for insertion of cDNAs or intact genomic fragments lacking a functional promoter; these residual β -globin gene elements of vector pEC3 have been shown to increase the overall expression levels of heterologous cDNA molecules, as well as providing mRNA processing and maturation signals. This construct of β -globin promoter / cDNA expression cassette was then transferred to the locus control region containing vector pGSE417. As with hPCN1 above, this expression construct was linearised and introduced into MEL cells by electroporation, and then selected by using G418 sulphate. Electrophysiological screening of separate clonal cell lines was carried out after DMSO induction to find those cell lines that successfully expressed the channel protein stably.

2.2 Cell Culture Methods

The maintenance of a cell culture line expressing cloned potassium channels of interest offers many advantages. Foremost is the possession of very large uniform population of cells, which may be repeatedly subcultured, effectively giving an immortal supply.

Under appropriate well-defined conditions in tissue culture dishes, most cells can live, proliferate and even express differentiated properties of development.

Cells vary in their requirements. The liquid media used contained a chemically well-defined mixture of salts, amino acids, vitamins, some type of whole serum and other nutrients such as glucose. Antibiotics were added to inhibit the growth of bacteria, or with a dominant selectable marker to select cells. Tissue culture dishes containing medium and cells were kept in an incubator at 37 °C in a humidified 5 % CO₂ atmosphere. The medium contains a pH indicator dye such as phenol red, so that it is easy to monitor the pH that the cells grow in.

Cell culture lines can also be stored indefinitely in liquid nitrogen at a temperature of -196 °C, and still be viable upon thawing.

2.2.1 Maintenance, storage and induction of Murine

Erythroleukemia (MEL) cells

The semi-adherent MEL-C88 murine erythroleukemia cell line was used. All preparation of media and handling of cells was carried out in a horizontal laminar flow cabinet (Medical Air Technology, Manchester) and sterile techniques were employed.

2.2.1.1 Incubation Media

Stock cultures were maintained in Dulbecco's Modified Eagle Medium (DMEM, with Glutamax®, with 4500 mg / l glucose, with 25 mM HEPES (N-[2-hydroxyethyl] piperazine-n-[2-ethanesulphonic acid]), without sodium pyruvate) (Gibco BRL) supplemented with 10 % (v / v) foetal calf serum (FCS) (Seralab), Penicillin / Streptomycin antibiotic (1 µg / ml penicillin and 1 mg / ml streptomycin) (Gibco BRL) and 0.5 mg / ml Geneticin (G418 sulphate). Geneticin is an aminoglycoside used as a selective agent, toxic to both eukaryotic and prokaryotic cells. Resistance genes are bacterial in origin, and can be expressed in eukaryotic cells when the Neo DNA sequence is introduced. This enables cells to grow in media containing Geneticin.

This incubation medium was filtered through a 0.22 µm cellulose acetate membrane disposable filter (Corning) in order to remove any potential bacterial or other contamination at this stage. Cells were cultured in 3ml of incubation media in 5 cm plastic Nunclon® dishes (Gibco BRL), at 37 °C in a 5 % CO₂ atmosphere in a humidified incubator, giving the medium a pH of 7.2.

2.2.1.2 Subculture of cells

The MEL-C88 cells were found to be able to grow to a maximum density of about 2×10^6 cells / ml. This value was measured using a haemocytometer when the cells had formed a continuous or confluent layer, and were resuspended in the medium.

Generally, cell numbers doubled in approximately 12 hours. To maintain the cell line, dishes were subcultured when a density of 5×10^5 cells / ml was reached. This involved diluting cells from these dishes in fresh medium in new dishes. Adherent cells were dislodged by a sharp tapping of the side of the plastic culture dishes, and circular swirling of the incubation media. 30 to 60 μ l of incubation media containing cells was added to each dish containing 3 ml of fresh incubation media, depending upon the density of the cell growth. This represented a 1:100 to 1:50 dilution, with a 1:100 dilution of a confluent culture again reaching confluence in approximately 8 days.

2.2.1.3 Storage of cell stocks in liquid nitrogen

Stocks of all the MEL cells transfected with potassium channel genes studied in this project were stored cryogenically, frozen in liquid nitrogen. At a cell density of 1×10^6 cells / ml, medium containing cells was spun in a 10 ml cone base plastic tube (Northern Media Supply Ltd., North Humberside) at 1500 rpm for 15 minutes in a MSE Minor 'S' benchtop centrifuge (RW Jennings & Co., Nottingham) and the supernatant was carefully aspirated.

The cell pellet was gently resuspended in 1.5 ml of fresh medium, as above, but containing 20 % foetal calf serum and 10 % (v / v) dimethyl sulphoxide (DMSO) (Sigma Hybrimax, Sigma Chemical Co., St. Louis, MO). The elevated level of FCS and the addition of DMSO serve to prevent the formation of potentially lethal ice crystals within the cells during the cooling process.

200 µl aliquots were immediately transferred to Nunc® cryotubes (Gibco BRL) and placed in liquid nitrogen vapour for one hour to ensure slow cooling to -196 °C. The cryotubes were then immersed in liquid nitrogen in a LR40 cryostorage refrigerator (Jencons [Scientific] Ltd., Leighton Buzzard).

To restart a culture from frozen cells, cryotubes were taken from liquid nitrogen storage and immediately placed in a water bath at 37 °C to ensure quick thawing. 100 µl of cells were then added to 3 ml of normal incubation medium in the 5 cm plastic dishes, and placed in the incubator. A further subculture was carried out after two days and the culture was then maintained as normal, as described above.

2.2.1.4 Induction of transfected cells

Transfected MEL cells were induced to undergo erythroid differentiation and hence potassium channel gene expression using 2 % (v / v) DMSO added to cells in log-phase or exponential growth (generally a minimum of 4 days after subculture). No further medium changes were carried out subsequent to induction and before patch clamp use. Cells were used for electrophysiological patch clamp studies from day 2 through to day 7 post induction.

No enzymatic treatment was necessary before patch clamping. However, cells were prepared for patch clamping by washing the cells in the external bath solution to be used. This was achieved by adding 0.5 ml of medium plus induced cells and 4.5 ml of external bath solution to a 10 ml cone base plastic tube and spinning at 1500 rpm for two minutes. The supernatant was aspirated, leaving a few mm of fluid in which to gently resuspend the cell pellet.

The cells were then ready for patch clamping, having been concentrated and all traces of proteins from the incubation media foetal calf serum having been removed. The presence of any extraneous proteins might affect the interaction between the lipid molecules of the cell membrane and the glass electrode.

2.3 Electrophysiological Methods and Equipment

2.3.1 Micropipette fabrication

Micropipettes were made from hard borosilicate glass thin-walled 1.5 mm outer diameter filamented capillaries (GC150TF) (Clark Electromedical, Reading, Berks.). The fused internal filament greatly aids filling of micropipettes.

The micropipettes were pulled to a fine tip using a two stage Narishige PP-83 vertical puller (Narishige Scientific Instruments, Tokyo, Japan) in which gravity provides the pulling force. The micropipette is held clamped vertically at two points, the upper being fixed, and the lower on a vertical sliding track. The microelectrode passes through a coil of heating element, exactly half way between the two initial clamping points.

The first stage of the pull, with a high filament temperature, caused the glass inside the element to melt and elongate over a range of about 5 mm, before being stopped. This first pull leaves a tapered region like an hour-glass. The micropipette was then repositioned, with the centre of the tapered region replaced inside the element. The second pull was at a lower temperature, with a free drop producing two fine-tipped micropipettes as the narrowed region broke.

Patch micropipettes require blunt tips to prevent penetration of the tip into the cell during the process of seal formation when suction is applied. Fire polishing burns

away any deposits and smoothes the surface of the tip, promoting the formation of high resistance gigaohm seals between the cell membrane and the glass. Also, a round hole at the tip probably improves access to the cell interior in the whole cell configuration when the cell membrane enclosed within is disrupted.

Electrodes were fire-polished using a Narishige MF-83 fire-polisher (Narishige Scientific Instruments, Tokyo, Japan). This is coupled with an inverted microscope with high magnification to visualise the tip. Upon polishing, the tip can clearly be seen to constrict and smoothen, so reproducibility is enhanced with good optics. To prevent particles from the fire-polisher platinum wire from sputtering onto the micropipette, the wire is bent into a hairpin, and coated with micropipette glass, which forms a bead over the hairpin. The micropipette to be polished was brought close to the bead using micromanipulators.

The diameter of the tip can roughly be estimated at this stage by measuring the pressure required to expel air bubbles from the tip into methanol. A 10 ml syringe with a cannula was used for this purpose, the volume at which bubbles first appear being used as an indicator, the 'bubble number'. A lower bubble number requires greater pressure, and implies a smaller tip. Again this is an aid to reproducibility of micropipettes. Typical bubble numbers were 7 pre-polish and 5 after polishing. 5 corresponds to a pipette resistance of approximately 10 M Ω .

The resistance of the micropipettes when filled with internal pipette solutions ranged from 4 to 20 M Ω . A higher initial resistance leads to easier formation of seals, but pipettes with larger tips and thus a lower resistance give good electrical access and better interchange between micropipette contents and cell interior. These two considerations set the usable range of electrode sizes.

2.3.2 Solutions

All experimental electrophysiological solutions were made up with MilliQ distilled / deionised water, and filtered through a 0.2 μm filter under vacuum.

Additionally, filters were used with syringes at the time of experimentation, to ensure that stored solutions were free from particles at the time of use. This attention to cleanliness is essential in order to be able to form high resistance seals regularly between microelectrode pipette glass and plasma cell membranes.

All chemicals used were obtained from Sigma Chemical Co. (Poole, Dorset, UK). Experimental solutions were titrated to pH 7.2, using a Solex model 3100 pH meter, and magnetic stirrer at room temperature. Osmolarity of all solutions was measured using a Wescor 5100B vapour pressure osmometer.

2.3.2.1 External bath solutions

Table 2.1 Ionic composition of external bath solutions

SOLUTIONS	5 K _o	35 K _o ⁺	70 K _o ⁺	140 K _o ⁺
K ⁺	5 mM	35 mM	70 mM	140 mM
Na ⁺	135 mM	105 mM	70 mM	-
Ca ²⁺	2 mM	2 mM	2 mM	2 mM
Mg ²⁺	2 mM	2 mM	2 mM	2 mM
HEPES	10 mM	10 mM	10 mM	10 mM

The external bath solutions used for whole cell recording are shown in Table 2.1 (above), represented by 5 K_o⁺, 35 K_o⁺ and 70 K_o⁺. These contained varying ratios of potassium and sodium ions, in the form of KCl and NaCl added in appropriate volumes from freshly made molar stock solutions. The aim in each case was to ensure a cation concentration of approximately 140 mM. Ca²⁺ and Mg²⁺ were added in appropriate volumes from commercially produced molar stock solutions of CaCl₂ and MgCl₂.

2.3.2.2 Internal pipette solutions

Table 2.2 Ionic composition of internal pipette solutions.

Solutions	2 mM Mg ²⁺	Mg ²⁺ free
K ⁺	140 mM	140 mM
Mg ²⁺	2.36 mM	-
HEPES	10 mM	10 mM
EGTA	10 mM	-
EDTA	-	10 mM

All internal pipette solutions contained 140 mM K⁺ and 10 mM HEPES buffer. The final total 140 mM K⁺ was made up from 110 mM KCl and 30 mM KOH, with the final pH adjustment to pH 7.2 in mind.

EGTA (ethylene glycol bis(B-aminoethyl ether)N,N,N',N'-tetraacetic acid) is a chelator of Ca²⁺ ions. This is important, because, as pointed out in the Molecular Biology Methods (above), a native Ca²⁺-activated potassium channel has been described in control untransfected MEL cells (Arcangeli, Wanke, Olivotto, Campagni, and Ferroni, 1987). EGTA therefore minimises the presence of free Ca²⁺ ions in the internal pipette solutions, whether they exist as an impurity in either water or added chemicals, or indeed leaching from the glass used in making the micropipettes.

Unfortunately, EGTA also tends to chelate free Mg²⁺ ions, as does EDTA to a much greater extent. This was allowed for by using a computer program, 'FRION' to

calculate free ion concentrations in solutions containing EGTA. 'FRION' was written in FORTRAN language on a PDP 11 / 73 computer by Dr. Noel Davies and Dr. Helmut Zucker, based on stability constants given in Martell & Smith (1974) and using a procedure described by Storer & Cornish Bowden (1976).

Using 'FRION', it was calculated that adding 2.36 mM Mg^{2+} to a solution containing 10 mM EGTA, would give 2 mM of free Mg^{2+} . The Mg^{2+} -free internal pipette solution used 10 mM EDTA (ethylenediaminetetraacetic acid) in place of EGTA, since this is a stronger chelator of Mg^{2+} than is EGTA.

The osmolarities of the internal pipette solutions and external bath solutions were measured and compared. If necessary, supplementary sucrose was added to the internal pipette solution, adjusting the osmolarity to exceed that of the external bath solution by approximately 20 mOs / kg. This was found to help in the formation of seals between the micropipette and the cell membrane, by exposing the enclosed membrane to a solution which is hypertonic compared to the cell interior.

All solutions were stored in a refrigerator at 4 °C. Before adding cells, or using in a micropipette, solutions were allowed to reach room temperature.

2.3.3 The patch clamp set-up

For electrophysiological recording, approximately 100 μ l of washed induced MEL cells were placed in a 35 mm plastic dish containing about 2 ml of filtered external bath solution which had been allowed to reach room temperature. The cells were allowed to settle for half an hour, after which time they adhered sufficiently to the surface of the dish to make micropipette approach and seal formation easier.

The plastic dish was placed in a perspex bath chamber, resting directly on the stage of the microscope.

2.3.3.1 Microscope

An inverted Nikon microscope was used to visualise the cells in their dish and the micropipette, from entry into the external bath solution, through approach, and contact with the surface of an appropriate cell to seal formation (see Seal Formation, below). Thus, the space between the objective lenses and the condenser contained the amplifier headstage, the electrode holder, the electrode and the cells. This arrangement allowed the visualisation at high magnification of the micropipette tip, from entry into the bath, right down to cell level.

2.3.3.2 Micromanipulator

The headstage of the amplifier was fixed solidly to a plexiglass plate rigidly attached to the micromanipulator, in an attempt to decrease mechanical vibration. The micromanipulator utilised both coarse mechanical movement and fine, motorised, remote-control movement, both in three dimensions.

2.3.3.3 Air Table and Faraday Cage

The microscope, and all equipment physically attached to it, were placed on an air suspension table, inside a Faraday cage. The air suspension table (Wentworth Laboratories Ltd., Bedford) consists of a heavy top resting on pneumatic supports, kept inflated using a nitrogen gas cylinder. An earthed Faraday cage was used to shield the amplifier headstage, microscope etc. from stray radiative interference, such as 50 Hz line frequency noise from artificial lighting or power sockets, noise from other electrical components of the patch clamp set-up such as computers, or even from external sources such as radio wave transmitters. The Faraday cage is connected to ground through a low resistance connection. Alternating current electric field signals are converted to current by interaction with the extruded aluminium material of the cage, and this is conducted to ground. It is important for all conductive material within the Faraday cage to be grounded at the same single point as the cage, and for this connection not to form any loops which could cause induction.

The micromanipulator remote control and its 12 V power supply were placed outside the cage.

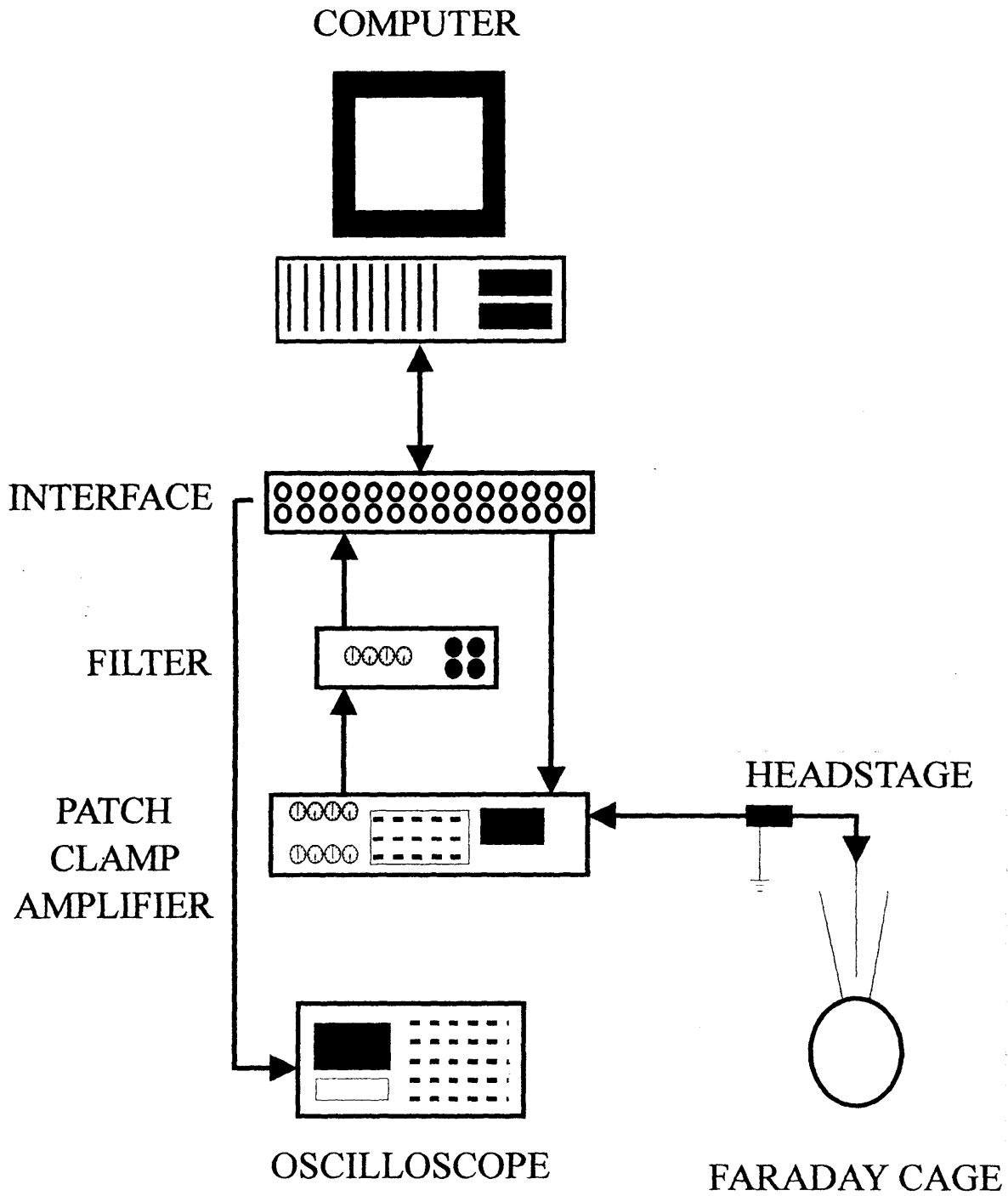


FIGURE 2.1: The patch clamp set-up.

2.3.3.4 Headstage and Amplifier

Currents were recorded using the Axopatch 200A amplifier (Axon Instruments, Foster City, CA, USA). With this amplifier in whole-cell voltage clamp mode, the amplifier headstage works using the principle of resistive feedback (Figure 2.2A)

The amplifier converts the tiny membrane currents recorded by the pipette into voltage signals using a feedback resistor R_f of extremely high resistance, typically 500 M Ω , to provide adequate gain. The amplifier also controls the potential of the pipette, allowing it to effectively voltage clamp the whole cell.

It is the potential difference between the operational amplifier inverting (-) and non-inverting (+) inputs that is amplified. The current source being measured is attached to the inverting input, which (assuming that the inputs have infinitely high resistance) draws no current, forcing the measured current to pass through the feedback resistor, R_f . Basically, the circuit uses negative feedback through R_f to maintain the inverting input of the operational amplifier at virtual ground. The operational amplifier output develops a voltage, V_0 , proportional to the input current, I_m , (Ohm's Law) such that:

$$V_0 = -I_m R_f$$

(Equation 2.1)

Command voltages, V_{com} , are applied to the non-inverting (+) input of the operational amplifier, and through feedback, applied to the pipette (Figure 2.3B). The

voltage recorded at the output of the headstage operational amplifier is thus the sum of $V_0 (= -IR_f)$ and the command voltage, V_{com} .

A subsequent differential operational amplifier in a boost circuit subtracts the V_{com} , and gives the value of V_0 . These stages are followed by several other amplification and filtering circuits.

The resistance value of the feedback resistor puts a limit on the maximum size of current that the circuit can measure; the lower the resistance, the greater the upper limit of output voltage. A 500 M Ω feedback resistor can only measure currents up to 30 nA, if the 15 V power supply of the amplifier is taken as the maximum value of V_0 (Ohm's Law). Taking into account the fact that the thermal current noise of a resistor is inversely proportional to the value of the resistance, and therefore decreases with a higher resistance value, a compromise must be reached. A 500 M Ω feedback resistor allows a good signal-to-noise ratio, and the currents recorded in this project were well within the limit stated above.

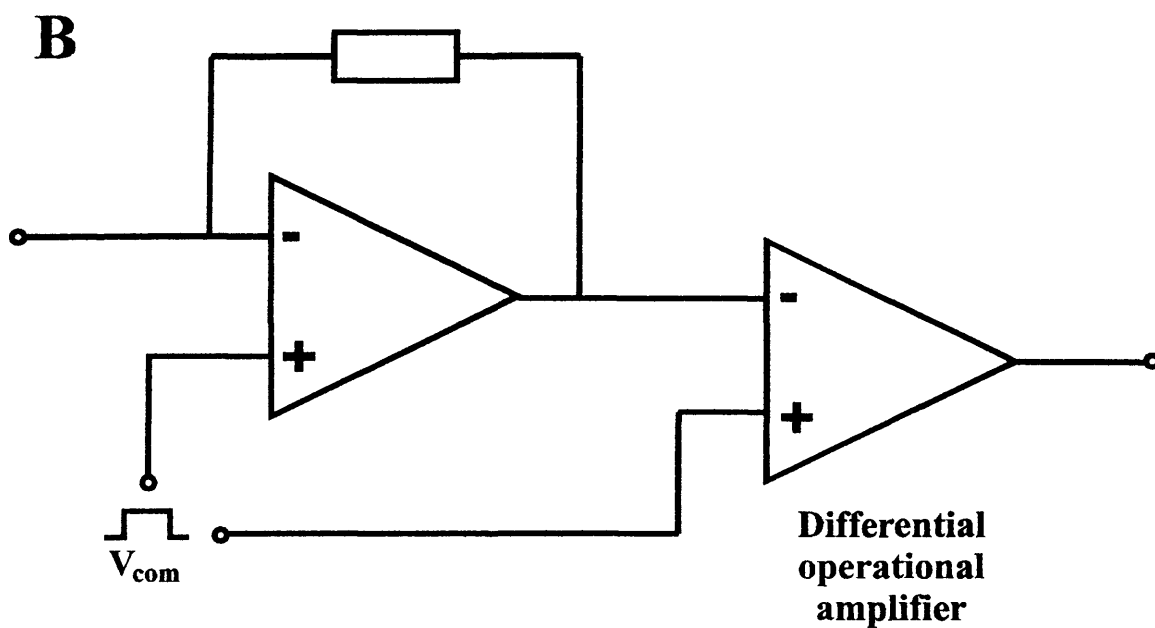
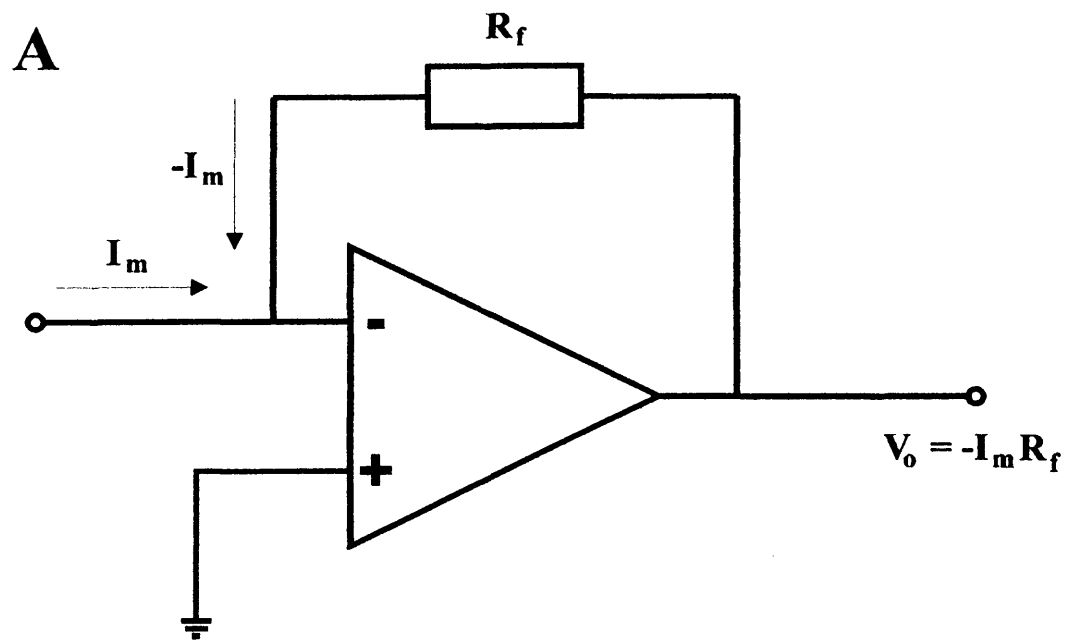


Figure 2.2 A: The patch clamp headstage is a resistive feedback current to voltage converter. **B** Command potentials are applied to the pipette and removed from subsequent headstage recorded operational amplifier voltage output via a differential operational amplifier.

2.3.3.5 Computer and interface

A Dell 486/P66 personal computer (Dell Computer Corporation, Bracknell, Berks) was used to control the Axopatch 200A patch clamp amplifier through the Labmaster TL-1 Digital to Analogue Converter Interface (Axon Instruments). This was achieved using software written using the AxoBASIC subroutine library (Axon Instruments) (Davies, 1993) to produce voltage pulse protocols, and then to record the resultant data directly to hard disk

Voltage pulses from the interface were sent to the external command input of the amplifier. The resulting current output is available to the computer for storage after digitisation (analogue to digital conversion) by the interface.

2.3.3.6 Oscilloscope

A Gould 420 digital storage oscilloscope (Gould Instruments, Ilford, Essex) was triggered from an output of the interface, and connected to the amplifier, to monitor currents. This proved to be very versatile due to the ease of change of gain, sweep speeds and so on, without affecting recordings, and because the storage facility and persistence allowed currents to be retained and examined.

2.3.3.7 Filters

Filtering is used to improve signal - to - noise ratios. An 8-pole low-pass Bessel filter of variable cut-off frequency (-3 dB) was used in addition to the built-in low-pass Bessel filter of the Axopatch 200A amplifier. According to the correction for a number of filters connected in cascade, the overall cut-off frequency, f_c , is given by:

$$\frac{1}{f_c^2} = \frac{1}{f_1^2} + \frac{1}{f_2^2} + \dots + \frac{1}{f_N^2}$$

(Equation 2.2)

where $f_{1\dots N}$ are the cut-off filter frequencies of N filters in cascade. So, the filters were set such that the final corrected frequency was approximately 1 kHz; for example, Bessel filter set at 1 kHz and Axopatch 200A filter at 10 kHz gave a corrected value of 995 Hz

2.3.4 Recording using the Axopatch 200A amplifier

The high resistance gigaohm seal formed between the micropipette glass and the cell membrane in patch clamp recording is highly stable, both electrically and mechanically. Typical values of tens of gigaohms for the resistance enable good

electrical isolation of the patch enclosed within the micropipette, and help to reduce the background noise. Thus, microscopic single channel currents can be resolved.

The whole-cell configuration allows direct access to the cytoplasm, and interchange of contents between the micropipette and the cytoplasm. The following paragraphs describe the methods used in order to form a seal, and set up the MEL cell in the whole cell configuration, ready for the recording of macroscopic whole-cell currents.

Micropipettes were usually fire polished just prior to use to ensure that they were smooth and free from any debris that might interfere in the sealing process. Internal pipette solution was introduced into the micropipette using a syringe fitted with a 0.22 μm filter and 0.2 ml plastic Gilson tip (drawn out to a fine tip using heat). The micropipette was filled to about a third of its length to enable contact between the silver/silver chloride internal reference electrode and the internal pipette solution. This solution therefore provides the final connection from the cell interior to the electrode. It was important to remove any small bubbles that might be occluding the micropipette tip. This was done by shaking or gently flicking the micropipette with a finger.

To avoid damage to the delicate circuitry of the headstage by static electricity, a grounded metal object was touched prior to touching the headstage to discharge any static build up. The micropipette was mounted into a polycarbonate and Teflon (for low noise and insulation) holder which holds it firmly and forms an airtight seal. The silver/silver chloride internal reference electrode feeds into the micropipette at one end and to a small pin at the other end for connection to a Teflon input connector in the amplifier headstage.

The circuit is completed by connecting the gold-plated headstage case ground to the bath electrode, a silver/silver chloride pellet which sits in a well in the perspex bath chamber, which is filled with internal pipette solution. This well is connected to the cell dish by a capillary tube filled with internal pipette solution.

The micropipette was lowered into the bath solution, with positive pressure applied with a syringe and polythene tubing through the pipette holder. This forces the internal pipette solution to flow out through the tip, preventing the build up of contaminating particles on the smooth end of the tip from the surface of the liquid, or indeed from within the bath solution.

The computer was used to apply 1 mV test pulses of 50 ms duration through the digital to analogue interface, in order to monitor the progress of seal formation. The resulting current through the pipette tip appeared as square pulses on the oscilloscope and computer, the amplitude of which depends upon the pipette resistance. No holding potential was applied at this stage.

A suitable cell was found, and the micropipette moved close to (but not touching) the cell, using the coarse mechanical manipulator first, and then the motorised remote control micromanipulator. Generally, round cells which appear phase bright under the microscope have been found to be easier to form gigaohm seals with than cells which appear flat.

At this stage the pipette offset was monitored in the 'TRACK (I=0)' mode, with the meter switched to V_{TRACK} . This shows any voltage offset between the bath electrode and the internal reference electrode in the micropipette, and was adjusted to zero. The pipette was gently touched against the cell, taking care not to pierce the cell membrane. Upon contact, the current pulse decreased in size, indicating that the

pipette resistance had increased. The pipette offset was again adjusted to zero if necessary, the mode switched to 'V-CLAMP' and the meter switched to V_m .

Disconnecting the syringe, and releasing the positive pressure is often enough to cause the formation of a gigaohm seal as the area of membrane enclosed within the tip springs back from its initial deformation. This is seen as a decrease in the amplitude of the current pulse (an increase in resistance) on the oscilloscope and computer. If a gigaohm seal has formed, the rectangular pulse shrinks down to a flat line with spikes of capacity current at the rising and falling edges of the voltage pulse.

Often, gentle suction was required to achieve this final stage. Changing the size of the voltage pulse to 10 mV, or changing the gain on the oscilloscope makes it easier to judge whether the endpoint has been reached, and the resistance of the seal can easily be calculated this way.

The capacitance spikes are due to the voltage change resulting from the rectangular pulse causing charging of the pipette and holder capacitances, and also stray capacitance at the headstage. The spikes have a large, fast component, and a smaller, slower tail, which appears to be characteristic of the glass type. These can be responsible for saturating the head stage output, and a sufficiently large voltage step can result in the fast capacity transient saturation persisting for times in the order of ms. The capacitance spikes can be reduced or even cancelled using the amplifier pipette capacitance compensation circuits, which inject a charging current by a separate pathway.

A holding potential of - 80 mV was set. The whole cell configuration was achieved by applying strong suction with the syringe. Rupture of the enclosed cell membrane is indicated by the appearance of large capacity transients, which are due entirely to the whole cell capacitance (if all the pipette capacitance has already been

compensated for). This cell capacitance is charged through the series resistance (access resistance of the pipette and ruptured membrane junction), which can cause problems due to the IR voltage drop, the bandwidth of current measurement, and the noise associated with the voltage clamp. When a current, I_m flows, the presence of the series resistance causes an error between the clamped pipette potential, V_{com} , and the actual value of the cell's membrane potential:

$$\text{voltage error} = I_m R_s$$

(Equation 2.3)

that is it say, an ionic current of 2 nA through a series resistance of 5 M Ω will result in a 10 mV error between the applied command potential and the actual membrane potential experienced by the cell.

For voltage clamp of voltage-activated ionic currents, it is particularly important for there to be accurate control of the cell membrane potential to prevent errors of estimation of the voltage-dependence of resultant currents.

The Axopatch 200A WHOLE CELL CAP. and SERIES RESISTANCE controls were used to minimise the size of the capacitance transient. This was sometimes made easier by first physically reducing the series resistance of the ruptured patch, by repeated strong suction pulses from the syringe, while taking care not to break the seal. This resulted in shorter duration capacitance spikes, though since the area under the spike is equal to the unchanged capacitance of the cell, the spikes increased in amplitude. Series resistance compensation minimises the size of the voltage drop across the access resistance by adding a signal to V_{com} that is proportional to the current. After adjustment with the controls minimised the size of

the spikes, the settings on the WHOLE CELL CAP. and SERIES RESISTANCE controls represented the actual values of these parameters, unique to the cell clamped by that particular pipette.

2.3.5 Data Analysis

2.3.5.1 Data Storage and Software

The STIMTOR programme, written in Microsoft V.7.1. BASIC using the AxoBASIC subroutine library (Axon Instruments) (Davies, 1993), was used to apply voltage pulse protocols and simultaneously acquire data. This data was displayed on screen, and could be written to files on the personal computer hard drive. The files were subsequently manipulated and analysed using the TRACAN trace analysis programme, which allowed direct control over the data arrays and internal parameters such as gain. TRACAN also allowed the facilities of further export of data to spreadsheets and graph drawing packages for production of figures.

2.3.5.2 Leak subtraction

A 'P / 6' method of leak subtraction was used to subtract capacitive and leakage currents from whole cell records in data files. During voltage pulse protocols, each test pulse was followed by 12 pulses of $1 / 6^{\text{th}}$ of the amplitude of the test pulse. These 12 pulses were too small to activate any membrane currents. Thus the resulting

current comprised only capacitive and leakage current. These leak pulses were written to the data files along with the membrane currents of the test pulse.

Assuming that the amplitude of the capacitive and leakage currents are linearly proportional to the size of the voltage step, these currents were scaled to the test pulses, and digitally subtracted from the membrane currents. The subtracted currents were written to a new file, for further analysis and manipulation.

2.3.5.3 Curve fitting

Curve fitting software was used to obtain the best fit of a suitable mathematical function to a set of data points. The parameters of the function describe the behaviour or shape of the set of data points, or when a theoretical function describing the data is known for example exponential decay or rise, parameters such as time constants can be extracted from the fit. Curve fitting software follows iterative procedures, from starting parameter estimates, continually refining parameter values to optimise the fit. The fits were obtained by minimising least squares using a SIMPLEX routine.

Fitting functions to data records using TRACAN involved manually setting fit and parameter limits, for example, time, $t = 0$, or the fit limits on tail currents to be fitted by a function describing exponential decay. After setting further conditions, such as number of exponentials to be fitted, offsets, 'fit every x^{th} point' etc, the function was repeatedly fitted until no improvement was found, and the curve fit displayed with the data points, and fit parameters.

Fitting functions to derived data from spreadsheets etc. for example using the graph-drawing package SigmaPlot (Jandel Scientific, San Rafael, CA, USA) followed a similar iterative process to fit defined mathematical fit functions, such as Boltzmann equations (see below, Chapters 3 and 4).

The data were statistically tested using SigmaStat (Jandel Scientific, San Rafael, CA, USA) performing paired Students t-test with significance at $p < 0.05$. All numerical values are presented as means \pm standard error of the means (SEM).

CHAPTER THREE

Whole Cell Recording of Voltage-Activated Delayed Rectifier Potassium Currents from Kv1.5 / hPCN1 Channels

3.1 Introduction

Delayed rectifier currents are characteristically activated upon depolarisation from the resting membrane potential, with a sigmoidal, delayed onset (though activation is rapid, typically in the order of milliseconds). Delayed rectifiers were classically called such in comparison to the much faster activation of sodium channels. This class of channel remain open whilst depolarisation persists, since inactivation tends to be very slow or absent altogether. Delayed rectifiers limit the duration of single action potentials because they open during depolarisation, playing a major role in action potential repolarisation.

The gene for hPCN1 (or Kv1.5) encodes a delayed rectifier potassium channel in the human heart. hPCN1 is the human homologue of the rat heart potassium channel RK4 (Roberds and Tamkun, 1991). Both of these homologues have been designated Kv1.5 since they are 86% identical. Most of the differences in the sequences occur in the amino - and carboxyl - terminal regions (64 % and 74 % identity respectively). Although the nomenclature of Chandy, Douglass, Gutman, Jan, Joho, Kaczmarek, McKinnon, North, Numa, Philipson, Ribera, Rudy, Salkoff, Swanson, Steiner, Tanouye and Tempel (1991) has standardised the naming of such 'identical' clones, I have also used some of the non-standard names here to emphasise the nature of the tissue - specific isolation and characterisation of homologues before identification. It is likely that the small differences in overall identity represent simple variation between species rather than indicating that the human, rat, canine, bovine, rabbit (and so on) channels are different isoforms.

Using Northern blot analysis of total RNA from each tissue with probes specific for the clone, Kv1.5 has been found, in the rat, to be abundant throughout the atrium, ventricle and aorta of the heart as well as in skeletal muscle, and to a lesser degree in brain (Roberds and Tamkun, 1991). The gene has also been cloned from human islet β -cells (although the clone was isolated from a human insulinoma cDNA library, RNA amplification by the polymerase chain reaction has demonstrated the presence of Kv1.5 RNA in normal human islets indicating that this potassium channel may be involved in normal islet function; Philipson, Hice, Schaefer, LaMendola, Bell, Nelson and Steiner, 1991); canine gastrointestinal smooth muscle (85 % overall identity with the human homologue; Overturf, Russell, Carl, Vogalis, Hart, Hume, Sanders and Horowitz, 1994); bovine adrenal medulla (clone entitled BAK5, using a cDNA library from the medulla and a bovine genomic library; Garcia-Guzman, Sala, Criado and Sala, 1994) and human, canine, rat and mouse skeletal muscle.

In the rabbit heart, the cDNA clone isolated, termed RBKv1.5 (Sasaki, Ishii, Nunoki, Yamagishi and Taira, 1995), also had about 85% overall shared amino acid identity with clones from the other species. In the human heart, Kv1.5 has been cloned from both ventricle (initially termed HK2; Snyders, Tamkun and Bennett, 1993; Tamkun, Bennett and Snyders, 1994) and atrium (Fedida, Wible, Wang, Fermini, Faust, Nattel and Brown, 1993).

Thus, one of the most important steps in correlation of the cloned channels with endogenous currents has to be in terms of easily measured biophysical properties, using a

heterologous expression system where the individual channel system can be studied using physiological solutions, without other contaminating currents.

3.2 Results

Here, experiments were carried out in the whole cell configuration of the patch clamp technique to determine the biophysical characteristics of cloned Kv1.5 channels from the gene transfected into MEL cells, as described in Materials and Methods.

External bath solutions contained (except where stated) 140 mM NaCl, 5 mM KCl, 2 mM CaCl₂, 2 mM MgCl₂ and 10 mM HEPES. Internal pipette solutions contained 140 mM KCl, 2 mM free Mg²⁺ (though 5.8 mM total MgCl₂ was used), 10 mM EGTA, 10 mM HEPES and 20 mM glucose. All solutions were adjusted to pH 7.2.

Current records were filtered using an 8-pole Bessel filter set at a cut off frequency of 1 kHz (-3 dB) and where two filters were used in series, the composite frequency was also kept at approximately 1 kHz, as described in Materials and Methods. All the currents shown in this chapter have been leak subtracted as described in Materials and Methods. There was no correction for junction potentials (see below).

3.2.1 The voltage dependence of Kv1.5

The Kv1.5 whole cell current was characterised under voltage clamp conditions. The whole cell current-voltage relationship was investigated, to show how the size of the current passing through the channel varied with the potential of applied voltage steps. Figure 3.1A shows a family of currents elicited by applying 50 ms depolarising voltage steps in increments of +10 mV, from -60 mV to +60 mV, all steps being applied from, and returning to, a holding potential of -80 mV. This voltage pulse protocol is shown below the current family on the same time scale.

The family of currents was characteristic of voltage-activated delayed rectifiers, with sigmoidal onset, and no apparent decay over the course of the 50 ms pulse. The size of the outward current increased with more positive pulses.

Figure 3.1A represents the response to very brief pulses. If longer depolarising pulses in the order of seconds were applied, current inactivation became apparent for the more positive potential steps. Figure 3.1B shows currents recorded using pulses to the same voltages as in Figure 3.1A, but of 4 seconds duration. The extent of the current inactivation over this period can be seen, with substantial inactivation for voltage pulses positive to about 0 mV.

To construct a current-voltage relation, the peak values of the leak subtracted currents elicited at each step during the 50ms pulse were plotted versus the membrane potential of the step (Figure 3.1C). Outward current was first apparent at membrane potentials positive to about -30 mV, and increased with more positive pulses, as expected

for delayed rectifier channels, as more channels opened, and the driving force grew due to the increasing electrochemical gradient for potassium ions across the cell membrane.

3.2.2 The reversal potential and selectivity of Kv1.5

The reversal potential for Kv1.5 under physiological conditions was found by measuring an instantaneous current-voltage relationship. The reversal potential is that voltage at which there is no net current flow.

The tail currents shown in Figure 3.2A are the result of repolarising steps back to varying potentials following a common 50 ms duration first pulse to +40 mV, which maximally activated the current, while being too short for appreciable inactivation to occur. Repolarising steps to potentials more negative than -20 mV step lead to deactivation, as channels close, and current declines exponentially. The initial, instantaneous value of this tail current varied with the repolarising step potential. It decreased with more negative potentials of the repolarising step, that is, as the driving force on the movement of potassium ions through the channel given by membrane potential, V , minus potassium equilibrium potential, E_K decreased, and it finally reversed direction.

$$\text{driving force} = (V - E_K)$$

(Equation 3.1)

To obtain an estimate of the initial current, a single exponential, as shown in Equation 3.2 below, was fitted to the tail currents at each potential, as described in the Methods, and extrapolated to the beginning of the repolarising step. The value of the initial, or instantaneous current was given by I_0 :

$$I_t = I_0 e^{(-t/\tau)}$$

(Equation 3.2)

where I_t represents the current at time t and τ is the time constant of deactivation fitted to the decay of the current. This gives an estimated value for instantaneous current, I_0 , at the beginning of the variable pulse. I_0 was plotted against repolarising pulse potential, as shown in Figure 3.2B, and the reversal potential of Kv1.5 channel currents found from the intercept on the x-axis, in other words, where the direction of the tail current reverses. In 5 mM external K^+ , this was found to be -77.3 mV (± 0.8 mV, $n = 12$). The expected value for the reversal potential under these ionic conditions (assuming perfect selectivity for potassium ions) was estimated from the Nernst equation for the potassium equilibrium potential:

$$E_K = \frac{RT}{F} \ln \frac{[K^+]_o}{[K^+]_i}$$

(Equation 3.3)

where E_K is the potassium equilibrium potential, R is the gas constant

($8.315 \text{ J K}^{-1} \text{ mol}^{-1}$), T is the absolute temperature (293.16 K), F is Faraday's constant ($9.648 \times 10^4 \text{ C mol}^{-1}$), and the subscripts o and i represent outside and inside the cell respectively.

For these external and internal solutions, E_K at 20 °C was calculated to be -83.3 mV. It can be seen that the reversal potential actually found for the current through Kv1.5 channels was not quite as negative as that calculated given perfect selectivity for potassium ions.

Tail currents were also used to measure reversal potentials using external solutions of (i) 70 mM external K^+ (with 70 mM external Na^+) in Figure 3.2C and (ii) 35 mM external K^+ (with 105 mM external Na^+) shown in Figure 3.2D. The values of E_K were calculated from the Nernst equation to be -17.3 mV and -34.7 mV respectively for these solutions. These compare to measured reversal potential values of -12.5 mV (± 0.5 , $n = 6$) and -29.6 mV (± 0.9 , $n = 7$) in 70 and 35 mM external potassium respectively. As mentioned at the beginning of the results for this chapter, there was no correction for liquid junction potentials carried out. Junction potentials exist at the pipette tip in patch clamp recording when the bath solution and pipette solutions are of different ionic composition. This is because, in the case of a pipette containing KCl and bath solution of mostly NaCl, K^+ ions have a higher ionic mobility than Na^+ ions, and therefore diffuse out of the patch pipette more rapidly than Na^+ ions in, producing a net negative charge on the pipette with respect to the bath. The results shown above for reversal potentials in 5, 70 and 35 mM external potassium bath solutions show a difference of +6, +4.8 and +5.1 mV respectively between calculated theoretical and average measured values and this may indicate the presence of liquid junction potentials.

It can be seen from the instantaneous current-voltage relations for the three external solutions, Figures 3.2B, C and D, that instantaneous current points plotted at more depolarised potentials appear to follow a linear relationship with voltage, there appearing to be a curvature (this can be described as a type of ‘rectification’) at more negative potentials with decreased external potassium. This effect diminishes with increasing external $[K^+]_o$, that is in 70 mM K^+_o , the instantaneous current-voltage relation is closer to a straight line than that in 5 mM. This curvature was predicted by the constant field theory, a model of the movement of ions through the membrane first produced by Goldman in 1943, and later expanded by Hodgkin and Katz (1949). This model was so called because the electrical gradient across the membrane was assumed to be linear. The membrane was assumed to be homogenous, and ions were predicted to cross the membrane independently of each other and at a rate proportional to that in free solution. The curvature of the data in Figures 3.2B, C and D can be fitted with an expression such as

$$I_K = P_K \frac{VF^2}{RT} \left\{ \frac{[K^+]_i e^{(VF/RT)} - [K^+]_o}{e^{(VF/RT)} - 1} \right\}$$

(Equation 3.4)

where I_K is the potassium current at membrane potentials V taken from the data points in the above plots, and P_K represents a permeability coefficient for potassium, in this case with the units $\text{cm}^3 \text{s}^{-1}$. The values of P_K returned from the fit of the above constant field

current equation were 6.0×10^{-8} , 6.4×10^{-8} and $5.4 \times 10^{-8} \text{ cm}^3 \text{ s}^{-1}$ respectively for the experiments in 5, 35 and 70 mM external potassium bath solutions respectively

The above analyses in comparing the calculated and measured values of reversal potential and the quite precise fitting of a constant field current equations to the curvature of measured data are still somewhat limited. This is because one permeant ion, K^+ , is assumed. Because the measured reversal potentials were found to be more positive than the calculated equilibrium potentials for potassium ions using those particular experimental solutions, this may pose questions about the selectivity of the channel for potassium ions.

In order to estimate the selectivity of a channel in the membrane, it is necessary to compare the permeabilities of the channel to ions other than just K^+ . To take into account the permeability to both K^+ and Na^+ , a derivative of the Hodgkin-Katz constant field voltage equation was used. This equation has the advantage of taking into account the imperfect selectivity of the channel for K^+ ions, and describes the relationship between the permeabilities of both potassium and sodium ions:

$$E_{\text{rev}} = \frac{RT}{F} \ln \left(\frac{[\text{K}]_o + \alpha[\text{Na}]_o}{[\text{K}]_i} \right)$$

(Equation 3.5)

where E_{rev} represents the reversal potential, and $\alpha = P_{Na} / P_K$, the ratio of the permeability to sodium ions to the permeability to potassium ions. This measure of permeability ratios is therefore useful as an indicator of selectivity.

Figure 3.3 shows theoretical calculated values of E_{rev} at all different external potassium concentrations shown as the solid line determined from calculations using the Nernst equation as above, and assuming that the channel is perfectly selective for potassium ions. For this line, a value of 140 mM was used for $[K^+]_i$, a value of 25.24 for used RT/F . E_{rev} was calculated for all the values of $[K^+]_o$ used. The values of all the reversal potentials found as shown in Figure 3.2 above were plotted as the open circles against $\log [K^+]_o$ for the three different concentrations of external potassium used (hence three clusters of circles). These data were fitted with a function based on Equation 3.5 above, in order to generate a best fit value for α . To allow for possible uncorrected liquid junction potentials, a value of +5 mV was assumed and added to the right hand side of the equation. The broken line on the graph represents the value of reversal potential measured at each external potassium concentration, and adjusted with the Hodgkin-Katz equation as above. It was found that the results were best fitted with a permeability ratio of 0.0025. This suggests that this channel is $1 / 0.0025 = 400$ times more permeable to K^+ ions than for Na^+ ions. The characteristic high ionic selectivity of voltage-gated potassium channels (Hille, 1992) is thus confirmed for Kv1.5. This result must be presented with caution however, since the size of uncorrected liquid junction potentials must be a factor, as well as the limited range of different bath solutions used. Note the curvature at lower concentrations of external potassium of the Hodgkin-Katz adjusted line

which described the measured data, away from the theoretical perfectly selective Nernst equation line.

Fitting a single exponential to the decay of these deactivating tail currents also gives a time constant for deactivation, $\tau_{\text{deactivation}}$. Deactivation occurs when the stimulus ends, the membrane potential is returned to a negative value, so that channels close. Thus, it is distinguished from inactivation which is a kinetically distinct process that begins at the same time as activation, and occurs under continued depolarisation, continuing even while the stimulus is still present. The variation of this time constant of deactivation with membrane potential is shown in Figure 3.4. $\tau_{\text{deactivation}}$ was plotted on a log scale versus the membrane potential for 5 mM, 35 mM and 70 mM external potassium bath solutions (shown as circles, triangles and squares respectively). In each case, the time constant was found to be voltage-dependent, with deactivation being much quicker with increasingly negative potentials. It was also found that large standard errors of mean (represented by the error bars) occurred for the points which coincided with the average values of E_{rev} found for each external potassium concentration. This is due to the difficulty in accurately fitting the deactivating tail currents at potentials close to E_{rev} where tail currents are very small.

3.2.3 Voltage dependence of steady-state activation for Kv1.5

Tail currents were also used to study the voltage dependence of activation of Kv1.5 as is shown in Figure 3.5A, with the arrow illustrating expanded tail currents fitted with exponentials.

Generally, the size of macroscopic current through a homogenous population of channels, I , can be expressed in terms of the single channel current, i , the total number of channels, N , and the channel open probability, P_{open} , by the relationship:

$$I = NiP_{\text{open}}$$

(Equation 3.6)

The voltage pulse protocol shown in Figure 3.5A has a 50 ms potential first pulse, to a series of potentials in 10 mV steps from -60 mV to +70 mV, resulting in the activation of K^+ channels. The size of the current due to this first pulse is proportional to the respective N , i and P_{open} at each potential. On repolarising back to the constant voltage pulse of -40 mV for 100 ms, the driving force for the tail current becomes the same in all cases, so that i becomes constant. This results in an instantaneous current proportional to the number of open channels ($= N \cdot P_{\text{open}}$) at the instant of stepping back to -40 mV, because the channels do not have time to close. This means that the voltage-dependence of P_{open} can be obtained by varying the potential of the first pulse, whilst keeping the repolarising pulse constant. Thus, the number of open channels depends

upon the membrane potential of the first pulse, and the driving force due to the second, repolarising pulse is constant. Instantaneous currents were found (as above) by fitting an exponential to the tails, as illustrated for three of the records, and these instantaneous current values were normalised to the maximal current value and plotted versus membrane potential of the initial variable pulse.

It is reasonable to assume that N , the total number of available channels, does not change during the course of the pulse protocol. The plot of instantaneous current versus the membrane potential of the first pulse therefore shows how P_{open} changes with membrane potential, since N and i are constant during the measurements in this experiment. Figure 3.5B shows averaged data \pm SEM for the activation plots from 13 cells. The activation curve for each set of data was fitted with a Boltzmann function:

$$f = \frac{I}{I_{\text{max}}} = \frac{1}{\left(1 + \exp\left[\left(\frac{V_{1/2} - V}{k}\right)\right]\right)}$$

(Equation 3.7)

where I represents instantaneous tail current and I_{max} equals maximal instantaneous tail current; $V_{1/2}$ equals the membrane potential at which the value of I is one-half of I_{max} , that is where half the available channels are activated; and k , the 'slope factor', is proportional to the steepness of the voltage dependence, and is a function of the gating charge indicating the equivalent number of channel protein charges that must move within the membrane voltage field to allow the conformational change leading to channel opening. $k = 24$ mV for the movement of one elementary charge.

The value of $V_{1/2}$ was found to be $-6.8 \text{ mV} (\pm 1.3 \text{ mV}, n = 13)$ and the mean value of slope factor, k to be $6.8 \text{ mV} (\pm 0.3 \text{ mV})$ for experiments in $5 \text{ mM } [K^+]_o$.

The slope factor value of approximately 6.8 mV indicates the equivalent movement of $24 / 6.8 = 3.529$ elementary charges across the width of the membrane voltage field, that is, gating charge is approximately 3.5 elementary charges.

Figures 3.6A and 3.6B show averaged activation curves for Kv1.5 in 70 mM , and $35 \text{ mM } [K^+]_o$; fitting the Boltzmann equation to the each set of activation curves gave mean values of $-9.2 \text{ mV} (\pm 1.1 \text{ mV}, n = 7)$ and $-3.7 \text{ mV} (\pm 2.1 \text{ mV}, n = 8)$ respectively for $V_{1/2}$; $6.8 \text{ mV} (\pm 0.2 \text{ mV})$ and $9.0 \text{ mV} (\pm 0.6 \text{ mV})$ respectively for k .

Student's t-tests were carried out to compare these mean values with those in $5 \text{ mM } K^+$. There was no significant difference between mean values of half-maximal activation ($P = 0.22$ and 0.19 respectively for 70 mM and 35 mM external potassium) between those in 5 mM external potassium and each of 35 mM and 70 mM external potassium solutions. The mean value for slope factor from the 70 mM external potassium data was almost identical to that for 5 mM ($P = 0.94$), but the mean value for slope factor using 35 mM external potassium was calculated to be significantly different ($P = 0.001$). However, the tail currents were elicited by a voltage pulse to -40 mV (Figure 3.5). Using these internal and external potassium concentrations, the closeness of this to the reversal potential, -34.7 mV , calculated from the Nernst equation (Equation 3.3), probably indicates the inaccuracy of the parameters found from the exponential fit to the inward

tail currents in this solution. Using 70 mM external potassium however, much larger inward tail currents were elicited, making accurate measurement easier.

3.2.4 Hodgkin-Huxley activation kinetics

Hodgkin and Huxley created a model describing permeability changes, accurately predicting features of excitability in terms of movements of independent charged particles within the cell membrane. Activation and inactivation were described as independent processes, activation being rapid, and opening channels during a depolarisation, whereas inactivation is slower, and closes channels during a depolarisation. Inactivated channels cannot be activated until inactivation is removed either by repolarisation or hyperpolarisation. The model allowed conductance changes to be expressed in terms of voltage and time only. The sigmoidal shape of the increase in potassium conductance on depolarisation can be described by the increase of current such that

$$I_t = I_\infty \left[1 - e^{(-t/\tau)} \right]^n$$

(Equation 3.8)

where I_t is the current at time t , I_∞ is the final value of the current, τ is the time constant of activation, and n represents the number of independent particles that need to be in the correct position within the membrane to allow channel opening for example. In Hodgkin

and Huxley's model, n was set at 4 (for easier calculations). This gave a good fit. This equation then suitably describes the rise of current on activation.

This function was fitted to the rise of Kv1.5 currents such as those shown in Figure 3.5A. It was found that a better fit was achieved with n constrained to 5. An example of a fitted current is shown in Figure 3.7A. $\tau_{\text{activation}}$, the time constant of activation was thus measured, and plotted on a linear scale, as in Figure 3.7B, and a common log scale, as in Figure 3.7C against the membrane potential of the activating pulse. The points on the graphs represent mean values of $\tau_{\text{activation}} \pm \text{SEM}$ for 10 cells.

The voltage dependence of this time constant can be seen. For a depolarising pulse of -30 mV, the average value of $\tau_{\text{activation}}$ is about 22.6 ms. For a pulse to -20 mV, the average value of $\tau_{\text{activation}}$ is 11.8 ms, or about half that at -30 mV. However, as the potential of the depolarisation increases, the time constants become less steeply voltage dependent. The value of $\tau_{\text{activation}}$ at +60 mV, 1.5 ms, is nearly half of that (3.1 ms) for a depolarisation of +20 mV. From the activation curve in Figure 3.5B, it can be seen that at potentials above +20 mV, a plateau phase is seen, that is to say, all available channels are activated.

3.2.5 Steady state inactivation in Kv1.5

Inactivation was more difficult to examine than activation because Kv1.5 is a very slowly inactivating delayed rectifier. The voltage pulse protocol used initially, employing a 5 second pulse to try to inactivate the channels to reach steady state was found to be too

short for inactivation to develop fully. The voltage pulse protocol was therefore modified so that the cell was held for a 60 second conditioning pre-pulse at variable potentials before a single test pulse to +20 mV. Currents elicited by the test pulse became larger as the first pulse was made increasingly more negative, reaching a plateau level, usually at potentials more negative than -40 mV. This is shown for the averaged data from 3 cells in Figure 3.8A. The peak values of current were normalised to the average of the values at this plateau, and plotted versus the potential of the conditioning pre-pulse.

Again, each of the resulting curves were fitted with a Boltzmann function as in Equation 3.7 above. Mean values of half maximal steady state inactivation occurred at -22.0 mV (± 0.5 mV, $n = 3$) and the slope factor, k was found to be 6.3 mV (± 0.4 mV) corresponding to a gating charge of approximately 3.8 elementary charges.

Steady state inactivation curves for Kv1.5 in 70 mM, and 35 mM $[K^+]_o$ gave mean values of -26.0 mV (± 1.2 mV, $n = 5$) and -20.5 mV (± 1.8 mV, $n = 7$) respectively for half-maximal inactivation; 5.7 mV (± 0.4 mV) and 8.3 mV (± 1.1 mV) respectively for k . Statistical analysis by Student's t -test again showed no significant difference between recordings in physiological 5 mM and in high external potassium (35 mM and 70 mM), either with half-maximal activation values ($P = 0.62$ and 0.05 respectively) or slope factor ($P = 0.26$ and 0.11 respectively).

3.2.6 The recovery from inactivation of Kv1.5

Increasing the interval between two equal voltage pulses produced information on the rate of recovery from inactivation. Comparison of the amplitude of the currents produced by these pulses, shown in Figure 3.10B gives a measure of how many channels have recovered from inactivation during the interval. Pulses of +40 mV were separated by between 200 ms and 10 seconds (Figure 3.10C), and fractional recovery plotted against separation time. This is shown for averaged data from 5 cells in Figure 3.10A.

Fractional recovery was defined as the amplitude of the peak current of the second pulse (C) minus 'steady state' current of the first pulse (B), divided by the peak (A) minus the steady state of the first pulse, or as shown in the figure,

$$\text{Fractional recovery} = \frac{(C - B)}{(A - B)}$$

(Equation 3.9)

As the interval was increased, it can be seen that more current was activated by the second pulse, as more inactivation was removed. A 10 second interval led to nearly complete recovery from inactivation.

A single, rising exponential of the form:

$$f = 1 - e^{(-t/\tau)}$$

(Equation 3.10)

was fitted to each set of data, to give a mean value of $\tau_{\text{recovery}} = 2.8$ seconds (± 0.2 seconds).

3.3 Discussion

MEL cells transfected with Kv1.5 were found to show delayed rectifier potassium currents, as described previously in many types of native cells and various expression systems. Some of these are described in the introduction to this chapter.

In the 'electrically silent' MEL cell expression system (with no voltage-activated currents found in native, untransfected cells), this resulted in a pure population of transfected channels. The channels were found to be highly selective in passing almost exclusively potassium ions.

These Kv1.5 currents were found to have biophysical parameters characteristic of delayed rectifiers in general. Activation was found to occur in response to depolarising voltage pulses positive to typical resting membrane potentials. Significant activation began to occur at about -30 mV. From the activation curve in Figure 3.5B, it can be seen that all available channels were fully activated at potentials above +30 mV. Currents activated with a sigmoidal shape over a period of milliseconds, and inactivated over a much longer time, in the order of seconds. Steady-state inactivation was found to be removed by hyperpolarisation, with a time course again in the order of seconds.

Table 3.1 Comparison of activation parameters of Kv1.5 with previous studies.

	$V_{1/2}$	k
This study	-6.8 mV	6.8 mV
Philipson <i>et al.</i> (1991) (<i>Xenopus</i> oocytes)	-6.0 mV	6.4 mV
Shelton <i>et al.</i> (1993) (MEL cells)	-4.0 mV	8.5 mV
Grissmer <i>et al.</i> (1994) (MEL cells)	-14.0 mV	12.0 mV

Activation parameters measured for cells in physiological 5 mM external potassium ($V_{1/2} = -6.8$ mV and $k = 6.8$ mV) compared to values of $V_{1/2} = -6.0$ mV (± 0.6 mV) and $k = 6.4$ mV (± 0.5 mV) for Philipson, Hice, Schaefer, LaMendola, Bell, Nelson and Steiner (1991) in *Xenopus* oocytes; $V_{1/2} = -4.0$ mV (± 2 mV) and $k = 8.5$ mV (± 0.7 mV) for Shelton, Davies, Antoniou, Grosveld, Needham, Hollis, Brammar and Conley (1993) in MEL cells and $V_{1/2} = -14.0$ mV (± 3 mV) and $k = 12.0$ mV (± 1 mV) for Grissmer, Nguyen, Aiyar, Hanson, Mather, Gutman, Karmilowicz, Auperin and Chandy (1994) also in MEL cells. All of the above (except Grissmer and colleagues) used the method of instantaneous tail currents at constant driving force to derive the activation parameters as used in this study. The method of Grissmer and colleagues was to calculate

the normalised peak conductance values from the peak current amplitudes at different potentials and fitting a Boltzmann function to the data. This may explain the disagreement of their parameters to the others, including this present study.

Inactivation parameters ($V_{1/2} = -22.0$ mV and $k = 6.3$) compared to values of half-maximal steady state inactivation of -25.3 mV (± 0.4 mV) and $k = 3.5$ mV (± 0.2 mV) for Philipson, Hice, Schaefer, LaMendola, Bell, Nelson and Steiner (1991), in *Xenopus* oocytes.

A more recent study (Uebele, England, Chaudhary, Tamkun, and Snyders, 1996) found functional differences in the kinetics and voltage dependence of activation and inactivation parameters for Kv1.5 currents expressed in various mammalian cell lines, due to the presence of endogenous Kv β 2.1 subunit. Though β subunits are not required for α subunit expression, it appears that the Kv β 2.1 subunit can alter Kv1.5 α subunit expression. Following expression of Kv1.5 in HEK 293 cells and mouse L-cells, some difference was found in the values of the above parameters.

For HEK 293 cells transfected with Kv1.5, in the absence of the Kv β 2.1 subunit, $V_{1/2}$, half maximal activation and inactivation occurred at -0.2 mV (± 2.0 mV) and -9.6 mV (± 1.8 mV) respectively. In the presence of the Kv β 2.1 subunit however, these values became -14.1 mV (± 1.8 mV) and -22.1 mV (± 3.7 mV) respectively, these second set of values being very similar to those from L-cells. L-cells have been shown to have an endogenous Kv β 2.1 subunit which assembles with the transfected Kv1.5 protein.

Interestingly, the value of -22.0 mV for half maximal inactivation measured in this present study, appears close to that found in the L-cells and HEK 293 (with co-transfected Kv β 2.1 subunit). Although Uebele and co-workers used molecular cloning,

immunopurification and Western blot analysis to identify endogenous Kv β subunits in other heterologous expression systems such as *Xenopus* oocytes, L-cells, CHO cells, HEK 293 cells, etc., at present this has not been carried out with MEL cells.

Figure 3.1 Voltage dependence of Kv1.5

A,B Typical whole currents recorded from Kv1.5 in response to a series of depolarising steps. These current records have been corrected for leakage and capacitance currents.

A Currents recorded in response to depolarising voltage steps of 50 ms duration, from a holding potential of -80 mV, in +10 mV steps from -60 mV to +60 mV. The voltage pulse protocol is shown below.

B Currents recorded in response to longer (4000 ms) depolarising pulses.

C Peak values of the current due to the 50 ms pulse plotted against membrane potential to give a typical current-voltage relationship for Kv1.5.

Figure 3.1

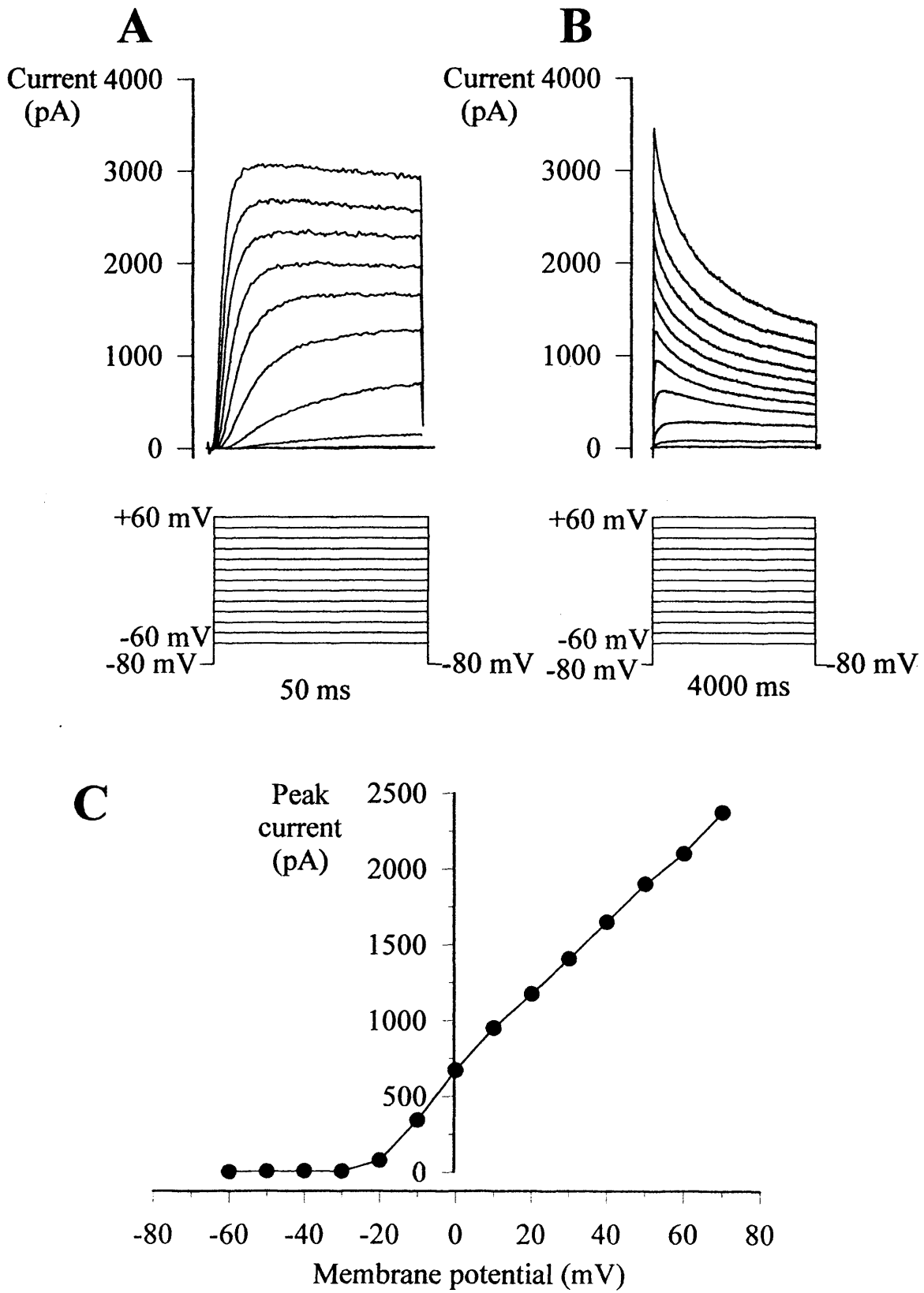


Figure 3.2 Reversal potential and selectivity of Kv1.5

A Currents recorded in an experiment to determine the reversal potential for cells transfected with Kv1.5. In the example illustrated, 5 mM external potassium bath solution was used. Currents were elicited by a brief (50 ms) +40 mV pulse from a holding potential of -80 mV, to open channels, followed by a series of variable potential voltage steps, from -30 mV to -130 mV, in 5 mV increments. The voltage protocol is shown above. The reversal potential was found by fitting a single exponential to each resulting deactivating tail current, to give a value for instantaneous current at the beginning of each variable pulse. The resulting plot of instantaneous current versus the variable potential crosses the voltage axis at the reversal potential, in other words, this is the voltage at which the current is equal to zero.

B Plot of instantaneous tail currents versus membrane potential from a cell exposed to 5 mM external potassium. The reversal potential can be seen to occur at approximately -75 mV, with 5 mM external potassium. The data were fitted with a constant field current equation as described in the text.

C,D Instantaneous current-voltage relationships for Kv1.5 in 70 mM and 35 mM external potassium respectively (these plots are all from different cells). Again, the data were fitted with a constant field current equation

Figure 3.2

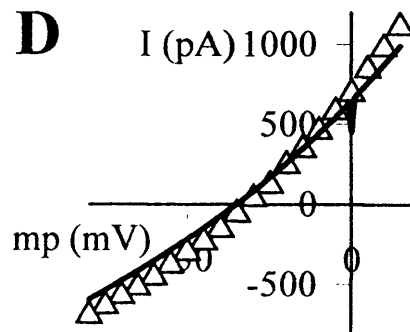
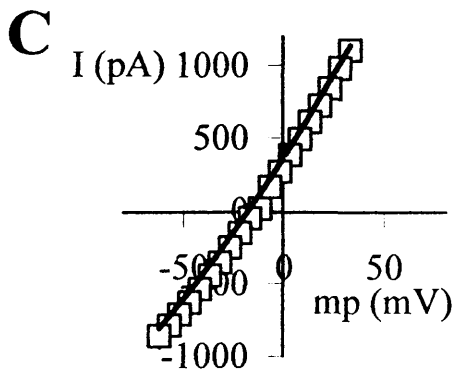
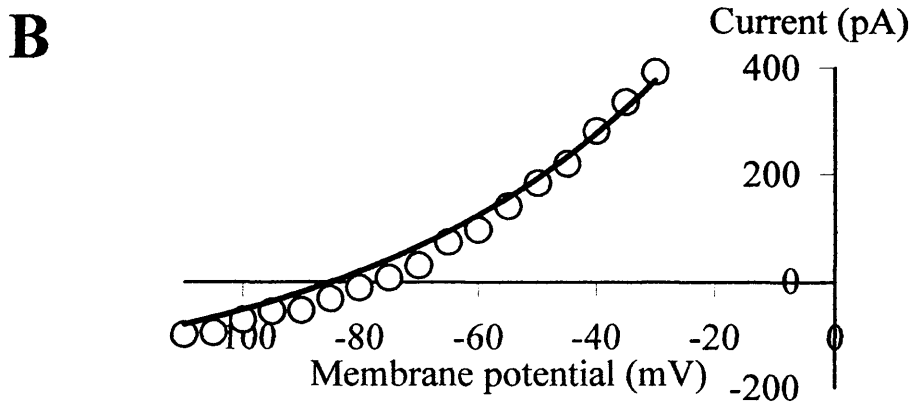
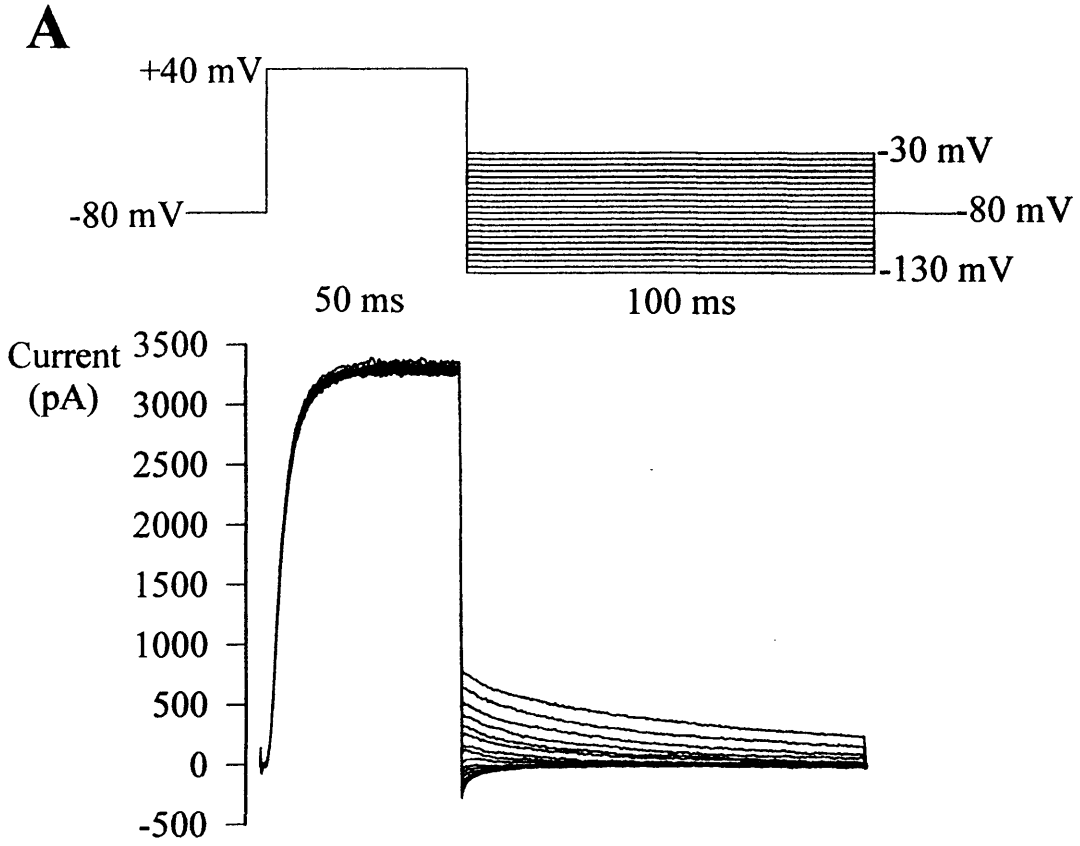


Figure 3.3 Selectivity of Kv1.5

Measured values of E_{rev} as found in Figure 3.2 (open circles) plotted against the external potassium concentration expressed on a log scale. Theoretical calculated values of E_{rev} at all different external potassium concentrations are shown as the solid line, determined from calculations using the Nernst equation (in text), and assuming that the channel is perfectly selective for potassium ions. For this theoretical line, a value of 140 mM was used for $[K^+]_i$. The broken line is the best fit to the measured E_{rev} data using a function of the Hodgkin-Katz equation (in text), with an adjustment for relative permeability of sodium ions, and an estimated adjustment for possible uncorrected liquid junction potentials. The data were best fitted with a value of α ($= p_{Na} / p_K$) found to be 0.0025.

Figure 3.3

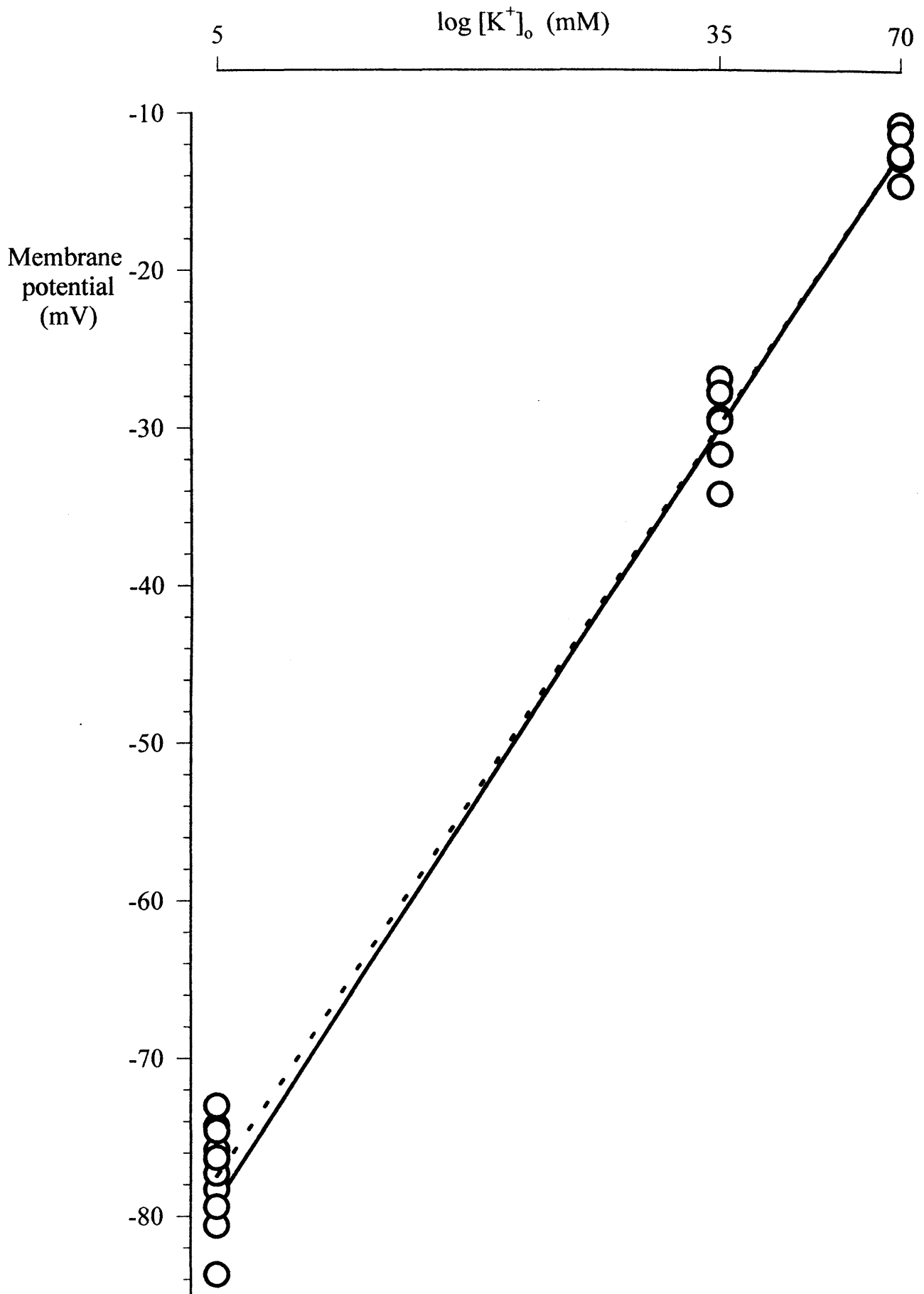


Figure 3.4 Time constants of deactivation

Change of time constant of deactivation with membrane potential for the deactivating tail currents such as those illustrated in Figure 3.2A. 5 mM, 35 mM and 70 mM external potassium are represented by circles, triangles and squares respectively.

Points represent means \pm SEM for 12, 7 and 6 cells respectively.

Note the large SEM for the points which coincide with the average value of reversal potential, E_{rev} , in each external potassium concentration. This was due to difficulties in accurately fitting exponentials to the deactivating tails at potentials close to E_{rev} in each case.

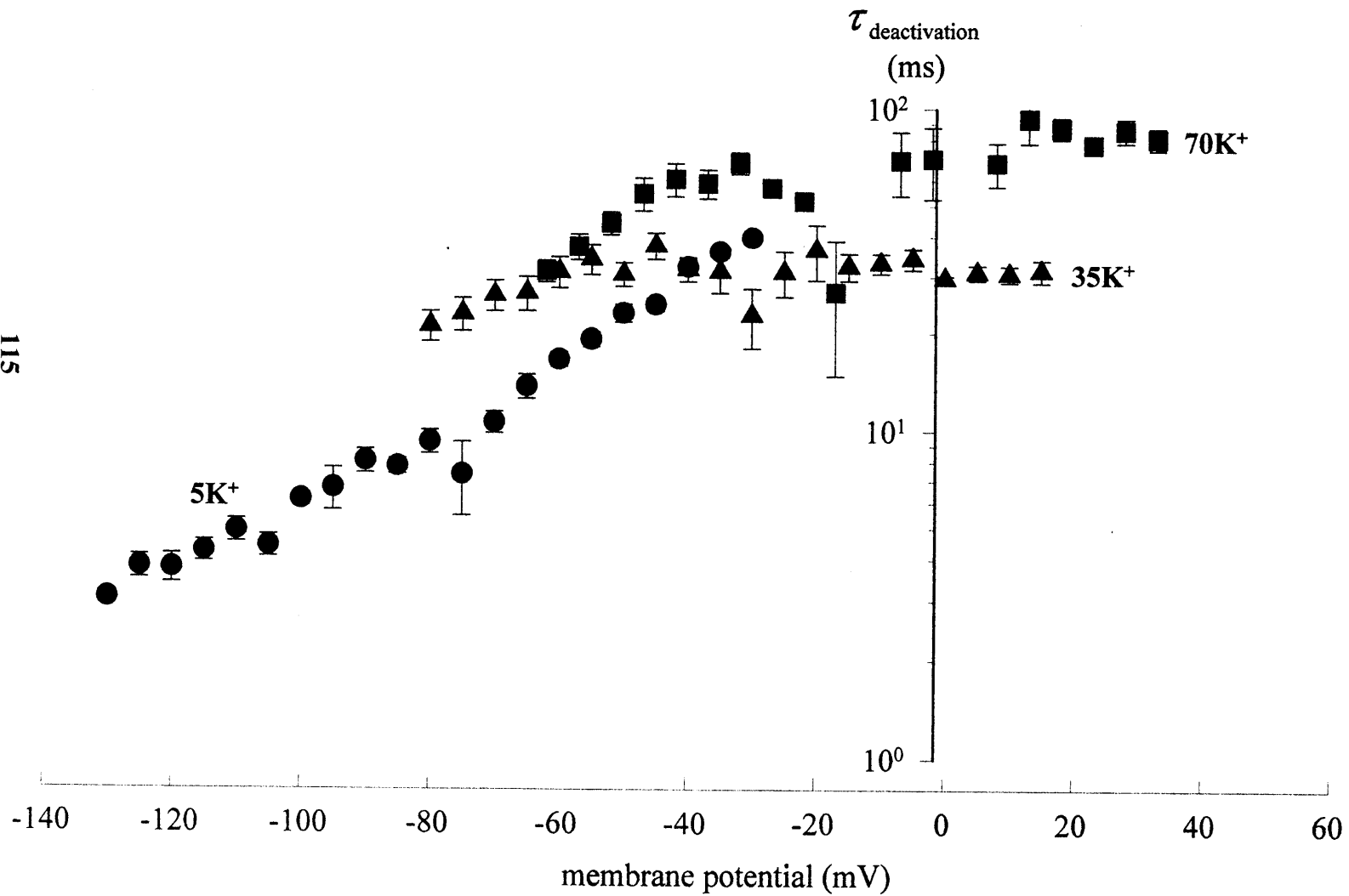


Figure 3.4

Figure 3.5 Voltage dependence of activation for Kv1.5.

A Family of Kv1.5 potassium currents elicited by 50 ms voltage steps from -60 mV to +70 mV in 10 mV increments, activating K⁺ channels, followed by a return to a fixed voltage of -40 mV for 100 ms, giving a variable tail current with instantaneous current proportional to the number of open channels. Instantaneous current magnitudes were found by fitting an exponential to the tails, as illustrated for three of the tail currents by the arrow.

C Values of instantaneous current were normalised and plotted versus membrane potential of the initial variable pulse to give an activation curve for Kv1.5 (voltage dependence with constant driving force for a measure of channel open probability). Points represent means \pm SEM for 13 cells. A Boltzmann function fitted to the averaged data illustrated in this figure gave half maximal activation, $V_{1/2}$ at -5.8 mV and slope factor of 8.0 mV. The mean value of $V_{1/2}$ returned from fitting the Boltzmann function to each individual activation curve was -6.8 mV (\pm 1.3 mV) and mean slope factor $k = 6.8$ mV (\pm 0.3 mV).

Figure 3.5

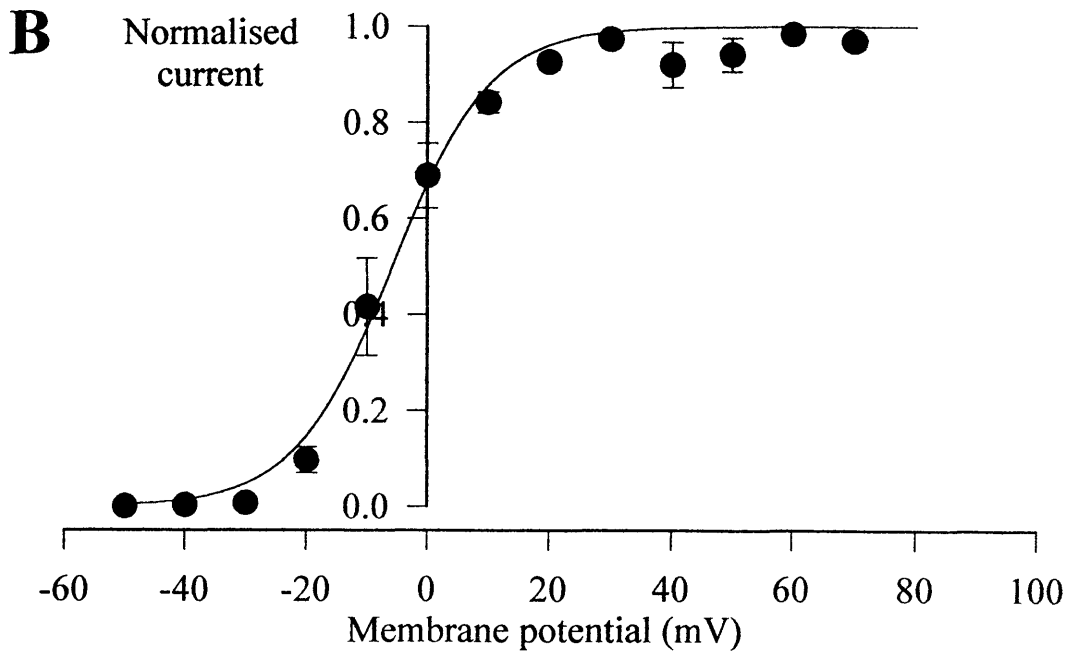
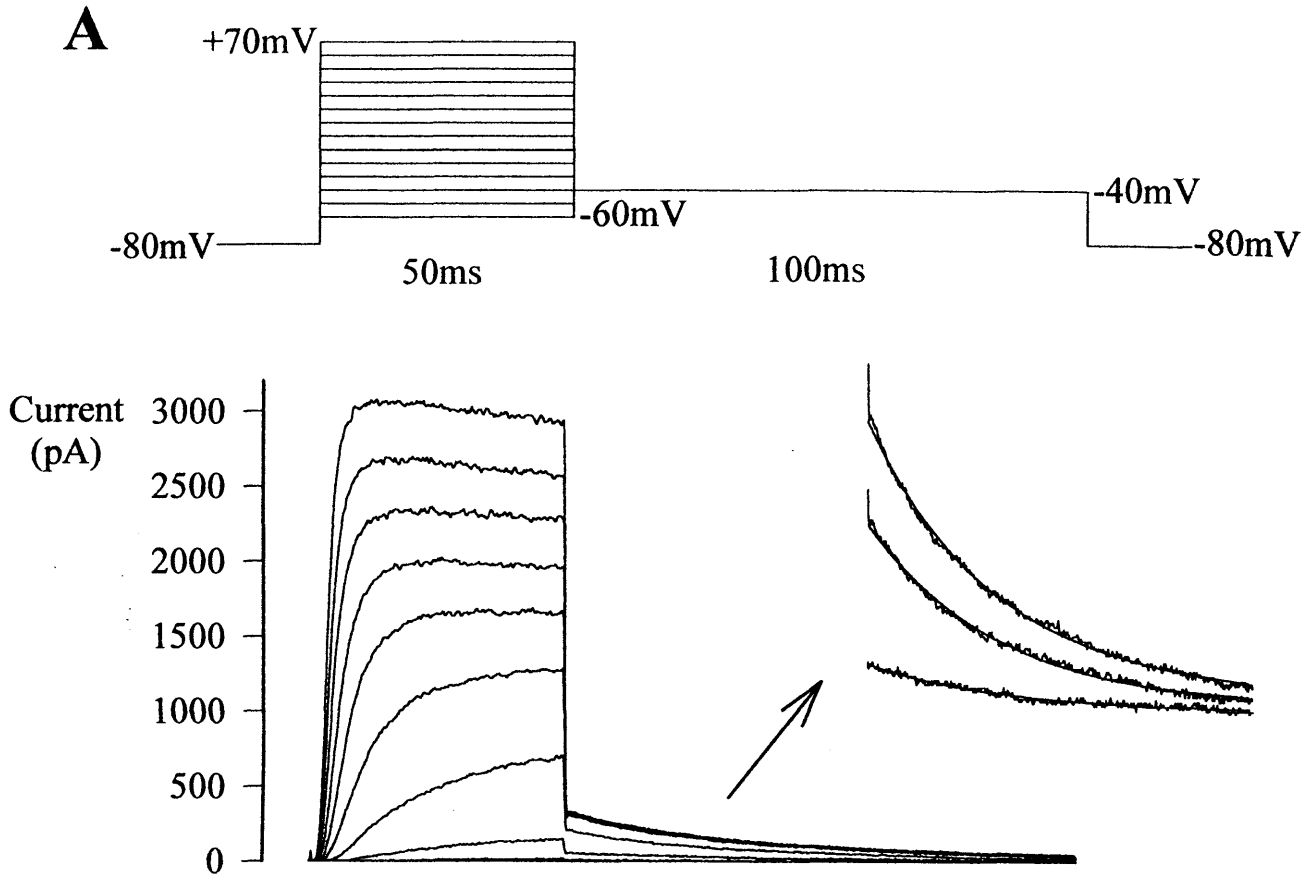


Figure 3.6 Activation curves with increased external potassium

A,B Activation curves for Kv1.5 as above, but with 70 mM (squares) and 35 mM (triangles) external potassium. Activation parameters were found to be -9.2 mV (± 1.1 mV, n = 7) and -3.7 mV (± 2.1 mV, n = 8) respectively for the mean value of $V_{1/2}$; 6.8 mV (± 0.2 mV) and 9.0 mV (± 0.6 mV) respectively for the mean value of k.

Figure 3.6

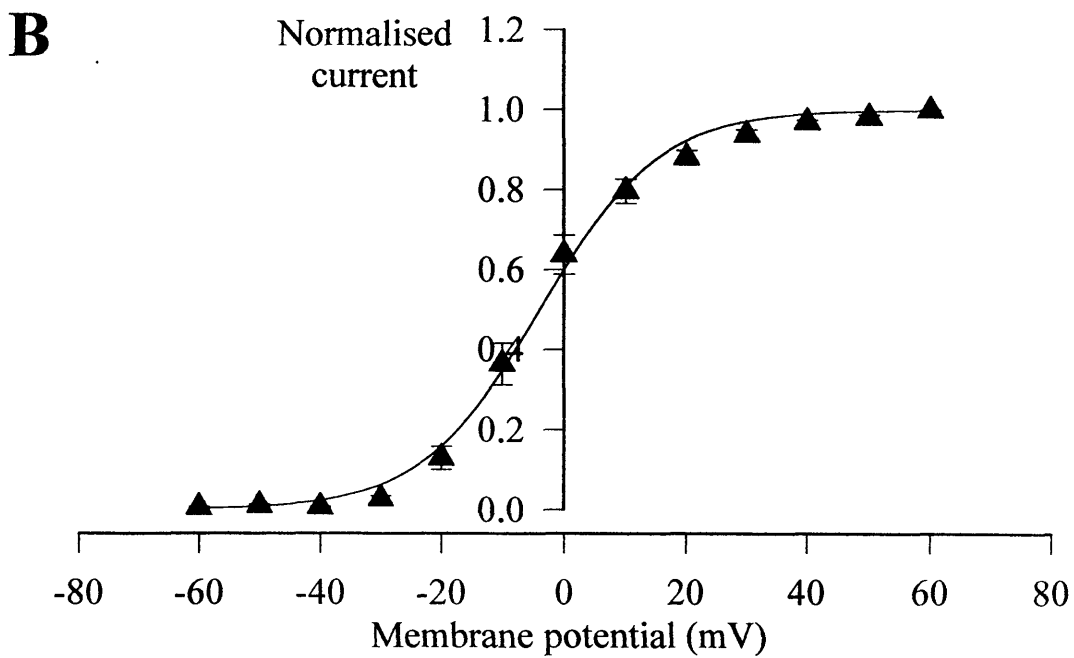
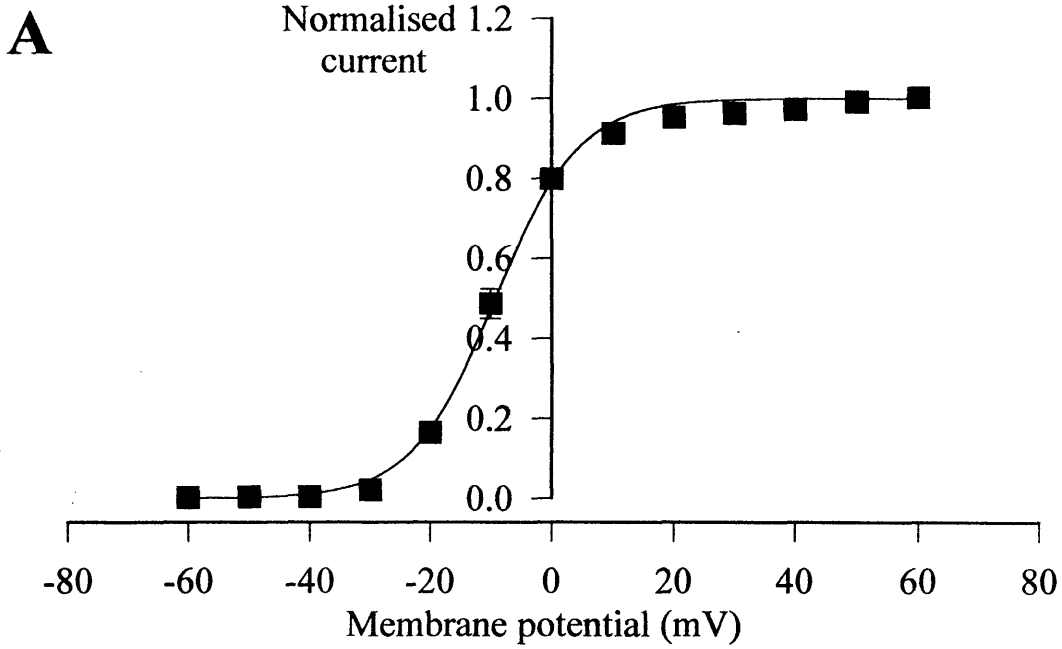


Figure 3.7 Hodgkin-Huxley activation kinetics.

A A fit of classical Hodgkin-Huxley formula describing the exponential rise of current on activation of the channel to a record of a Kv1.5 current. Values of the time constant of activation, $\tau_{\text{activation}}$ were obtained from the parameters of Equation 3.7 (in text) fitted to the activation of Kv1.5 currents elicited due to the voltage pulse protocols described earlier in Figure 3.5. The fit is illustrated here for a current elicited by a depolarisation to +60 mV.

B $\tau_{\text{activation}}$ on a linear scale against membrane potential. Points represent means \pm SEM for 11 cells.

C $\tau_{\text{activation}}$ on a common log scale against membrane potential.

These plots illustrate the voltage dependence of the time constant of activation.

Figure 3.7

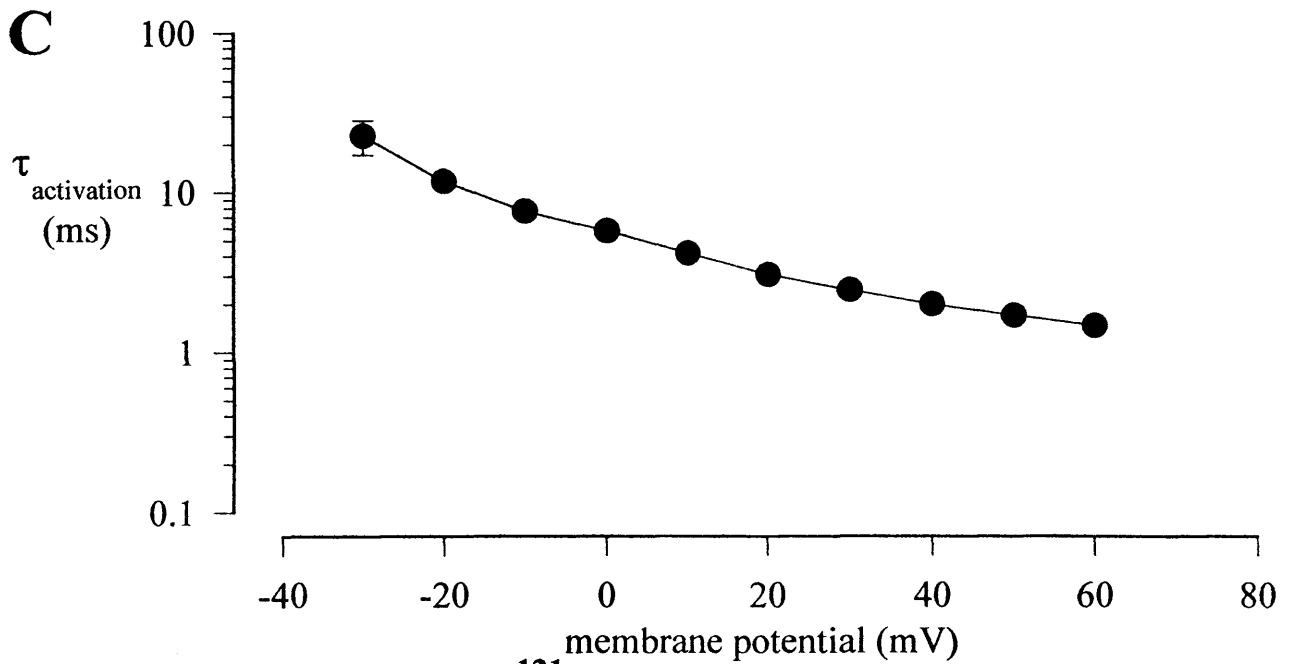
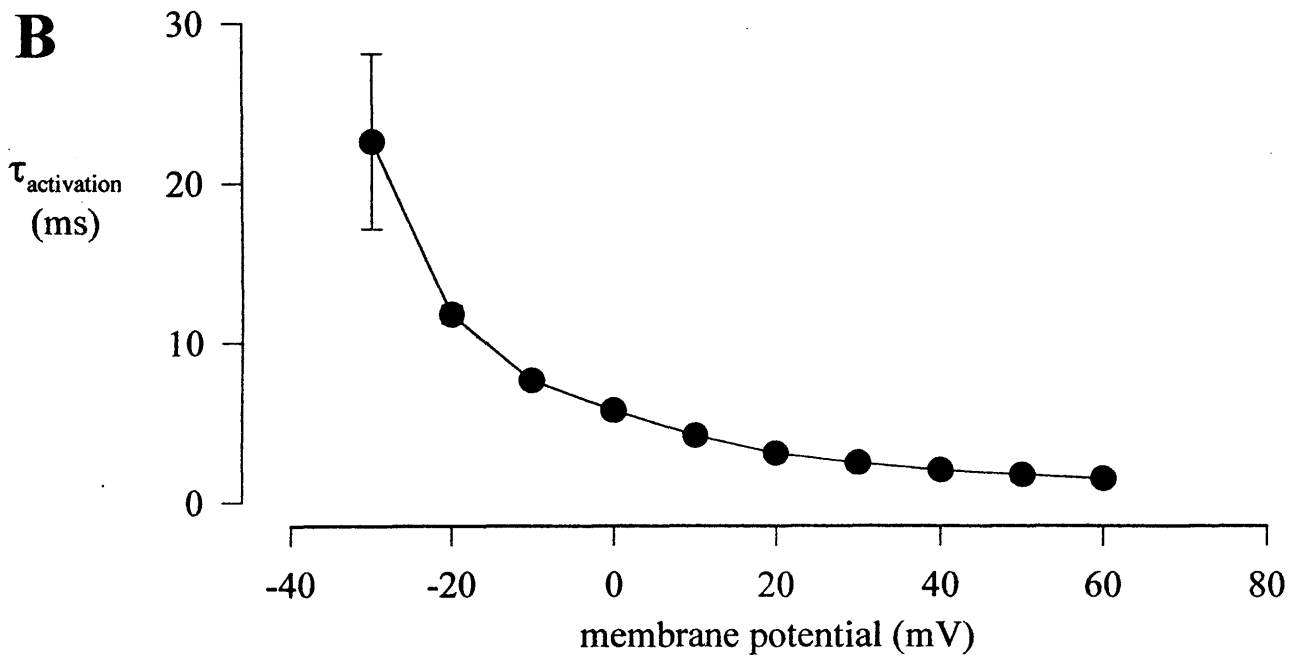
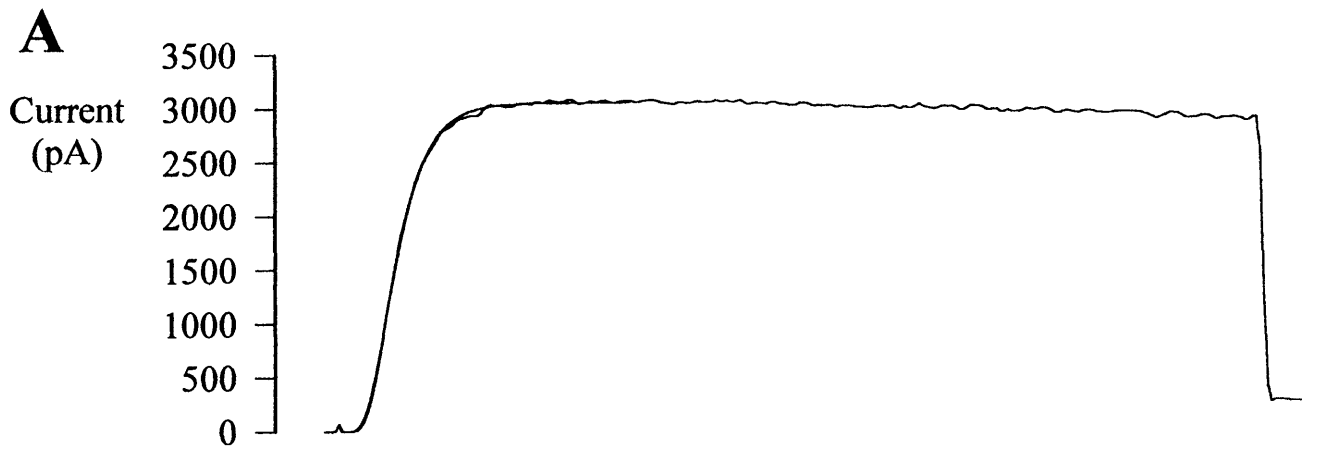
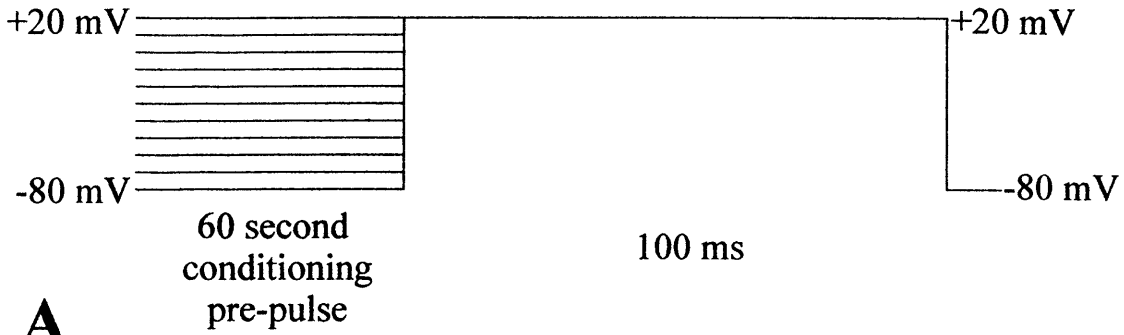


Figure 3.8 Kv1.5 Steady state inactivation.

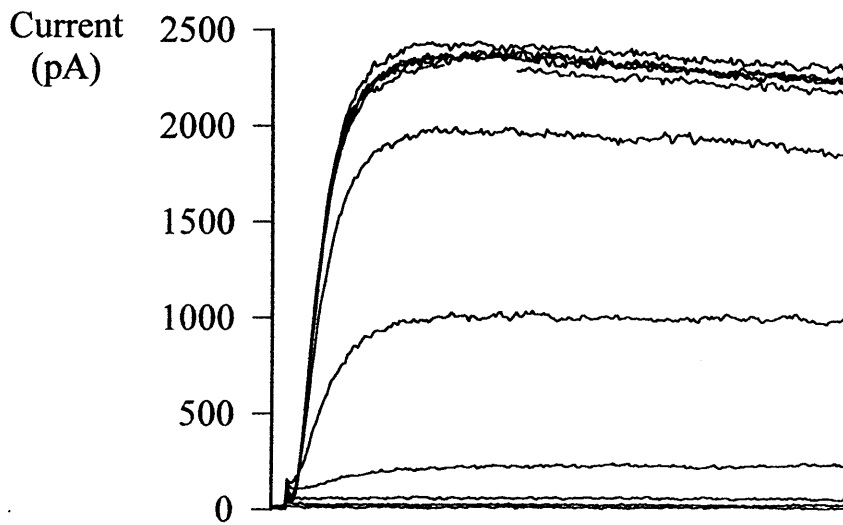
A Family of currents elicited by 100 ms test pulse at +20 mV, following a 60 second conditioning pre-pulse at variable potentials. A long pre-pulse was necessary to ensure steady state inactivation.

B Peak current due to the test pulse was normalised, and plotted versus the potential of the variable pre-pulse. Points represent averaged data \pm SEM for 3 cells. A Boltzmann function fitted to the averaged data gave half maximal steady state inactivation at -22.0 mV and slope factor, k, of 6.3 mV. The mean value of $V_{1/2}$ returned from fitting the Boltzmann function to each individual inactivation curve was at -22.0 mV (\pm 0.4 mV) and mean value of slope factor, k, of 6.3 mV (\pm 0.3 mV).

Figure 3.8



A



B

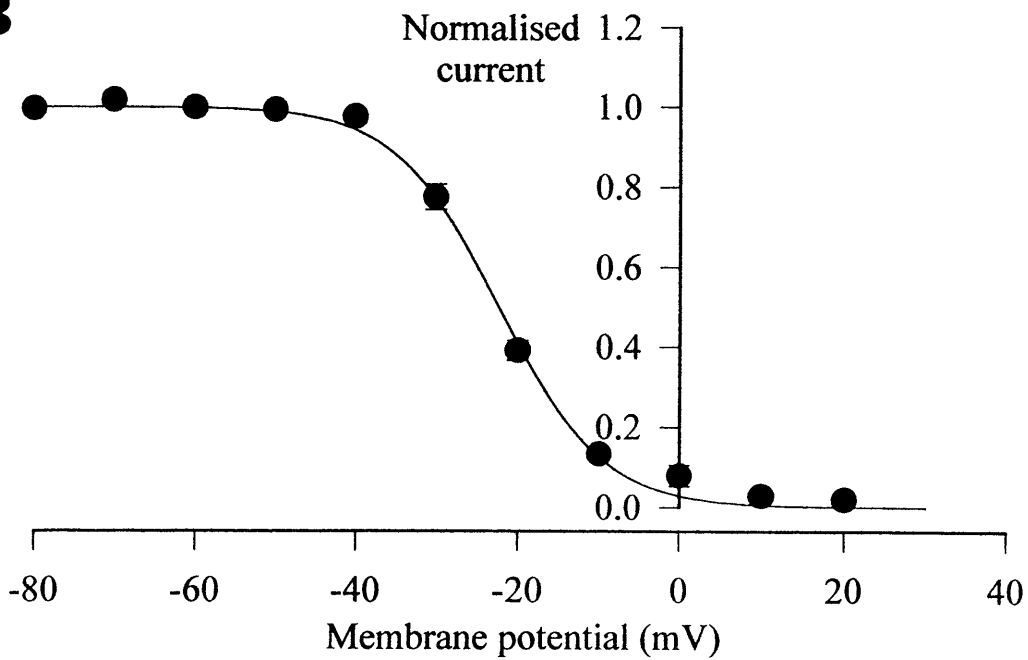


Figure 3.9 Steady state inactivation with increased external potassium

A,B Steady state inactivation curves (as in Figure 3.7B) for Kv1.5 in 70 mM (squares) and 35 mM (triangles) external potassium. Mean inactivation parameters were found to be -26.0 mV (± 1.2 mV, $n = 5$) and -20.5 mV (± 1.8 mV, $n = 7$) respectively for half-maximal inactivation; 5.7 mV (± 0.4 mV) and 8.3 mV (± 1.1 mV) respectively for k.

Figure 3.9

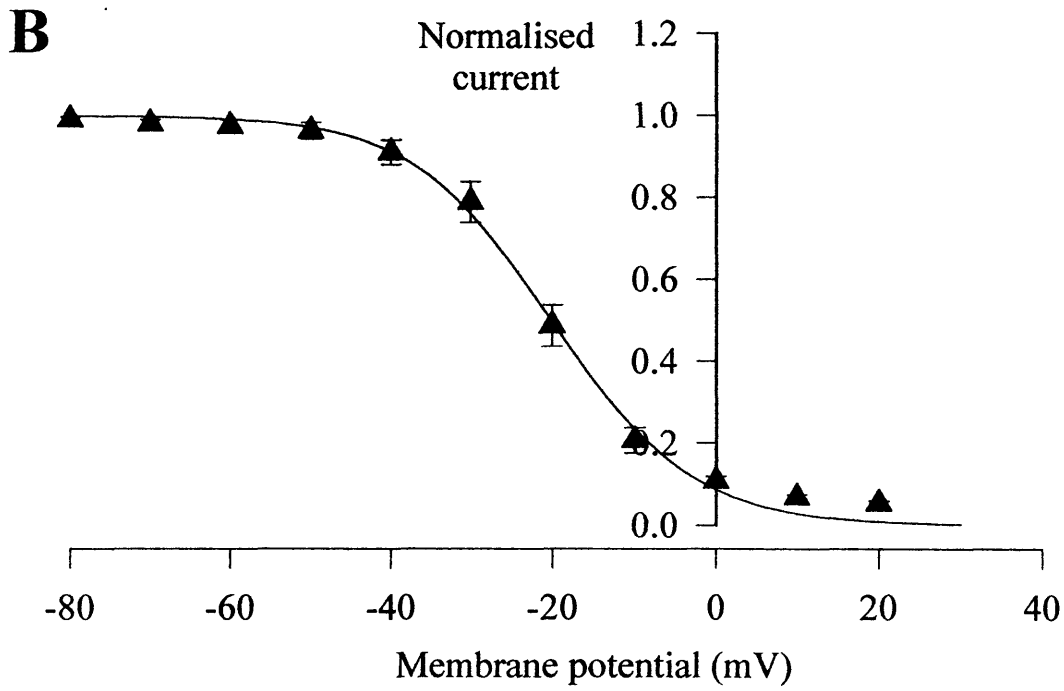
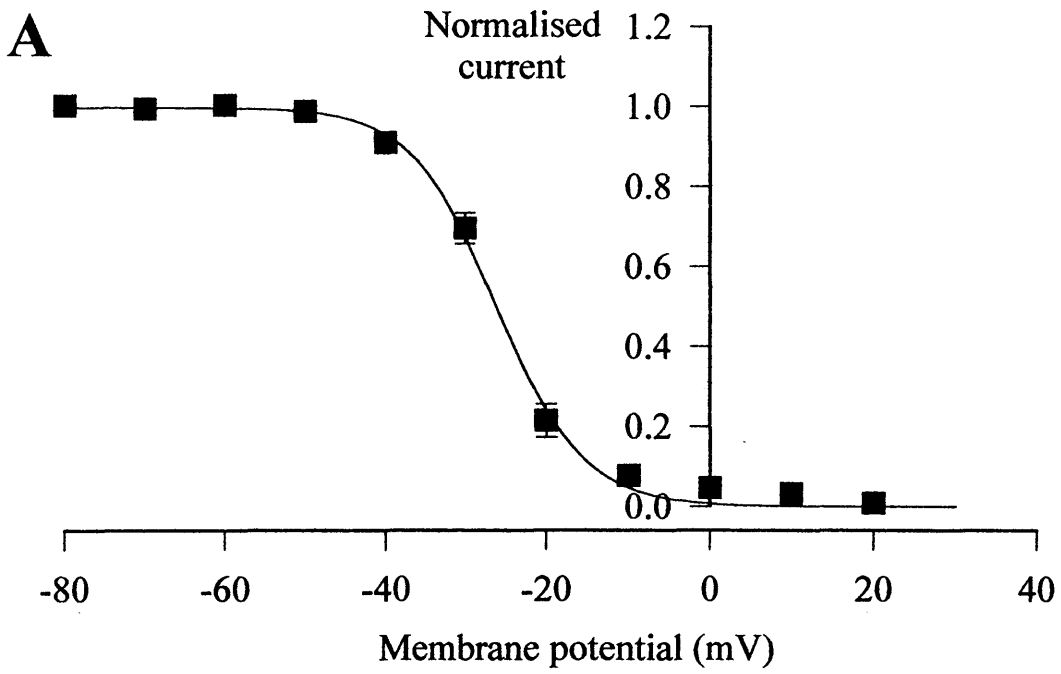


Figure 3.10 Recovery from inactivation for Kv1.5.

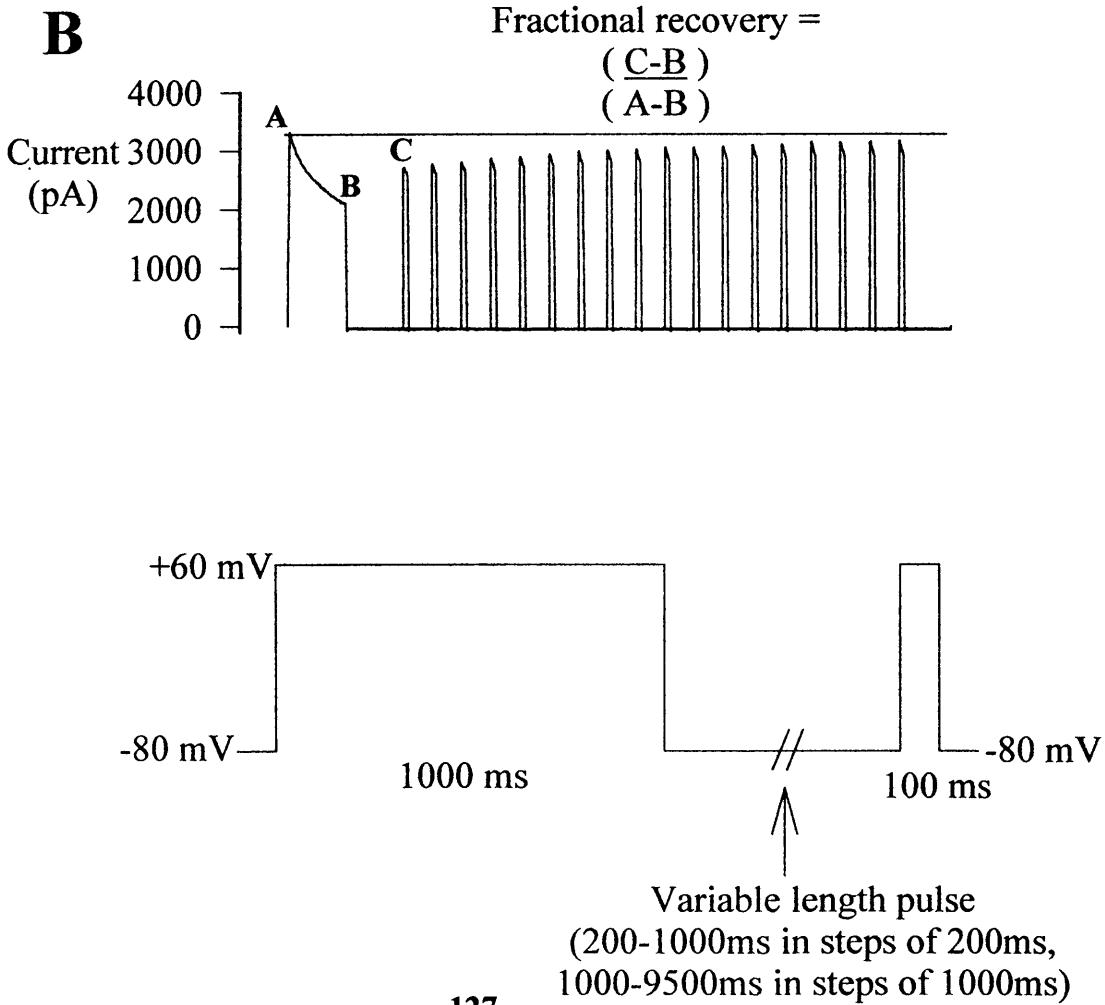
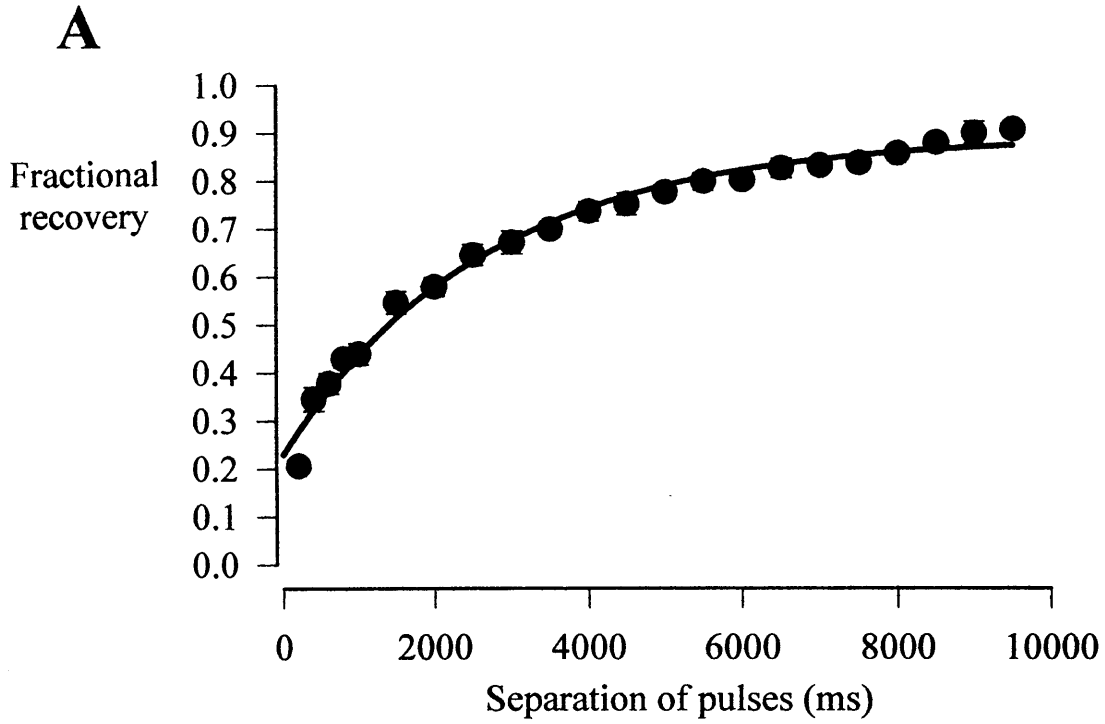
A Plot of fractional recovery from inactivation giving a value for time constant of recovery. Two pulses at +40 mV, applied from a holding potential of -80 mV, and separated by an increasing interval between pulses, from 200 to 9500 ms resulted in currents which showed an increase in amplitude for the current due to pulse 2 with increasing inter-pulse separation, very nearly recovering all the initial current after 10 seconds. Fractional recovery was defined as the amplitude of the peak current of the second pulse minus 'steady state' current of the first pulse, all divided by the peak current minus steady state current of the first pulse.

$$\text{Fractional recovery} = \frac{(C - B)}{(A - B)}$$

Points on the plot of fractional recovery versus separation represent mean data \pm SEM, for 5 cells. A single exponential fitted to this plot gave $\tau_{\text{recovery}} = 2.8$ seconds (± 0.2 seconds).

B Example of current trace used to construct the plot of fractional recovery from inactivation, and the voltage pulse protocol employed. Point A represents amplitude of peak current for pulse 1; point B represents amplitude of steady state current for peak 1; point C represents amplitude of peak current for pulse 2.

Figure 3.10



CHAPTER FOUR

Whole Cell Recording of Voltage-Activated Transient Potassium Currents From Kv4.2 / RShal1 Channels

4.1 Introduction

The A-type or transient outward potassium current is so called because it is characteristically activated upon depolarisation from the resting membrane potential more rapidly than the delayed rectifier, the current reaches a peak within a few milliseconds, and then the current decreases rapidly as the channel inactivates back completely to base level within hundreds of milliseconds or less. This makes the opening of the channel 'transient' compared to that of the delayed rectifier which doesn't show a discernible peak on this order of time scale, and is much slower to inactivate, typically over several seconds.

A currents fulfil the role of spacing repetitive responses such as controlling action potential frequencies; they regulate the frequency of the firing rate. As mentioned above, A-type channels activate in response to depolarisation, and rapidly become inactivated. This inactivation is removed by the period of hyperpolarisation occurring immediately after the action potential. As the next depolarisation commences, the A current is again activated, and works against the effect of the depolarisation which is to activate the next action potential at the threshold frequency. Therefore, the A current serves to space out successive action potentials, by limiting the rate and magnitude of depolarisation (Connor and Stevens, 1971).

A currents have been described in many different vertebrate neuronal cells, cardiac cells and muscle cells (Rudy, 1988). The gene for RShal1 (or Kv 4.2) encodes an A-type potassium channel, first isolated from rat hippocampus (Baldwin, Tsaur, Lopez, Jan and Jan, 1991). Northern blots revealed that the mRNA encoding this channel subunit was expressed at a similar level in the heart and the brain. At the same time, the homologue RK5 was found (Roberds and Tamkun, 1991), which was

almost identical at the amino acid level to RShal1 except for a distinct carboxyl terminus. Again this was also found in the brain and cardiac cells, and also smooth muscles, but not skeletal muscle. RK5 was also designated as Kv4.2 on the basis of sequence identity. Blair, Roberds, Tamkun and Hartshorne (1991) subsequently expressed this clone in the *Xenopus* oocytes system. The functional voltage-dependence and kinetic characteristics led them to suggest that this channel contributes to the transient outward current involved in the heart action potential. The expression of Kv4.2 in heart muscle was assessed using a ribonuclease (RNase) protection assay, and a gradient of Kv4.2 mRNA expression was found to exist across the ventricular wall as well as differences in levels between the atrium and ventricle (Dixon and McKinnon, 1994) which explains observations of the variation of the transient outward potassium current in heart. Further from this, the levels of protein in the heart representing Kv4.2 amongst others were measured using Western blots, confirming detectable levels (Barry, Trimmer, Merlie and Nerbonne, 1995). These results suggested that potassium channel expression in heart muscle is under the control of transcriptional regulation, in order to produce a precise required variation in the phenotype of the different myocytes in different regions of the heart.

Similarly, differences in neuronal excitability within the nervous system may also arise from fine transcriptional regulation and differential expression of the various potassium channel genes, for example in a cell-type specific manner or in response to specific neuronal activity. Examination of the distribution of mRNA in rat brain hippocampus following seizure activity found the Kv4.2 mRNA to be reduced (Tsauro, Sheng, Lowenstein, Jan and Jan, 1992). Kv4.2 mRNA was found to be the most abundant *Shal*-related transcript in rat brain RNA preparations. An antisense oligonucleotide based on this sequence was quite efficient in arresting the expression

in *Xenopus* oocytes (using brain poly-(A) RNA) of a potassium A current that activates transiently near the threshold for Na⁺ action potential generation seen in somatic recordings from neurons.

Again, the use of a heterologous expression system is a tremendously powerful tool in order to correlate the properties and confirm the identity of cloned channels with an endogenous current.

4.2 Results

Experiments were carried out in the whole cell configuration of the patch clamp technique in order to determine the biophysical characteristics of the RShal1 channel transfected into MEL cells, as described in Materials and Methods.

External bath solutions contained (except where stated) 140 mM NaCl, 5 mM KCl, 2 mM CaCl₂, 2 mM MgCl₂ and 10 mM HEPES. Internal pipette solutions contained 140 mM KCl, 2 mM free Mg²⁺ (5.8 mM total MgCl₂ was added to the solutions), 10 mM EGTA, 10 mM HEPES and 20 mM glucose. All solutions were titrated to pH 7.2, and all experiments carried out at room temperature.

Current records were filtered using an 8-pole low pass Bessel filter set at 1 kHz and where two filters were used in series, the composite frequency was also kept at approximately 1 kHz, as described in Materials and Methods.

All records were leak subtracted subsequent to recording, again as described in Materials and Methods.

4.2.1 The voltage dependence of Kv4.2

A current - voltage relationship for Kv4.2 was constructed. A typical family of Kv4.2 currents in response to a series of depolarising pulses is shown in Figure 4.1A. A conditioning hyperpolarising pre-pulse was necessary in order to ensure that all channels were in the closed state, and to remove steady-state inactivation. This is explained by the range of the inactivation curve shown later in this chapter (Figure 4.6). A 50 ms step to -100 mV, from the holding potential of -80 mV was thus the first step in this protocol. This was followed by 100 ms long depolarising pulses, commencing from -60 mV, and rising to +90 mV in increments of +10 mV.

The onset of the resulting outward currents was sigmoidal, but for those elicited by the more positive potential pulses, the currents quickly reached a peak, typically in the order of five milliseconds, before decaying quite rapidly back towards zero in approximately 100 ms. These currents resembled typical voltage-activated, fast transient, or A-type currents previously described in many studies (see Hille, 1992).

There was no plateau seen after the current had reached its maximum value for these more positive potentials, in contrast to recordings from Kv1.5 over this range of pulse lengths (Figure 3.1A).

A simple current-voltage relationship for Kv4.2 is shown in Figure 4.1B. These values of peak current were plotted against membrane potential. It can be seen that the Kv4.2 channels open at membrane potentials above -40 mV.

4.2.2 Hodgkin-Huxley activation parameters

Hodgkin and Huxley created a model describing permeability changes, correctly predicting features of excitability in terms of movements of independent charged particles within the cell membrane. Activation and inactivation were described as independent processes, activation being rapid, and opening channels during a depolarisation, whereas inactivation is slower, and closes channels during a depolarisation. Inactivated channels cannot be activated until inactivation is removed by repolarisation. The model allowed conductance changes to be expressed in terms of voltage and time only. As shown in chapter 3, the sigmoidal shape of the increase in potassium conductance on depolarisation can be described by the increase of current such that

$$I_t = I_\infty (1 - e^{(-t/\tau)})^n$$

(Equation 3.8)

where I_t is the current at time t , I_∞ is the final value of the current, τ is the time constant of activation, and n represents the number of independent particles responsible for being in the correct position within the membrane to allow channel opening. In Hodgkin and Huxley's model, n was set at 4 (for easier calculations). This equation then approximately describes the rise of current on activation.

However, fitting this equation to the currents elicited by the Kv4.2 channel would produce an underestimate for time constant of activation, because this equation does not take into account the process of inactivation, which commences at the same

time as activation. A component representing the inactivation process can be included in Equation 3.8 (see also Adams and Gage, 1979). An expression describing the inactivation, represented by a falling exponential function is multiplied with I_t thus:

$$I_t = I_\infty (1 - e^{(-t/\tau_1)})^n \cdot e^{(-t/\tau_2)}$$

(Equation 4.1)

where τ_1 and τ_2 represent the time constants of activation and inactivation respectively. These are subsequently referred to as $\tau_{\text{activation}}$ and $\tau_{\text{inactivation}}$.

This expression was fitted to the currents as previously shown in Figure 4.1. Instead of using $n = 4$ as Hodgkin and Huxley did, it was found that better fits were achieved with n being equal to 5.

An example to illustrate the fit is shown in Figure 4.2A. This is a current trace elicited by a pulse to +70 mV. Values of $\tau_{\text{activation}}$ obtained from the parameters of the equation were plotted against membrane potential. Figure 4.2B shows $\tau_{\text{activation}}$ on a linear scale, and in C, on a common log scale. These illustrate that the time constant of activation decreases with depolarisation.

With reference to the activation curve in Figure 4.3, which shows that maximal activation of channels occurs at potentials above +40 mV, it can also be seen from panel B that $\tau_{\text{activation}}$ is less steeply voltage dependent above about +40 mV.

4.2.3 Voltage dependence of activation

A different approach was needed in order to obtain information about the activation of Kv4.2, from that used for Kv1.5. As described in the previous chapter for Kv1.5, exponentials were fitted to tail currents measured at a constant potential, after the Kv1.5 channel had been activated by a variable potential first pulse. This protocol gave a constant driving force for the tail currents, resulting in an instantaneous current proportional to the number of open channels.

This method proved to be unsuitable for Kv4.2. It was extremely difficult to design a voltage pulse protocol that enabled a tail current to begin at the peak of the current. This can clearly be seen from the current family in Figure 4.1A and the single current in Figure 4.2A; there is no plateau of current as seen with Kv1.5, because of the more rapid inactivation over this order of time.

Therefore, the chord conductance method was used to measure the voltage dependence of channel activation. In the discussion of the previous chapter, I mentioned that Grissmer, Nguyen, Aiyar, Hanson, Mather, Gutman, Karmilowicz, Auperin and Chandy (1994) did not use the method of instantaneous tail currents at constant driving force to derive the activation parameters for Kv1.5 as I did in this study. The method of Grissmer and colleagues was to calculate the normalised peak conductance values from the peak Kv1.5 current amplitudes at different potentials and fitting a Boltzmann function to the data, which is similar to the method I used for Kv4.2 in this study. However, due to the rapid inactivation of Kv4.2 currents, it was necessary to correct the peak of the current for this slight decrease in magnitude.

Exponentials of the type:

$$f = I_0 e^{-t/\tau}$$

(Equation 4.2)

were fitted to the decay of the current, as illustrated for seven of the current records in Figure 4.3A. In Equation 4.2, I_0 represents current at time, $t = 0$, and τ in this case is a time constant of decay. From the resulting fit, I_0 was obtained.

I_0 can be used as a value for current corrected for inactivation, assuming that inactivation begins at time $t = 0$ when the voltage changes in the pulse protocol, and also assuming that inactivation proceeds exponentially. Figure 4.4 illustrates the nature of this correction. A fitted current trace is shown, at a voltage step to +50 mV. The dotted line is placed at the point where the current peaks; this peak current is shown as I_t , and time elapsed is t . Now, since inactivation proceeds exponentially, the current at time is equal to t will be reduced by inactivation by a factor, B , where:

$$B = e^{-t/\tau}$$

(Equation 4.3)

where τ is the time constant of inactivation. Since I_t , the current at time t has been reduced by the factor B due to inactivation, the corrected current, $I_{\text{corrected}}$ at time t will be:

$$I_{\text{corrected}} = I_t \times \frac{1}{B}$$

(Equation 4.4)

Now, if an exponential is fitted to the decay of the current and this exponential curve passes through, or very close to the peak current, then I_0 the extrapolated value of the current at time = t can be assumed to be the value of $I_{\text{corrected}}$. This is because, from Equation 4.2,

$$I_t = I_0 e^{-t/\tau}$$

(Equation 4.5)

Thus,

$$I_0 = I_t \times \frac{1}{e^{-t/\tau}}$$
$$\Rightarrow I_0 = I_t \times \frac{1}{B}$$

From Equation 4.4, this implies that $I_0 = I_{\text{corrected}}$.

From Ohm's Law,

$$I = \frac{V}{R}$$

(Equation 4.6)

where I is current, V is voltage and R is resistance. Conductance, g, is the reciprocal of resistance, so that:

$$I = g V$$

(Equation 4.7)

Now, to express the conductance as a function of the electrochemical driving force on potassium ions, $(V-E_K)$, where V equals the membrane potential, and E_K is the potassium equilibrium potential, a 'chord' was constructed to the current - voltage relationship using the following equation in calculations:

$$I_0 = g(V - E_K)$$

(Equation 4.8)

Therefore, at lower membrane potentials, chord conductance decreases as the slope of the chord decreases. One must exercise some caution however with the method of investigating activation using chord conductances. As mentioned in the previous chapter, the constant field current equation predicts that the values of the current data obtained from instantaneous current-voltage relationships at more negative potentials deviate away from a straight line and this was found to be the case for Kv1.5. The implication of this is that at more negative potentials the current is no longer linearly proportional to the potential difference across the membrane, and since the driving force $(V-E_K)$ is used in these calculations, if there is also this rectification with Kv4.2, then some error may occur. This is the real difference in the methods I used to investigate the voltage dependences of activation of Kv4.2 and Kv1.5; with

the latter, after activating channels, tail currents were elicited at constant driving force by clamping the membrane potential to the same constant voltage pulse. With Kv4.2 however, the peak current was divided by the magnitude of the driving force at that particular pulse potential.

Chord conductances were normalised and plotted against membrane potential to construct the activation curve shown in Figure 4.3B. Points shown in this figure represent the means \pm SEM for 5 cells. A Boltzmann function of the type:

$$f = \frac{g}{g_{\max}} = \frac{1}{1 + \exp\left[\left(\frac{V_{\frac{1}{2}} - V}{k}\right)\right]}$$

(Equation 4.9)

was fitted to the normalised set of data for each cell, to give the following parameters:

$V_{\frac{1}{2}}$, the membrane potential at which half the available channels are activated, was found to occur at -9.5 mV (\pm 2.3 mV, $n = 5$), and the slope factor, k , of 10.8 mV (\pm 1.0 mV) indicated the equivalent movement of $24 / 10.8 = 2.2$ elementary charges across the width of the membrane voltage field. This implied a gating charge of approximately 2 elementary charges. The Kv4.2 current can be seen to be maximally activated at potentials positive to about +40 mV. This can be seen from the plateau of the points on the activation curve.

Activation was also investigated with increased external potassium in the bath solution. The resulting currents and activation curve constructed in the same way as

above, can be seen in Figure 4.5. The arrow in Figure 4.5A points to inward going currents. These occurred in response to those membrane pulses lying between the threshold for activation (about -40 mV, from Figure 4.1B) and the reversal potential, which is calculated to be -17.3 mV for these solutions. At potentials positive to this, outward currents were seen.

Using 70 mM external potassium instead of physiological 5 mM external potassium, half-maximal activation now occurred at -1.2 mV (± 1.3 mV, $n = 7$), and k , the slope factor, was found to be 9.0 mV, indicating the equivalent movement of $24 / 9 = 2.6$ elementary charges across the width of the membrane voltage field.

Student's t-tests were carried out to compare the values of half- maximal activation and slope factor for Kv4.2 channels with 5 mM and 70 mM external potassium. The result for $V_{1/2}$ ($P = 0.009$) suggest a significant difference though it must be remembered that using chord conductances to calculate the voltage dependence of activation is a more inaccurate method than using tail currents as for Kv1.5. There was no statistical difference found in comparing the measured values of slope factor for Kv4.2 channels with 5 mM and 70 mM external potassium.

Further information was obtained from the exponential fits to the decay of currents as shown previously in Figures 4.1A and 4.3A. This is illustrated again in Figure 4.6A, showing an exponential fit to the decay of the current due to a +90 mV pulse of 100 ms length.

Values of τ_{decay} were obtained from the fitted exponentials, as in Equation 3.8, and these were plotted versus the membrane potential of the pulse. Figures 4.6B and C show τ_{decay} plotted on a linear and common log scale respectively. It was extremely difficult to fit the function to the decay of current due to pulses below -10 mV when

70 mM external potassium was used. Again this was due to the proximity to the reversal potential.

The voltage dependence of this time constant can clearly be seen. For cells in 5 mM external potassium (represented by circles in Figure 4.6B), τ_{decay} for a pulse to -20 mV was nearly half the value of that for a pulse to -40 mV. This means that the current inactivates more quickly at positive potentials. The time constant was distinctly less steeply voltage dependent at potentials above 0 mV.

It was also observed that the relationship between τ_{decay} and voltage was shifted up and to the right with increased external potassium. At any potential, τ_{decay} was greater, and the time constant was less steeply voltage-dependent at potentials above +20 mV with 70 mM external potassium.

4.2.4 Voltage dependence of steady-state inactivation.

The transient nature of the Kv4.2 current compared to Kv1.5 again required a different method in order to derive information on inactivation parameters. As illustrated in Figure 4.7A, from a holding potential of -80 mV, a 50 ms long conditioning pre-pulse to -100 mV ensured that all channels were in the closed state. This brief hyperpolarisation also ensured that any previous inactivation was removed from channels. The following set of two pulses elicited current families. The first, a conditioning 100 ms depolarising pulse of variable potential, ranging from -100 mV up to +20 mV in steps of +10 mV, produced currents which started at pulses positive to -40 mV, and increased to a maximum with increasing depolarisation. The second pulse, a constant 100 ms step to +40 mV, produced currents which decreased from the

initial maximum value (when the variable first pulse was at -100 mV) down to zero, as the first pulse became more depolarised. This meant that the size of the current due to the second pulse reflected how many of the channels became inactivated during the first pulse.

The magnitude of the current due to the second pulse was normalised to its maximal value, and plotted against the membrane potential of the first pulse, to give a steady-state inactivation curve, as shown for averaged data \pm SEM for 6 cells, in Figure 4.6B. Boltzmann functions fitted to the steady state inactivation curve data from each cell, as previously, gave a value for half-maximal inactivation, $V_{1/2}$ at -49.8 mV (\pm 1.4 mV, $n = 6$), and slope factor, k , of 8.3 mV (\pm 1.1 mV). This corresponded to a gating charge of approximately 2.9 elementary charges.

4.3 Discussion

MEL cells transfected with Kv4.2 were found to pass currents which had the characteristics previously described for A currents in native cells and various heterologous expression systems.

Activation of Kv4.2 currents was found to occur in response to depolarising voltage pulses, with significant activation occurring positive to about -30 mV. From the activation curve, it can be seen that all the available channels are activated at potentials above +40 mV, though the method used to construct the activation curve here is less accurate than that used for Kv1.5 in the previous chapter, as discussed

above. This can be seen from the potentials negative to -20 mV; measurements were difficult with small currents as found at these potentials.

Table 4.1 Comparison of activation parameters of Kv4.2 with previous studies

	$V_{1/2}$	k
This study	-9.5mV	10.8 mV
Baldwin <i>et al.</i> (1991) (<i>Xenopus</i> oocytes)	-4.0 mV	20.3 mV
Blair <i>et al.</i> (1991) (<i>Xenopus</i> oocytes)	-1.0 mV	-

The values of half maximal activation, $V_{1/2}$, and slope factor, k, measured in this study were -9.5 mV, and 10.8 mV respectively. These compare with $V_{1/2} = -4.0$ mV (± 1.9 mV) and $k = 20.3$ mV (± 0.9 mV) for Baldwin, Tsaur, Lopez, Jan and Jan (1991) using functional expression of the cDNA in *Xenopus* oocytes, and a value of -1 mV for $V_{1/2}$ by Blair, Roberds, Tamkun, and Harthorne (1991), also using oocytes. Baldwin, Tsaur, Lopez, Jan and Jan constructed a conductance - voltage curve by plotting the amplitude of the peak current divided by the driving force across the membrane using a reversal potential of -100 mV obtained by extrapolation from measured reversal potentials at 20, 40 and 89 mM external K^+ . Conductance values were normalised to the maximum conductance and plotted versus the membrane potential. Half maximal activation and slope factor were obtained from a Boltzmann

equation fitted to the data. Blair , Roberds, Tamkun, and Harthorne assumed a reversal potential of -100 mV in order to calculate the conductance and fitted a Boltzmann equation to a conductance - voltage curve in the same way.

Table 4.2 Comparison of steady state inactivation parameters of Kv4.2 with previous studies

	$V_{1/2}$	k
This study	-49.8mV	8.3 mV
Baldwin <i>et al.</i> (1991) (<i>Xenopus</i> oocytes)	-48.0 mV	9.2 mV
Yeola & Snyders (1996) (Mouse L cells)	-41.0 mV	6.4 mV

Similarly, in comparing parameters for inactivation, in this study, values of half-maximal inactivation, $V_{1/2}$ at -49.8 mV , and slope factor, k, of 8.3 mV compared remarkably closely with the values of -48.0 mV (± 2.5 mV), and 9.2 mV (± 0.6 mV) for Baldwin, Tsauro, Lopez, Jan and Jan (1991). They used a 500 ms pre-pulse to a series of membrane potentials, followed by a 100 ms test pulse to +60 mV, normalising to the maximal peak current during the test pulse, and fitting a Boltzmann equation to the resultant curve with membrane potential of pre-pulse. A study by Yeola and Snyders (1996) of Kv4.2 expressed in a mouse L-cell line gave a value of half-maximal inactivation at -41 mV (± 1 mV) and slope factor 6.4 mV (± 0.1 mV). They used a 400 ms conditioning pre-pulse to a series of membrane potentials,

followed by a test pulse to +50 mV. Again, the maximal peak of the test current was used to normalise, and a Boltzmann equation used for the fit.

Interestingly, Yeola and Snyders fitted single exponentials to the decline in Kv4.2 current, similar to τ_{decay} that I have used in Figure 4.6. They were assessing the effect of flecainide and quinidine on the rate of decline of current, and both of these compounds accelerated the apparent rate of inactivation. Their value for this time constant for a current at +50 mV was 30 ms. This compares to my data giving a mean value of 11 ms at this potential.

Overall, these values for the midpoint potentials of activation are quite similar to those for Kv1.5, but for inactivation, there was a negative shift of over 25mV. This indicates that, at a membrane potential of for example, -40 mV, very few Kv1.5 channels would become inactivated, whereas, at this voltage almost all of the Kv4.2 channels would be expected to become inactivated. After a depolarisation which activates Kv4.2, unless the membrane potential returns to below -80mV, all of the Kv4.2 channels will not be available, because those channels that become inactivated will not have this inactivation reversed.

One of the consequences of this are that, though the Kv4.2 channel becomes activated by depolarisations to membrane potentials positive to about -40 mV, once it is activated, it will operate at membrane potentials negative to -40 mV. Also, it is very possible that the Kv4.2 channel is expressed with an accessory β -subunit *in vivo*. As discussed in the previous chapter, the Kv β 2.1 subunit shifted the half-maximal activation and inactivation of the Kv1.5 α subunit more negative by 13.9 and 12.5 mV respectively (Uebele, England, Chaudhary, Tamkun and Snyders, 1996). Therefore, although the voltage range found in this study over which the Kv4.2 currents are

activated may appear to be too depolarised, the reality under physiological conditions may well be different. The Kv4.2 current may therefore work against the effect of the depolarisation and allow the next action potential to occur at the threshold frequency. In the steady state, the channel conducts within quite a narrow window of negative potentials.

Figure 4.6 shows the time constant of decay of Kv4.2 current at various membrane potentials. This time constant was very steeply voltage dependent up to 0 mV, and less so at membrane potentials positive to this. The mean value of this time constant for the decay in current at -40 mV was found to be 57 ms in this study, and at 0 mV, it was 15 ms. The larger the depolarisation is, the greater the magnitude of the Kv4.2 current, and the quicker the channels inactivate.

There are large differences in relative abundance in the comparison of atrial and ventricular RNA samples of transcripts from the Kv4.2 (RShal1) gene (Dixon and McKinnon, 1994), suggesting that there is variation of transcriptional regulation within cardiac muscle, contributing to spatially regulated control of the action potential. The work of Yeola and Snyders mentioned above indicated that the functional properties of Kv4.2, particularly flecainide sensitivity, resemble those of I_{to} , the transient outward potassium current in the heart more than other potential A-type candidates such as Kv1.4, confirming the importance of this channel in the control of the cardiac action potential.

Figure 4.1 Current-voltage relationship for Kv4.2

A A typical family of whole cell currents recorded from Kv4.2 in response to a series of depolarising voltage steps of 100 ms length. From a holding potential of -80 mV, an initial conditioning 50 ms step to -100 mV ensured that all channels were closed, followed by 100 ms depolarising steps in increments of +10 mV from -60 mV to +90 mV.

B A simple current-voltage relationship constructed using the values of peak current from the records shown in Figure 4.1A plotted versus membrane potential.

Figure 4.1

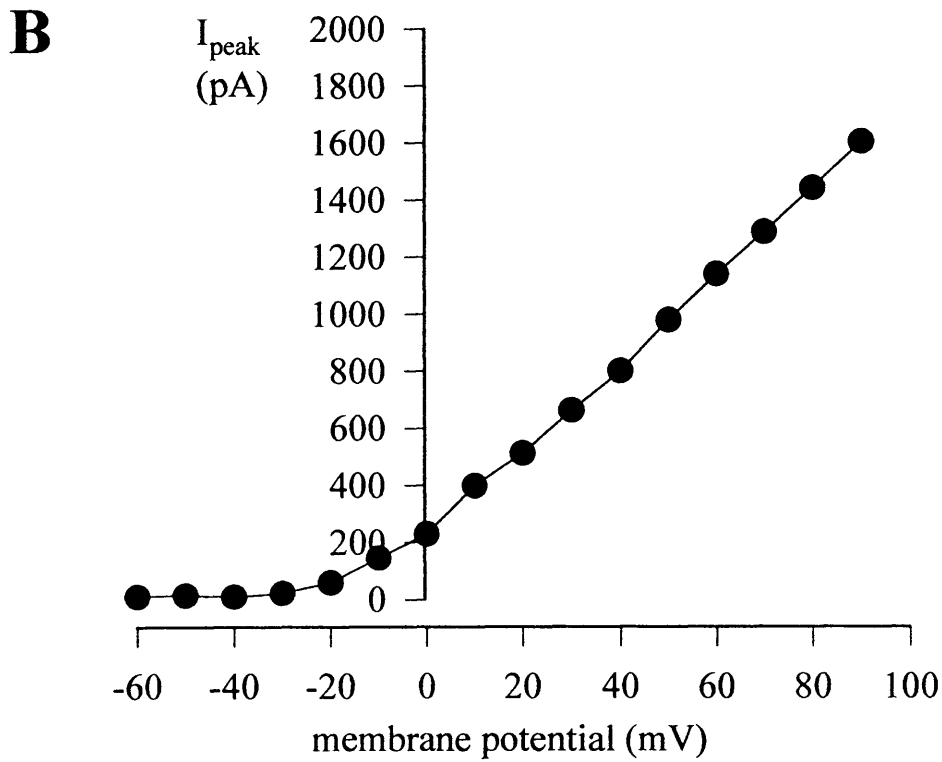
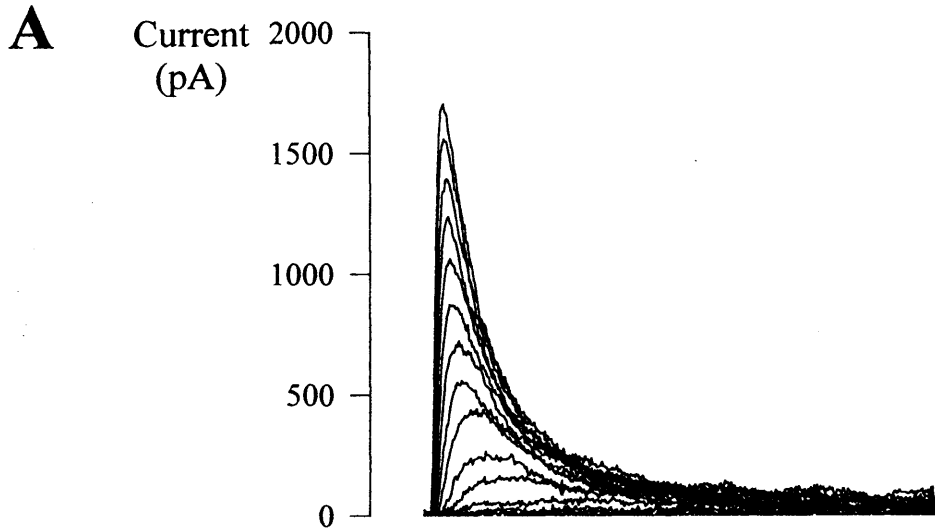
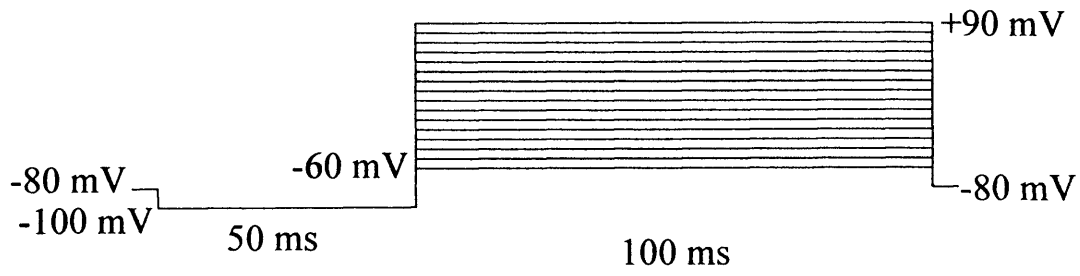


Figure 4.2 Hodgkin-Huxley activation parameters

A A fit of classical Hodgkin-Huxley formula describing a channel showing both activation and inactivation, to a record of a Kv4.2 current. Values of $\tau_{\text{activation}}$, a time constant of activation, were obtained from the parameters of the equation described in the text fitted to currents elicited due to the voltage pulse protocols described above in Figure 4.1A and later again in Figure 4.3A.

B $\tau_{\text{activation}}$ plotted on a linear scale against membrane potential.

C $\tau_{\text{activation}}$ plotted on a common log scale against membrane potential.

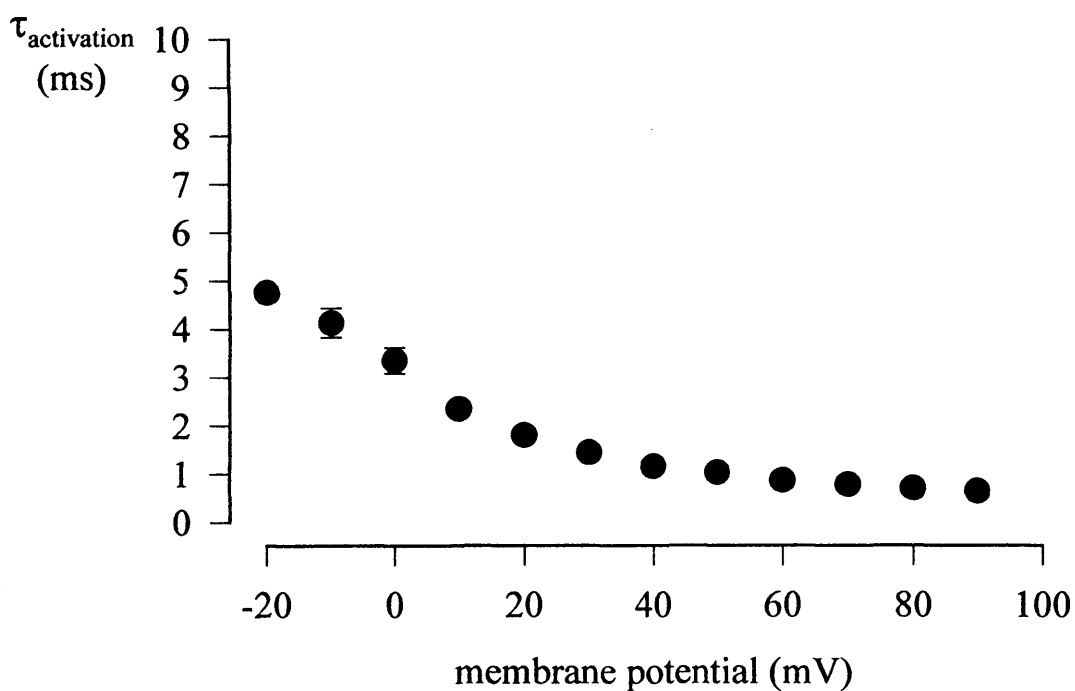
These illustrate the voltage dependence of the activation time constant and represent means \pm SEM for 5 cells.

Figure 4.2

A



B



C

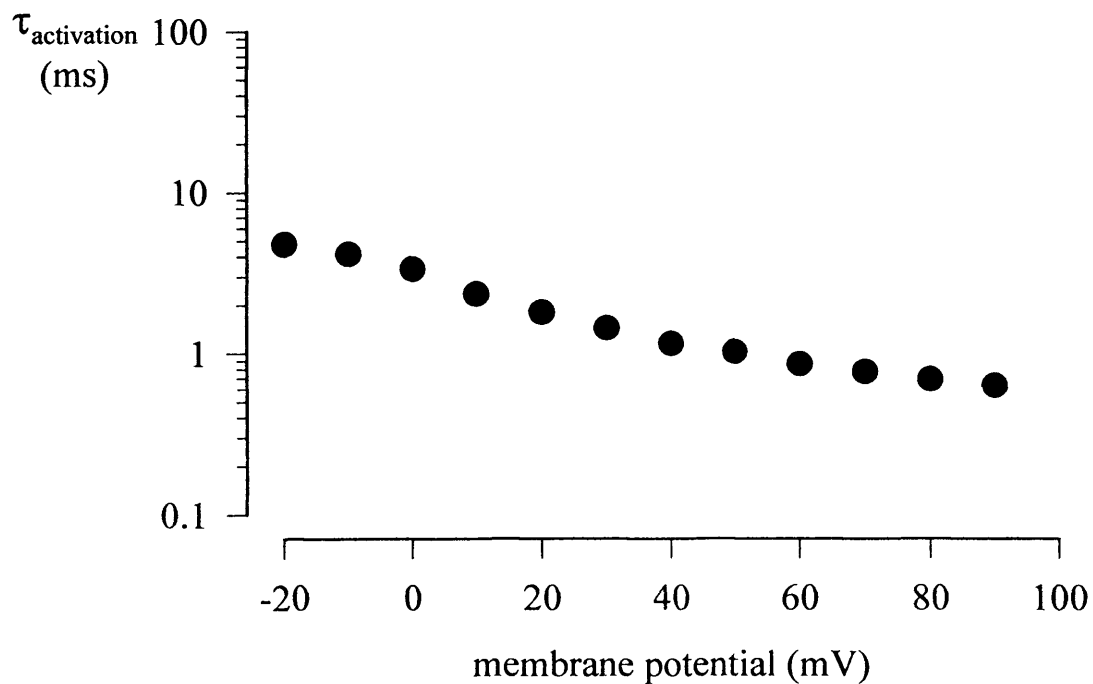


Figure 4.3 Voltage dependence of activation of Kv4.2

A A typical family of whole cell currents recorded from Kv4.2 in response to a series of depolarising voltage steps of 100 ms length. From a holding potential of -80 mV, an initial conditioning 50 ms step to -100 mV ensured that all channels were closed, followed by 100 ms depolarising steps in increments of +10 mV from -60 mV to +90 mV. Inset are exponential fits to the decay of the Kv4.2 currents elicited by the pulses between +40 mV and +90 mV to illustrate the origin of the parameters used in subsequent manipulations. For clarity, only these seven exponential fits are shown, and the time base and current scale is not the same as for the main family of currents.

B The voltage dependence of activation for Kv4.2, a measure of the channel open probability due to constant driving force. Chord conductance at each potential was calculated with respect to the value for I_0 , initial current elicited from the exponential fit to the decay of current (as illustrated in Figure 4.1A above) divided by the driving force at that potential. Values of conductance were normalised to maximal values, and plotted against membrane potential to give an activation curve. Points on this graph of averaged data represent means \pm SEM for 5 cells. A Boltzmann function fitted to this illustrative curve gave half-maximal activation, $V_{1/2}$ at -9.5 mV, and slope factor, $k = 11.5$. The mean value of $V_{1/2}$ returned from fitting the Boltzmann function to each individual activation curve was -9.5 mV (± 2.3 mV) and mean slope factor $k = 10.8$ mV (± 1.0 mV).

Figure 4.3

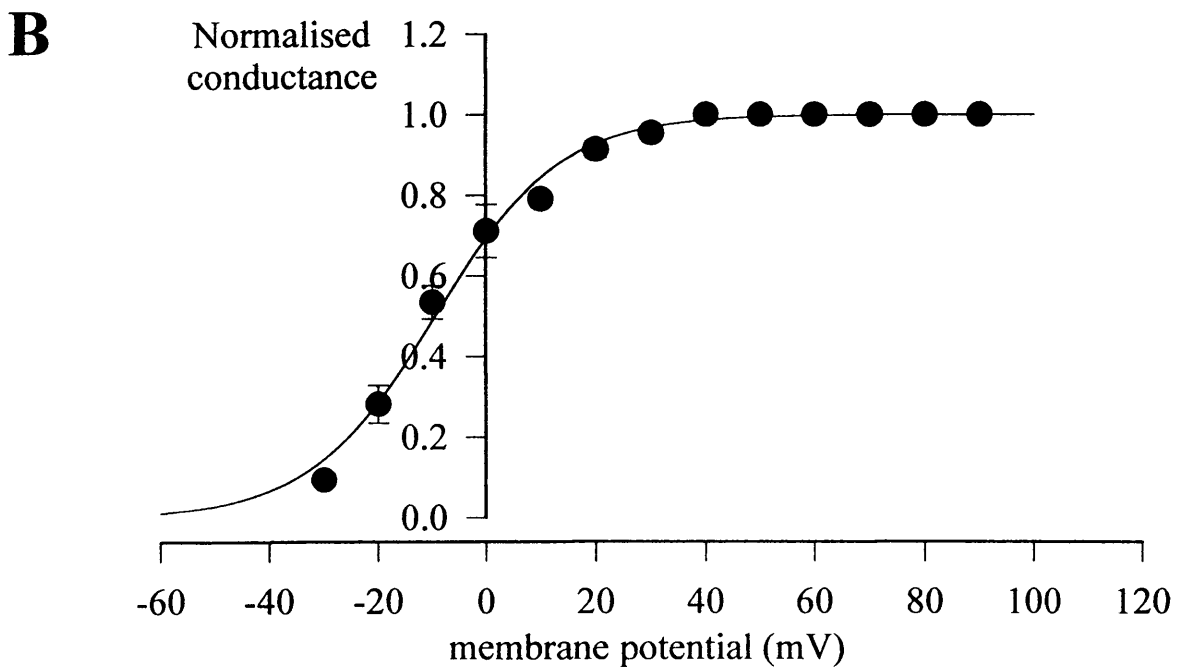
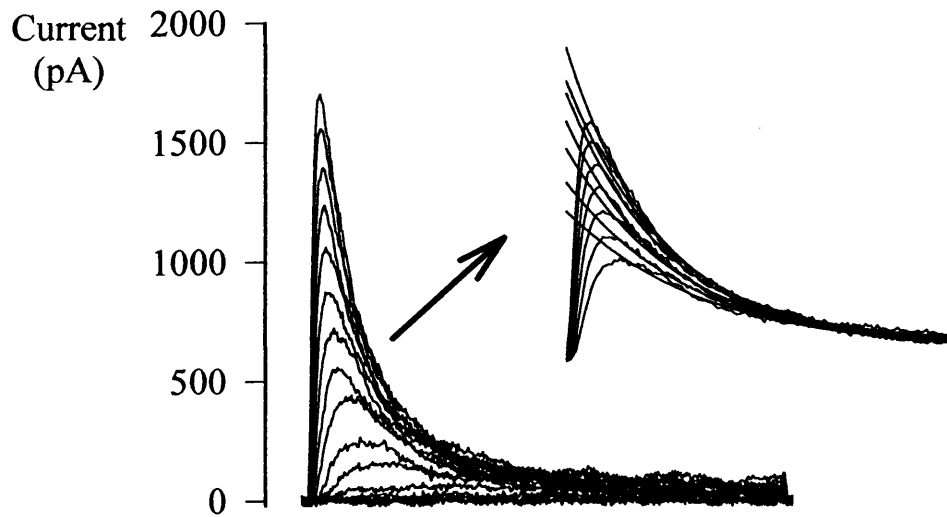
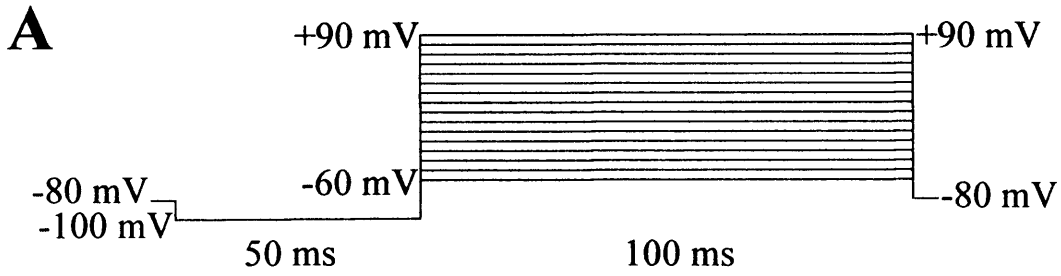


Figure 4.4 Correction of reduction in peak current due to inactivation

A fitted current traces is shown, at a voltage step to +50 mV. The dotted line is placed at the point where the current peaks; this peak current is shown as I_p , and time elapsed is time = t . A full explanation is in the text.

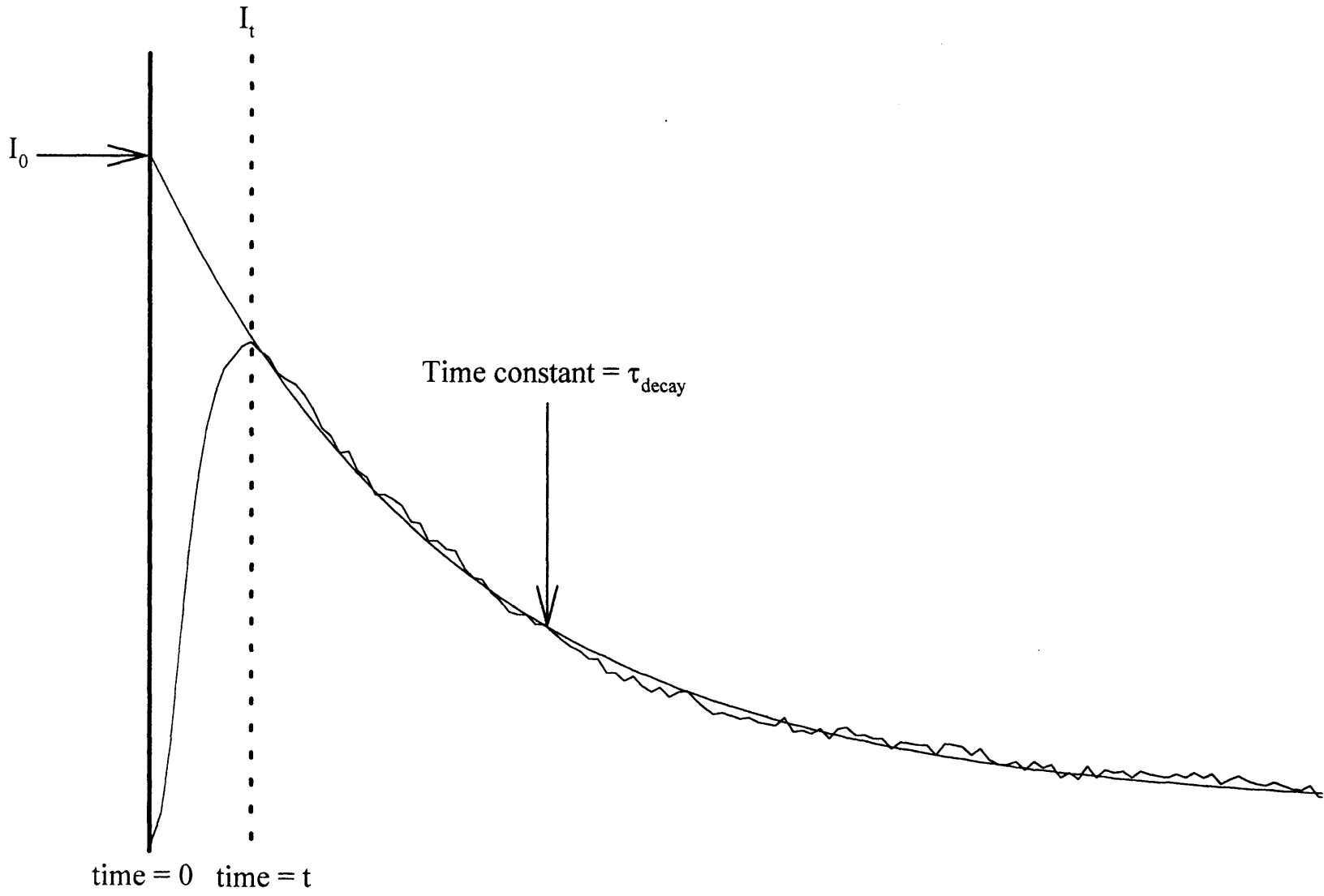


Figure 4.4

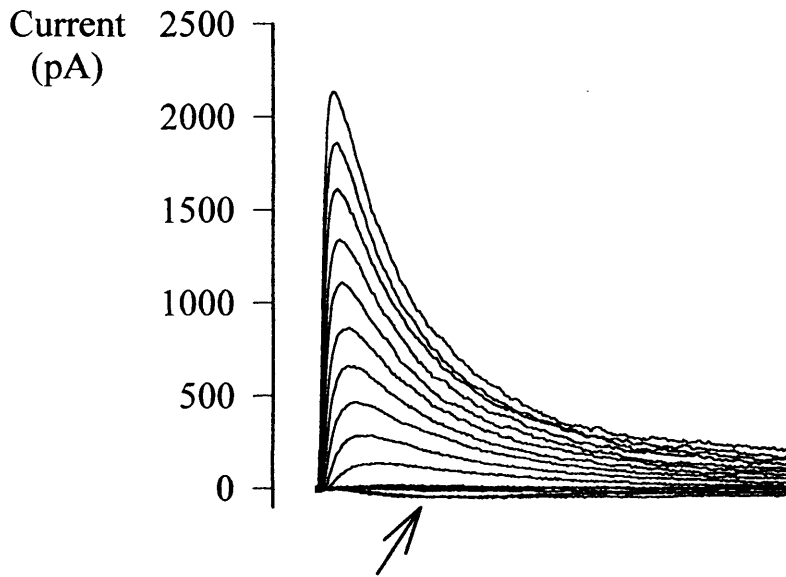
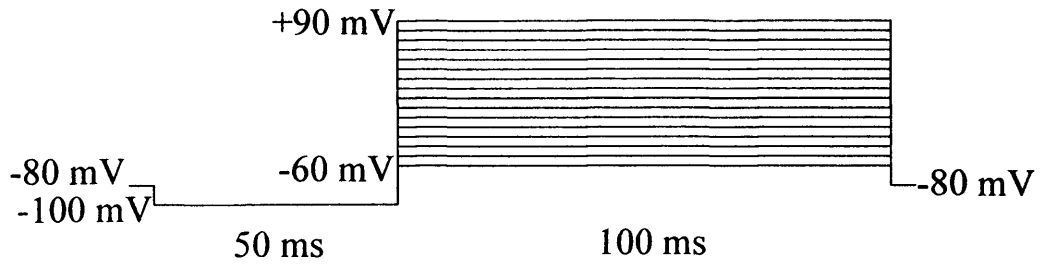
Figure 4.5 Activation curve with 70 mM K⁺ external bath solution

Whole cell currents, voltage pulse protocol and activation curve as in Figure 4.3, but with 70 mM external K⁺ instead of physiological 5 mM K⁺. Points represent means \pm SEM for 7 cells. A Boltzmann function fitted to the individual activation curve data for each cell gave a mean value of half-maximal activation, $V_{1/2}$ at -1.2 mV, and a mean value of slope factor, $k = 9.0$ mV.

The arrow in A shows currents that are inward in direction.

Figure 4.5

A



B

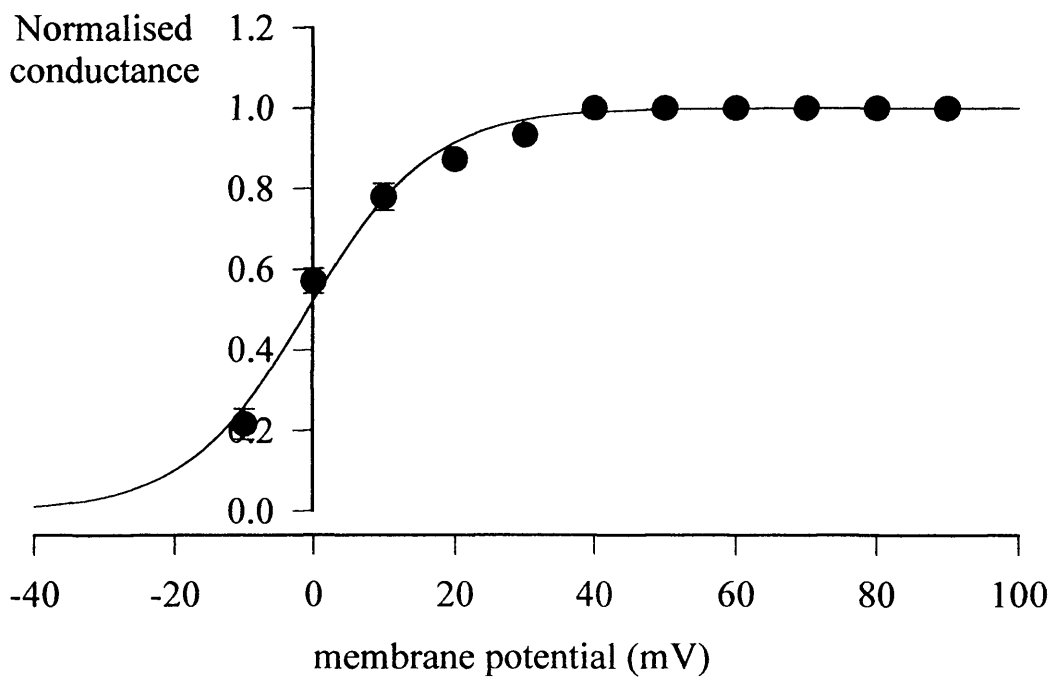


Figure 4.6 Plots of τ_{decay} against membrane potential

A An exponential fit to the decay of the Kv4.2 current in response to a +90 mV pulse. Values of τ_{decay} , a time constant of decay of current were obtained from the exponential fit parameters for currents elicited due to the voltage pulse protocols described earlier in Figure 4.3A.

B,C τ_{decay} plotted on a linear scale (panel B) and common log scale (panel C) against membrane potential for both physiological 5 mM K^+ (circles) and 70 mM K^+ (squares) external bath solutions. Points represent means \pm SEM for 5 and 7 cells respectively.

Figure 4.6

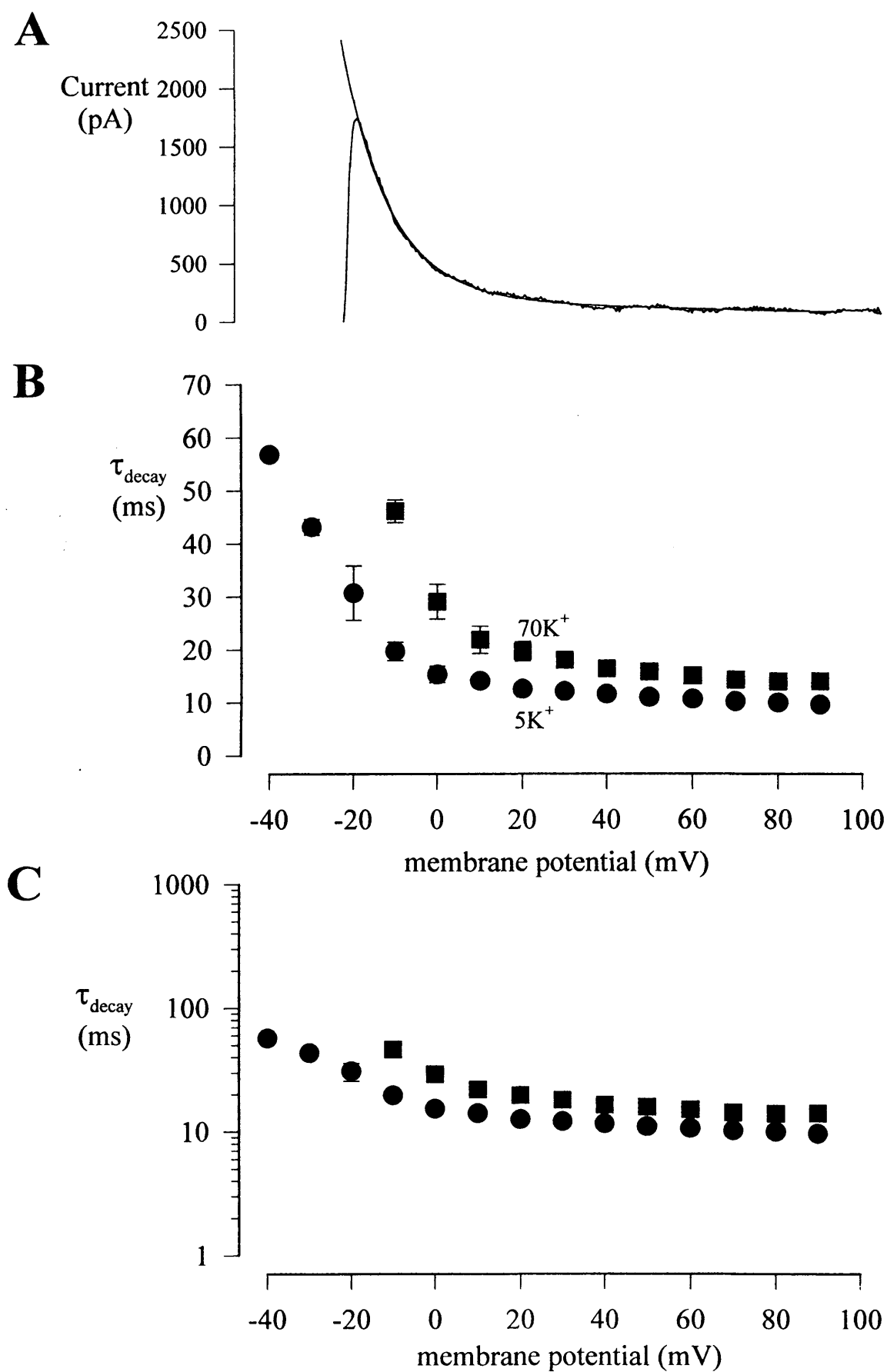


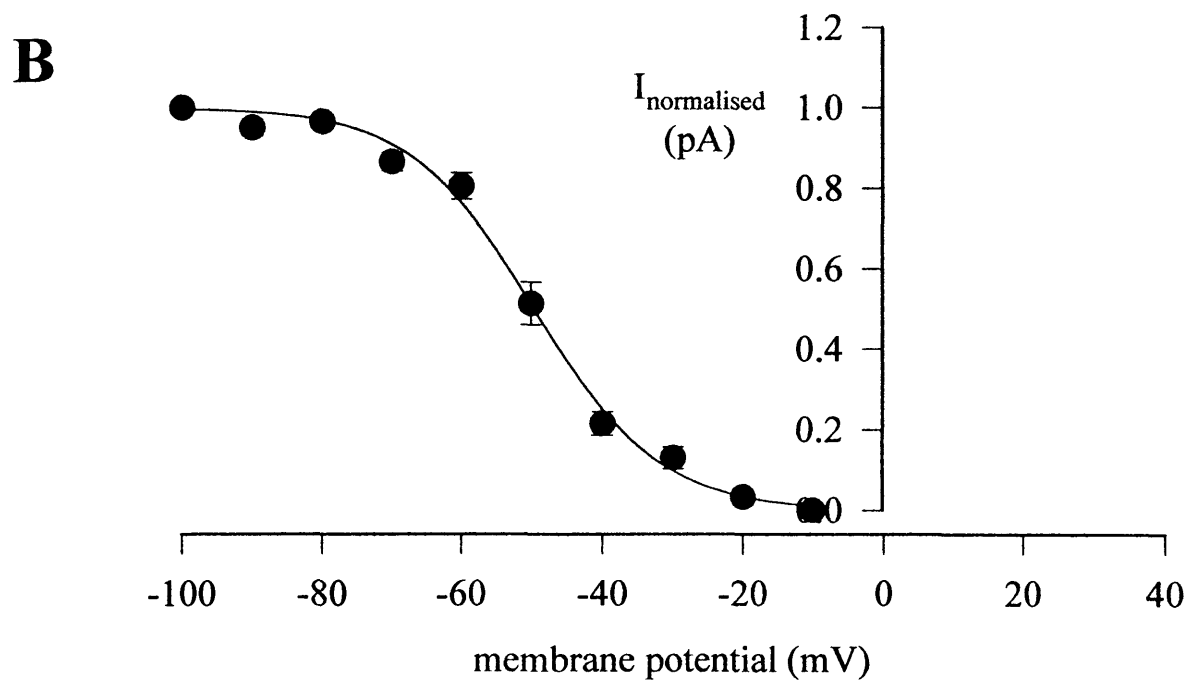
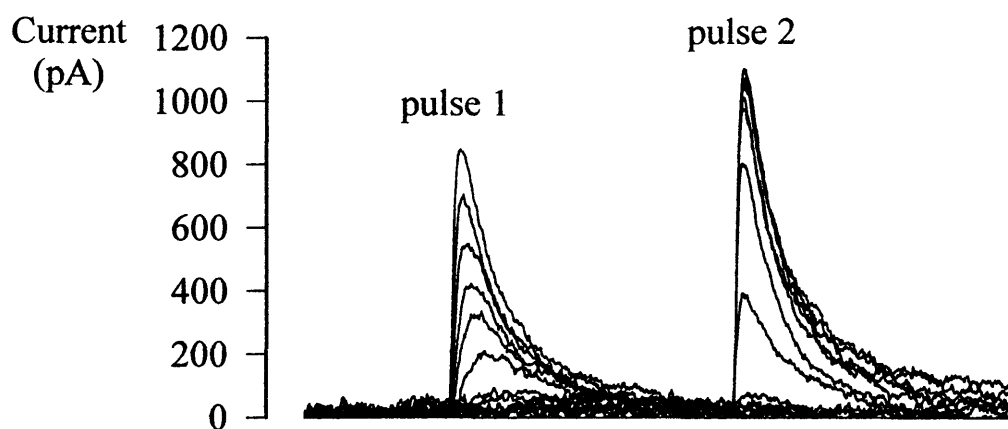
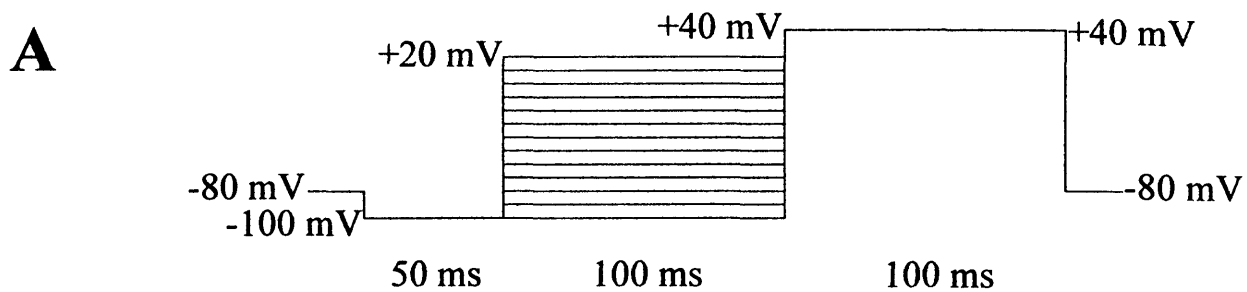
Figure 4.7 Voltage dependence of steady state inactivation of Kv4.2

A The voltage pulse protocol used to produce an inactivation curve for Kv4.2.

From a holding potential of -80 mV, a conditioning 50ms pre-pulse to -100 mV ensured that all channels were closed and inactivation was removed. This was followed by a variable potential 100 ms pulse (pulse 1), depolarising from -100 mV to +20 mV in increments of +10 mV. The final step was a 100 ms constant +40 mV pulse. The current families beneath the voltage pulse protocol show the results of this. The size of the current produced by pulse 1 increased to the maximum with increasing depolarization. Conversely, the size of current due to pulse 2 decreased from the initial maximum value down to zero.

B The magnitude of the current due to pulse 2 was normalised and plotted versus membrane potential to give an inactivation curve. Points represent means \pm SEM for 6 cells. A Boltzmann function fitted to these data gave half-maximal inactivation, $V_{1/2} = -49.8$ mV (± 1.4 mV), and slope factor, $k = 8.3$ (± 1.1 mV).

Figure 4.7



CHAPTER FIVE

The effect of ShakerB inactivating ball peptides on Kv1.5 and Kv4.2 whole cell currents

5.1 Introduction

The 'ball and chain' model for fast inactivation of voltage-activated potassium channels was investigated using MEL cells stably transfected with either Kv1.5, coding for a delayed rectifier current, or Kv4.2, coding for an A-type current.

An inactivation 'ball' particle tethered on the intracellular surface of the channel by a chain at the amino-terminus of the polypeptide, is able to move to a receptor site on the intracellular mouth of the pore to bind and block the pore (Armstrong and Bezanilla, 1977). This model was conceived after experiments with sodium currents in squid giant axon which were altered by proteolytic enzyme treatment of the cytoplasmic face of the channels; after treatment, previously inactivating currents were changed to currents that did not inactivate (Armstrong, Bezanilla and Rojas, 1973).

Hoshi, Zagotta and Aldrich (1990) corroborated this evidence using deletion mutants of the amino terminal cytoplasmic domain of the *Shaker*B potassium channel expressed in *Xenopus* oocytes. The ball and chain model was entirely consistent with their results with this channel as it was with the sodium channel. Deletion of the first 22 amino acid residues at the amino-terminus resulted in a disruption of inactivation. This region is a good candidate for the inactivation ball, with 11 hydrophobic uncharged amino acid residues followed by a hydrophilic, highly polar stretch of 8 amino acids, including four positively charged amino acids. These first 19 residues are followed by an extended sequence of about 60 or more hydrophilic amino acid residues, which was said to be a candidate for the chain. Large deletions restricted to

this chain region alone resulted in inactivation being speeded up as might be expected if the shorter chain would get the ball to the pore more quickly.

According to this model, the ball region should be able to interact with the rest of the channel and produce inactivation, even when not attached by the chain. This was found to be the case.

Synthetic peptides corresponding to the first 20 amino acid portion of the *ShakerB* amino-terminus were found to restore fast inactivation to ShB Δ 6-46, a non-inactivating 41 amino acid deletion mutant of *ShakerB* with most of the amino-terminus removed (Zagotta, Hoshi and Aldrich, 1990). Inactivation was found to be restored in a concentration-dependent manner. Synthetic ball peptides were added to the intracellular side of the cell membrane in the inside-out configuration of the patch clamp technique, and inactivation was readily reversed when peptide-free solution was perfused onto the cell membrane.

Isacoff, Jan and Jan (1991) reported a putative cytoplasmic receptor for the inactivation ball in this model. They proposed that the S4-S5 loop forms part of the receptor, lying at or near the cytoplasmic mouth of the permeation pathway for potassium ions. Mutations here of highly-conserved amino acid residues affected the inactivation of wild-type *ShakerB* channels. The process of diffusion of ball peptide to the receptor site is facilitated by electrostatic interaction. The positively charged and hydrophobic amino acid residues of the ball region are thought to interact with a receptor at the intracellular mouth of the pore, thus the ball can occlude the pore. This receptor may include the amino acid residues in the short intracellular loop between the S4 and S5 transmembrane segments contributing along with the H5 region between S5 and S6, with both regions of the sequence also contributing to the formation of the lower part of the pore. In addition to this, tetraethylammonium ions

applied internally compete with this type of rapid inactivation, and tetraethylammonium ions block the pore (Choi, Aldrich and Yellen, 1991).

The inactivation receptor must be conserved amongst many potassium channel families regardless of their native inactivation rates because the synthetic ball peptides were found to even cause inactivation of cyclic nucleotide-gated channels (Kramer, Goulding and Siegelbaum, 1994) and calcium-activated potassium channels in porcine coronary smooth muscle (Toro, Stefani and Latorre, 1992), rat brain (Foster, Chung, Zagotta, Aldrich and Levitan, 1992) and rat skeletal muscle (Beirão, Davies and Stanfield, 1994), but ATP-dependent potassium channels in rat skeletal muscle were found not to be blocked. The explanation for this is that the highly conserved ion-conducting pore region amongst the potassium channel superfamily must also be the site of interaction of the inactivating ball, since the above channels do not normally display inactivation. ATP-dependent potassium channels lack any homologue for the S1-S4 region of the above channels, and belong to a different family.

Functional voltage-activated potassium channels are tetramers, and inactivation has been shown to involve only one of the four amino-terminal domains to block the pore of each channel. There is evidence to suggest that the synthetic ball peptide binds to the same or similar site to the tethered amino-terminal version in that the peptide preferentially binds to open channels (Zagotta, Hoshi and Aldrich, 1990). Also, one of the point mutations made at the amino-terminus (leucine-7 to glutamic acid) of *ShakerB* by this group had the effect of disrupting the ability of synthetic ball peptides to block the non-inactivating deletion mutant of the *ShakerB* channel.

There is a wide spectrum of inactivation kinetics amongst the alternatively spliced *Shaker* variants, and the *Shaker*-like voltage-activated potassium channel gene subfamilies, ranging from the fast inactivating A-type to delayed rectifiers, which display little or no appreciable inactivation of this type. The aims of the experiments in this chapter were to investigate the effects of using synthetic ball peptides based on the amino-terminal domain of the *ShakerB* channel to block Kv1.5, a delayed rectifier, and Kv4.2, an A-type potassium channel. The *ShakerB* inactivating ball peptide will be referred to as ShB inactivating ball peptide. Rates of block were measured from the decay of whole cell currents recorded with synthetic ball peptide in the internal pipette solution, and the effects of changing concentration were investigated, as well as using different ball peptides with increased positive charges.

5.2 Results

Again, all the experiments here were carried out in the whole cell configuration of the patch clamp technique. External bath solutions contained (except where stated) 140 mM NaCl, 5 mM KCl, 2 mM CaCl₂, 2 mM MgCl₂ and 10 mM HEPES. Control internal pipette solutions contained 140 mM KCl, 2 mM free Mg²⁺ (though 5.8 mM total MgCl₂ was used), 10 mM EGTA, 10 mM HEPES and 20 mM glucose. Synthetic ShB inactivating ball peptide were made by the Peptide and Nucleic Acid Chemistry Laboratory at the University of Leicester, using an Applied Biosystems 431A peptide synthesiser according to the sequences given by Zagotta, Hoshi and Aldrich (1990). The carboxy-terminus of the peptides was amidated to

avoid introducing an additional negative charge that might affect peptide activity. The peptides were purified to a single peak by reversed phase, high pressure liquid chromatography, and purity confirmed by mass spectrometry. The molecular weights of the ShB and ShB:E12K,D13K peptides (see Table 5.1 below) were measured to be 2228 and 2240 respectively. Peptides were stored in solution at -20 °C, and added to the patch pipette at the required concentrations before each experiment. All solutions were adjusted to pH 7.2. The high molecular weight of the peptides caused some concern with regard to mobility and access of the peptide to the cell interior once the whole cell configuration was established. However, in practice it was found that during lengthy periods of recording from the same cell, results obtained earlier or later in the experiment were not much different. On three occasions of recording over 30 minutes, I compared the change in peak current due to + 60 mV pulses (from a holding potential of -80 mV); with ShB peptide present in the pipette, these currents declined by 1.6, 4.9 and 0.4% over approximately half an hour. If one assumes that the effect of the peptide is concentration-dependent, this implies that block of current did not increase to any great degree over the time of recording.

Table 5.1 Amino acid sequence and net charges of *ShakerB* derived synthetic ball peptides.

Peptide	Amino acid sequence	Net charge
ShB	MAAVAGLYGLGEDRQHRKKQ ---+ +++	2+
ShB:L7E	MAAVAGEYGLGEDRQHRKKQ - ---+ +++	1+
ShB:E12K,D13K	MAAVAGLYGLGKKRQHRKKQ +++ +++	6+

All current records were filtered using an 8-pole Bessel filter set at a cut off frequency of 1 kHz (-3 dB) and where two filters were used in series, the composite frequency was also kept at approximately 1 kHz, as described in Materials and Methods. All the currents shown in this chapter have been leak subtracted as described in Materials and Methods.

Several assumptions were made. The ShB inactivating ball peptide was assumed to bind reversibly to a single binding site on the channel and it was assumed that the ball peptide binds to channels in the open state preferentially (Demo and Yellen, 1991); binding of the ball peptide to the site blocked the current through that channel without affecting the binding of other ball peptides to other channels. It was assumed that activation is coupled with inactivation,. The rate of block was measured from the time course of decay phase of whole cell currents elicited by depolarising voltage steps.

The decay phase of the current was fitted with the sum of three exponentials. This was found to give a much easier and better fit than with two exponentials; this is discussed in greater detail in Figure 5.6, where a control current is shown fitted well with just two components, but the test current requires three components to achieve as good a fit. A test current fitted with only two components is also compared.

The time constant of the fast component of inactivation τ_{fast} was taken to be dependent upon peptide block. The C-type inactivation process which was described by Hoshi, Zagotta and Aldrich (1991) in *Shaker* potassium channels, and occurs by a separate molecular mechanism, was not investigated here. C-type inactivation, the

slow component of inactivation has a time constant in the order of several hundred or thousand milliseconds.

Murrell-Lagnado and Aldrich (1993a; 1993b) working with *ShakerB* potassium channels with NH₂-terminal deletions and synthetic peptides of the alternative-spliced variants of the NH₂-terminal sequences of *Shaker*, fitted two exponentials to the decline in current, and took the amplitude of the slow component to be the steady state level of current remaining after peptide block. To get an estimated value for the steady state current as a fraction of peak current in the *absence* of peptide (I_S), they divided the amplitude of the slow component by the sum of the amplitudes of the fast and slow components, that is

$$I_S = \frac{\text{amp}_{\text{slow}}}{\text{amp}_{\text{slow}} + \text{amp}_{\text{fast}}}$$

(Equation 5.1)

where amp_{slow} and amp_{fast} are the amplitudes of the fast and slow components respectively.

Now, due to my use of the sum of three exponentials in fitting the decay of the currents, the value of the amplitude of the slow component is not clear. However, I estimated the fraction of current not blocked by the peptide as:

$$I_S = \frac{I_0 - \text{amp}_{\text{fast}}}{I_0}$$

(Equation 5.2)

that is, the value of amplitude of initial current, I_0 (found by extrapolation) minus the amplitude of the fast component, divided by the amplitude of the initial current. I considered this to be a good estimate of I_S in Equation 5.1 without the complications of finding the amplitude of the steady state current. The problems associated with this are discussed below, and in Figure 5.6.

Further from this, Murrell-Lagnado and Aldrich showed that

$$k_b = \frac{1 - I_S}{\tau_{fast}}$$

(Equation 5.3)

and,

$$k_{ub} = \frac{I_S}{\tau_{fast}}$$

(Equation 5.4)

that is, k_b and k_{ub} , the rates of block and unblock of peptide can be calculated from the above manipulations and τ_{fast} , the time constant of the fast component of inactivation.

Both k_b and k_{ub} have the units s^{-1} .

If blocking rates are equated with binding rates, that is a reversible bimolecular reaction with ball peptide and binding site as reactants, then the association rate constant, k_{on} is obtained by dividing k_b by the concentration of peptide (units are $M^{-1}s^{-1}$), and the dissociation rate constant, k_{off} is not dependent upon peptide concentration and is simply equal to k_{ub} , with the same units, s^{-1} .

The binding of the ball peptide with the binding site can be characterised by an equilibrium dissociation constant, K_D defined in terms of the association and

dissociation rate constants. K_D was calculated by dividing $k_{\text{off}} / k_{\text{on}}$ and has the units M.

5.2.1 The effects of ShB inactivating ball peptide on Kv1.5 currents

Firstly, the effects of the synthetic wild-type ShB inactivating ball peptide on Kv1.5 were investigated. Figure 5.1 shows the effect of including 200 μM ShB inactivating ball peptide in the intracellular pipette solution, in the whole cell patch clamp configuration. Depolarising voltage steps of four second length were applied to control cells in the absence of peptide. The family of currents shown in Figure 5.1A, as shown previously in Chapter 3, were corrected for leakage and capacitance currents. Outward currents became apparent at membrane potentials positive to about -30 mV, and increased with more positive pulses. Current inactivation became apparent for the more positive pulses. Figure 5.1B shows a family of currents recorded with 200 μM ShB inactivating ball peptide included in the internal pipette solution. The extent of the current inactivation for each current trace here can be compared to that of control cells above. It can clearly be seen, particularly with those current traces due to the more positive pulse potentials, that the decline in current at comparative times during the pulse was greater for cells in the presence of the inactivating ball peptide compared to control cells. The slope of the decline in current was greater, especially during the initial 500 ms of the pulse. In the example shown for control cells here, the current due to the +60 mV pulse declined to approximately half of its peak after four seconds. This compares to a decline to approximately a

quarter of the peak current after four seconds for the example of the cell exposed to 200 μ M ShB inactivating ball peptide.

A more valid comparison can be made if the magnitudes of the peak current in the control and test cells were the same. To achieve this, the data array for the current trace at +60 mV in the presence of 200 μ M ShB inactivating ball peptide was multiplied using TRACAN trace analysis software (Davies, 1993) to scale 1:1 with the equivalent trace for control cells. The result is shown in Figure 5.2A over four seconds, and in Figure 5.2B over the initial 50 ms. In panel A, it can be seen that the current declines more steeply in cells exposed to 200 μ M ShB inactivating ball peptide than in control cells, and to a level approximately one half of that in control cells after four seconds. Even after just 50 ms, there is a definite difference in the levels of current decline, as shown in panel B.

5.2.2 Voltage dependence of steady state activation of Kv1.5

In order to investigate the effect of ShB inactivating ball peptide on the voltage dependence of the steady-state activation of Kv1.5, tail currents were used, as shown previously in Figure 3.5. Kv1.5 current was activated by a 50 ms first pulse to a series of potentials, followed by a repolarising step back to a constant -40 mV for 100ms. The instantaneous current due to the second pulse was proportional to the number of open channels at the instant of stepping back to -40 mV from the variable potential first pulse. Instantaneous current values obtained by fitting exponentials to the tail currents were normalised to the maximal current value and plotted versus the membrane potential of the initial variable pulse. This is shown in Figure 5.3A for averaged data \pm SEM for 5 cells. A Boltzmann function (Equation 3.7) fitted to the

activation curve for each cell gave an average value of $V_{1/2}$, the potential at which half maximal activation occurs, to be $-6.6 \text{ mV} (\pm 0.9 \text{ mV})$, and the average value of slope factor, k , which is proportional to the steepness of the voltage dependence, to be $6.0 \text{ mV} (\pm 0.4 \text{ mV})$.

Student's t -tests were carried out to compare these mean values with those in control cells in the absence of ShB inactivating ball peptide (half maximal activation at -6.8 mV and slope factor of 6.8 mV). There was no significant difference for mean values of half-maximal activation ($P = 0.937$) and slope factor ($P = 0.177$) between control cells, and those in the presence of $200 \mu\text{M}$ ShB inactivating ball peptide.

5.2.3 Voltage dependence of steady state inactivation of Kv1.5

Similarly, the effect of ShB inactivating ball peptide on the voltage dependence of inactivation of Kv1.5 was investigated and compared to that in control cells. The voltage pulse protocol used ensured that steady state inactivation had developed fully by holding the cell at variable potentials for a 60 second conditioning pre-pulse before a single 100 ms test pulse to $+20 \text{ mV}$. As shown for control cells in Figure 3.8, currents elicited by the test pulse became larger as the first pulse was made increasingly more negative. These currents reached a plateau level, usually at potentials negative to -40 mV . The peak values of current were normalised to the average of the values at this plateau, and plotted versus the potential of the conditioning pre-pulse, to give an inactivation curve as shown in Figure 5.3B for average data \pm SEM for 5 cells.

Again the inactivation curves for each cell were fitted with a Boltzmann function. Mean values of half maximal steady state inactivation occurred at -24.9 mV (± 1.2 mV, $n = 5$) and the slope factor, k was found to be 6.1 mV (± 0.2 mV) corresponding to a gating charge of approximately 3.9 elementary charges.

Statistical analysis by Student's t-tests showed no significant difference in the inactivation parameters of half maximal steady state inactivation ($P = 0.174$) and slope factor ($P = 0.445$) between control cells (half maximal inactivation at -22.3 mV and slope factor of 6.3 mV), and those in the presence of 200 μ M ShB inactivating ball peptide.

5.2.4 Recovery from inactivation

The recovery from inactivation in the presence of 200 μ M ShB inactivating ball peptide was investigated. The same set of voltage pulse sequences were used as shown for control Kv1.5 transfected cells in Figure 3.10. Increasing the interval between two equal voltage pulses and comparing the amplitude of the currents produced by these pulses gave a measure of how many channels had recovered from inactivation during the interval. Fractional recovery was plotted against separation time. This plot of peptide blocked data was fitted with the sum of two rising exponentials, because the curve obtained using one exponential did not accurately fit the data. This is shown for averaged data \pm SEM for 5 cells in Figure 5.4. As in control cells, as the interval was increased, it was seen that more current was activated by the second pulse, as more inactivation was removed. A 10 second interval led to nearly complete recovery from inactivation. A plot of fractional recovery against

recovery time for each cell in the presence of 200 μM ShB inactivating ball peptide was fitted with the expression to give two time constants of recovery from inactivation, with mean values of 0.29 seconds ($\pm 1.2 \times 10^{-3}$ seconds, $n = 5$) and 3.8 seconds (± 0.2 seconds).

To be able to compare this set of data with that from control cells, as shown in Figure 3.10, the control data was also re-fitted with the sum of two rising exponentials, even though that was well-fitted with an expression containing just one exponential. The control data gave mean values of 0.26 seconds ($\pm 2.8 \times 10^{-3}$ seconds, $n = 5$) and 4.5 seconds (± 0.8 seconds) for the fast and slow components respectively. Student's t-tests comparing these mean values of data from control Kv1.5 cells and from Kv1.5 cells in the presence of 200 μM ShB inactivating ball peptide for the fast component showed that there was not a statistically significant difference ($P = 0.497$) between the two groups of data. Similarly, for the slow component time constant of recovery from inactivation, there was not a statistically significant difference ($P = 0.516$) between the two groups of data.

Thus, it was found that neither the voltage dependence of steady state inactivation of Kv1.5, nor the time constants of recovery from inactivation were altered when 200 μM ShB inactivating ball peptide was included in the internal pipette solution. The main difference evaluated by this experiment was that although the recovery from inactivation for control cells could be reasonably well described by a single exponential function, adding another exponential to the expression used for fitting gave a much more accurate fit. It appears that another factor is introduced for cells in the presence of inactivating ball peptide, because a single exponential did not give as good fits as the control data.

5.2.5 Inactive mutant variant of the ShB inactivating ball peptide

Figure 5.5 shows that the use of the inactive mutant inactivating ball peptide ShB:L7E had the expected result of not affecting the inactivation of the Kv1.5 current. This version of the peptide has a point mutation at position 7 from a neutral leucine to negatively charged glutamate, and has previously been shown to be inactive (Zagotta, Hoshi and Aldrich, 1990; Toro, Stefani and Latorre, 1992; Beirão, Davies and Stanfield, 1994). Figure 5.5A shows the data array for a four second current trace at +60 mV in the presence of 200 μ M ShB:L7E ball peptide multiplied to scale 1:1 with the equivalent trace for control cells. This control trace is the same as that used in Figure 5.2A. This result is also shown in Figure 5.2B over the initial 50 ms. In panel A, it can be seen that there is little difference in the rate of current decline between the trace from the control cell and that from cells in the presence of ShB:L7E ball peptide. Indeed, over the first two seconds the current from the control trace had actually declined to a slightly greater degree than that with ShB:L7E ball peptide before a 'cross over' point; after four seconds, the final level of control current was just slightly more than that of test current. This final level of current after four seconds is approximately one half of the peak current for membrane pulses to +60 mV in all control and ShB:L7E ball peptide exposed cells (other data not shown). After just 50 ms, there is little difference in the levels of current decline between the traces, as shown in panel B for scaled data from control and ShB:L7E ball peptide exposed cells different to those in panel A.

5.2.6 The kinetics of the block of Kv1.5 by ShB inactivating ball peptide

Before I discuss the various blocking/unblocking rates, association on and off rate constants and dissociation rate constants, Figure 5.6 explains some of the parameters used in the equations defined above used to determine these parameters. Figure 5.6A shows a typical Kv1.5 whole cell current trace recorded with 200 μ M ShakerB inactivating ball peptide in the internal pipette solution. This trace is shown here fitted with the sum of three exponentials using the TRACAN trace analysis programme (Davies, 1993). This figure illustrates how the peak current in the absence of any inactivation was estimated by extrapolating the curve back to time $t = 0$. The numerical results of this fit return the estimated value of the magnitude of peak current in the absence of any inactivation, termed I_0 . This figure also shows how difficult it was to obtain an estimate of I_{ss} , the magnitude of the steady state current. It is difficult to say whether the current remaining at the end of the four second depolarising pulse is steady state or not.

The same current trace in Figure 5.6A is shown in both Figure 5.6C and Figure 5.6D, fitted with the sum of three and two exponentials with time constants τ_1 and τ_2 (and τ_3 with three exponentials) respectively. The exponential curve in panel C overlays the data points quite closely throughout compared to the exponential curve in panel D which particularly misses the initial section following the peak of the current. Thus, two components were deemed to be unsatisfactory for fitting the decline of peptide blocked currents. In contrast, panel B shows a control current, recorded in the absence of ball peptide, fitted with two components. The decline of current here was well fitted, and in contrast to the ball peptide blocked current shown in panel D, the

initial part of the current following the peak was not missed by the fit. The implication of this is that the ball peptide introduces the third, fastest element in the decline of the whole current, and justifies the use of the fast component of block in my calculations, and the subtraction of the unblocked steady state portion of the current.

τ_1 represents τ_{fast} in my calculations used in this chapter. The amplitude of this time constant was also returned by the exponential fitting routine.

As mentioned above in the Methods section, Murrell-Lagnado and Aldrich took the amplitude of the slow component to be the steady state level of current remaining after peptide block and estimated the value of the steady state current as a fraction of peak current in the absence of peptide by dividing the amplitude of the slow component by the sum of the amplitudes of the fast and slow components.

As mentioned above, Figures 5.6A and C confirm that the use of the sum of three exponentials in fitting the decay of the currents provided a more accurate result for the initial decline in current after the peak, than if the sum of two exponentials had been used. Unfortunately, the numerical value of the amplitude of the slow component was not always meaningful or clear; sometimes a negative value was returned.

However, I estimated the fraction of current not blocked by the peptide as the value of amplitude of initial peak current in the absence of peptide, I_0 (found by extrapolation) minus the amplitude of the fast component, divided by the amplitude of the initial current (Equation 5.2). I_0 minus fast component amplitude is equivalent to the slow component amplitude (if one assumes that the sum of the amplitudes of fast and slow components is equal to the amplitude of the peak current in the absence of peptide).

Blocking rates, k_b and unblocking rates, k_{ub} of 200 μ M ShakerB inactivating ball peptide with Kv1.5 were calculated after fitting four second current traces such as those in Figure 5.1B with the sum of three exponentials. The parameters discussed above returned from the fitting process were used in Equations 5.3 and 5.4 to give blocking and unblocking rates. The rate of block and unblock were derived, as explained above, from the estimate of the steady state current as a fraction of the peak current not blocked by peptide (I_s). Since the fast time component of inactivation was taken to be dependent upon peptide block, the blocking rate was defined as $(1 - I_s)$ divided by time constant of this fast component, and the unblocking rate as I_s divided by the fast component time constant.

These rates were plotted versus membrane potential, as shown in Figure 5.7A. Points on this graph, and in panels B and C represent means \pm SEM for 3 cells. Blocking rates, k_b are represented by circles, and unblocking rates, k_{ub} by squares. Both rates appear to be voltage-dependent. At a membrane potential of 0 mV, k_b is equal to a mean value of 0.5 s^{-1} ($\pm 0.1 \text{ s}^{-1}$); it rises with a linear relationship with membrane potential, and at a membrane potential of 100 mV, k_b is equal to 1.6 s^{-1} ($\pm 0.2 \text{ s}^{-1}$). At 0 mV, k_{ub} is equal to 0.8 s^{-1} ($\pm 0.2 \text{ s}^{-1}$), rising linearly to 5.9 s^{-1} ($\pm 0.2 \text{ s}^{-1}$) at a membrane potential of 100 mV.

Figure 5.7B shows association rate constants, k_{on} (circles), and dissociation rate constants, k_{off} (squares), for 200 μ M ShakerB inactivating ball peptide with Kv1.5 plotted versus membrane potential. Association rate constant is related to the blocking rate by dividing by the peptide concentration, which is constant here. Thus, the plot of k_{on} also shows voltage dependence, rising linearly from a mean value of $2.3 \times 10^3 \text{ M}^{-1} \text{ s}^{-1}$ ($\pm 0.7 \times 10^3 \text{ M}^{-1} \text{ s}^{-1}$) at 0 mV to a mean value of $8.2 \times 10^3 \text{ M}^{-1} \text{ s}^{-1}$ ($\pm 1.0 \times 10^3 \text{ M}^{-1} \text{ s}^{-1}$) for a membrane potential of 100 mV. Since the dissociation rate constant, k_{off}

describes the reverse of binding by peptide, it is not dependent upon peptide concentration. Thus, k_{off} is simply equal to k_{ub} , with the same units, s^{-1} , and the plot is the same as in Figure 5.7A.

The equilibrium dissociation constants, K_D , for 200 μM ShakerB inactivating ball peptide with Kv1.5 are shown plotted versus membrane potential in Figure 5.7C. This graph is derived from the data in Figure 5.7B. There is some scatter here as might be expected for data derived from other data rather than from direct measurements, though the trend appears to be for the equilibrium dissociation constants to be almost voltage independent.

Figure 5.8 shows data (in the same format as in Figure 5.7) for Kv1.5 currents recorded with 100 μM ShB inactivating ball peptide in the internal pipette solution rather than 200 μM . k_b and k_{ub} were calculated in the same way. These rates were again plotted versus membrane potential, as shown in Figure 5.8A. Points on this graph represent means \pm SEM for 3 cells. Blocking rates, k_b are represented by circles, and unblocking rates, k_{ub} by squares. Both rates again appear to be voltage-dependent. At a membrane potential of 0 mV, k_b is equal to a mean value of 0.3 s^{-1} ($\pm 0.1 \text{ s}^{-1}$); it rises with a linear relationship with membrane potential, and at a membrane potential of 100 mV, k_b is equal to 1.3 s^{-1} ($\pm 0.2 \text{ s}^{-1}$). At 0 mV, k_{ub} is equal to 1.2 s^{-1} ($\pm 0.2 \text{ s}^{-1}$), rising linearly to 6.4 s^{-1} ($\pm 0.3 \text{ s}^{-1}$) at a membrane potential of 100 mV. Figure 5.8B shows k_{on} (circles), and k_{off} (squares), for 100 ShakerB inactivating ball peptide with Kv1.5 plotted versus membrane potential. The plot of k_{on} is derived from the data for k_b by dividing by the peptide concentration, 100 μM . Here, it also shows voltage dependence, rising from a mean value of $2.7 \times 10^3 \text{ M}^{-1}\text{s}^{-1}$ ($\pm 0.8 \times 10^3 \text{ M}^{-1}\text{s}^{-1}$)

at 0 mV to a mean value of $12.5 \times 10^3 \text{ M}^{-1}\text{s}^{-1}$ ($\pm 1.8 \times 10^3 \text{ M}^{-1}\text{s}^{-1}$) for a membrane potential of 100 mV. Again, the plot of k_{off} is the same as that for k_{ub} . The equilibrium dissociation constants, K_{D} , for 100 μM ShakerB inactivating ball peptide with Kv1.5 are shown plotted versus membrane potential in Figure 5.8C. As for Figure 5.7C above, the equilibrium dissociation constants here appear to be voltage independent.

5.2.7 A mutant of the ShB inactivating ball peptide with increased positive charge

The effect of the ShB:E12K,D13K inactivating ball peptide on Kv1.5 currents was investigated. This form of the peptide has point mutations at positions 12 and 13 from negatively charged glutamate and aspartate respectively, both to positively charged lysine. This has the effect of increasing the net charge of +2 in wild type ShB inactivating ball peptide to +6 in this variant.

Figure 5.9 illustrates the effect of the ShB:E12K,D13K inactivating ball peptide on Kv1.5 currents using superimposed scaled currents as previously shown. Figure 5.9A matches the magnitude of the peaks of the current traces in response to the +60 mV voltage pulse of 4000 ms duration for a typical control Kv1.5 current, and one each in the presence of 200 μM ShB and 200 μM ShB:E12K,D13K inactivating ball peptides. The result was quite dramatic; the trace for 200 μM ShB:E12K,D13K inactivating ball peptide showed a very rapid decline in current over the first 200 ms of the voltage pulse even compared to the wild type peptide. The current had declined to approximately 33 % of its peak value after this first 200 ms; this compares to a

decline to approximately 55 % of the peak of the current in the presence of 200 μM ShB inactivating ball peptide, and a decline to 66 % of peak in control cells over this same initial time period. After 200 ms, the slope of the current decline flattened out so much that over the remaining 3800 ms of the +60 ms voltage pulse, the current in the presence of 200 μM ShB:E12K,D13K inactivating ball peptide declined to 20 % of the peak. The final level of current at the end of the pulse was very similar to that in the presence of wild type peptide.

Figure 5.9B has superimposed scaled current traces showing the effect of 200 μM ShB:E12K,D13K and ShB inactivating ball peptides on Kv1.5 currents over a shorter time, 50 ms. Again, the current in the presence of 200 μM ShB:E12K,D13K declined to a much greater degree than that in the presence of 200 μM ShB inactivating ball peptide and that in control cells. The peak of the 200 μM ShB:E12K,D13K current trace can be discerned more easily than the others, and the time to peak from the beginning of the voltage pulse at approximately 6 ms was shorter than that with wild-type ball peptide (10-14 ms), which in turn was shorter than that in control cells (12-17 ms). Over 50 ms, the Kv1.5 current in the presence of 200 μM ShB:E12K,D13K inactivating ball peptide resemble those from a typical A-type potassium channel, such as Kv4.2.

Figure 5.10 shows the variation with membrane potential of 100 μM ShB:E12K,D13K inactivating ball peptide blocking/unblocking rates, association/dissociation rate constants and Equilibrium dissociation constants in cells transfected with Kv1.5. Points represent means \pm SEM for 3 cells in each panel of this figure. Blocking rates, k_b (circles), and unblocking rates, k_{ub} (squares), of 100 μM ShB:E12K,D13K inactivating ball peptide with Kv1.5 are shown in Figure 5.10A. At

a membrane potential of 0 mV, k_b is equal to a mean value of $6.1 \text{ s}^{-1} (\pm 1.8 \text{ s}^{-1})$; it rises with a linear relationship with membrane potential, and at a membrane potential of 100 mV, k_b was equal to $33.7 \text{ s}^{-1} (\pm 0.4 \text{ s}^{-1})$. At 0 mV, k_{ub} was equal to $9.0 \text{ s}^{-1} (\pm 1.0 \text{ s}^{-1})$, rising linearly to $15.6 \text{ s}^{-1} (\pm 0.6 \text{ s}^{-1})$ at a membrane potential of 100 mV. The plot of k_{on} (Figure 5.10B) was once again derived from the data for k_b by dividing by the peptide concentration, 100 μM . Here, it increased from a mean value of $6.1 \times 10^4 \text{ M}^{-1} \text{ s}^{-1} (\pm 18 \text{ M}^{-1} \text{ s}^{-1})$ at 0 mV to a mean value of $3.4 \times 10^5 \text{ M}^{-1} \text{ s}^{-1} (\pm 4.1 \text{ M}^{-1} \text{ s}^{-1})$ for a membrane potential of 100 mV. Again, the plot of k_{off} is the same as that for k_{ub} . Equilibrium dissociation constants, K_D , for 100 μM ShB:E12K,D13K inactivating ball peptide with Kv1.5 are shown plotted versus membrane potential in Figure 5.10C. As previously, the equilibrium dissociation constants, a measure of affinity for the peptide, appeared to be largely voltage independent, though it might be argued that over the range shown, there is a slight downward slope with increasing membrane potential, indicating an increase of affinity with increasing voltage.

Figure 5.11 uses histogram plots to compare blocking and unblocking rates, association rate constants and Equilibrium dissociation constants for 100 and 200 μM ShB and 100 μM ShB:E12K,D13K inactivating ball peptides with Kv1.5 at a +60 mV pulse. In all four cases, shown by the four panels of this figure, there was statistically no significant difference in the mean values of the respective parameters between 100 and 200 μM ShB inactivating ball peptide data. However, in each case, there was a significant difference between data from both concentrations of wild type peptide compared to that from 100 μM ShB:E12K,D13K peptide. The blocking and unblocking rates, and association rate constants were greatly increased for Kv1.5

currents recorded with the mutant form of the ball peptide in the internal pipette solution compared to those recorded with two concentrations of the wild-type peptide. The mutant form of the peptide carries four extra positive charges compared to wild-type.

Figure 5.11A compares the blocking rate k_b for mean data (\pm SEM) from three cells in each case. Mean values were 1.3 s^{-1} ($\pm 0.6 \text{ s}^{-1}$), 1.1 s^{-1} ($\pm 0.1 \text{ s}^{-1}$) and 26.8 s^{-1} ($\pm 6.0 \text{ s}^{-1}$) respectively for 200 μM ShB, 100 μM ShB and 100 μM ShB:E12K,D13K inactivating ball peptides. Student's t-tests applied to these data showed that wild type peptide data at the two concentrations was not significantly different ($P = 0.83$), but both of these sets of data were significantly different ($P < 0.05$) to that with the mutant form of the peptide.

Figure 5.11B shows the unblocking rate k_{ub} . In this panel, again from data for three cells in each case, mean values were 2.9 s^{-1} ($\pm 0.8 \text{ s}^{-1}$), 3.8 s^{-1} ($\pm 0.3 \text{ s}^{-1}$) and 13.6 s^{-1} ($\pm 0.1 \text{ s}^{-1}$) respectively for 200 μM ShB, 100 μM ShB and 100 μM ShB:E12K,D13K inactivating ball peptides at voltage pulses to +60 mV. There was no significant difference between 200 μM ShB and 100 μM ShB mean values ($P = 0.57$) -one would not expect there to be a difference since for a bimolecular reaction, the unblocking rate should be independent of concentration. Comparing these wild-type values to mean values with 100 μM ShB:E12K,D13K gave a significant difference in both cases ($P = 0.001$ and $P < 0.001$ respectively).

The association rate constant k_{on} is compared in Figure 5.11C. Since this rate constant is derived from the relationship between the blocking rate and concentration of peptide, it was unsurprising that the statistical analysis of yielded the same result as that above for these sets of data. The mean values of association rate constant as shown in the histogram were $6.6 \times 10^3 \text{ M}^{-1} \text{ s}^{-1}$ ($\pm 2.9 \times 10^3 \text{ M}^{-1} \text{ s}^{-1}$), $1.1 \times 10^4 \text{ M}^{-1} \text{ s}^{-1}$

($\pm 1.1 \times 10^3 \text{ M}^{-1} \text{ s}^{-1}$) and $2.7 \times 10^5 \text{ M}^{-1} \text{ s}^{-1}$ ($\pm 6.0 \times 10^3 \text{ M}^{-1} \text{ s}^{-1}$) respectively for 200 μM ShB, 100 μM ShB and 100 μM ShB:E12K,D13K inactivating ball peptides at voltage pulses to +60 mV. Again, there was no significant difference between the sets of data for wild-type peptide ($P = 0.277$) but there was between these and data for mutant peptide ($P < 0.05$ in both cases). The comparison of blocking rate and association rate constant between the two concentrations of the wild-type peptide did not yield the expected result, pointing perhaps to problems with access of the peptides to the interior of the cell. This will be elaborated upon in the discussion for this chapter.

Finally, Figure 5.11D compares equilibrium dissociation constant K_D , for 100 and 200 μM ShB, and 100 μM ShB:E12K,D13K inactivating ball peptides with Kv1.5 at a pulse potential of +60 mV. Values of this parameter, which represents the ratio of dissociation and association rate constants, were $4.5 \times 10^{-4} \text{ M}$ for 200 μM ShB, $3.4 \times 10^{-4} \text{ M}$ for 100 μM ShB and $5.1 \times 10^{-5} \text{ M}$ for 100 μM ShB:E12K,D13K. As expected, there was a higher affinity for the more positively charged variant of the ball peptide, indicated by the lower value of K_D .

Figure 5.12 is another histogram representation of data, this time comparing the values of τ_{fast} returned from fitting the decline of current traces due to voltage pulses to +60 mV. This time, it was valid to include the mean data for control cells (from seven cells) in the absence of peptide, together with data for three cells each in the presence of 100 and 200 μM ShB, and 100 μM ShB:E12K,D13K inactivating ball peptides. Mean values were 246.4 ms (± 14.9 ms) for Kv1.5 currents recorded from control cells, and 176.3 ms (± 7.8 ms), 124.4 ms (± 5.5 ms) and 25.9 ms (± 5.3 ms) respectively for currents recorded in the presence of 100 and 200 μM ShB, and

100 μ M ShB:E12K,D13K inactivating ball peptides. Student's t-tests showed a significant difference for values of τ_{fast} between control cells and 100 μ M ShB ($P < 0.05$), between 100 μ M ShB and 200 μ M ShB ($P < 0.01$) and between 200 μ M ShB and 200 μ M ShB:E12K,D13K ($P < 0.001$)

5.2.8 The effects of the ShB:E12K,D13K inactivating ball peptide on Kv4.2 currents

I will now discuss the Kv4.2 whole cell experiments I conducted with 200 μ M ShB:E12K,D13K inactivating ball peptide in the internal pipette solution. Kv4.2 is a rapidly activating and inactivating A-type potassium channel, and these recordings were made with the form of the peptide (from those available for these experiments) and concentration that would show the greatest effect. As mentioned later in the discussion, the peptide concentration can be critical in many ways, for example, ease of seal formation and actual amount of peptide available to the inside of the channels; a balance needs to be struck.

Figure 5.13 shows the effect on Kv4.2 currents of including 200 μ M ShB:E12K,D13K inactivating ball peptide in the internal pipette solution. Panels A and B show typical whole cell currents recorded from Kv4.2 in the absence and presence of peptide respectively. Records have been corrected for leakage and capacitance currents. Currents were recorded in response to depolarising voltage steps of 100 ms duration, from a holding potential of -80 mV, in +10 mV steps from 0 mV to +90 mV. A 50 ms pre-pulse to -100 mV ensured that all channels were in the closed non-inactivated state. The voltage pulse protocol is shown above the currents.

It can be seen that current traces in the presence of the peptide reached their peak much more quickly and showed a very rapid decline in current over the first 10 - 20 ms of the voltage pulse, with current traces due to more positive pulses declining fastest. Even the residual amount of steady state current remaining at the end of the pulse was much less for test cells compared to control.

When the current traces due to the +90 mV pulse were scaled and superimposed, as for Kv1.5 currents previously in this chapter, this effect was even more apparent (Figure 5.14). Panel A shows the currents over 100 ms, and Panel B shows the same traces over 10 ms. In this example, control current reached a peak between 3 and 4 ms, but the current in the presence of inactivating ball peptide peaked after about 1 ms. After 100 ms, there was nearly four times as much residual control current remaining compared to that of test current. After 10 ms, the test current had declined to approximately 30 % of peak current, compared to nearly 84 % of peak current with the control current trace.

5.2.9 The effect of peptide on the voltage dependence of steady state activation and inactivation in Kv4.2

The effect of 200 μ M ShB:E12K,D13K inactivating ball peptide on the voltage dependence of activation and inactivation of Kv4.2 was investigated, as shown in Figures 5.15. An activation curve, Figure 5.15A, was constructed as before by calculating chord conductance at each potential; initial current elicited from the exponential fit to the decay of current was divided by the driving force at that potential. Conductance values were normalised to maximal values and plotted versus membrane potential. Points represent means \pm SEM for 3 cells. A Boltzmann function fitted to the data from each cell gave a mean half maximal activation, $V_{1/2}$ at -10.4 mV (\pm 1.0 mV) and mean slope factor $k = 14.0$ mV (\pm 0.3 mV). Statistical analysis by Student's t-test showed no significant difference between these mean values and those in control data (as shown in Chapter 4), where half maximal activation is at -9.5 mV and k is 10.8 mV ($P = 0.787$ and $P = 0.061$ respectively for half-maximal activation and slope factor).

Steady state inactivation curve for Kv4.2 with 200 μ M ShB:E12K,D13K inactivating ball peptide in the internal pipette solution is shown in Figure 5.15B. As shown previously in Figure 4.7, a conditioning 50ms pre-pulse to -100 mV was followed by a variable potential 100 ms pulse depolarising from -100 mV to +20 mV in increments of +10 mV. The final step was a 100 ms constant +40 mV pulse. The magnitude of the current due to the final step was normalised and plotted versus membrane potential to give an inactivation curve. Points represent means \pm SEM for

3 cells. A Boltzmann function fitted to the data from each cell gave a mean half maximal steady state inactivation at $-53.6 \text{ mV} (\pm 1.4 \text{ mV})$ and average slope factor k of $7.0 \text{ mV} (\pm 0.4 \text{ mV})$. Again, t-tests did not provide any evidence of a statistically significant shift in the voltage dependence of inactivation ($P = 0.171$ for half-maximal inactivation, and $P = 0.428$ for slope factor) from control values of -49.8 mV and 8.3 mV respectively.

5.2.10 Hodgkin-Huxley parameters

The voltage dependence of steady state activation and inactivation were thus found to be unchanged. The Hodgkin-Huxley activation and inactivation parameters that I have used in this project are with respect to time, so the time course of activation and inactivation over a range of membrane potentials can be examined, rather than the relative magnitude of activation or inactivation over the voltage range.

Figure 5.16 shows the results of fitting a function based upon Equation 4.1 on the current records for control cells in the absence of peptide and test cells with 200 μM ShB:E12K,D13K inactivating ball peptide. Again, n was constrained to 5, to achieve a better fit to the data. Values of $\tau_{\text{activation}}$ and $\tau_{\text{inactivation}}$ were both returned from the fit, and plotted on a common log scale against membrane potential, as shown in panels A and B respectively. There was a decrease in the magnitude of $\tau_{\text{activation}}$ as the potential became more positive, for both control and test cells. At 0 mV, the mean value of $\tau_{\text{activation}}$ for control cells was 3.3 ms (± 0.3 ms, $n = 3$), compared to 1.6 ms (± 0.1 ms, $n = 3$). Both sets of data were quite linear with respect to membrane potential up to about +50 mV, then they level off slightly. The curves converged as the membrane potential becomes more positive; at +90 mV, mean values were 0.6 ms (± 0.03 ms) and 0.6 ms (± 0.07 ms) respectively. Although the Hodgkin-Huxley model requires activation and inactivation to be separate independent processes, this graph implies that the synthetic peptides do speed up activation in a voltage dependent manner, although at +90 mV, the presence of extra synthetic peptide in free solution

makes no difference to that speed of activation seen in control cells with just the N-terminal tethered ball and chain structure.

The plot of $\tau_{\text{inactivation}}$ against membrane potential similarly showed voltage dependence for both control and test cells in the presence of ball peptide. At 0 mV, the mean value of $\tau_{\text{inactivation}}$ for control cells was 17.1 ms (± 1.9 ms, $n = 3$), compared to 6.8 ms (± 1.2 ms, $n = 3$) in test cells. The curves of $\tau_{\text{inactivation}}$ were more steeply voltage dependent up to about +40 mV; at potentials more positive to this, they both levelled off and became flatter.

5.2.11 The kinetics of the block of Kv4.2 by 200 μM ShB:E12K,D13K inactivating ball peptide

The variation of 200 μM ShB:E12K,D13K inactivating ball peptide blocking and unblocking rates of Kv4.2 with membrane potential were investigated. Figure 5.17A shows blocking rates, k_b for Kv4.2 control cells in absence of peptide (filled circles) and with 200 μM ShB:E12K,D13K inactivating ball peptide (open circles) plotted versus membrane potential on a common log scale. Control cell data have been fitted with the same functions and equations as for test cells, assuming that the endogenous amino-terminal tethered ball and chain binds in the same manner. Points represent means \pm SEM for 4 control cells and 3 test cells. At a membrane potential of 0 mV, k_b was equal to a mean value of 67.5 s^{-1} ($\pm 1.3 \text{ s}^{-1}$) compared to 81.1 s^{-1} ($\pm 2.9 \text{ s}^{-1}$) in test cells; both curves rose with a linear relationship with membrane potential, and at a membrane potential of 90 mV, k_b was equal to 109.3 s^{-1} ($\pm 6.6 \text{ s}^{-1}$) for control cells, and 136.1 s^{-1} ($\pm 9.8 \text{ s}^{-1}$) for test cells. Student's t-test analysis of data at +60 mV

(in line with Kv1.5 data above) showed a statistical difference ($P < 0.05$) between the means of 91.9 s^{-1} ($\pm 5.8 \text{ s}^{-1}$) in control cells and 128.8 s^{-1} ($\pm 10.4 \text{ s}^{-1}$) for test cells at this potential.

Figure 5.17B shows unblocking rates, k_{ub} for Kv4.2 control cells in absence of peptide (filled circles) and with $200 \mu\text{M}$ ShB:E12K,D13K inactivating ball peptide plotted versus membrane potential on a common log scale. Here again, k_{ub} increased linearly with membrane potential for both test and control cells; however, the data for the two curves lay quite closely. At 0 mV , k_{ub} for control cells in absence of peptide was equal to 4.2 s^{-1} ($\pm 0.7 \text{ s}^{-1}$), rising to 14.5 s^{-1} ($\pm 2.0 \text{ s}^{-1}$) at a membrane potential of 100 mV . For test cells, k_{ub} was equal to 6.4 s^{-1} ($\pm 2.7 \text{ s}^{-1}$) at 0 mV , increasing to 38.8 s^{-1} ($\pm 6.9 \text{ s}^{-1}$) at a membrane potential of 100 mV . For data at $+60 \text{ mV}$, mean values of k_{ub} for control data, 10.5 s^{-1} ($\pm 3.0 \text{ s}^{-1}$) and for test data 20.4 s^{-1} ($\pm 8.4 \text{ s}^{-1}$) were found not to be significantly different ($P = 0.346$).

Finally, association and dissociation rate constants for the block of Kv4.2 by $200 \mu\text{M}$ ShB:E12K,D13K inactivating ball peptide at different membrane potentials were examined. Figure 5.18A shows association rate constants k_{on} (squares), and dissociation rate constants k_{off} (circles), plotted versus membrane potential. Points represent means \pm SEM for 3 cells. As for k_b , from which this data was derived (by dividing by concentration of peptide), there was a linear relationship with membrane potential, with k_{on} increasing with more positive pulse potential. Mean values increased from $4.1 \times 10^5 \text{ M}^{-1} \text{ s}^{-1}$ ($\pm 1.5 \times 10^4 \text{ M}^{-1} \text{ s}^{-1}$) at 0 mV to $6.8 \times 10^5 \text{ M}^{-1} \text{ s}^{-1}$ ($\pm 4.9 \times 10^4 \text{ M}^{-1} \text{ s}^{-1}$) at $+90 \text{ mV}$. At $+60 \text{ mV}$, the mean value of k_{on} was found to be $6.4 \times 10^5 \text{ M}^{-1} \text{ s}^{-1}$ ($\pm 5.2 \times 10^4 \text{ M}^{-1} \text{ s}^{-1}$)

Equilibrium dissociation constants, K_D , for 200 μ M ShB:E12K,D13K inactivating ball peptide with Kv4.2 are shown plotted versus membrane potential in Figure 5.18B. There is a clear linear voltage-dependent relationship here. The value of K_D at +60 mV was 3.2×10^{-5} M. However, the result here is counter-intuitive; one would expect the affinity between peptide and binding site to increase with depolarisation. This would be represented graphically in this plot by a decrease of K_D with increasing membrane potential.

5.3 Discussion

This chapter describes experiments where synthetic peptides based upon the first 20 amino acid portion of the *ShakerB* amino-terminus were added to the internal pipette solution in whole cell patch clamp recordings from MEL cells stably transfected with Kv1.5 and Kv4.2 potassium channels.

Previous work with these synthetic peptides involved adding the peptide solution to the intracellular side of the cell membrane in the inside-out configuration of the patch clamp technique. Zagotta, Hoshi and Aldrich (1990) recorded macroscopic currents from inside-out patches from RNA injected *Xenopus* oocytes, as did Murrell-Lagnado and Aldrich (1993). Beirão, Davies and Stanfield (1994) used inside-out patches from rat skeletal muscle sarcolemmal vesicles. Toro, Stefani and Latorre (1992) used porcine coronary smooth muscle K_{Ca} channels reconstituted into lipid bilayers; similarly, Foster, Chung, Zagotta, Aldrich and Levitan (1992) inserted rat skeletal muscle or rat brain K_{Ca} channels into lipid bilayers.

This study has characterised the block of Kv1.5 and Kv4.2 channels by synthetic 20 amino acid ball peptides based upon the first 20 amino acid portion of the *ShakerB* amino-terminus or point mutations of this sequence. Kv1.5 is a typical delayed rectifier voltage-activated potassium channel, with very slow inactivation characteristics. The action of the wild-type ShB inactivating ball peptide transformed these inactivation characteristics. This is shown by scaled currents in this chapter; current decline was faster with respect to time, and there was less than half of the current remaining at the end of a four second pulse, compared to that with control cells in the absence of ShB peptide. However, there was no statistically significant

change in the voltage dependence of steady state activation and inactivation, or in the time of recovery from inactivation. This result for steady state inactivation seems to be counter-intuitive, and cannot be explained. One would expect the range for inactivation to be altered in the presence of ball peptide because channels were becoming inactivated earlier in the pulse than for control cells, and the steady state current remaining at the end of the pulse, as a proportion of peak current, was decreasing. Half-maximal inactivation (the membrane potential at which half of the available channels would be expected to become inactivated) must surely shift in this case; for a pulse at the same membrane potential, more channels were becoming inactivated for test data compared to control data.

A point mutation of the amino acid sequence of the peptide (L7E) that replaced a neutral leucine with a negatively charged glutamate, and has previously been shown to be inactive (Zagotta, Hoshi and Aldrich, 1990; Toro, Stefani and Latorre, 1992; Beirao, Davies and Stanfield, 1994), had no effect on this channel. A version of the peptide (ShB:E12K,D13K) that replaces negatively charged glutamate and aspartate with positively charged lysine had an even greater effect than wild-type peptide. The peak of the current occurred earlier during a depolarisation compared to that in control cells in the absence of peptide. An even greater relative decrease in current occurred with respect to time; with higher concentrations of this ShB:E12K,D13K version of the peptide, the current characteristics began to resemble those of a typical A-type current.

As expected, the association rate constant, which represents the rate of onset of inactivation, increased with an increase of the charge of the peptide by four positive charges. There was an unexpected result with the increase in the dissociation rate constant (or unblocking rate). This is also counter-intuitive; one would expect this

rate to remain the same or even decrease, as if the peptide were held more strongly by long-range electrostatic interactions with the negatively charged surface in or around the inner mouth of the channel. This anomaly perhaps also explains the strange trend of constant or decreasing affinity with increasing depolarisation between the peptide and its binding site, as reported in the results section above (and also particularly for Kv4.2 also in this chapter). The values of K_D are derived from the calculations of the unblocking rate, and any inaccuracy here is also apparent in the derived equilibrium dissociation constant plots. The method of subtraction of the steady state blockage used in order to calculate the rates of block and unblock by the peptide may be introducing some errors.

There was no significant increase in the time constants of recovery from inactivation with wild-type peptide, compared to control cells in absence of peptide. Although this experiment was not repeated with the ShB:E12K,D13K mutant inactivating ball peptide, this may indicate that the unblocking rate would not be limiting on the recovery from inactivation. Certainly, A-type potassium channels tend to have a quicker time constant for recovery from inactivation compared to delayed rectifiers. It is a consequence of this property that A-type potassium channels can recover between repeated firings of action potentials, and serve to set the spacing time.

Using this potent mutant of the peptide even had an effect on Kv4.2 currents. Kv4.2 is a fast inactivating A-type or fast transient potassium channel. To give some idea of the inactivation characteristics of this channel compared to Kv1.5, an exponential fitted to the decline in Kv4.2 current to a depolarising pulse to +60 mV would have a time constant in the order of 15 ms. This compared to a similarly fitted

time constant to the decline of a Kv1.5 current at this potential in the region of 150 - 200 ms. Scaled Kv4.2 currents in the absence of, and in the presence of the ball peptide showed quite a difference; again, the peak of current occurred earlier, and the current declined much more quickly. Although a slight decrease in length of time to peak might be expected if inactivation is known to be accelerated (and therefore beginning to reduce the current earlier), the scaled currents in Figure 5.14B seem to imply more than this. One would not expect the peptide to accelerate activation, though the data in Figure 5.16A derived from fits of the Hodgkin-Huxley activation parameters points to this. Although hyperpolarising pre-pulse potentials were used in all voltage pulse protocols, it may be possible that the presence of some residual inactivation before the test pulses was present. This could introduce such errors. There was no statistically significant change in the voltage dependence of steady state activation and inactivation.

As discussed in Chapter One, the mammalian homologues of the *Shaker* protein were found to be significantly more closely related to the *Drosophila Shaker* protein in the S1-S6 region than to the other mammalian sub-family members within a species. The mouse versions of the *Shaker* gene was found to have more than 70 % identity with that of the *Drosophila*, compared to only about 40 % identity with the mouse versions of the other subfamily genes. Now, this suggests that the inactivation receptor site for the peptide, thought to include the short intracellular loop between the S4 and S5 transmembrane segments along with the H5 region between S5 and S6, is conserved between the different potassium channel subfamilies, with greater homology within the *Shaker*-like Kv1 subfamily. Certainly, the evidence cited in the introduction to this chapter points to the conservation of the receptor site beyond just

the Kv1 subfamily, with even K_{Ca} channels being affected by the peptide. The results for Kv4.2, a member of the *Shal*-like Kv4.2 subfamily, where the rate of inactivation (already at the quick end of the spectrum for this property amongst the voltage-activated potassium channels) was significantly faster compared to the control with no external synthetic peptide support this.

The blocking rate and association rate constant data presented here are voltage-dependent implying that the binding site which reputedly includes the pore region must be within electric field of the membrane.

The data presented here support the idea of 'free' peptides in solution binding to the Kv4.2 channel even in the presence of the amino-terminal 'ball and chain', and these free peptides binding faster than the tethered ball. Blocking rates and unblocking rates were estimated for control Kv4.2 cells in the absence of peptide by fitting control cell data with the same functions and equations as for test cells, assuming that the endogenous amino-terminal tethered ball and chain binds in the same manner. Although unblocking was unchanged, the blocking rate was increased significantly. This increased blocking rate is a composite of the binding of tethered and free ball to the receptor site. This could suggest that at the +60 mV potential of the comparison, perhaps some peptide receptor sites which are free in the control cells are being occupied with the ball peptide. However, at this membrane potential, examination of the steady state inactivation curves for Kv4.2 (Figure 5.15B) suggest that most of the channels become inactivated; the plot of $\tau_{inactivation}$ from the Hodgkin-Huxley model (Figure 5.16B) suggests that the time constant of inactivation gets smaller, i.e. the rate of inactivation increases. But, there is no convergence in the data points from the comparison of k_b between control and test cells, the curves remain parallel throughout the range displayed; if the free and tethered peptides were binding

at the same rate then at the increasingly positive potentials where the peptide receptors became saturated (all channels inactivated) the blocking rate would become the same - the difference in the blocking rate could not be explained by extra receptors being bound by free peptide.

The inactivity of the L7E mutant tends to suggest that there is some degree of specificity; removal of this positive charge may be crucial in preventing binding at the receptor site. In the case of the mutant ShB:E12K,D13K of the peptide increasing the positive charges at positions 12 and 13 had a greater increasing effect on the rate of block and association rate constants. This supports the idea that simple electrostatic interactions are involved in bringing receptor and peptide together. The experiments of Hoshi, Zagotta and Aldrich (1990) showed that the ball itself in the model is a concentration of positively charged amino acid residues. The negatively charged pore of the channel can be thought of as being important in attracting these positive charges.

Of course, C-type inactivation, associated with the C-terminal region of the channel is also present, and this fact may be complicating the picture. The traces in Figure 5.9 for currents recorded in the presence of the peptides still seem to be reaching a steady state level - interestingly, this is at virtually the same point for the wild-type and ShB:E12K,D13K mutant - albeit one which is about half of that with control cells. Thus, one cannot simply say that the time constants τ_{fast} and τ_{slow} represent the two inactivation processes, N-type and C-type, since they occur concurrently. This was highlighted by the difficulties in ascertaining steady state blockage accurately mentioned above.

There were some problems associated with making whole cell recordings from MEL cells with synthetic ball peptides included in the pipette solution. It became

quite difficult to form gigaohm seals. This was found to be worse with a higher concentration of peptide. Control recordings were usually done with patch pipettes typically of 4 - 10 MΩ resistance. After long periods of frustration, in order to increase the likelihood of gigaohm seal formation, patch pipettes of higher resistance were used, typically 10 - 20 MΩ. This resulted in a smaller pipette tip, and associated with this were problems of access of ball peptide to the interior of the cell. This can explain some inconsistencies of blocking rate data. The value of k_b for 200 μM ShB inactivating ball peptide should be double that for 100 μM ShB at the same membrane potential. The actual mean values were $1.3 \text{ s}^{-1} (\pm 0.6 \text{ s}^{-1})$ and $1.1 \text{ s}^{-1} (\pm 0.1 \text{ s}^{-1})$ respectively. The histogram in Figure 5.11 and statistical analysis show no significant difference between these sets of data at that potential. Since the association rate constant is related to the concentration of the peptide (in units of $\text{M}^{-1}\text{s}^{-1}$), the values of k_{on} should be similar for the two concentrations of the peptide, but instead, k_{on} for the lower concentration is actually higher, indicating that for some reason, less than expected concentrations of peptide were available to the binding site.

It is interesting to compare the values of the association and dissociation rate constants measured by Murrell-Lagnado and Aldrich (1993a) with those from the present study. With the *ShakerB* deletion mutant channel with ShB wild-type peptide, for a +50 mV pulse, they found a k_{on} of $4.7 \times 10^6 \text{ M}^{-1} \text{ s}^{-1}$ and k_{off} of 13.8 s^{-1} . My results with Kv1.5 were k_{on} of $7.0 \times 10^4 \text{ M}^{-1} \text{ s}^{-1}$ and k_{off} of 3.8 s^{-1} . With the mutant ShB:E12K,D13K peptide, for a + 50 mV pulse, they had a k_{on} of $140 \times 10^6 \text{ M}^{-1} \text{ s}^{-1}$ and k_{off} of 24 s^{-1} . My results with Kv1.5 were k_{on} of $2.5 \times 10^5 \text{ M}^{-1} \text{ s}^{-1}$ and k_{off} of 13.4 s^{-1} , and with Kv4.2, a k_{on} of $5.4 \times 10^5 \text{ M}^{-1} \text{ s}^{-1}$ and k_{off} of 13.1 s^{-1} . Although this may indicate that the specificity of the peptide for these channels may inherently

be less, it is more than likely that there was a lower concentration of peptide than expected with my recordings. However, it seems that the access of the peptide to the interior of the cell did not increase significantly with time during lengthy periods of whole cell recording from the same cell, so there was no material difference between results obtained earlier or later in the experiment. These problems with success of seal formation with the peptide in the patch pipette, and perhaps achieving sufficient delivery of the required concentrations of peptide to the inner pore of the channel could be overcome, if all relevant conditions were optimised.

Despite the complications of the system, the methods and calculations used here to investigate the block of mammalian Kv channels by synthetic peptides proved to be quite successful.

Figure 5.1 The effect of ShakerB inactivating ball peptide on Kv1.5.

A,B Typical whole cell currents recorded from Kv1.5 in the absence and presence of ShakerB inactivating ball peptide. Records have been corrected for leakage and capacitance currents.

A Currents recorded from a control cell (no ball peptide present in the patch pipette) in response to depolarising voltage steps of 4000 ms duration, from a holding potential of -80 mV, in +10 mV steps from -40 mV to +60 mV. The voltage pulse protocol is shown above.

B Currents recorded from a different cell in response to the same voltage pulse protocol as above, but with 200 μ M ShakerB inactivating ball peptide in the internal solution in the patch pipette.

Figure 5.1

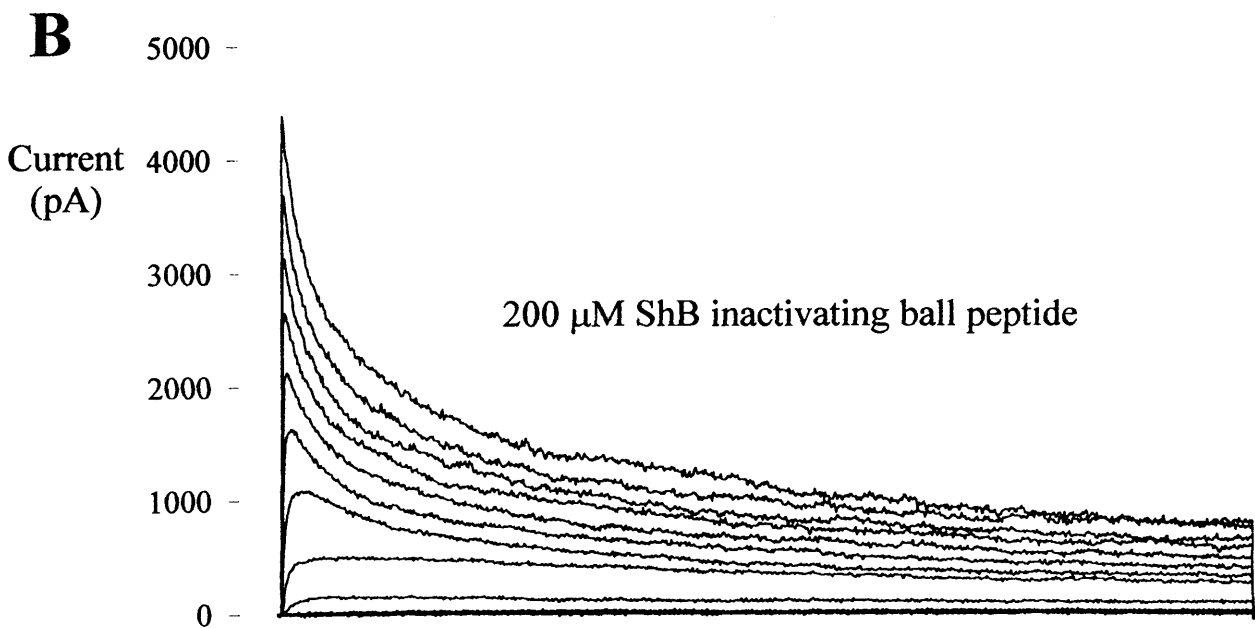
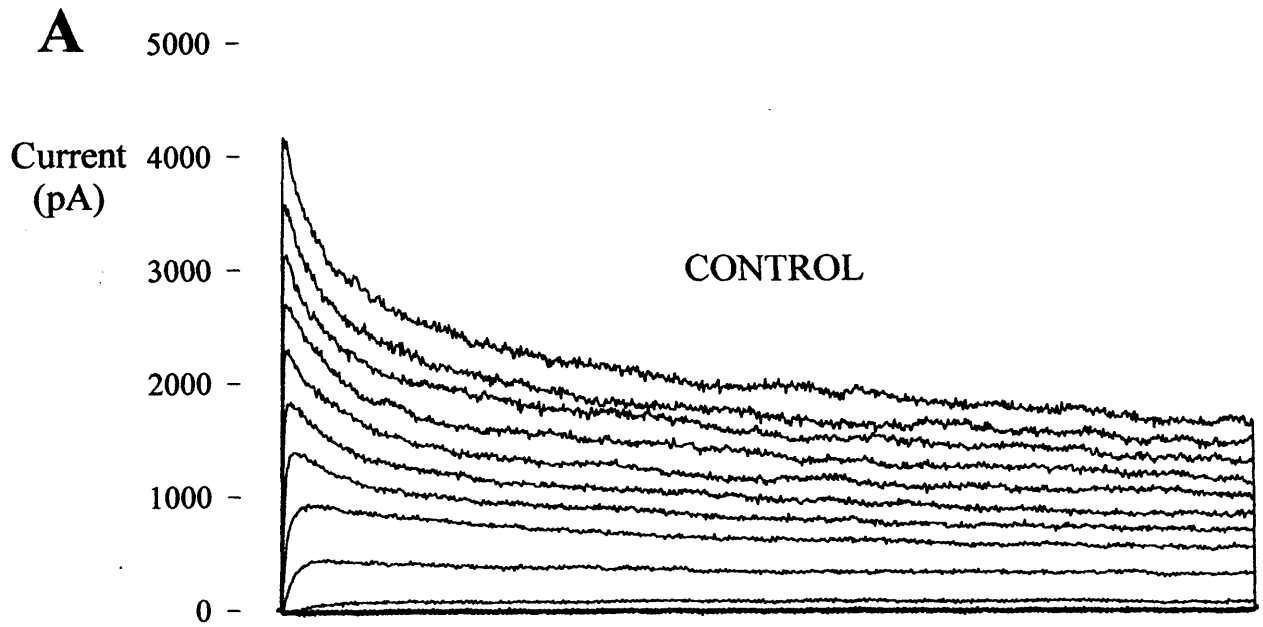
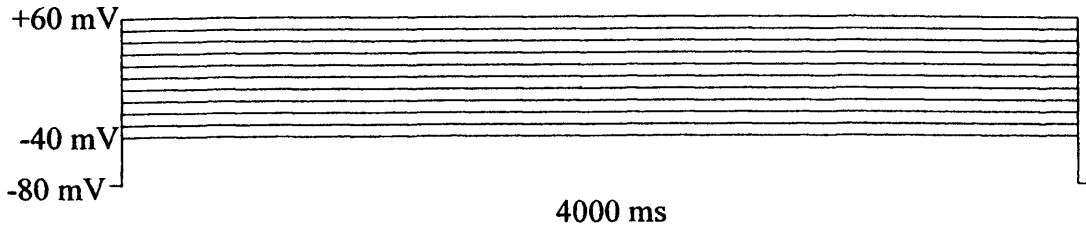


Figure 5.2 The effect of ShakerB inactivating ball peptide illustrated using scaled current traces.

A The extent of the inactivation of Kv1.5 current due to ShakerB inactivating ball peptide illustrated by matching, by multiplication, the magnitude of the peaks of the current traces in response to the +60 mV voltage pulse of 4000 ms duration shown in Figures 5.1 and 5.2. These scaled current traces, in the absence and presence of 200 μ M ShakerB inactivating ball peptide respectively are shown superimposed.

B Superimposed scaled current traces showing the effect of 200 μ M ShakerB inactivating ball peptide on Kv1.5 currents from two different cells, over a shorter time, 50 ms.

Figure 5.2

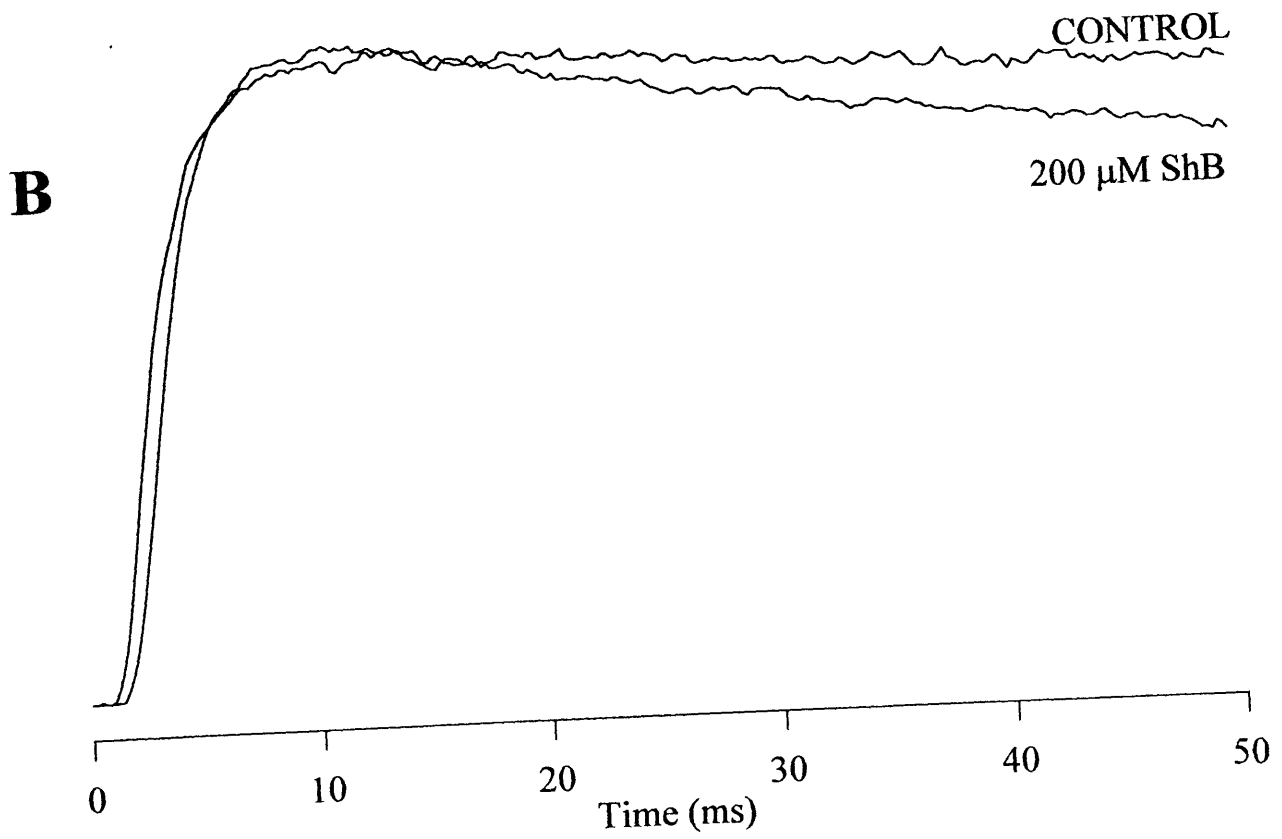
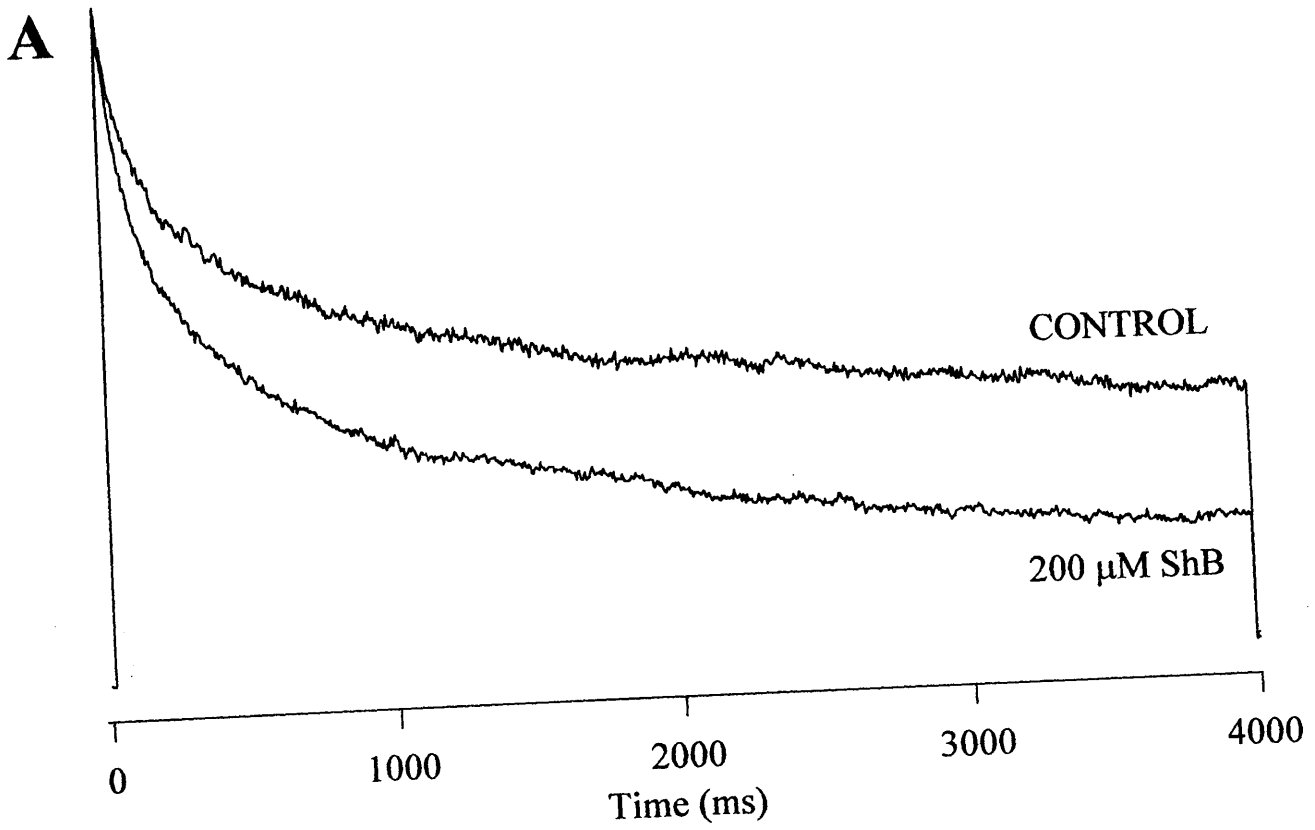


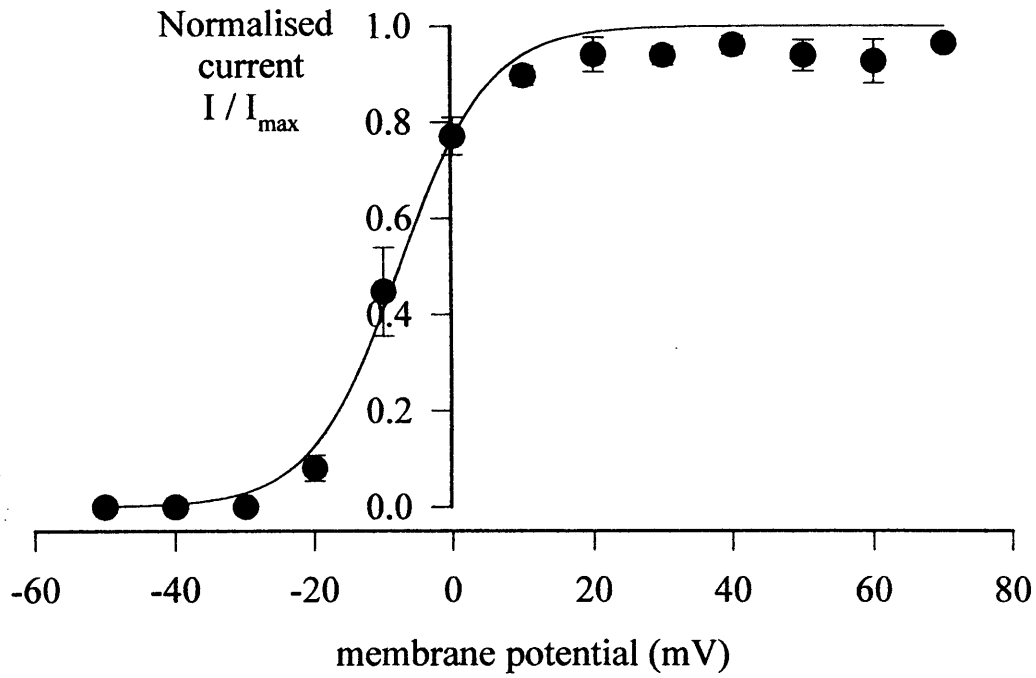
Figure 5.3 The effect of ShakerB inactivating ball peptide on the voltage dependence of activation and inactivation of Kv1.5.

A The voltage dependence of the activation for Kv1.5 with 200 μ M ShakerB inactivating ball peptide in the internal pipette solution. As shown in Figure 3.5, values of the instantaneous tail current elicited by a return to a fixed voltage step after an initial variable voltage step were normalised and plotted against the potential of the initial variable voltage step to give an activation curve. Points represent means \pm SEM for 5 cells. A Boltzmann function fitted to the data from each cell gave a mean half maximal activation, $V_{1/2}$ at -6.6 mV (\pm 0.9 mV) and mean slope factor $k = 6.0$ mV (\pm 0.4 mV). The illustrated curve has $V_{1/2}$ at -7.7 mV and $k = 6.4$ mV.

B Steady state inactivation of Kv1.5 with 200 μ M ShakerB inactivating ball peptide in the internal pipette solution. As shown in Figure 3.8, a family of currents was elicited by a 100 ms test pulse at +20 mV following a 60 second conditioning pre-pulse at variable potentials. Peak currents due the test pulse were normalised and plotted versus the potential of the variable pre-pulse. Points represent means \pm SEM for 5 cells. A Boltzmann function fitted to the data from each cell gave a mean half maximal steady state inactivation at -24.9 mV (\pm 1.2 mV) and average slope factor k of 6.1 mV (\pm 0.2 mV). The illustrated curve has $V_{1/2}$ for inactivation at -24.9 mV and $k = 6.2$ mV

Figure 5.3

A



B

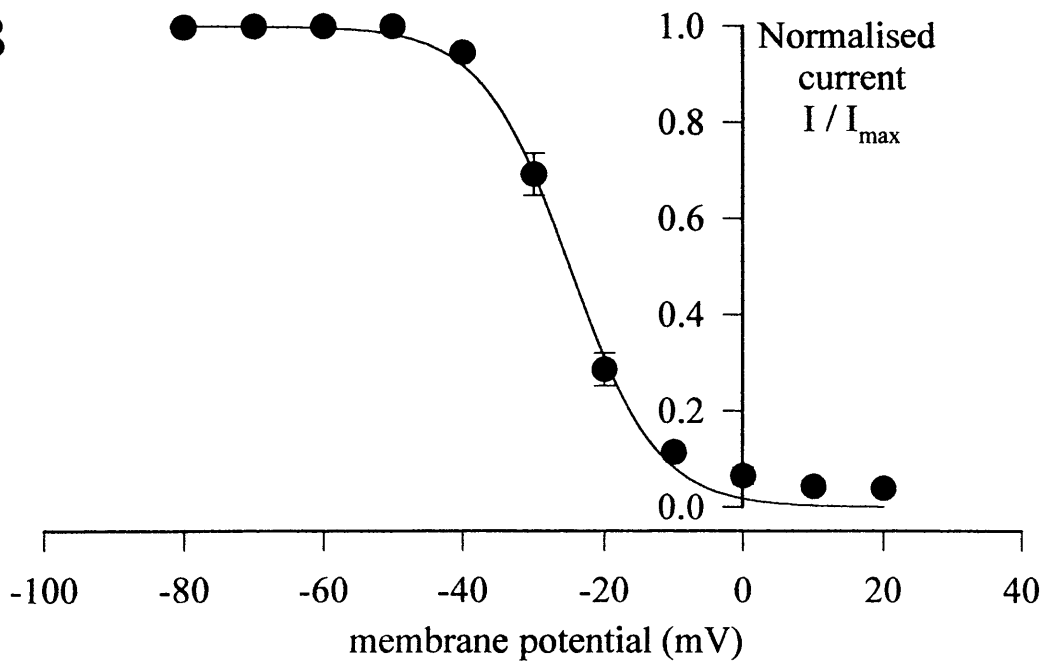


Figure 5.4 The effect of ShakerB inactivating ball peptide on the recovery from inactivation of Kv1.5.

Plot of fractional recovery from inactivation giving a value for time constant of recovery, as shown in Figure 3.10. Points on the plot of fractional recovery versus separation represent mean data \pm SEM for 5 cells. A double exponential fitted to the data for each cell gave a mean values of the fast and slow time constants of recovery to be 0.29 seconds ($\pm 1.2 \times 10^{-3}$ seconds) and 3.8 seconds (± 0.2 seconds) respectively. The illustrated curve fitted to the averaged data points had fast and slow time constants of recovery of 0.28 seconds and 3.8 seconds respectively.

Figure 5.4

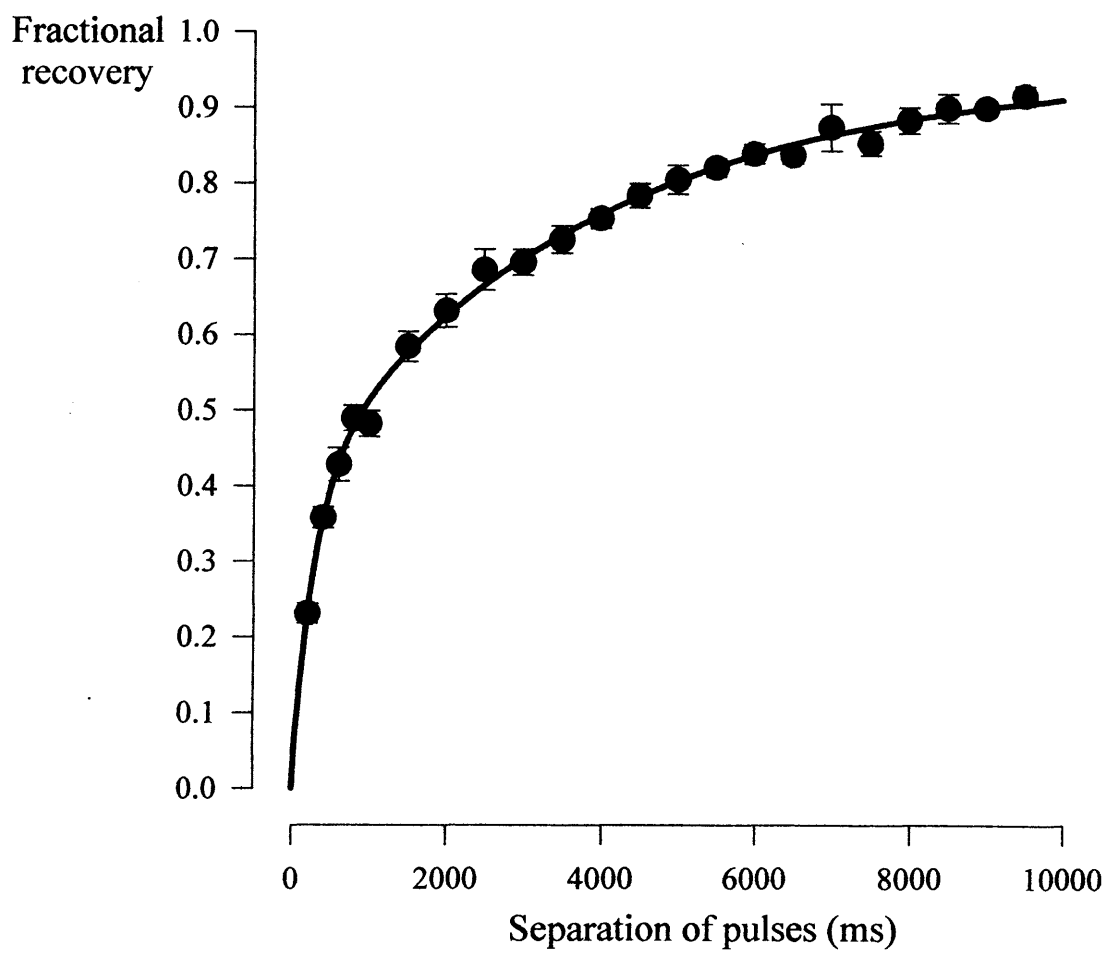


Figure 5.5 The effect of the inactive ShBL7E ball peptide illustrated using scaled currents.

A The effect of the L7E point mutation of the ShakerB inactivating ball peptide (ShB,L7E) on Kv1.5 currents. As in Figure 5.2A, the magnitude of the peaks of the current traces in response to the +60 mV voltage pulse of 4000 ms duration were matched. These scaled current traces, in control cells and in the presence of 200 μ M ShB,L7E ball peptide are shown superimposed.

B Superimposed scaled current traces showing the effect of 200 μ M ShB,L7E ball peptide on Kv1.5 currents, over a shorter time, 50 ms.

Figure 5.5

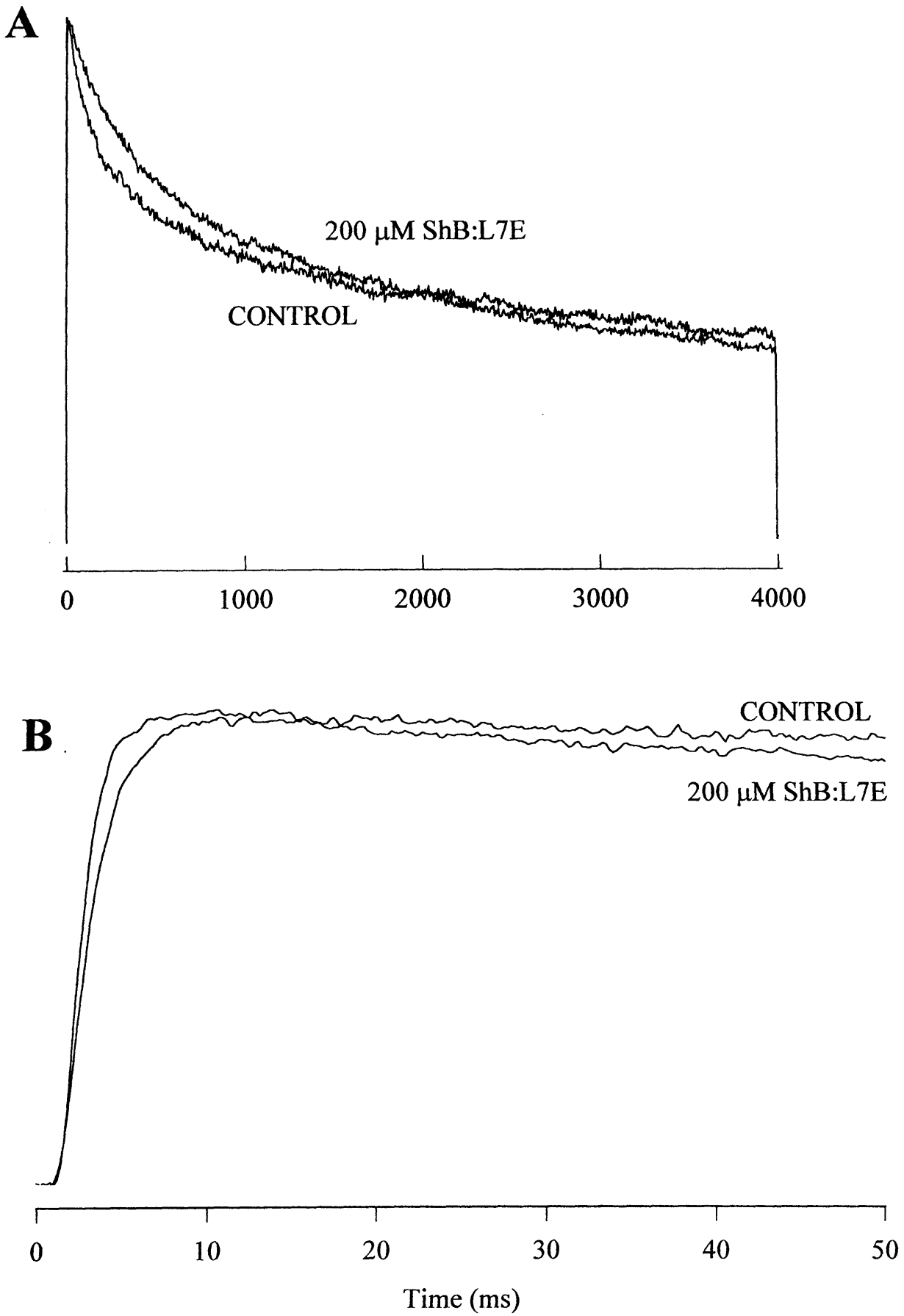


Figure 5.6 An explanation of the parameters used in the equations used to determine blocking rates etc.

A A typical whole cell current trace recorded with 200 μM ShakerB inactivating ball peptide in the internal pipette solution, shown here fitted with the sum of three exponentials using the TRACAN trace analysis programme (Davies, 1993). This figure illustrates how extrapolating the curve back to time $t = 0$ gives the magnitude of I_0 , an estimate of the peak current in the absence of any inactivation. I_{ss} , the magnitude of the steady state current is also shown.

B A typical control whole current shown here fitted with the sum of two exponentials.

C,D The same current trace as shown in A above is shown here, fitted with the sum of three and two exponentials with time constants τ_1 and τ_2 (and τ_3 with three exponentials) respectively. Note how the curve in B overlays the data points quite closely throughout compared to the curve in C which particularly misses the initial section following the peak of the current. τ_1 represents τ_{fast} in calculations used in this chapter.

Figure 5.6

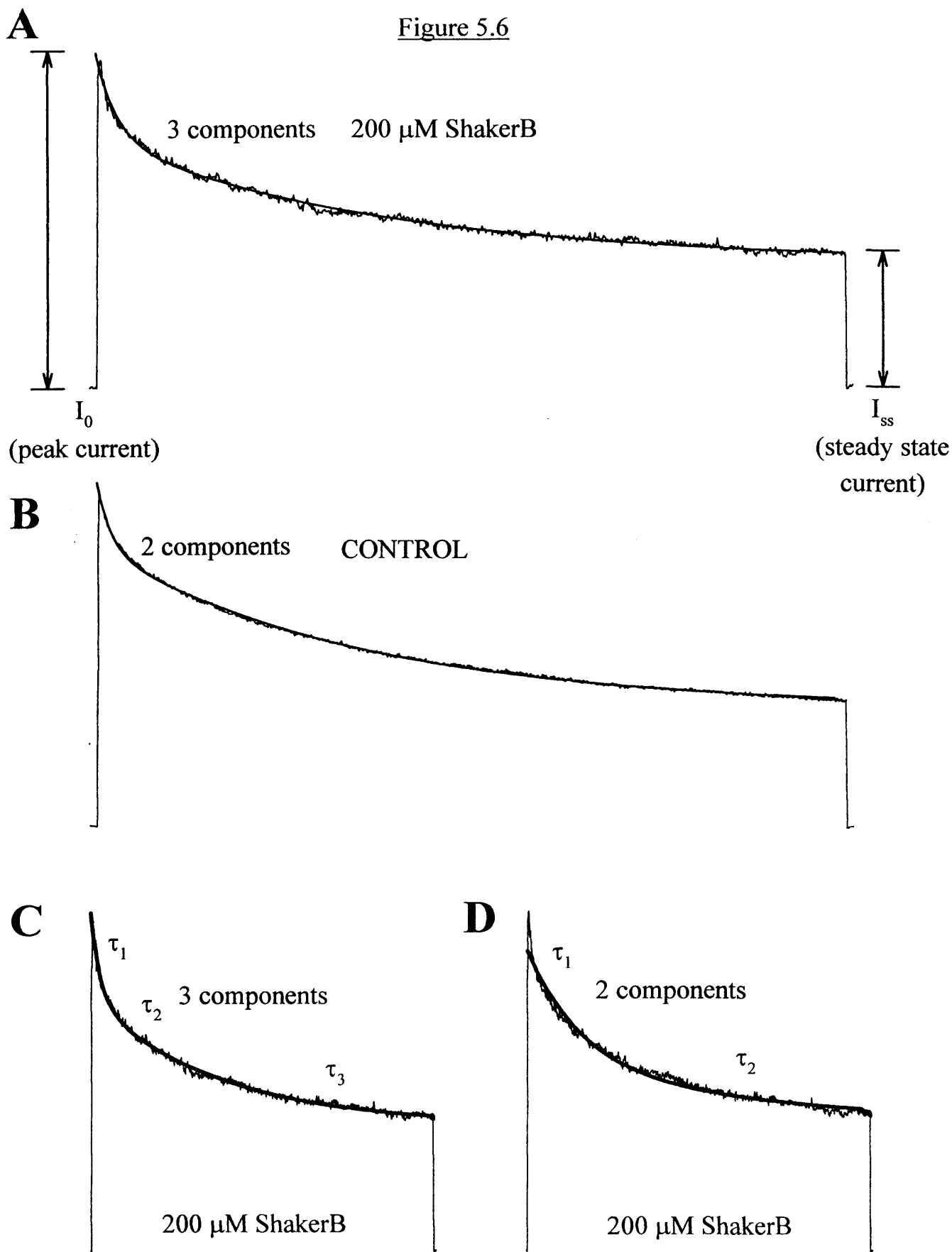


Figure 5.7 The variation of 200 μ M ShakerB inactivating ball peptide blocking/unblocking rates, association/dissociation rate constants and Equilibrium dissociation constants of Kv1.5 with membrane potential.

A Blocking rates, k_b (circles), and unblocking rates, k_{ub} (squares), of 200 μ M ShakerB inactivating ball peptide with Kv1.5 plotted versus membrane potential. Points represent means \pm SEM for 3 cells.

B Association rate constants, k_{on} (circles), and dissociation rate constants, k_{off} (squares), for 200 μ M ShakerB inactivating ball peptide with Kv1.5 plotted versus membrane potential. Points represent means \pm SEM for 3 cells.

C Equilibrium dissociation constants, K_D , for 200 μ M ShakerB inactivating ball peptide with Kv1.5 plotted versus membrane potential. Points represent means \pm SEM for 3 cells.

Figure 5.7

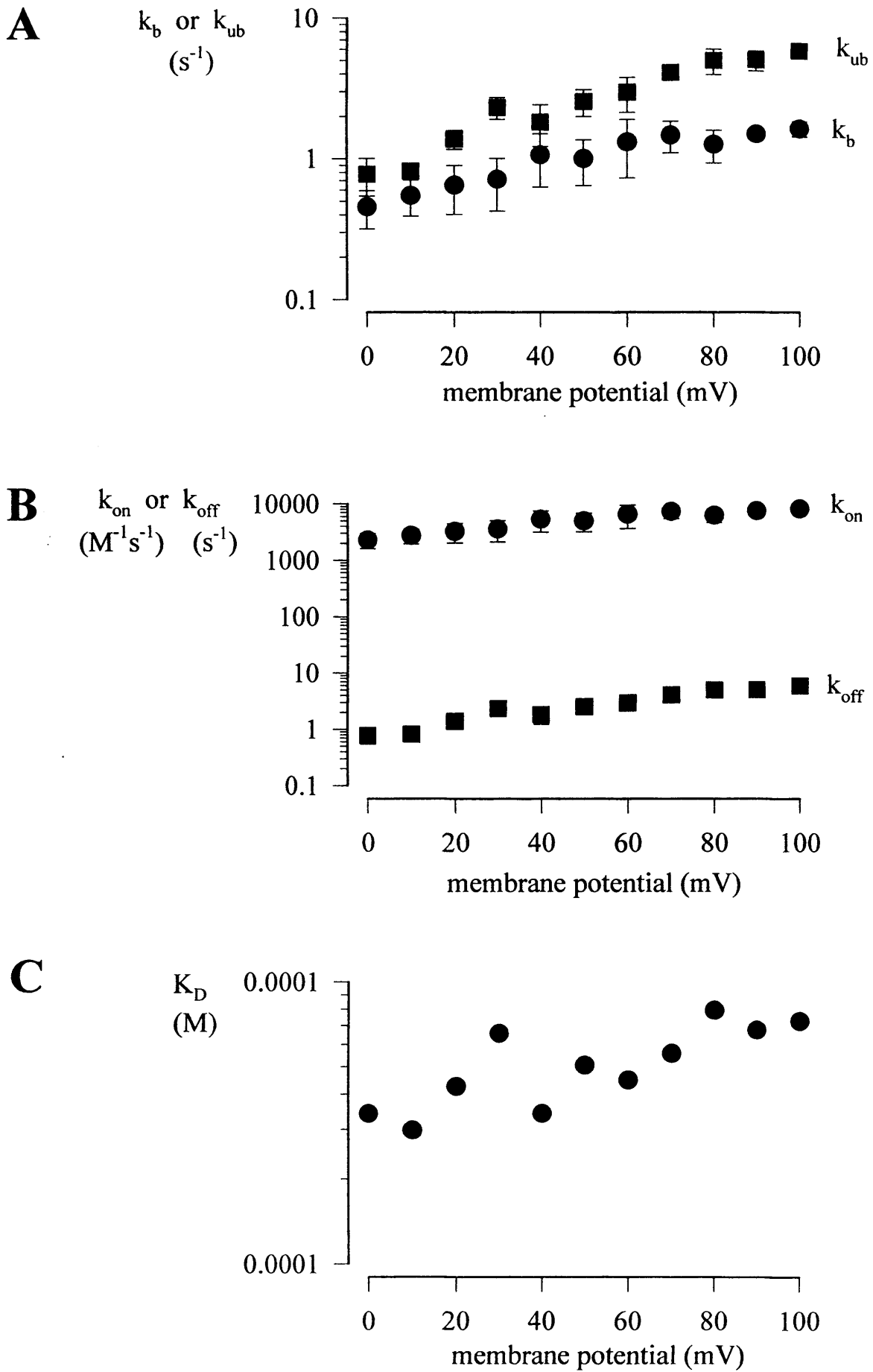


Figure 5.8 The variation of 100 μ M ShakerB inactivating ball peptide blocking/unblocking rates, association/dissociation rate constants and Equilibrium dissociation constants of Kv1.5 with membrane potential.

A Blocking rates, k_b (circles), and unblocking rates, k_{ub} (squares), of 100 μ M ShakerB inactivating ball peptide with Kv1.5 plotted versus membrane potential. Points represent means \pm SEM for 3 cells.

B Association rate constants, k_{on} (circles), and dissociation rate constants, k_{off} (squares), for 100 μ M ShakerB inactivating ball peptide with Kv1.5 plotted versus membrane potential. Points represent means \pm SEM for 3 cells.

C Equilibrium dissociation constants, K_D , for 100 μ M ShakerB inactivating ball peptide with Kv1.5 plotted versus membrane potential. Points represent means \pm SEM for 3 cells.

Figure 5.8

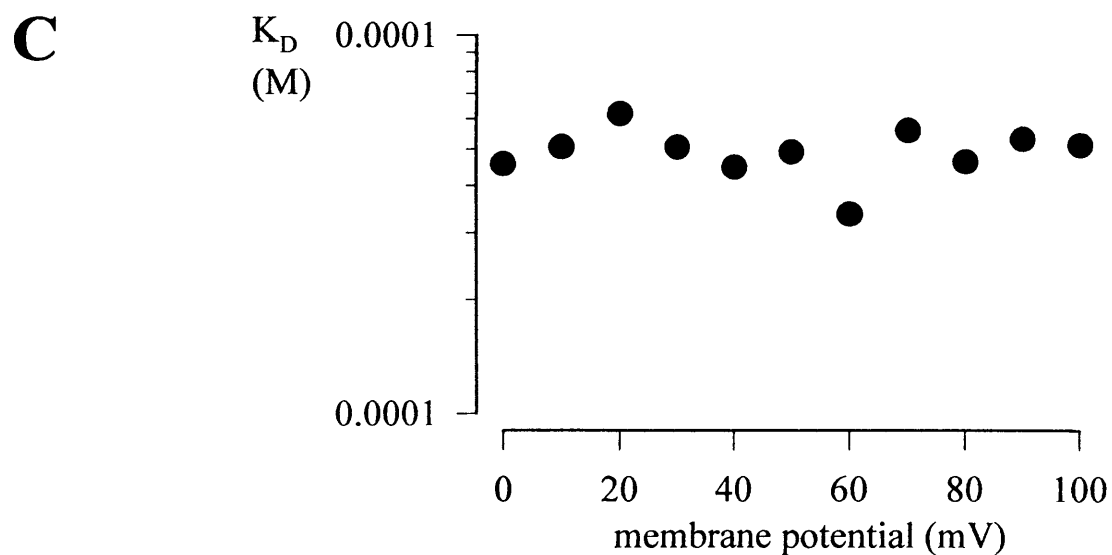
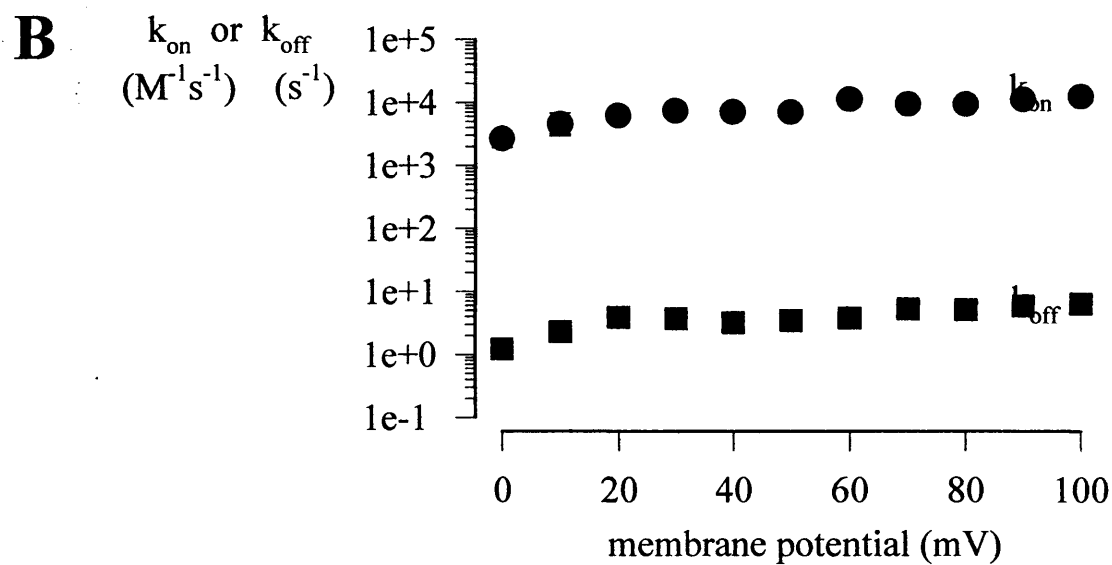
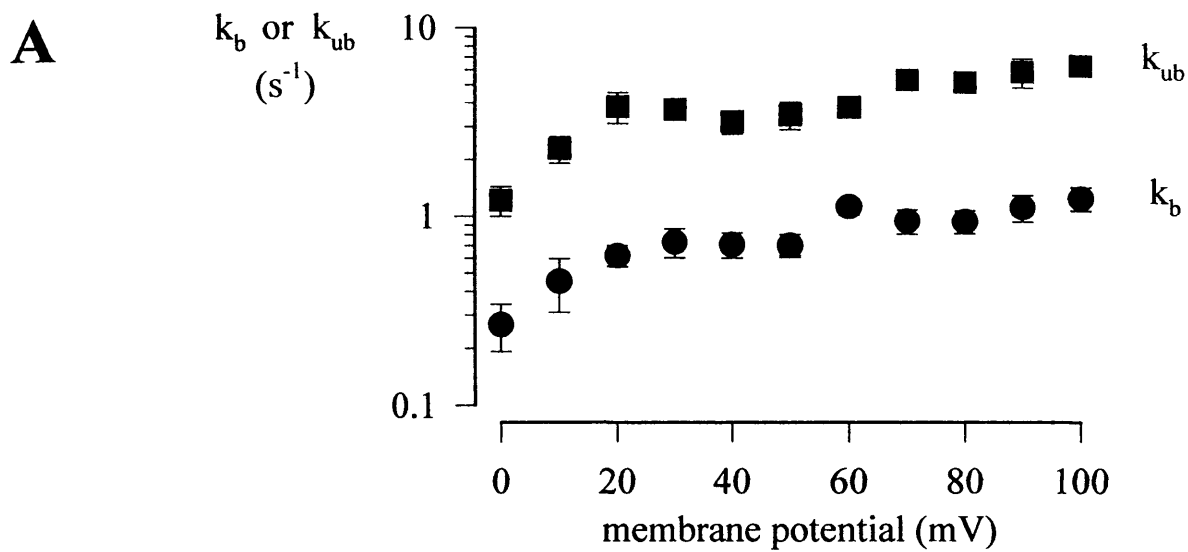


Figure 5.9 The effect of ShB:E12K,D13K inactivating ball peptide on Kv1.5
illustrated using scaled currents.

A The effect of the E12K,D13K mutation of the ShakerB inactivating ball peptide (ShB,E12K,D13K) on Kv1.5 currents. As in Figure 5.2A, the magnitude of the peaks of the current traces in response to the +60 mV voltage pulse of 4000 ms duration were matched. These scaled current traces shown are typical of those in control cells in the absence of peptide, and in the presence of 200 μ M ShB:E12K,D13K and ShB inactivating ball peptides.

B Superimposed scaled current traces showing the effect of 200 μ M ShB:E12K,D13K and ShB inactivating ball peptides on Kv1.5 currents over a shorter time, 50 ms.

Figure 5.9

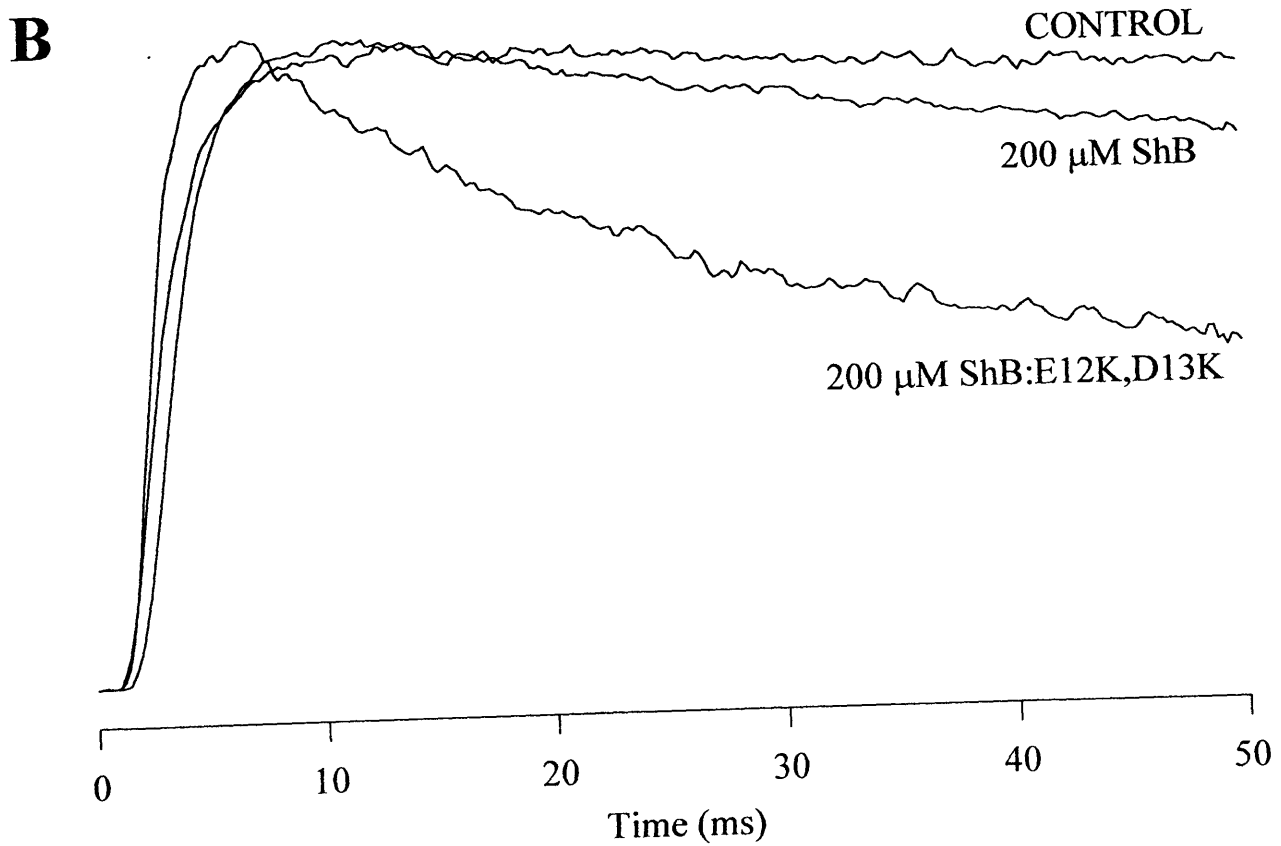
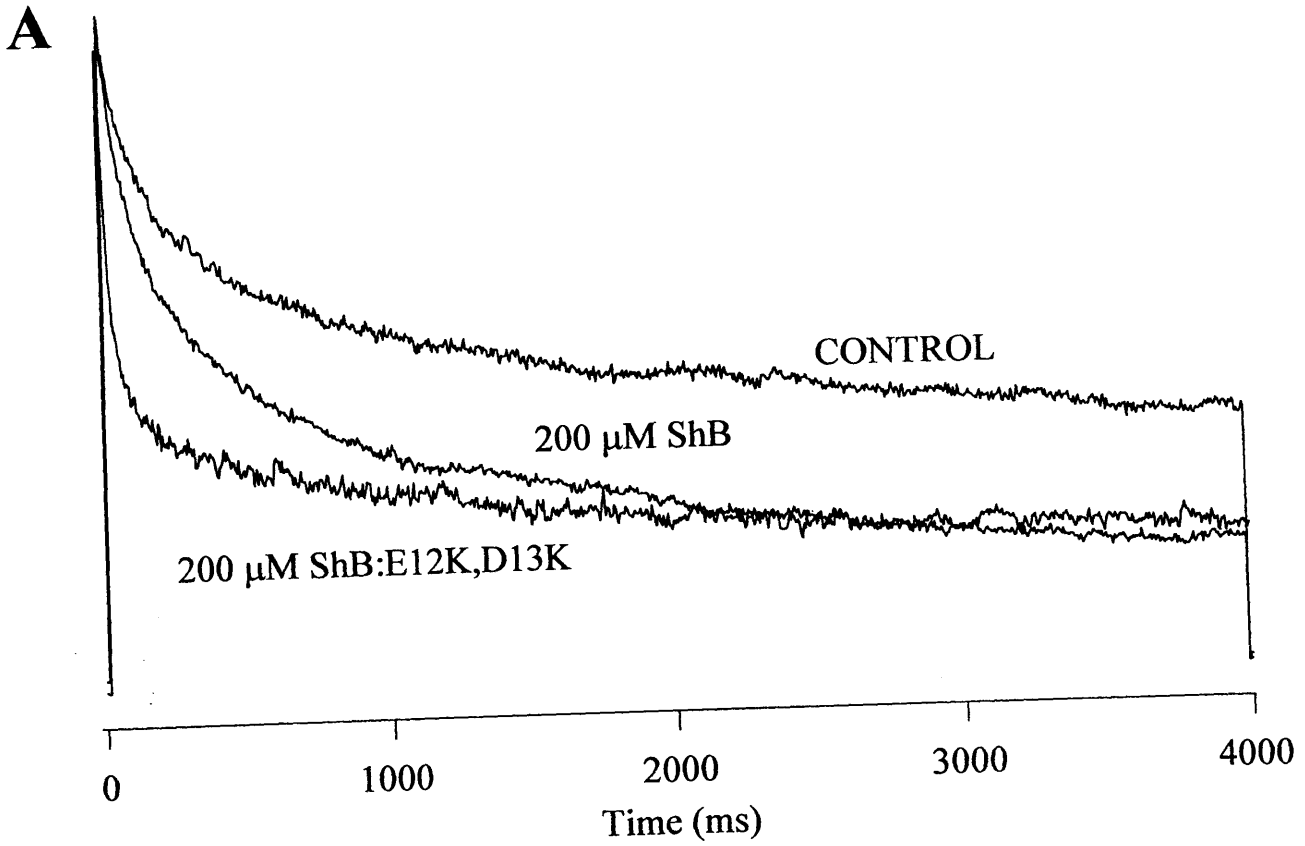


Figure 5.10 The variation of 100 μ M ShB:E12K,D13K inactivating ball peptide blocking/unblocking rates, association/dissociation rate constants and Equilibrium dissociation constants of Kv1.5 with membrane potential.

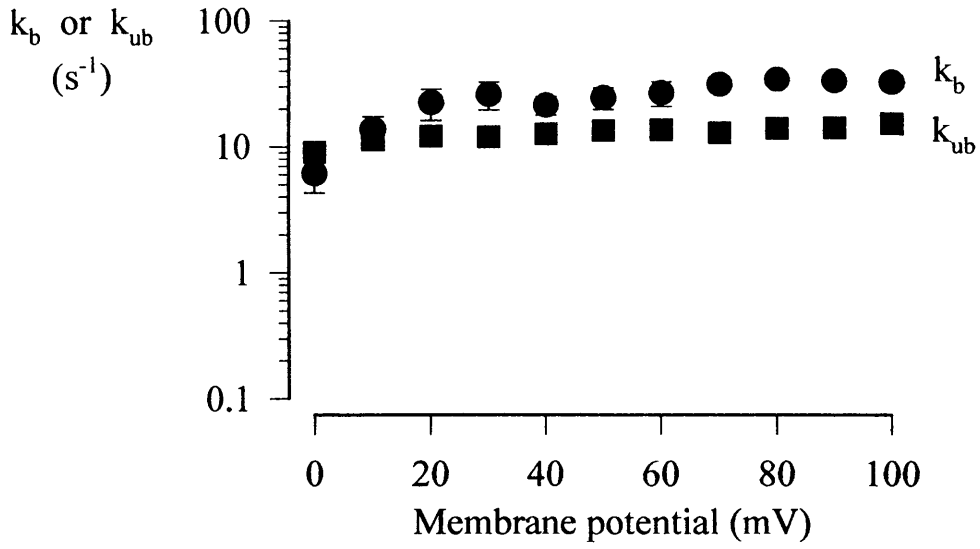
A Blocking rates, k_b (circles), and unblocking rates, k_{ub} (squares), of 100 μ M ShB:E12K,D13K inactivating ball peptide with Kv1.5 plotted versus membrane potential. Points represent means \pm SEM for 3 cells.

B Association rate constants, k_{on} (circles), and dissociation rate constants, k_{off} (squares), for 100 μ M ShB:E12K,D13K inactivating ball peptide with Kv1.5 plotted versus membrane potential. Points represent means \pm SEM for 3 cells.

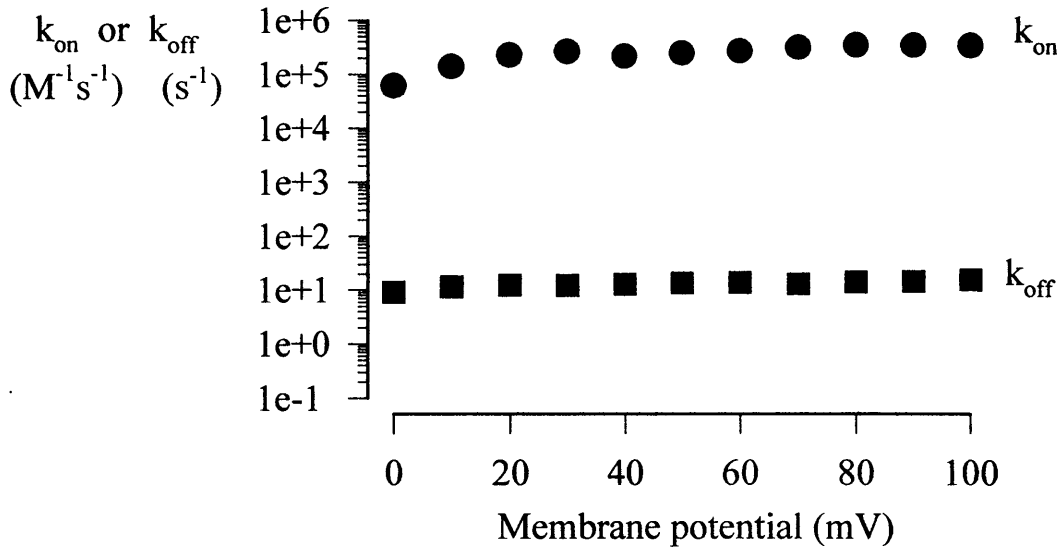
C Equilibrium dissociation constants, K_D , for 100 μ M ShB:E12K,D13K inactivating ball peptide with Kv1.5 plotted versus membrane potential. Points represent means \pm SEM for 3 cells.

Figure 5.10

A



B



C

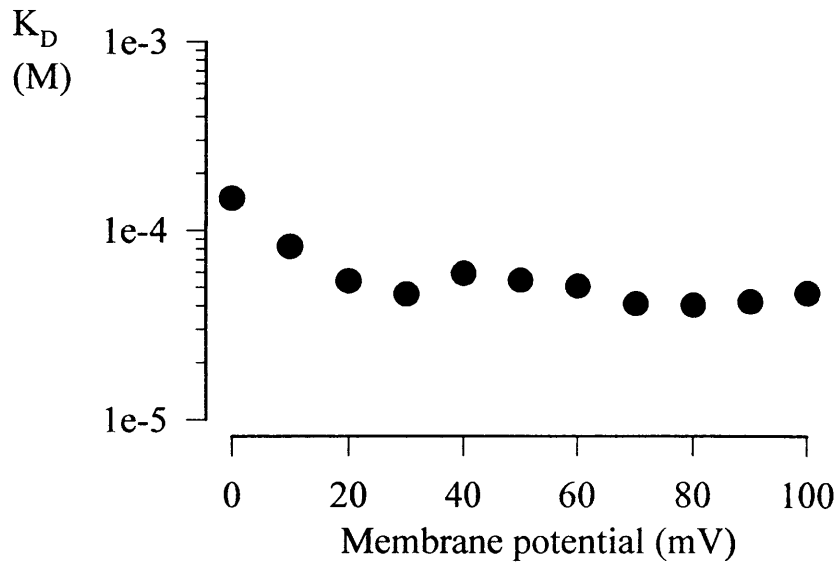
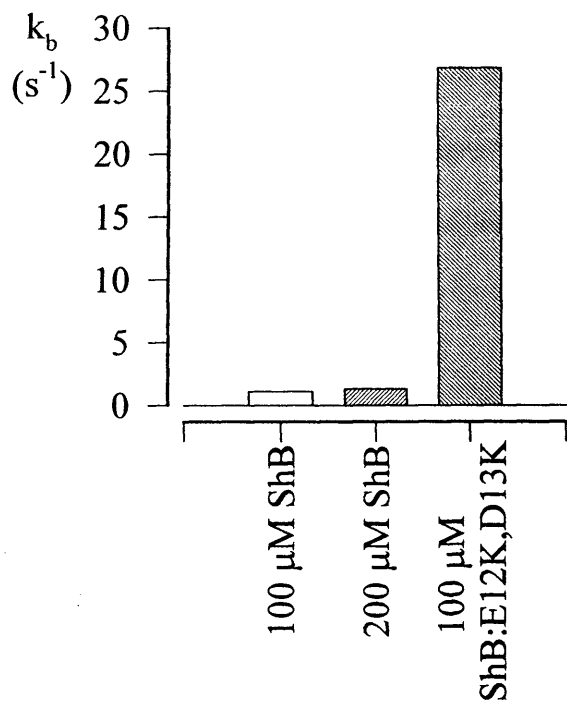


Figure 5.11 Comparison of blocking and unblocking rates, association rate constants and Equilibrium dissociation constants for different peptides with Kv1.5 at a +60 mV pulse.

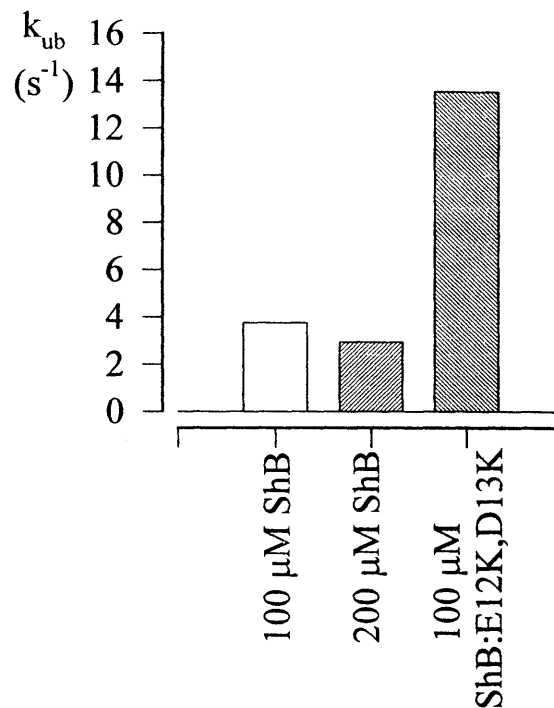
Histogram plots of **A** blocking rate k_b , **B** unblocking rate k_{ub} , **C** association rate constant k_{on} and **D** equilibrium dissociation constant K_D , for 100 and 200 μM ShakerB, and 100 μM ShB:E12K,D13K inactivating ball peptides with Kv1.5 at a pulse potential of +60 mV. Bars represent averaged data for 3, 3, and 3 cells respectively in all panels of this figure.

Figure 5.11

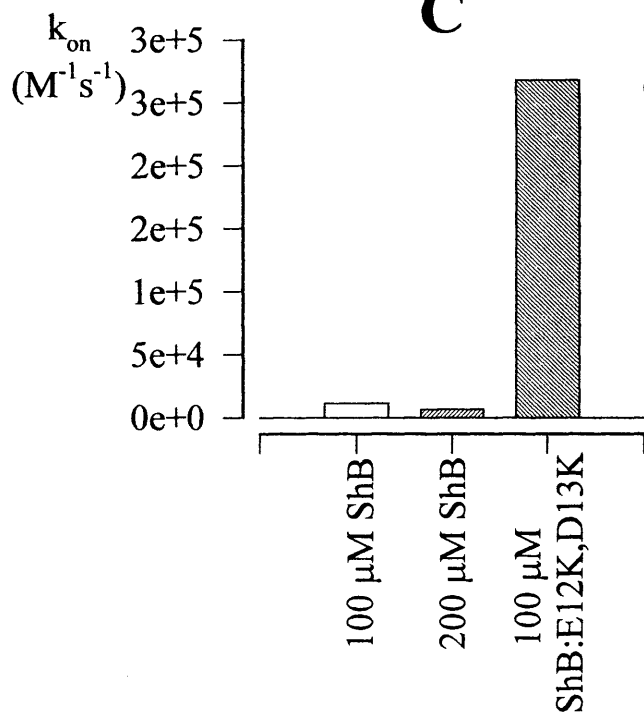
A



B



C



D

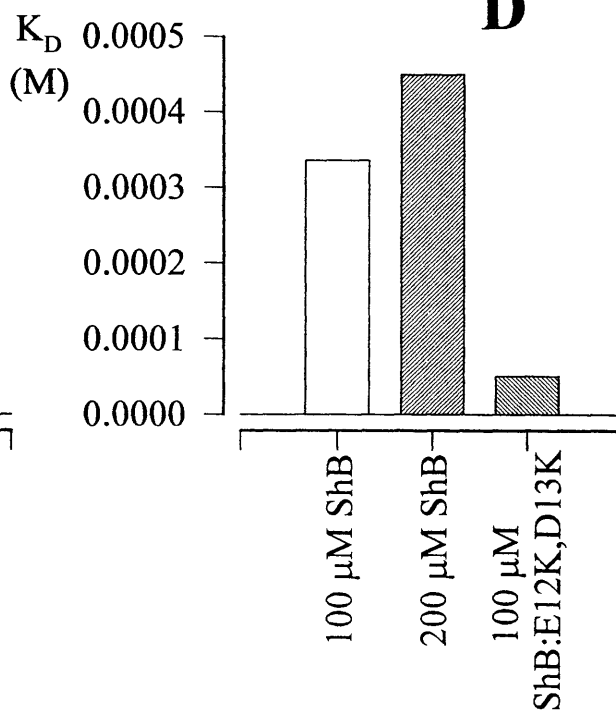


Figure 5.12 Comparison of τ_{fast} values at +60 mV.

Histogram plot of τ_{fast} fitted to the decline of the Kv1.5 current at a + 60 mV pulse for control cells , and cells in the presence of 100 and 200 μ M ShakerB, and 100 μ M ShB:E12K,D13K inactivating ball peptides. Bars represent average data for 7, 3, 3 and 3 cells respectively.

Figure 5.12

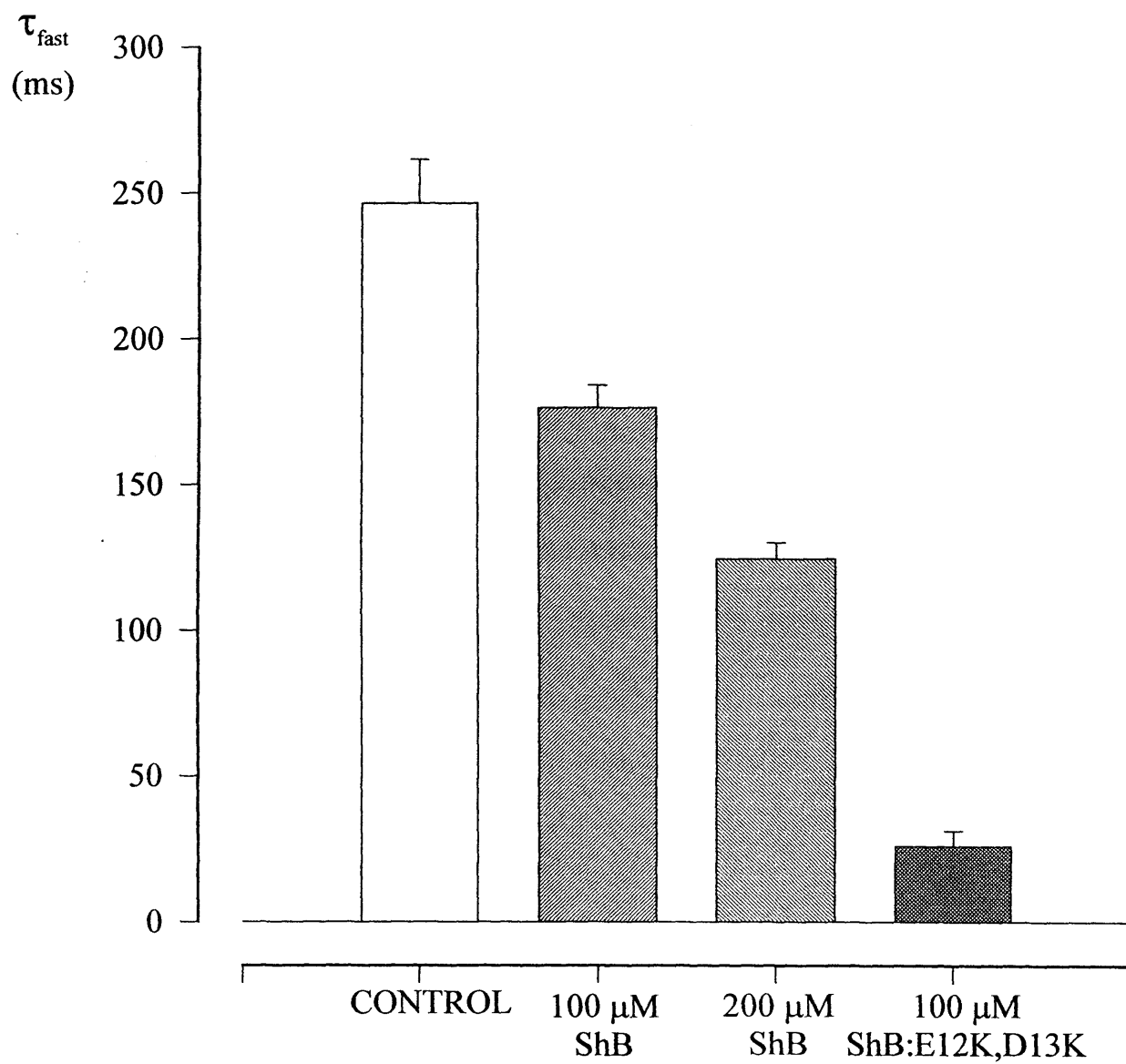


Figure 5.13 The effect of 200 μ M ShB:E12K,D13K inactivating ball peptide on Kv4.2.

A,B Typical whole cell currents recorded from Kv4.2 in the absence and presence of 200 μ M ShB:E12K,D13K inactivating ball peptide. Records have been corrected for leakage and capacitance currents.

A Currents recorded from a control cell (no ball peptide present in the patch pipette) in response to depolarising voltage steps of 100 ms duration, from a holding potential of -80 mV, in +10 mV steps from 0 mV to +90 mV. The voltage pulse protocol is shown above.

B Currents recorded from a different cell in response to the same voltage pulse protocol as above, but with 200 μ M ShB:E12K,D13K inactivating ball peptide in the internal solution in the patch pipette.

Figure 5.13

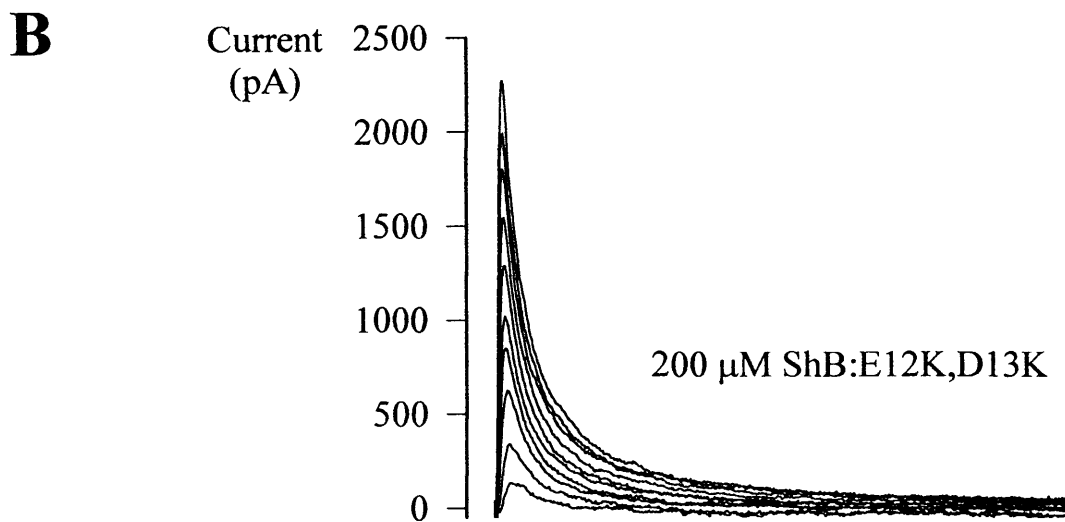
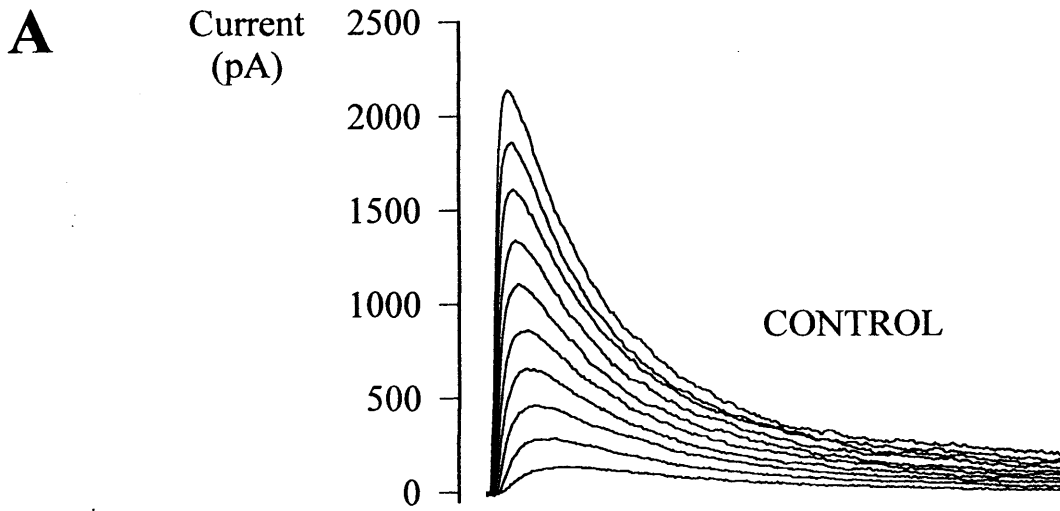
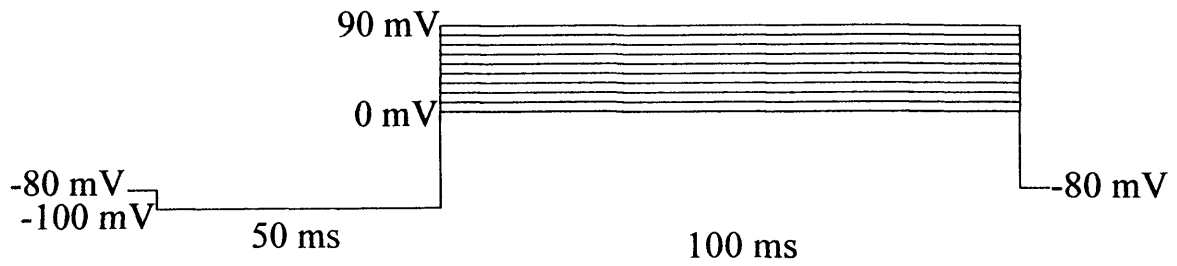


Figure 5.14 The effect of ShB,E12K,D13K inactivating ball peptide on Kv4.2
illustrated using scaled currents.

A The magnitude of the peaks of the current traces in response to the +90 mV voltage pulse of 100 ms duration were matched. These scaled current traces shown are typical of those in control cells in the absence of peptide, and in the presence of 200 μ M ShB:E12K,D13K inactivating ball peptide. Note how the peak of the current is reached much more quickly.

B Superimposed scaled current traces showing the effect of 200 μ M ShB:E12K,D13K inactivating ball peptide on Kv4.2 currents over a shorter time, 10 ms. These are the same current traces as in Figure 5.14A above.

Figure 5.14

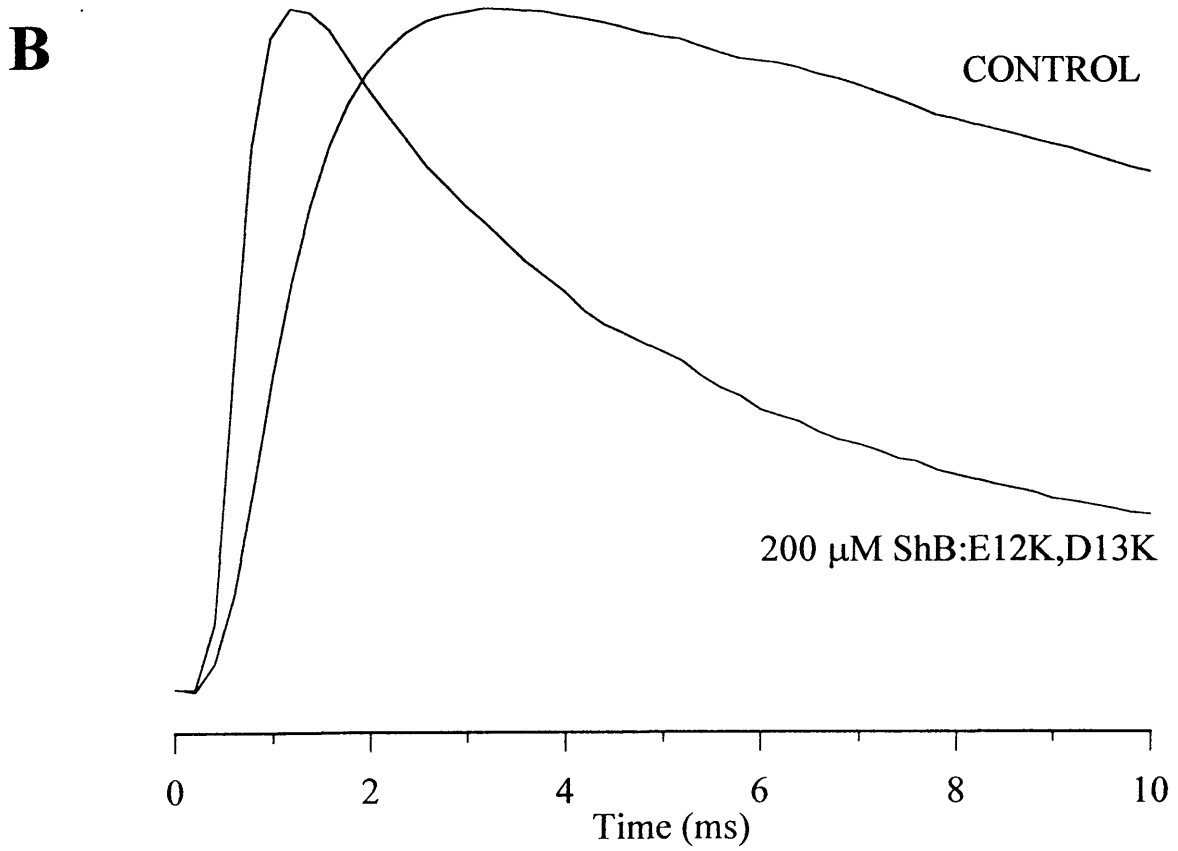
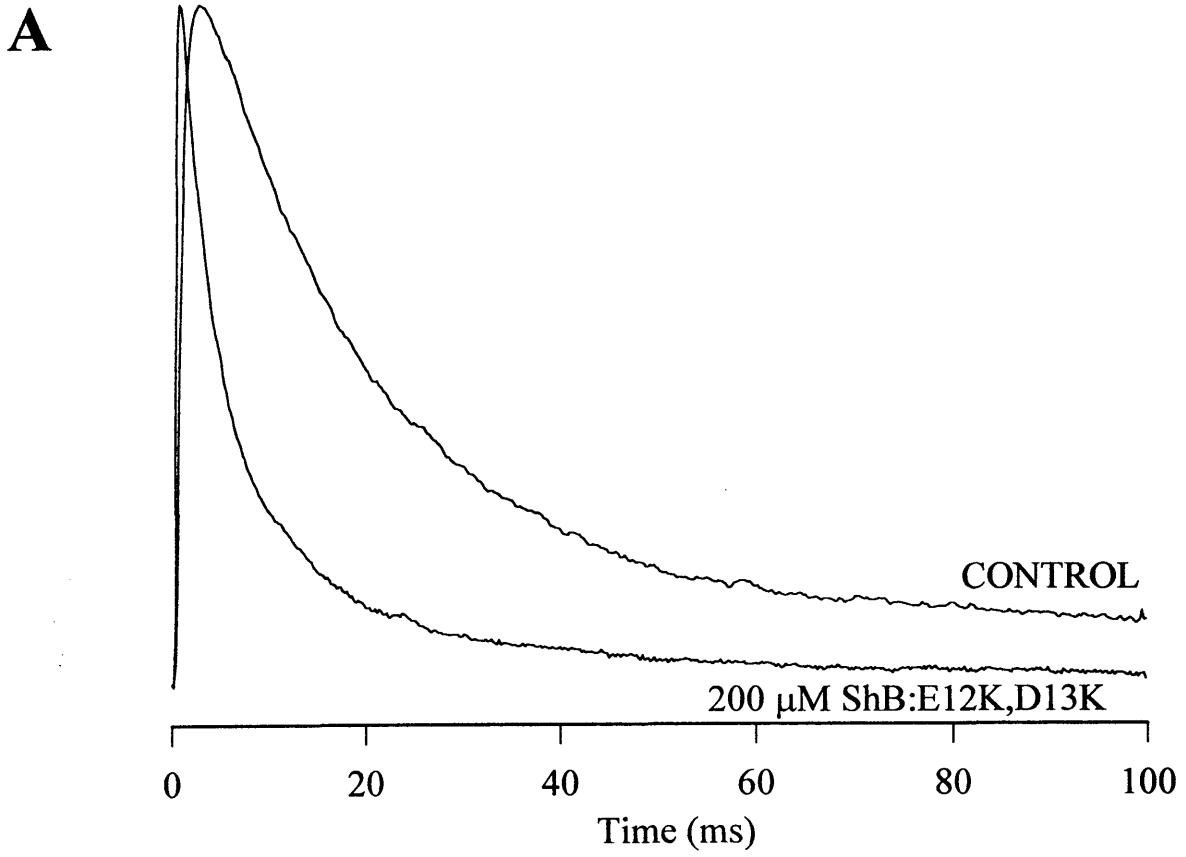


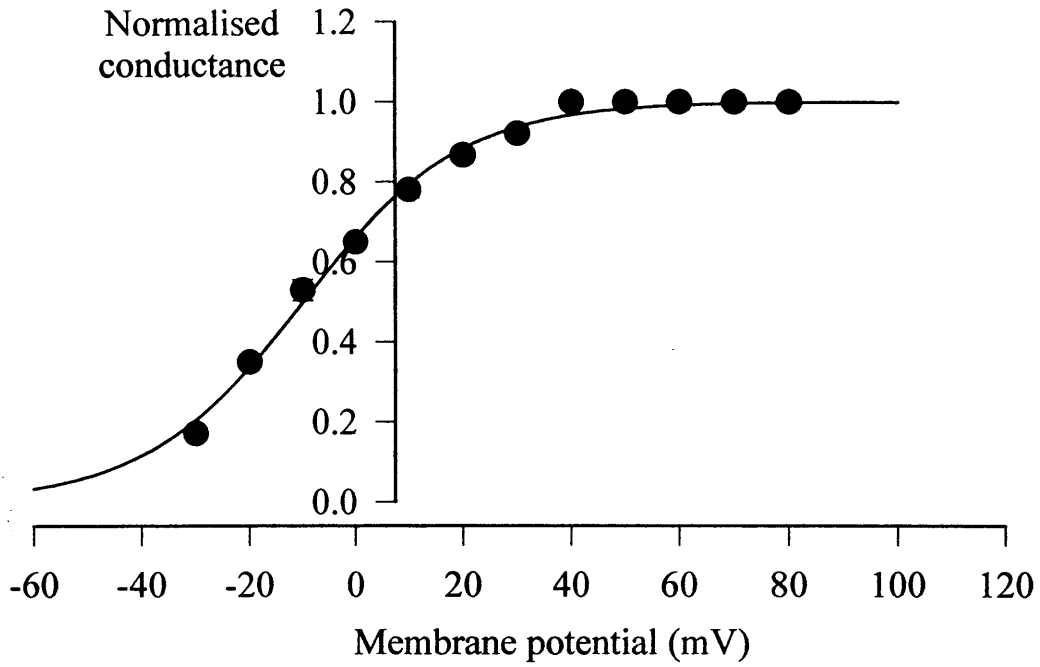
Figure 5.15 The effect of 200 μ M ShB:E12K,D13K inactivating ball peptide on the voltage dependence of activation and inactivation of Kv4.2.

A The voltage dependence of the activation for Kv4.2 with 200 μ M ShB:E12K,D13K inactivating ball peptide in the internal pipette solution. Chord conductance at each potential was calculated with respect to the value for I_0 , initial current elicited from the exponential fit to the decay of current divided by the driving force at that potential. Conductance values were normalised to maximal values to give an activation curve. Points represent means \pm SEM for 3 cells. A Boltzmann function fitted to the data from each cell gave a mean half maximal activation, $V_{1/2}$ at -10.4 mV (\pm 1.0 mV) and mean slope factor $k = 14.0$ mV (\pm 0.3 mV). The illustrated curve has $V_{1/2}$ at -9.9 mV and $k = 13.8$ mV.

B Steady state inactivation of Kv4.2 with 200 μ M ShB:E12K,D13K inactivating ball peptide in the internal pipette solution. As shown in Figure 4.7, a conditioning 50ms pre-pulse to -100 mV was followed by a variable potential 100 ms pulse depolarising from -100 mV to +20 mV in increments of +10 mV. The final step was a 100 ms constant +40 mV pulse. The magnitude of the current due to the final step was normalised and plotted versus membrane potential to give an inactivation curve. Points represent means \pm SEM for 3 cells. A Boltzmann function fitted to the data from each cell gave a mean half maximal steady state inactivation at -53.6 mV (\pm 1.4 mV) and average slope factor k of 7.0 mV (\pm 0.4 mV). The illustrated curve has $V_{1/2}$ for inactivation at -53.6 mV and $k = 7.3$ mV

Figure 5.15

A



B

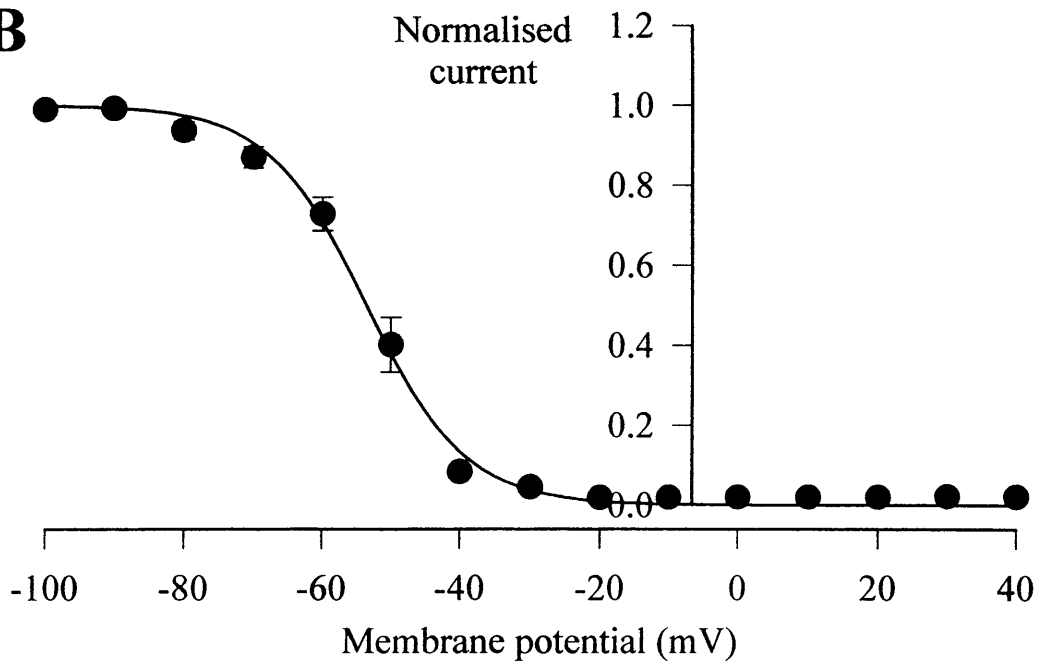


Figure 5.16 Hodgkin-Huxley activation parameters

A Values of $\tau_{\text{activation}}$, a time constant of activation derived from the fit of a classical Hodgkin-Huxley formula describing a channel showing both activation and inactivation to current traces. $\tau_{\text{activation}}$ was obtained from the parameters of Equation 4.1 (described in the text of Chapter 4) fitted to currents elicited due to the voltage pulse protocols described above in Figure 5.13A. $\tau_{\text{activation}}$ is plotted on a common log scale against membrane potential for control cells in the absence of peptide (open circles) and to Kv4.2 test cells in the presence of 200 μM ShB:E12K,D13K inactivating ball peptide (filled circles).

B $\tau_{\text{inactivation}}$ for currents from control cells in the absence of peptide (open circles) and from Kv4.2 test cells in the presence of 200 μM ShB:E12K,D13K inactivating ball peptide (filled circles) plotted on a common log scale against membrane potential.

These illustrate the voltage dependence of the activation time constant and represent means \pm SEM for 3 cells in each case.

Figure 5.16

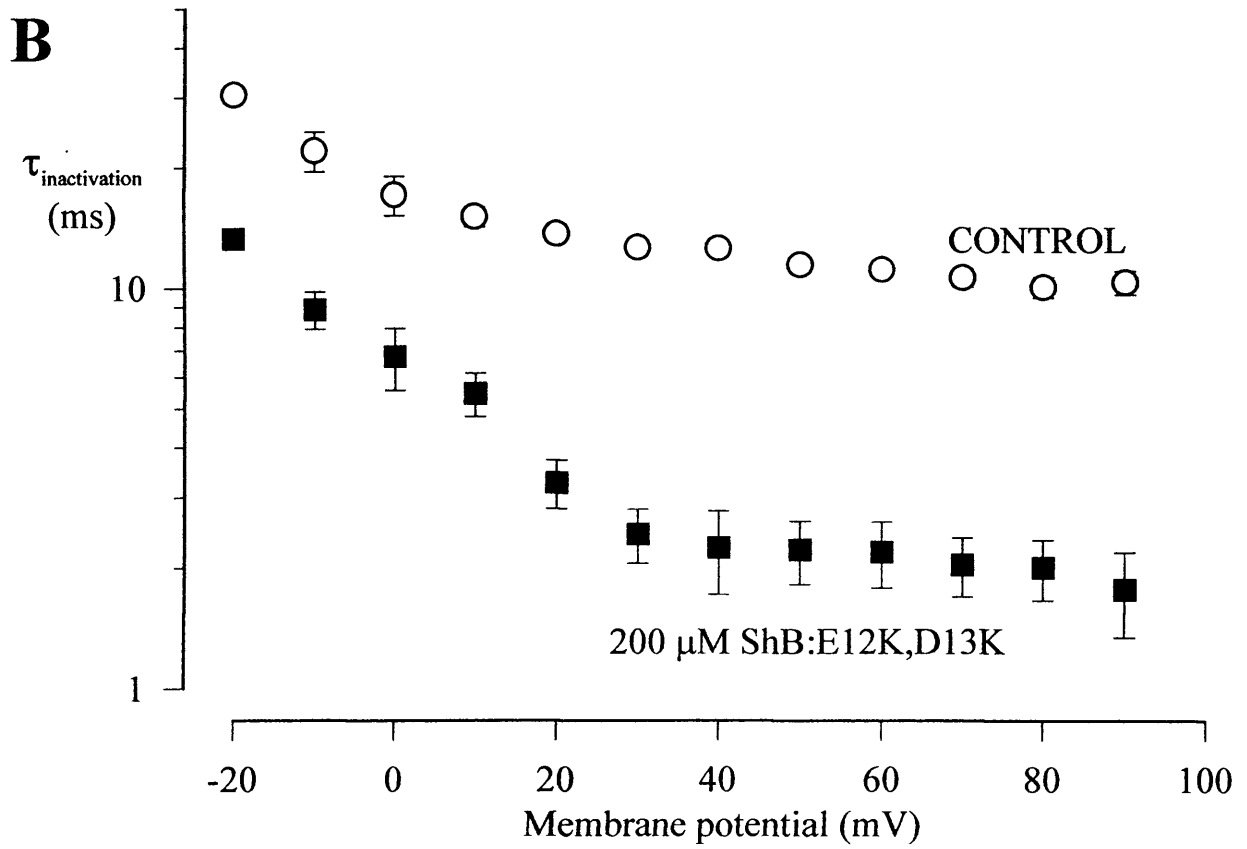
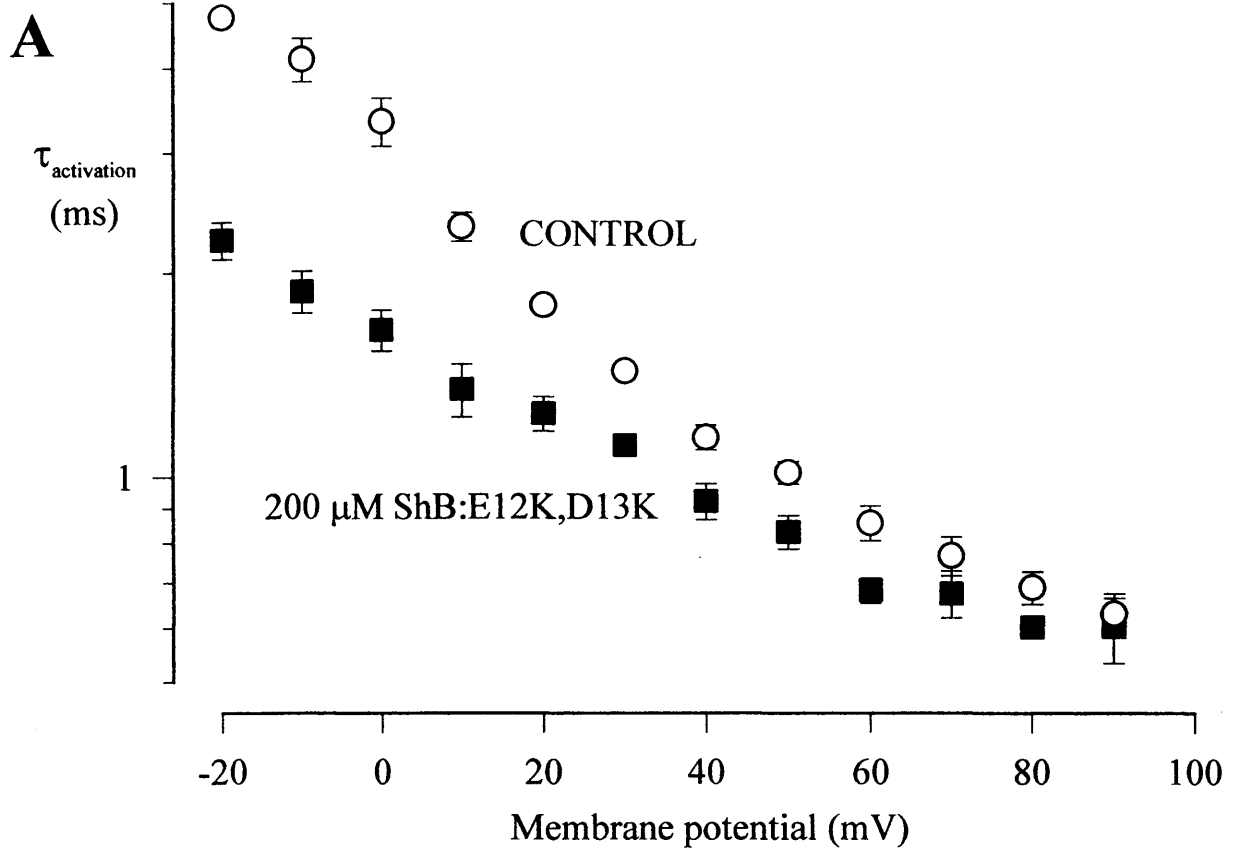


Figure 5.17 The variation of 200 μ M ShB:E12K,D13K inactivating ball peptide blocking and unblocking rates of Kv4.2 with membrane potential.

A Blocking rates, k_b for Kv4.2 control cells in absence of peptide (filled circles) and 200 μ M ShB:E12K,D13K inactivating ball peptide with Kv4.2 (open circles) plotted versus membrane potential. Control cell data have been fitted with the same functions and equations as for test cells, assuming that the endogenous N-terminal ball is binding in the same manner. Points represent means \pm SEM for 3 cells for control and test cells.

B Unblocking rates, k_{ub} for Kv4.2 control cells in absence of peptide (filled circles) and 200 μ M ShB:E12K,D13K inactivating ball peptide with Kv4.2 (open circles) plotted versus membrane potential. Points represent means \pm SEM for 3 cells for control and test cells.

Figure 5.17

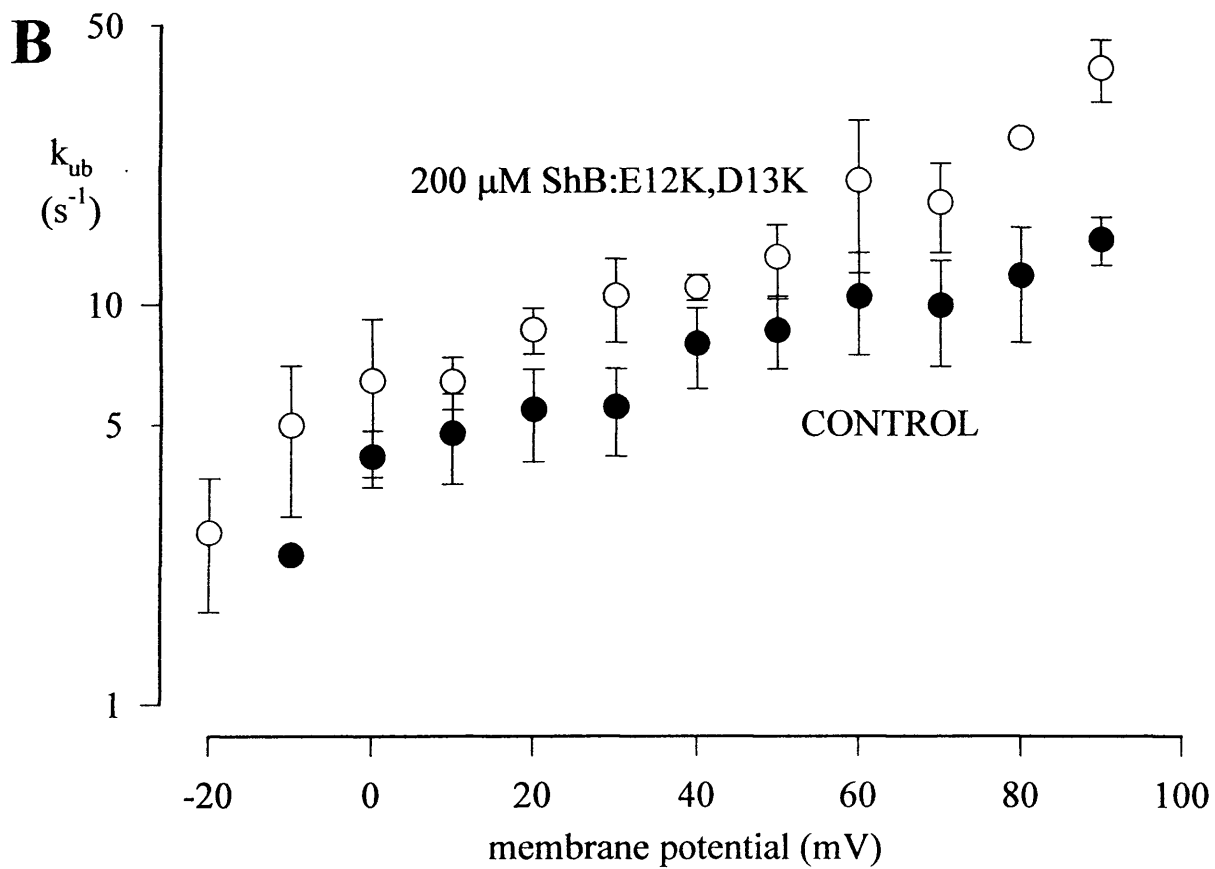
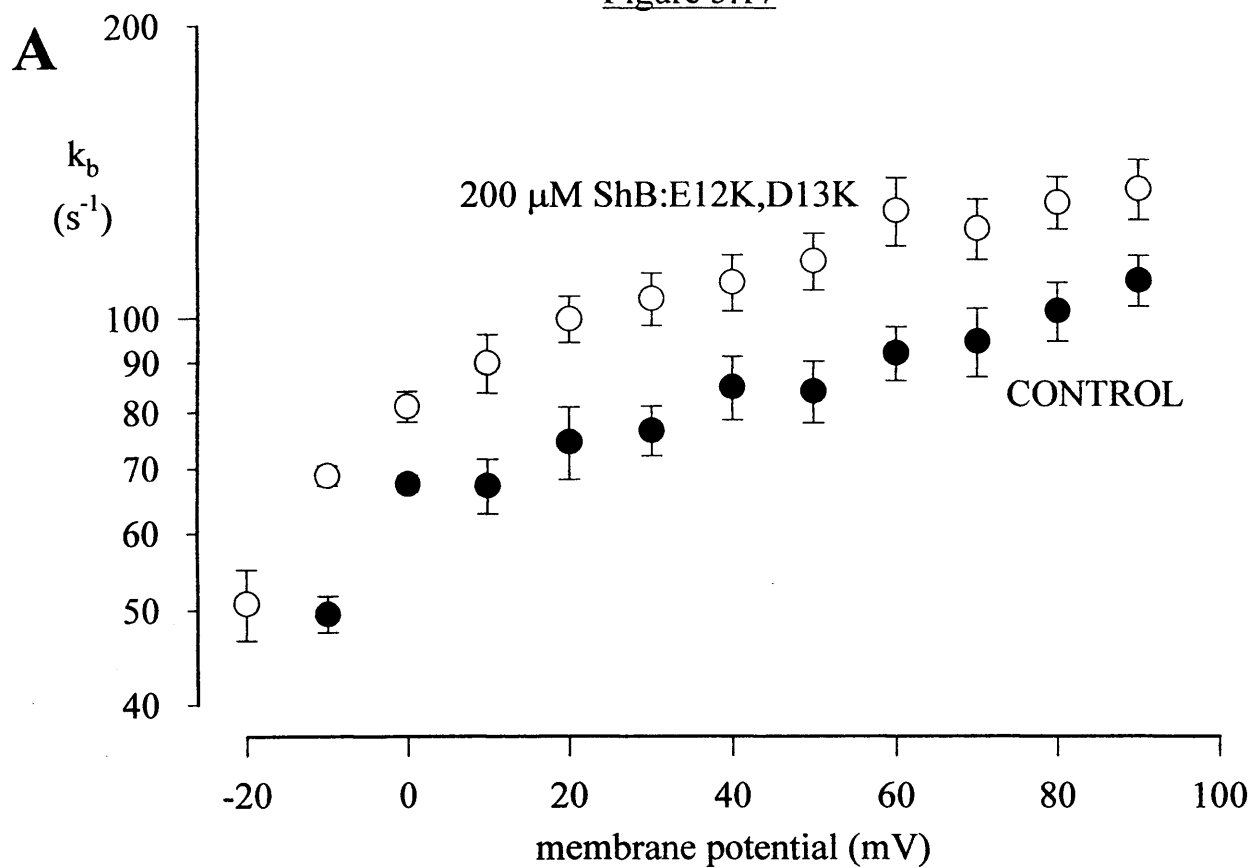
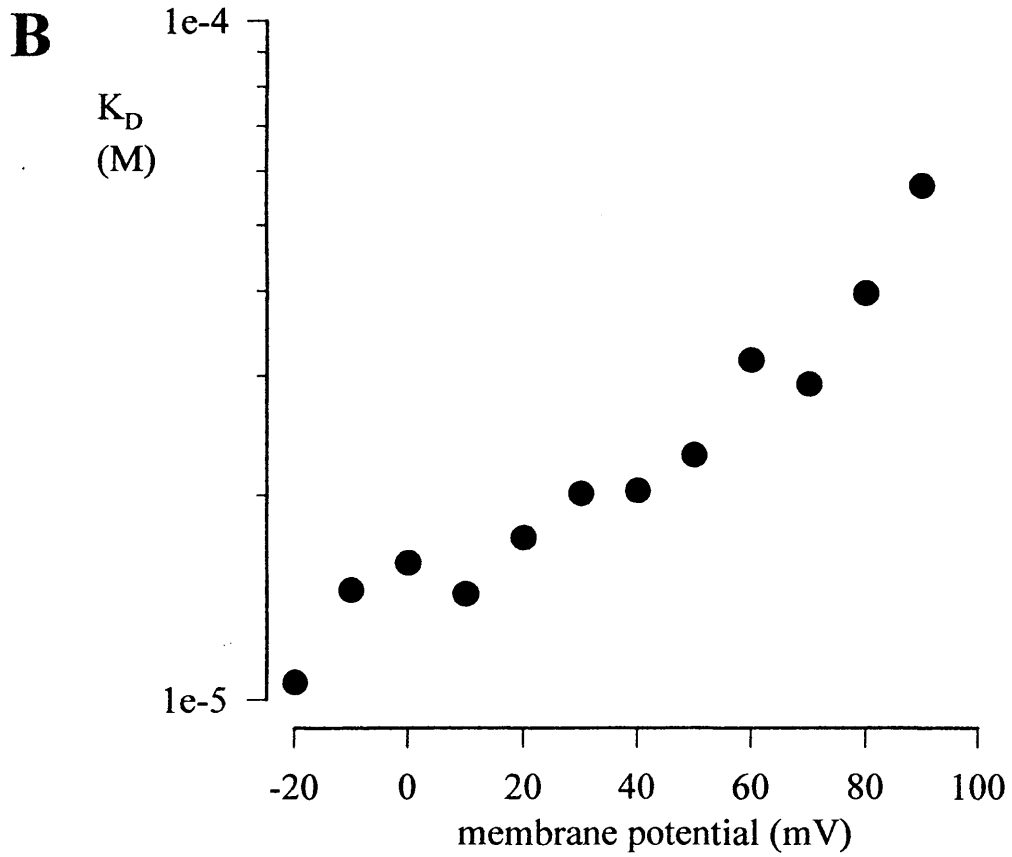
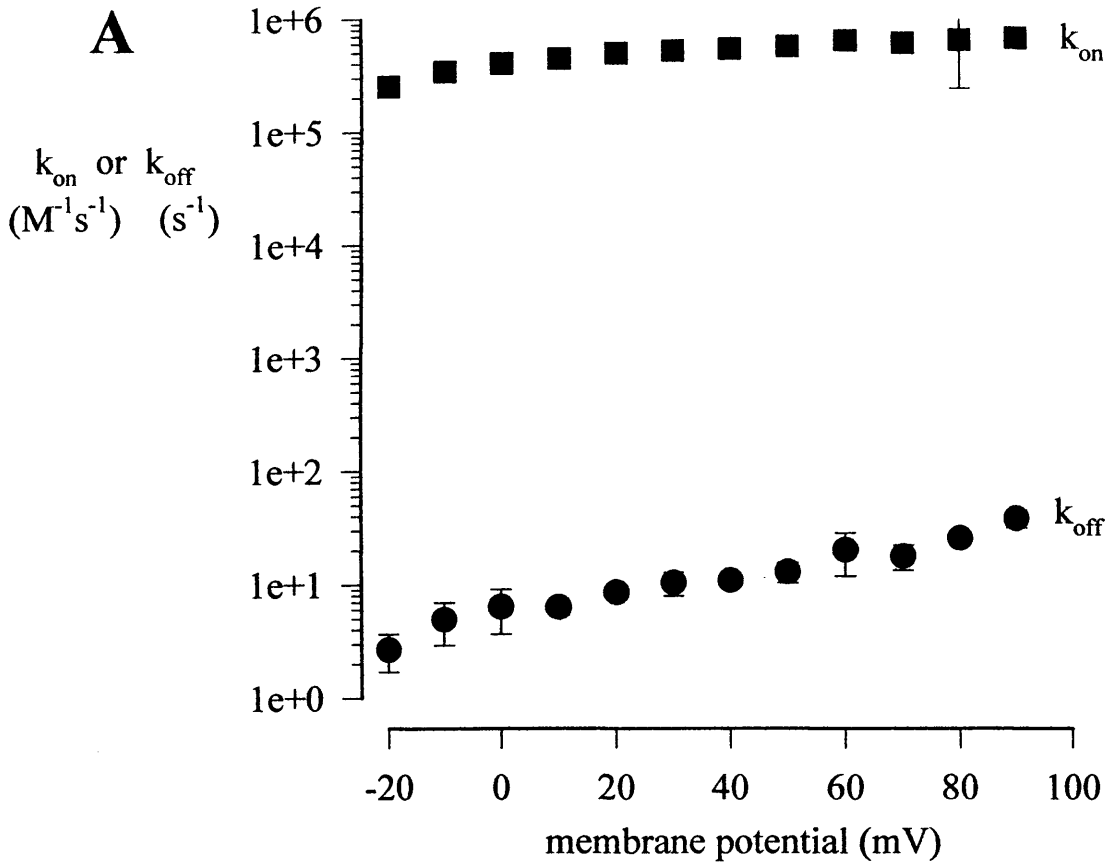


Figure 5.18 The variation of 200 μM ShB:E12K,D13K inactivating ball peptide association/dissociation rate constants and Equilibrium dissociation constants of Kv4.2 with membrane potential.

A Association rate constants k_{on} (squares), and dissociation rate constants k_{off} (circles), 200 μM ShB:E12K,D13K inactivating ball peptide with Kv4.2 plotted versus membrane potential. Points represent means \pm SEM for 3 cells.

B Equilibrium dissociation constants, K_{D} , for 200 μM ShB:E12K,D13K inactivating ball peptide with Kv4.2 plotted versus membrane potential. Points represent means \pm SEM for 3 cells.

Figure 5.18



CHAPTER SIX

General Discussion

The aim of this study was to research the biophysical properties of two voltage-activated potassium channels, the delayed rectifier Kv1.5, and the A-type Kv4.2. These potassium channels were stably transfected by electroporation into a mammalian cell line, Murine Erythroleukemia (MEL) cells.

MEL cells are erythrocyte precursors that can be induced to undergo erythroid differentiation and maturation if chemically induced with compounds such as dimethyl sulphoxide. The production of globin proteins during this maturation process in MEL cells was useful, in that it enabled transfected DNA encoding for the channels to be expressed and the channel protein to be produced, packaged and inserted into the membrane. This was able to take place when the DNA for the respective channels was linked to and regulated by the locus control region of the human β -globin gene, which produced human globin proteins alongside those of the mouse. Functional channels were detectable in the membrane about 7 hours after the induction of stably transfected cells, although most of my experiments were conducted at least 48 hours after induction.

MEL cells proved to be relatively easy to form gigaohm seals with, using conventional internal and external solutions. The lack of endogenous currents enables the single type of channel transfected to be studied in isolation. This is difficult in native cells due to the interference from other channel currents in recordings. Although one can use drugs or toxins to block specific channels, or apply complex voltage pulse protocols to activate/inactivate relevant channels, or even alter the composition of solutions by substituting non-permeating ions for physiological ions, the ideal approach would be to find a cell line with no endogenous ion channels. This MEL cell expression system had several advantages over the main expression system used at the time of these experiments, namely mRNA expression in *Xenopus* oocytes. Whole cell experiments are impossible with

Xenopus oocytes due to their large size. Expression in a mammalian cell line may mean that the post-translational modifications of channel proteins after synthesis resemble those in native cells more closely than expression in amphibian cells. Finally, the factor of ease of use is important – as a stably transfected cell line, channels continued to be expressed giving currents consistently at similar levels in MEL cells through over 20 passages of these cells in culture. Cells survived well in liquid nitrogen, so stocks of early passage cells (soon after transfection) could be frozen. Apart from regular subculture of cell lines, the process, from adding DMSO in order to commence induction through to using the cells proved to be very easy compared to regularly harvesting oocytes from the *Xenopus* toad, preparation of oocytes, through to the laborious injection of mRNA into individual oocytes.

The whole cell configuration of the patch clamp technique was used to characterise the biophysical properties of two voltage-activated potassium channels, Kv1.5 and Kv4.2. These characterisations are described in Chapters Three and Four. Studies of ion channels encompass a wide range of experimental techniques from a variety of disciplines. A combination of electrophysiology, molecular biology, pharmacology, biochemistry and biophysical approaches has advanced our understanding enormously. Using techniques such as Northern blot analysis of total RNA, RNA amplification by the polymerase chain reaction and screening of cDNA and genomic libraries, KV1.5 and Kv4.2 have been found to be abundant throughout many tissues. One of the most important steps in correlation of the cloned channels with endogenous currents has to be in terms of easily measured biophysical properties such as half maximal activation or inactivation, in order to establish functional characteristics such as the voltage range of activation or the time course of recovery from inactivation. A heterologous expression system where

the individual channel system can be studied using physiological solutions, without other contaminating currents can offer many clues, which may be confirmed in native tissues. Pharmacological tools may also be useful – potassium channel sensitivities to blockers such as 4-aminopyridine differ between sub-types. Another example of this is the flecainide sensitivity of Kv4.2 established by Yeola and Snyders (1996) which resembles the flecainide sensitivity of I_{to} , the transient outward potassium current in the heart more than other potential A-type candidates in the heart such as Kv1.4. This confirms the importance of this channel in the control of the cardiac action potential. However, one must proceed carefully with comparison of functional biophysical parameters established from heterologous expression in cell lines to those in native tissues. For instance, the half-maximal inactivation values for I_{to} vary from -85 mV reported in the rabbit to -14 mV in ferret and humans (Campbell, Rasmusson, Qu and Strauss, 1993).

Since the experimental work was carried out for this thesis, the widespread existence in most tissues of an accessory subunit for mammalian potassium channels similar to those in sodium and calcium channels able to modulate current amplitude and inactivation kinetics has been confirmed. This was first shown by Rettig, Heinemann, Wunder, Lorra, Parcej, Dolly and Pongs (1994), who identified cDNA clones encoding two isoforms of the β -subunit of rat brain potassium channels. These subunits would not form channels when expressed in *Xenopus* oocytes but co-expression with the delayed rectifier RCK1 (Kv1.1) channel led to the expression of a rapidly inactivating current rather than the extremely slowly inactivating (functionally non-inactivating) current with RCK1 alone. It appears that the β -subunits possess an endogenous ball region in their amino-terminus, that can behave in a similar way to the *Shaker*B ball and chain. The ability of different potassium channels to form heteromultimers has been shown to occur only within

subfamilies, and not between subfamilies (Covarrubias, Wei and Salkoff, 1991) and this appeared to be true for β -subunits also. Sewing, Roeper and Pongs (1996) showed that co-expression of Kv β 1 subunit (i.e. assigned to subunit subfamily 1) with Kv1.5 resulted in faster inactivation, but there was no effect observed with Kv2 or Kv3 potassium channels.

However, Uebele, England, Chaudhary, Tamkun and Snyders (1996) found functional differences in the kinetics of and voltage dependence of activation and inactivation parameters for Kv1.5 currents expressed in various mammalian cell lines, due to the presence of endogenous Kv β 2.1 subunit. Uebele and co-workers used molecular cloning, immunopurification and Western blot analysis to identify endogenous Kv β subunits in heterologous expression systems such as *Xenopus* oocytes, L-cells, CHO cells and HEK293 cells. It appears that the Kv β 2.1 subunit can alter Kv1.5 α -subunit expression. For HEK293 cells transfected with Kv1.5 in the absence of the Kv β 2.1 subunit, half-maximal activation and inactivation occurred at -0.2 mV and -9.6 mV respectively. In the presence of the Kv β 2.1 subunit however, these values became -14.1 mV and -22.1 mV respectively, these second set of values being very similar to those from L-cells. L-cells have been shown to have an endogenous Kv β 2.1 subunit that assembles with the transfected Kv1.5 protein. This fact should be borne in mind when choosing a cell line for expression studies or when attempting to map cloned channel currents to native currents. The fact that β -subunits can change the properties of a channel potentially increases the diversity of potassium channels *in vivo* even further.

Chapter Five describes whole cell experiments on inactivation with both Kv1.5 and Kv4.2. Synthetic 'ball' peptides based upon the sequence of the amino-

terminal structural motif that causes fast inactivation (analogous to a 'ball and chain' occluding the pore internally) in *Shaker* potassium channels were included in the pipette solutions during recordings. Blocking/unblocking rates and association/dissociation rate constants were calculated in order to characterise the effect on Kv1.5 and Kv4.2 currents. Kv1.5 does not undergo fast inactivation unlike Kv4.2; it could be described as being functionally non-inactivating for the time periods of most physiological depolarisations. The synthetic inactivating ball peptides caused Kv1.5 inactivation to speed up to resemble an A-type current. The mutation L7E caused peptides to become inactive; the double mutation E12K,D13K made the peptide more potent. Even Kv4.2 currents inactivated significantly more quickly. These results imply that there is a high degree of conservation of the receptor site on the channel for the ball, from *Shaker* to Kv1.5 and Kv4.2. The problems I encountered with delivery of required concentrations of the peptides to the inner face of the channel could be assessed by performing experiments in the inside-out configuration of the patch clamp technique, and applying peptide in a flow solution rather than including it in the patch pipette.

The nature of N-type inactivation was more recently investigated using high resolution nuclear magnetic resonance (NMR) spectroscopy. Antz, Geyer, Fakler, Schott, Guy, Frank, Ruppersberg and Kalbitzer (1997) established that the N-terminal domains of the rapidly inactivating Kv1.4 and Kv3.4 channels do indeed contribute to the inactivation gate of each of these channels. Three-dimensional analysis of the inactivation ball domain revealed a compact structural arrangement with all positively charged residues clustered to one side of the ball, and the negatively charged residues forming a tail next to the hydrophobic region. The same group of workers also found, using NMR spectroscopy again, that synthetic ball domains have a similar non-random structure in an aqueous environment in

which they are biologically active such as the intracellular solutions used in this study (Schott, Antz, Frank, Ruppertsberg and Kalbitzer, 1998).

Fernandez-Ballester, Gavilanes, Albar, Criado, Ferragut and Gonzalezros (1995) found that the *Shaker*B inactivating ball peptide has a great tendency to adopt a highly stable beta-structure even in the presence of anionic phospholipid vesicles, an interaction with conformational restrictions that they postulated could partly imitate those at putative peptide binding elements at the mouth of the pore (a ring of anionic residues and a hydrophobic pocket) and be important in determining channel blockade. Interestingly, the inactive form of the peptide also used in this study, ShB:L7E, could not adopt the beta-structure under their experimental conditions and remained in a predominantly non-ordered conformation.

Other work on voltage-activated potassium channels that I carried out in this work with MEL cells, but not included in this thesis included preliminary studies of the intracellular block of Kv4.2 by Mg²⁺ ions. Rettig, Wunder, Stocker, Lichtinghagen, Mastiaux, Beckh, Kues, Pedarzani, Schröter, Ruppertsberg, Veh and Pongs (1992) described the block of Raw3 (Kv3.4) channels from rat brain expressed in *Xenopus* oocytes, and recorded in cell-attached macropatches or inside-out patches. In the absence of Mg²⁺, there was no rectification of the current-voltage relationship at potentials positive to 0 mV. In my whole cell experiments with Kv4.2, there was no such rectification of the current-voltage relationship, even with elevated levels of free Mg²⁺ (up to 10 mM from 2 mM) in the intracellular pipette solution, and the current-voltage relationship did not change with pipette solution lacking Mg²⁺. Unfortunately, none of the clones of rat Kv3.4 transfected into MEL cells that I screened appeared to be expressing functional channels. I also

screened clones of human Kv1.3 and rat Kv1.1 that did produce currents, both delayed rectifiers.

With the great advances in molecular biology cloning techniques of recent years, the versatility of a stable expression system such as this means that it is possible to attempt to recreate in a heterologous system, the diversity of potassium channel architecture *in vivo*.

REFERENCES

ADAMS, D.J. and GAGE, P.W. (1979) Characteristics of sodium and calcium conductance changes produced by membrane depolarization in an *Aplysia* neurone. *Journal of Physiology* **289**, 143-161.

ADAMS, P.R., CONSTANTIN, A., BROWN, D.A. and CLARK, R.B. (1982) Intracellular Ca^{2+} activates a fast voltage-sensitive current in vertebrate sympathetic neurones. *Nature* **246**, 746-749.

AGNEW, W.S. (1988) A Rosetta stone for K channels. *Nature* **331**: 114-115.

AIDLEY, D.J. and STANFIELD, P.R. (1996) *Ion Channels*. Cambridge University Press, Cambridge, Great Britain.

ALDRICH, R. (1993) Advent of a new family. *Nature* **362**: 107-108.

ANTONIOU, M. (1991) Introduction of erythroid-specific expression in Murine Erythroleukemia (MEL) cell lines. In *Methods in Molecular Biology Vol 7: Gene Transfer and Expression Protocols*. Edited by E.J. Murray 1991 The Humana Press Inc. Clifton NJ, USA.

ANTZ, C., GEYER, M., FAKLER, B., SCHOTT, M., GUY, H.R., FRANK, R., RUPPERSBERG, J.P. and KALBITZER, H.R. (1997) NMR structure of inactivation gates from mammalian voltage-dependent potassium channels. *Nature* **385**: 272-275.

ARCANGELI, A., WANKE, E., OLIVOTTO, M., CAMPAGNI, S. and FERRONI,

A. (1987) Three types of ion channel are present on the plasma membrane of Friend erythroleukemia cells. *Biochemical and Biophysical Research Communications* **146** (3): 1450-1457.

ARMSTRONG, C.M. (1981) Sodium channels and gating currents. *Physiological*

Reviews **61**: 644-683.

ARMSTRONG, C.M. and BEZANILLA, F. (1977) Inactivation of the sodium

channel. II. Gating current experiments. *Journal of General Physiology* **70**: 567-590.

ARMSTRONG, C.M., BEZANILLA, F. and ROJAS, E. (1973) Destruction of

sodium conductance inactivation in squid axons perfused with pronase.

Journal of General Physiology **62**: 375-391.

BALDWIN, T.J., TSAUR, M.-L., LOPEZ, G.A., JAN, Y.N. and JAN, L.Y. (1991)

Characterization of a mammalian cDNA for an inactivating voltage-sensitive K⁺ channel. *Neuron* **7**: 471-483.

BARRY, D.M., TRIMMER, J.S., MERLIE, J.P. and NERBONNE, J.M. (1995)

Differential expression of voltage-gated K⁺ channel subunits in adult rat heart: relationship to functional K⁺ channels? *Circulation Research* **77**: 361-369.

- BEIRÃO, P.S.L., DAVIES, N.W. and STANFIELD, P.R. (1994) Inactivating 'ball' peptide from *ShakerB* blocks Ca^{2+} -activated but not ATP-dependent K^+ channels of rat skeletal muscle. *Journal of Physiology* **474**: 269-274.
- BLAIR, T.A., ROBERDS, S.L., TAMKUN, M.M., and HARTSHORNE, R.P. (1991) Functional expression of RK5, a voltage-gated K^+ channel isolated from the rat cardiovascular system. *FEBS Letters* **295**: 211-213.
- BOYETT, M.R., HARRISON, S.M., JANVIER, N.C., MCMORN, S.O., OWEN, J.M. and SHUI, Z. (1996) A list of vertebrate cardiac ion currents: Nomenclature, properties, function and cloned equivalents. *Cardiovascular Research* **32**: 455-481.
- BROWN, D.A. and ADAMS, P.R. (1980) Muscarinic suppression of a novel voltage-sensitive K^+ -current in a vertebrate neurone. *Nature* **283**: 673-676.
- BUTLER, A., WEI, A., BAKER, K. and SALKOFF, L. (1989) A family of putative potassium channel genes in *Drosophila*. *Science* **243**: 943-947.
- CAMPBELL, D.L., RASMUSSEN, R.L., QU, Y. and STRAUSS, H.C. (1993) The calcium-independent transient outward potassium current in isolated ferret right ventricular myocytes. *Journal of General Physiology* **101**: 571-601.

CHANDY, K.G., DOUGLASS, J., GUTMAN, G.A., JAN, L., JOHO, R.,
KACZMAREK, L., MCKINNON, D., NORTH, R.A., NUMA, S.,
PHILIPSON, L., RIBERA, A.B., RUDY, B., SALKOFF, L., SWANSON,
R.A., STEINER, D., TANOUYE, M. AND TEMPLE, B.L. (1991)
Simplified gene nomenclature. *Nature* **352**: 26.

CHRISTIE, M.J., NORTH, R.A., OSBORNE, P.B., DOUGLASS, J. and
ADELMAN, J.P. (1990) Heteromultimeric potassium channels expressed
in *Xenopus* oocytes from cloned subunits. *Neuron* **2**: 405-411.

CHOI, K.L., ALDRICH, R.W. and YELLEN, G. (1991) Tetraethylammonium
blockade distinguishes two inactivation mechanisms in voltage-activated K⁺
channels. *Proceedings of the National Academy of Sciences USA* **88**:5092-
5095.

COLINO, A. and HALLIWELL, J.V (1987) Differential modulation of three
separate K-conductances in hippocampal CA1 neurons by serotonin. *Nature*
328: 73-77.

CONNOR, J.A. and STEVENS, C.F. (1971) Voltage clamp studies of a transient
outward membrane current in gastropod neural somata. *Journal of*
Physiology **213**: 21-30.

COVARRUBIAS, M., WEI, A. and SALKOFF, L. (1991) *Shaker*, *Shal*, *Shab* and
Shaw express independent K⁺ current systems. *Neuron* **7**: 763-773.

DAVIES, N.W. (1993) A suite of programs for acquisition and analysis of voltage- and patch-clamp data developed using the AxoBASIC library. *Journal of Physiology* **459**: 111P.

DEAL, K.K., ENGLAND, S.K. and TAMKUN, M.M. (1996) Molecular physiology of cardiac potassium channels. *Physiological Reviews* **76**(1): 49-67.

DEISSEROTH, A. and HENDRICK, D. (1978) Human alpha-globin gene expression following chromosomal dependent gene transfer into mouse erythroleukemia cells. *Cell* **15**: 55-63.

DELPIRE, E. and GULLANS, S.R. (1994) Cell volume and K⁺ transport during differentiation of mouse erythroleukemia cells. *American Journal of Physiology* **266** (*Cell Physiology* **35**): C515-C523.

DIXON, J.E. and M^cKINNON, D. (1994) Quantitative analysis of potassium channel mRNA expression in atrial and ventricular muscle of rats. *Circulation Research* **75**: 252-260.

DOUPNIK, C.A., DAVIDSON, N. and LESTER, H.A. (1995) The inward rectifier potassium channel family. *Current Opinion in Neurobiology* **5**: 268-277.

- FAKLER, B., BRANDLE, U., BOND, C.H., GLOWATZKI, E., KONIG, C.,
ADELMAN, J.P., ZENNER, H.P. and RUPPERSBERG, J.P. (1994). A
structural determinant of differential sensitivity of cloned inward rectifier K⁺
channels to intracellular spermine. *FEBS Letters* **356**: 199-203.
- FEDIDA, D., WIBLE, B., WANG, Z., FERMINI, B., FAUST, F., NATTEL, S. and
BROWN, A.M. (1993) Identity of a novel delayed rectifier current from
human heart with a cloned K⁺ channel current. *Circulation Research* **73**:
210-216.
- FERNANDEZ-BALLESTER, G., GAVILANES, F., ALBAR, J.P., CRIADO, M.,
FERRAGUT, J.A. and GONZALEZROS, J.M. (1995) Adoption of beta-
structure by the inactivating ball peptide of the *Shaker*B potassium channel.
Biophysical Journal **68** (3): 858-865.
- FICKER, E., TAGLIALATELA, M., WIBLE, B.A., HENLEY, C.M. and BROWN,
A.M. (1994) Spermine and spermidine as gating molecules for inward
rectifier K⁺ channels. *Science* **266**: 1068-1072.
- FOSTER, C.D., CHUNG, S., ZAGOTTA, W.N., ALDRICH, R.W. and LEVITAN,
I.B. (1992) A peptide derived from the *Shaker*B K⁺ channel produces short
and long blocks of reconstituted Ca²⁺-dependent K⁺ channels. *Neuron* **9**:
229-236.

FRASER, P.J. and CURTIS, P.J. (1987) Specific pattern of gene expression during induction of mouse erythroleukemia cells. *Genes & Development* **1**: 855-861.

FRIEND, C., SCHER, W., HOLLAND, J.G. and SAKO, T. (1971) Hemoglobin synthesis in murine virus induced leukemic cells *in vitro*: stimulation of erythroid differentiation by dimethyl sulfoxide. *Proceedings of the National Academy of Sciences of the U.S.A.* **68**: 377-382.

GARCIA-GUZMAN, M., SALA, F., CRIADO, M. and SALA, S. (1994) A delayed rectifier potassium channel cloned from bovine adrenal medulla: functional analysis after expression in *Xenopus* oocytes and in a neuroblastoma cell line. *FEBS Letters* **354** (2): 173-176.

GRISSEMER, S., NGUYEN, A.N., AIYAR, J., HANSON, D.C., MATHER, R.J., GUTMAN, G.A., KARMILOWICZ, M.J., AUPERIN D.D. and CHANDY, K.G. (1994) Pharmacological characterization of five cloned voltage-gated K⁺ channels, types Kv1.1, 1.2, 1.3, 1.5, and 3.1, stably expressed in mammalian cell lines. *Molecular Pharmacology* **45**: 1227-1234.

GUTMAN, G.A. and CHANDY, K.G. (1993) Nomenclature of mammalian voltage-dependent potassium channel genes. *Seminars in the Neurosciences* **5**: 101-106.

- HALLIWELL, J.V. and ADAMS, P.R. (1982) Voltage-clamp analysis of muscarinic excitation in hippocampal neurones. *Brain Research* **250**: 71-92.
- HAMILL, O.P., MARTY, A., NEHER, E., SAKMANN, B. and SIGWORTH, F.J. (1981) Improved patch-clamp techniques for high-resolution current recording from cells and cell-free membrane patches. *Pflügers Archiv* **391**: 85-100.
- HARTMANN, H.A., KIRSCH, G.E., DREWE, J.A., TAGLIALATELA, M., JOHO, R.H. and BROWN, A.M. (1991) Exchange of conduction pathways between two related K⁺ channels. *Science* **251**, 942-944.
- HEGINBOTHAM, L., ABRAMSON, T. and MacKINNON, R. (1992) A functional connection between the pores of distantly related ion channels as revealed by mutant K⁺ channels. *Science* **258**: 1152-1155.
- HILLE, B. (1967) The selective inhibition of delayed potassium currents in nerve by tetraethylammonium ion. *Journal of General Physiology* **50**: 1287-1302.
- HILLE, B. (1992) *Ionic channels of Excitable Membranes*. Sinauer, Sunderland, U.S.A.
- HO, K., NICHOLS, C.G., LEDERER, W.J., LYTTON, J., VASSILEV, P.M., KANAZIRSKA, M.V. and HEBERT, S.C. (1993) Cloning and expression

of an inwardly rectifying ATP-regulated potassium channel. *Nature* **362**: 31-38.

HODGKIN, A.L. and HUXLEY, A.F. (1952) A quantitative description of membrane current and its application to conduction and excitation in nerve. *Journal of Physiology* **117**: 500-544.

HODGKIN, A.L. and KATZ, B. (1949) The effect of sodium ions on the electrical activity of the giant axon of the squid. *Journal Of Physiology* **108**: 37-77.

HOLZ, R. and FINKELSTEIN, A. (1970) The water and non-electrolyte permeability induced in thin lipid membranes by the polyene antibiotics nystatin and amphotericin B. *Journal of General Physiology* **56**: 125-145.

HOSHI, T., ZAGOTTA, W.N. and ALDRICH, R.W. (1990) Biophysical and molecular mechanisms of *Shaker* potassium channel inactivation. *Science* **250**: 533-538.

HOSHI, T., ZAGOTTA, W.N. and ALDRICH, R.W. (1991) Two types of inactivation in *Shaker* K⁺ channels: effects of alterations in the carboxy-terminal region. *Neuron* **7**: 547-556.

HOSHI, T., ZAGOTTA, W.N. and ALDRICH, R.W. (1994) *Shaker* potassium channel gating I: transitions near the open state. *Journal of General Physiology* **103**: 249-278.

ISACOFF, E.Y., JAN, Y.N. and JAN, L.Y. (1990) Evidence for the formation of heteromultimeric potassium channels in *Xenopus* oocytes. *Nature* **345**: 530-534.

ISACOFF, E.Y., JAN, Y.N. and JAN, L.Y. (1991) Putative receptor for the cytoplasmic inactivation gate in the *Shaker* K⁺ channel. *Nature* **353**: 86-90.

ISHIHARA, K., MITSUIYE, T., NOMA A. and TAKANO, M. (1989) The Mg²⁺ block and intrinsic gating underlying inward rectification of the K⁺ current in guinea-pig cardiac myocytes. *Journal of Physiology* **419**: 297-320.

IVERSON, L.E., TANOUYE, M.A., LESTER, H.A., DAVIDSON, N. and RUDY, B. (1988) A-type potassium channels expressed from *Shaker* locus cDNA. *Proceedings of the National Academy of Sciences USA* **85**: 5723-5727.

JAN, Y.N., JAN, L.Y. and DENNIS, M.J. (1977) Two mutations of synaptic transmission in *Drosophila*. *Proceedings of the Royal Society of London Series B* **198**: 87.

JAN, L.Y. and JAN, Y.N. (1990) How might the diversity of potassium channels be generated? *Trends in Neuroscience* **13** (10): 415-419.

JAN, L.Y. and JAN, Y.N. (1992) Structural elements involved in specific K⁺ channel functions. *Annual Review of Physiology* **54**: 537-555.

KEYNES, R.D. and AIDLEY, D.J. (1991) *Nerves and Muscle*. Cambridge University Press, Cambridge, Great Britain.

KRAMER, R.H., GOULDING, E., and SIEGELBAUM, S.A. (1994) Potassium channel inactivation peptide blocks cyclic nucleotide-gated channels by binding to the conserved pore domain. *Neuron* **12**: 655-662.

KAMB, A., IVERSON, L.E., TANOUYE, M.A. (1987) Molecular characterization of *Shaker*, a *Drosophila* gene that encodes a potassium channel. *Cell* **50**: 405-413.

KUBO, Y., BALDWIN, T.J., JAN, Y.N. and JAN, L.Y. (1993) Primary structure and functional expression of a mouse inward rectifier potassium channel. *Nature* **362**: 127-133.

KUBO, Y., REUVENY, E., SLESINGER, P.A., JAN, Y.N. and JAN, L.Y. (1993) Primary structure and functional expression of a rat G protein-coupled muscarinic potassium channel. *Nature* **364**: 802-806.

LEECH, C.A. and STANFIELD, P.R. (1981) Inward rectification in frog skeletal muscle fibres and its dependence on membrane potential and external potassium. *Journal of Physiology* **319**: 295-309.

LI, M., JAN, Y.N. and JAN, L.Y. (1992) Specification of subunit assembly by the hydrophilic amino-terminal domain of the *Shaker* potassium channel.

Science **257**: 1225-1230.

LOPEZ, G.A., JAN, Y.N. and JAN, L.Y. (1994) Hydrophobic substitution mutations in the S4 sequence alter voltage-dependent gating in *Shaker* K⁺ channels. *Neuron* **7**: 327-336.

LUNEAU, C.J., WILLIAMS, J.B., MARSHALL, J., LEVITAN, E.S., OLIVA, C., SMITH, J.S., ANTANAVAGE, J., FOLANDER, K., STEIN, R.B., SWANSON, R., KACZMAREK, L.K. and BUHROW, S.A. (1991) Alternative splicing contributes to K⁺ channel diversity in the mammalian central nervous system. *Proceedings of the National Academy of Sciences of the USA* **88**: 3932-3936.

MacKINNON, R. (1991) Determination of the subunit stoichiometry of a voltage-activated potassium channel. *Nature* **350**: 232-235.

MATSUDA, H., SAIGUSA, A., and IRISAWA, H. (1987) Ohmic conductance through the inward rectifier K channel and blocking by internal Mg²⁺.

Nature **325**: 156-159.

MOORE, S.D., MADAMBA, S.G., JOELS, M. and SIGGINS, G.R. (1988) Somatostatin augments the M-current in hippocampal neurons. *Science* **239**: 278-280.

MURRELL-LAGNADO, R.D. and ALDRICH, R.W. (1993) Interactions of amino terminal domains of *Shaker* K channels with a pore blocking site studied with synthetic peptides. *Journal of General Physiology* **102**: 949-975.

MURRELL-LAGNADO, R.D. and ALDRICH, R.W. (1993) Energetics of *Shaker* K channels block by inactivation peptides. *Journal of General Physiology* **102**: 977-1003.

NEEDHAM, M., GOODING, C., HUDSON, K., ANTONIOU, M., GROSVELD, F. and HOLLIS, M. (1992) LCR/MEL: A versatile system for high-level expression of heterologous proteins in erythroid cells. *Nucleic Acids Research* **20** (5): 997-1003.

NEHER, E. and SAKMANN, B. (1976) Single channel currents recorded from membrane of denervated frog muscle fibres. *Nature* **260**: 799-802.

NEHER, E. and SAKMANN, B. (1992) The patch clamp technique. *Scientific American* March: 28-35.

NODA, M., TAKAHASHI, H., TANABE, T., TOYOSATO, M., FURUTANI, Y., HIROSE, T., ASAI, M., INAYAMA, S., MIYATA, T. and NUMA, S. (1982) Primary structure of α -subunit precursor of *Torpedo californica* acetylcholine receptor deduced from cDNA sequence. *Nature* **299**: 793-797.

NODA, M., SHIMUZU, S., TANABE, T., TAKAI, T., KAYANO, T., IKEDA, T.,
TAKAHASHI, H., NAKAYAMA, H., KANAOKA, Y., MINAMINO, N.,
KANGAWA, K., MATSUO, H., RAFTERY, M.A., HIROSE, T.,
INAYAMA, S., HAYASHIDA, H., MIYATA, T. and NUMA, S. (1984)
Primary structure of *Electrophorus Electricus* sodium channel deduced from
cDNA sequence. *Nature* **312**: 121-127.

NODA, M., IKEDA, T., SUZUKI, S., TAKESHIMA, H., TAKAHASHI, T.,
KUNO, M., and NUMA, S. (1986) Expression of functional sodium
channels from cloned cDNA. *Nature* **322**: 826-828.

OVERTURF, K.E., RUSSELL, S.N., CARL, A., VOGALIS, F., HART, P.J.,
HUME, J.R., SANDERS, K.M. AND HOROWITZ, B. (1994) Cloning and
characterization of a Kv1.5 delayed rectifier K⁺ channel from vascular and
visceral smooth muscles. *American Journal of Physiology* **267** (Cell
Physiology **36**): C1231-1238.

PAK, M.D., BAKER, K., COVARRUBIAS, M., BUTLER, A., RATCLIFFE, A.
and SALKOFF, L. (1991) mShal, a subfamily of A-type K⁺ channel cloned
from mammalian brain. *Proceedings of the National Academy of Sciences*
USA **88**: 4386-4390.

PAPAZIAN, D.M., SCHWARZ, T.L., TEMPEL, B.L., JAN, Y.N. and JAN, L.Y.
(1987) Cloning of genomic and complementary DNA from *Shaker*, a
putative potassium channel gene from *Drosophila*. *Science* **237**: 749-753.

- PAPAZIAN, D.M., TIMPE, L.C., JAN, Y.N. and JAN, L.Y. (1991) Alteration of voltage-dependence of *Shaker* potassium channel by mutations in the S4 sequence. *Nature* **349**: 305-310.
- PHILIPSON, L.H., HICE, R.E., SCHAEFER, K., LaMENDOLA, J., BELL, G.I., NELSON, D.J. and STEINER, D.F. (1991) Sequence and functional expression in *Xenopus* oocytes of a human insulinoma and islet potassium channel. *Proceedings of the National Academy of Sciences USA* **88**: 53-57.
- PONGS, O. (1992) Molecular biology of voltage-dependent potassium channels. *Physiological Reviews* **72** (4) (Suppl.): S69-S88.
- RETTIG, J., HEINEMANN, S.H., WUNDER, F., LORRA, C., PARCEJ, D.N., DOLLY, J.O. and PONGS, O. (1994) Inactivation properties of voltage-gated K⁺ channels altered by presence of β -subunit. *Nature* **369**: 289-294.
- RETTIG, J., WUNDER, F., STOCKER, M., LICHTINGHAGEN, R., MASTIAUX, F., BECKH, S., KUES, W., PEDARZANI, P., SCHRÖTER, K.H., RUPPERSBERG, J.P., VEH, R. and PONGS, O. (1992) Characterization of a *Shaw*-related potassium channel family in rat brain. *EMBO Journal* **11** (7): 2473-2486.
- ROBERDS, S.L. and TAMKUN, M.M. (1991) Cloning and tissue-specific expression of five voltage-gated potassium channel cDNAs expressed in rat

heart. *Proceedings of the National Academy of Sciences USA* **88**: 1798-1802.

RUDY, B. (1988) Diversity and ubiquity of potassium channels. *Neuroscience* **25** (3): 729-749.

RUPPERSBURG, J.P., FRANK, R., PONGS, O. and STOCKER, M. (1991)
Cloned neuronal I_K(A) channels reopen during recovery from inactivation.
Nature **353**: 657-660.

RUPPERSBURG, J.P., SCHRÖTER, K.H., SAKMANN, B., STOCKER, M.,
SEWING, S. and PONGS, O. (1990) Heteromultimeric channels formed by
rat-brain potassium channel proteins. *Nature* **345**: 535-537.

SALKOFF, L. (1983) Genetic and voltage-clamp analysis of a *Drosophila*
potassium channel. *Cold Spring Harbor Symposium on Molecular Biology*
48: 221-231.

SALKOFF, L., BAKER, K., BUTLER, A., COVARRUBIAS, M., PAK M.D. and
WEI, A. (1992) An essential 'set' of K⁺ channels conserved in flies, mice
and humans. *Trends in Neuroscience* **15** (5): 161-166.

SAMBROOK, J., FRITSCH, E.F. AND MANIATIS, T. (1989) *Molecular Cloning*
- a Laboratory Manual, 2nd edn. Cold Spring Harbor Press, New York.

SASAKI, Y., ISHII, K., NUNOKI, K., YAMAGISHI, T. and TAIRA, N. (1995)

The voltage-dependent K⁺ channel (Kv1.5) cloned from rabbit heart and facilitation of inactivation of the delayed rectifier current by the rat β-subunit. *FEBS Letters* **372** (1): 20-24.

SCHWARZ, T.L., TEMPEL, B.L., PAPAZIAN, D.M., JAN, Y.N. and JAN, L.Y.

(1988) Multiple potassium channel components are produced by alternative splicing at the *Shaker* locus in *Drosophila*. *Nature* **331**:137-142.

SCHOTT, M., ANTZ, C., FRANK, R., RUPPERSBERG, J.P. and KALBITZER,

H.R. (1998) Structure of the inactivating gate from the *Shaker* voltage-gated K⁺ channel analyzed by NMR spectroscopy. *European Biophysics Journal* **27** (2): 99-104.

SEWING, S., ROEPER J. and PONGS (1996) Kvβ1 subunit binding specific for

Shaker-related potassium channel α-subunits. *Neuron* **16** (2): 455-463.

SHELTON, P.A., DAVIES, N.W., ANTONIOU, M., GROSVELD, F.,

NEEDHAM, M., HOLLIS, M., BRAMMAR, W.J. and CONLEY, E.C.

(1993) Regulated expression of K⁺ channel genes in electrically silent mammalian cells by linkage to β-globin gene-activation elements. *Receptors and Channels* **1**: 25-37.

SHEN, N.V., CHEN, X., BOYER, M.M., PFAFFINGER, P.J. (1993) Deletion

analysis of K⁺ channel assembly. *Neuron* **11**: 67-76.

- SLESINGER, P.A., JAN, Y.N. and JAN, L.Y. (1993) The S4-S5 loop contributes to the ion selective pore of potassium channels. *Neuron* **11**: 739-749.
- SNYDERS, D.J., TAMKUN, M.M. and BENNETT, P.B. (1993) A rapidly activating and slowly inactivating potassium channel cloned from human heart. Functional analysis after stable mammalian cell culture expression. *Journal of General Physiology* **101** (4): 513-543.
- SOLC, C.K. and ALDRICH, R.W. (1988) Voltage-gated potassium channels in larval CNS neurons of *Drosophila*. *Journal of Neuroscience* **8**: 2556-2570.
- SOLC, C.K., ZAGOTTA, W.N. and ALDRICH, R.W. (1987) Single-channel and genetic analyses reveal two distinct A-type potassium channels in *Drosophila*. *Science* **236**: 1094-1098.
- STANFIELD, P.R., DAVIES, N.W., SHELTON, P.A., KHAN, I.A., BRAMMAR, W.J., STANDEN, N.B. and CONLEY, E.C. (1994) The intrinsic gating of inward rectifier K⁺ channels expressed from the murine IRK1 gene depends on voltage, K⁺, and Mg²⁺. *Journal of Physiology* **475**: 1-7.
- STANFIELD, P.R., DAVIES, N.W., SHELTON, P.A., SUTCLIFFE, M.J., KHAN, I.A., BRAMMAR, W.J. and CONLEY, E.C. (1994) A single aspartate residue is involved in both intrinsic gating and blockage by Mg²⁺ of the inward rectifier, IRK1. *Journal of Physiology* **478**: 1-7.

STANFIELD, P.R., DAVIES, N.W., SHELTON, P.A., KHAN, I.A., BRAMMAR, W.J., STANDEN, N.B. and CONLEY, E.C. (1994) Mutation of a single aspartate residue in the inward-rectifier potassium channel encoded by the murine IRK1 gene alters its voltage- and K⁺-dependent gating. *Journal of Physiology* **477**: 86P.

STÜHMER, W., CONTI, F., SUZUKI, H., WANG, X., NODA, M., YAHAGI, N., KUBO, H. and NUMA, S. (1989) Structural parts involved in activation and inactivation of the sodium channel. *Nature* **339**:597-603.

STÜHMER, W., RUPPERSBERG, J.P., SCHRÖTER, K.H., SAKMANN, B., STOCKER, M., GIESE, K.P., PERSCHKE, A., BAUMANN, A. and PONGS, O. (1989) Molecular basis of functional diversity of voltage-gated potassium channels in mammalian brain. *EMBO Journal* **8** (11): 3235-3244.

TAKUMI, T., OHKUBO, H. and NAKANISHI, S. (1988) Cloning of a membrane protein that induces a slow voltage-gated potassium current. *Science* **242**: 1042-1045.

TAMKUN, M.M., BENNETT, P.B. and SNYDERS, D.J. (1994) Cloning and expression of human cardiac K⁺ channels. *Cardiac Electrophysiology: From Cell to Bedside*, edited by D. Zipes and J. Jalife. Philadelphia, PA: Saunders, p. 21-31.

- TANABE, T., TAKESHIMA, H., MIKAMI, A., FLOCKERZI, V., TAKAHASHI, H., KANGAWA, K, KOJIMA, M., MATSUO, H., HIROSE, T., and NUMA S (1987) Primary structure of the receptor for calcium channel blockers from skeletal muscle. *Nature* **328**:313-318.
- TANOUE, M.A., FERRUS, A. and FUJITA, S. (1981) Abnormal action potentials associated with the *Shaker* complex locus of *Drosophila*. *Proceedings of the National Academy of Sciences USA* **78**: 6548-6552.
- TEMPEL, B.L., PAPAZIAN, D.M., SCHWARZ, T.L., JAN, Y.N. and JAN, L.Y. (1987) Sequence of a probable potassium channel component encoded at *Shaker* locus of *Drosophila*. *Science* **237**: 770-775.
- TIMPE, L.C., SCHWARZ, T.L., TEMPEL, B.L., PAPAZIAN, D.M., JAN, Y.N. and JAN, L.Y. (1988) Expression of functional potassium channels from *Shaker* cDNA in *Xenopus* oocytes. *Nature* **331**: 143-145.
- TORO, L., STEFANI, E. and LATORRE, R. (1992) Internal blockade of a Ca²⁺-activated K⁺ channel by *ShakerB* inactivating "ball" peptide. *Neuron* **9**: 237-245.
- TSAUR, M.L., SHENG, M., LOWENSTEIN, D.H., JAN, Y.N. and JAN, L.Y. (1992) Differential expression of K⁺ channel messenger-RNAs in the rat-

- brain and down-regulation in the hippocampus following seizures. *Neuron* **8** (6): 1055-1067.
- UEBELE, V.N., ENGLAND, S.K., CHAUDHARY, A., TAMKUN, M.M., and SNYDERS, D.J. (1996) Functional differences in Kv1.5 currents expressed in mammalian cell lines are due to the presence of endogenous Kv β 2.1 subunits. *Journal of Biological Chemistry* **271** (5):2406-2412.
- WANG, H., KUNKEL, D.D., MARTIN, T.M., SCHWARTKROIN, P.A. and TEMPEL, B.L. (1993) Heteromultimeric K⁺ channels in terminal and juxtaparanodal regions of neurons. *Nature* **365**: 75-79.
- WEI, A., COVARRUBIAS, M., BUTLER, A., BAKER, K., PAK, M. and SALKOFF, L. (1990) K⁺ current diversity is produced by an extended gene family conserved in *Drosophila* and mouse. *Science* **248**: 599-603.
- WIBLE, B.A., TAGLIALATELA, M., FICKER, E. and BROWN, A.M. (1994) Gating of inward rectifier K⁺ channels localized to a single negatively charged residue. *Nature* **371**: 246-249.
- YEOLA, S.W., and SNYDERS, D.J. (1997) Electrophysiological and pharmacological correspondence between Kv4.2 current and rat cardiac transient outward current. *Circulation Research* **33**: 540-547

YELLEN, G., JURMAN, M.E., ABRAMSON, T. and MACKINNON, R. (1991)

Mutations affecting internal TEA blockade identify the probable pore-forming region of a K⁺ channel. *Science* **251**, 939-942.

ZAGOTTA, W.N., HOSHI, T. and ALDRICH, R.W. (1990) Restoration of

inactivation in mutants of *Shaker* potassium channels by a peptide derived from ShB. *Science* **250**: 568-571.